ANTONIO F. CORNO

PIERLUIGI FESTA

Congenital
Heart Defects

DECISION MAKING
FOR SURGERY

3 CT-Scan and MRI

A. F. Corno
P. Festa

■ **Congenital Heart Defects**
Decision Making for Cardiac Surgery

Volume 3   CT-Scan and MRI

With compliments

PHILIPS

A. F. Corno
P. Festa

■ **Congenital Heart Defects**
Decision Making for Cardiac Surgery

Volume 3   CT-Scan and MRI

Dedicated to our loved children

Federica, Laura, Jonathan, Bean

Laura, Paula, Pablo, Kiko

A. F. Corno   P. Festa

Congenital Heart Defects

Decision Making for Cardiac Surgery

Volume 3   CT-Scan and MRI

Foreword by Richard Jonas

With 198 Figures in 400 Separate Illustrations

STEINKOPFF
VERLAG

Springer

Antonio F. Corno, MD, FRCS (Glasgow), FACC, FETCS
Cardiac Surgery
Alder Hey Royal Children Hospital
Eaton Road
Liverpool, L12 2AP
England, UK

Gigi P. Festa, MD
Pediatric Cardiologist
Ospedale Pediatrico Apuano "G. Pasquinucci", CNR
Via Aurelia Sud
54100 Massa
Italy

Foreword

The diagnosis and management of congenital heart disease has evolved rapidly over the last 30 years. In the 1970s, invasive cardiac catheterization was a high-risk procedure for the infant and particularly the duct dependent neonate. The introduction of noninvasive 2-dimensional echocardiography revolutionized the diagnosis and management of individuals with congenital heart disease. No longer was the cardiologist limited to a handful of images and patient positions but could spend hours if necessary defining every detail of an individual child's cardiac anomaly. The addition of Doppler and subsequently color Doppler further increased the importance of echocardiography in the decision making for congenital cardiac surgical procedures. And now we are fortunate to have further additions to the imaging and diagnostic armamentarium, namely cardiac CT and cardiac MRI.

In this most recent volume of the series entitled "Congenital Heart Defects: Decision Making for Surgery" Dr. Antonio F. Corno provides an up-to-date and comprehensive presentation of the new role that cardiac CT and cardiac MRI will play in the management of congenital heart disease. He has been ably assisted by a cardiologist, Dr. Gigi P. Festa.

The book provides a dazzling array of images derived by both techniques and covering the full range of congenital heart anomalies. Both the pre-operative and postoperative usefulness of these techniques is presented.

There is no doubt that these techniques will be particularly helpful in the older child and adult with congenital heart disease in assessing the late impact of a congenital heart anomaly and the surgical repair or palliation which may have been undertaken years previously.

The time is definitely right for a comprehensive presentation of these new diagnostic modalities and the manner in which they will influence the field of congenital heart management.

Dr. Corno is to be congratulated on seizing this opportunity and producing a beautifully illustrated textbook that will be the standard against which others will be measured.

Washington, DC   RICHARD JONAS, M.D.
August 2008

Preface

The first two volumes of this series on "Congenital Heart Defects – Decision making for surgery" have been dedicated to the "Most common defects (Volume 1)" and to "Less common defects (Volume 2)". The schema utilized for these two books was the same, with each chapter devoted to a single malformation, with incidence, morphology, associated anomalies, pathophysiology, diagnosis (including clinical pattern, electrocardiogram, chest X-ray, echocardiogram, and cardiac catheterization with angiography), indications for surgical treatment, details of surgical techniques, potential complications and literature references.

During the last few years computed tomography (CT) scan and magnetic resonance imaging (MRI) have emerged as valuable noninvasive cardiovascular diagnostic tools. Both CT scan and MRI are capable of producing stunning 3-dimensional pictures independent of body size. In particular cardiac MRI can provide unique anatomic and functional information not available by any other diagnostic modality previously available. Because of the progressively increasing role of CT scan and MRI in the pre- and postoperative evaluation of patients with congenital heart defects, it seemed natural to continue this series of volumes preparing a third book entirely dedicated to these two diagnostic techniques.

The sole author of the first two volumes (AFC) decided to involve Dr. Gigi P. Festa, cardiologist with extensive expertise particularly in cardiac MRI, in the current task. The choice was due not only to his competence in the matter, but to the fact that we worked together years ago, first in Milan, Italy, then in Paris, France, with Dr. Yves Lecompte. The mutual respect that develops among colleagues is not enough to write a book, particularly when working as nowadays in different departments and living in different countries, with different professional schedules and family commitments, despite the advantages of the communication feasible through the internet. A deep friendship is indispensable to reach agreement on every single detail, including the entire text and the choice of illustrations.

We agreed to maintain the extremely schematic format of the book, following the style of the first two volumes, in order to provide the essential information to the readers. Since our list of congenital heart defects is derived from the sum of malformations treated in the first two volumes in this series, most of the clinical data on conventional diagnostic techniques (electrocardiography, X-ray, echocardiography, cardiac catheterization with angiography), indication for surgery and surgical techniques have been omitted to avoid duplication with the other volumes of the series. Only a selected num-

ber of illustrations, as well as number of references, could be used because of space limitations. Finally, since the pre-operative and post-operative illustrations are coming from different departments and different periods, it is quite clear that the patients have been treated with either interventional cardiology or surgical techniques by different operators, not necessarily by the authors.

Liverpool and Massa, Summer 2008   ANTONIO F. CORNO
                                                          GIGI P. FESTA

Acknowledgements

Table of Contents

CHAPTER 3.0 | Introduction to CT scan and MRI

Introduction

Transthoracic echocardiography is the first-line imaging modality for diagnosis and follow-up of patients with congenital heart defects due to its low cost, widespread availability, portability, ease of use, and excellent temporal-spatial resolution, reducing the need for diagnostic cardiac catheterization and angiography in most patients. However, the diagnostic utility of echocardiography markedly diminishes with the growth of the patients and after surgical procedures through median sternotomy because acoustic windows become progressively more limited. Moreover extracardiac structures, such as the great arteries and great veins, complex intracardiac connections or surgically implanted conduits or baffles deeply located in the chest or behind the sternum, may also be difficult to resolve by ultrasound. Diagnostic cardiac catheterization carries risk of complications because it is invasive and is associated with radiation exposure; furthermore as a projection technique, it is limited in providing accurate anatomical information. In the last two decades, computed tomography (CT) scan and magnetic resonance imaging (MRI) have emerged as valuable noninvasive cardiovascular diagnostic tools capable of producing informative pictures, providing unique anatomic and functional information not available by any other diagnostic modality currently available. For the assessment of the anatomy of the extracardiac structures, the clinical indication for CT scan and MRI are somewhat similar, and very often the question which is better to

use is raised. The main differences as well as advantages and disadvantages are highlighted in Table 3.0.1.

The easy of use and the short time required for the complete investigation make the CT very attractive, particularly in children. However, according to the recent literature, its radiation exposure represents a major concern, mainly in children and its use should be limited whenever possible as recommended by the FDA in 2001. While the CT scan still remains a very valuable tool to provide detailed information about extracardiac structures, the available clinical experience with MRI is becoming richer than that with CT due its better capacity to assess intracardiac morphology and cardiac function, and its better versatility.

The choice between CT and MRI has to be based on the available institutional equipment and scheduling, the capability of the

Table 3.0.1. CT scan and MRI

	MRI	CT
▮ Examination time	+ (long)	++++ (short)
▮ Great vessels image resolution	+++	++++
▮ Tissue characterization	+++	+
▮ Calcification analysis	No	Yes
▮ Flow analysis	Yes	No
▮ Coronary artery imaging	++	+++
▮ Ventricular function analysis	++++	+
▮ Airway analysis	++	++++
▮ Ionizing radiation	No	Yes
▮ User friendly	+	+++
▮ Costs	+++	+

patient to cooperate, and the need to tailor the investigation to answer the specific question being asked. Cardiologists and radiologists should be provided accurate estimates of CT radiation doses to allow for a balanced and accurate assessment of the risk/benefits ratio when considering indication for a CT scan.

Computed tomography

◼ General principles

Computed tomography (CT) is a medical imaging method using tomography where digital geometry processing generates a 3-dimensional image from a large series of 2-dimensional X-ray images. Although historically the generated images were in the axial or transverse plane, orthogonal to the long axis of the body, modern computational techniques allow this volume data to be reformatted into various planes or even as 3-dimensional representations. CT has undergone staged evolution leading to increased spatial resolution and temporal resolution. Initial single slice CT has evolved into helically scanning CT in which large volumes could be included by the translation of the subject along the axis of scanner. By introducing multiple detectors (multislice CT) including arrays detectors, commonly 64 in the current clinical practice, increased resolution and/or volumes can be imaged on shorter time scales. This has led to the ability to perform high-resolution scans gated to the cardiac cycle.

◼ Patient preparation

The need of sedation in infants and children less than 6 years of age has decreased as the speed of CT scanning has increased. While the sedation rate for single-detector row CT was at least 30%, the sedation rate for young children undergoing multidetector row CT is less than 5%. Despite this improvement, sedation has not yet been eliminated, and knowledge of safe and effective use of sedation remains of paramount importance.

Oral administration of chloral hydrate is used as a sedative agent in children, while deep sedation (propofol) or general anesthesia (isoflurane) is used in infants. In older children adequate preparation with verbal reassurance and explanation of the procedure can generally obtain good cooperation.

◼ Methodology and technical aspects

◼ **Intravenous contrast material:** The issues in the administration of intravenous contrast material for CT angiography in pediatric patients include type and volume of contrast material, method of administration (manual versus power injection), and delay between the start of injection and the initiation of scanning. Intravenous contrast material is not required for routine investigation of the airways, but is essential in children with suspected para-tracheal malformation such as vascular rings or pulmonary artery slings. Through an intravenous cannula placed in the CT suite, the nonionic contrast material is administered at a dose of 2.0 mL/kg. The use of a nonionic agent minimizes the gastrointestinal side effects such as nausea and vomiting, the discomfort at the site of injection, the patient reaction during the administration of intravenous contrast material, and potential complications from contrast material extravasations. With multidetector row CT volumes as small as 2 mL/kg allow successful contrast enhancement for CT angiography. Intravenous contrast material can be administered by manual (hand) or power injection. The advantages of power over manual injection are the ability to precisely determine the timing of delivery of the contrast material and the uniformity of enhancement. The flow rates vary with the size of the intravenous catheter, from 1.5 to 2.0 mL/s for a 22-gauge catheter to 2 to 3 mL/s for a 20-gauge catheter. During the injection

of contrast material, the site of injection needs to be closely monitored to minimize the risk of extravasations. As a general rule the contrast material is administered with a flow rate calculated to deliver the entire volume of contrast material in a period equivalent to, or slightly less than, the duration of the CT acquisition. There is a low but nonnegligible level of risk associated with the intravenous administration of the contrast agent itself: severe and potentially life-threatening allergic reaction and renal insufficiency. Because of these risks, ionic contrast agents are generally avoided.

▪ **Scanning delay time:** The time between the start of the injection of contrast material and the start of the scan data acquisition is the delay time. Empirically the duration of the scanning time should be set to obtain the maximum of contrast concentration in the region of interest, in order to provide excellent vascular enhancement in children. An automated tracking system, taking into account variable factors such as cardiac output and circulation time, allows customization of contrast enhancement for each individual patient.

▪ **Technical parameters:** Before scanning is started, several technical parameters have to be selected, including collimator thickness, table speed, tube current or milliamperage, kilovoltage, and anatomic coverage required. Sections of 1 mm thickness are generally used in children, to maintain accurate definition without increasing the radiation dose. The table speed is set as fast as possible to increase the temporal resolution and to decrease the radiation combined with detector array dimensions. Electrocardiographic gating is able to reduce artifacts related to cardiac motion and arterial pulsation, but it does not affect the respiratory motion.

▪ **Radiation exposure:** In children the issue of radiation exposure is extremely important. Since children's organs are more radiosensitive than adults' and they have a longer life span than adults, the development of ra-

diation-induced malignancies is a real potential risk, particularly in younger children. On average, the radiation exposure during a CT scan reaches 2.0 to 2.5 rems, in comparison with 1.5 to 2.0 rems during a diagnostic cardiac catheterization with angiography. The radiation dose for a particular CT study depends on multiple factors: volume scanned, patient size, number and type of scan studies, and desired resolution and image quality. In general, multidetector row CT should be performed with techniques providing adequate quality of images with the lowest possible radiation exposure. These techniques include the use of the lowest milliamperage and kilovoltage settings, appropriate section thickness, and the fastest table speed. Adjustments of specific technical factors proved to minimize the radiation dose in children undergoing CT, particularly in state-of-the-art multisection spiral CT: such adjustments include setting the lowest diagnostic tube current according to the patient's weight and doubling the pitch, which reduces the radiation dose by half. The use of ECG prospective gating in multislice CT scan allows a further reduction of the radiation exposure, thanks to the acquisition of images limited to 70–80% of the R-R interval. In addition, multiphase studies should be used for selected indications rather than on a routine basis.

▪ **Anatomic coverage:** A minimal coverage for CT angiography should extend from the level of the diaphragm inferiorly to just below the thoracic inlet, in order to include the proximal aspects of the common carotid arteries and of the subclavian arteries in the CT scan. This inclusion allows visualization of the position of the aortic arch, presence of aortic coarctation, presence and degree of hypoplasia of the aortic arch, and anomalous origin of the head and neck vessels. The selected field of view has to approximate the cross-sectional size of the region being studied. A smaller field of view can reduce a waste of matrix space, a loss of resolution, and incidence of poor quality images.

■ **Breath holding:** CT scan investigations are performed with breath holding at suspended inspiration in cooperative grown-up children and during quiet respiration in children under sedation.

■ **Reconstruction algorithms:** A standard reconstruction algorithm is generally enough in routine CT angiography studies. A high resolution algorithm is used for 3-dimensional reconstructions involving the airways.

■ **Post-processing applications**

Various options are available for post-processing the volumetric data set.

■ **Multiplanar reconstructions:** Sections of multiplanar reformations can be displayed in any plane: coronal, sagittal, parasagittal or in curved isotropic datasets, such as along the axis of the mediastinal vessels or airways. This technique is fast and can be easily performed at the CT scanner, but it provides only a 2-dimensional display of data (Figs. 3.0.1
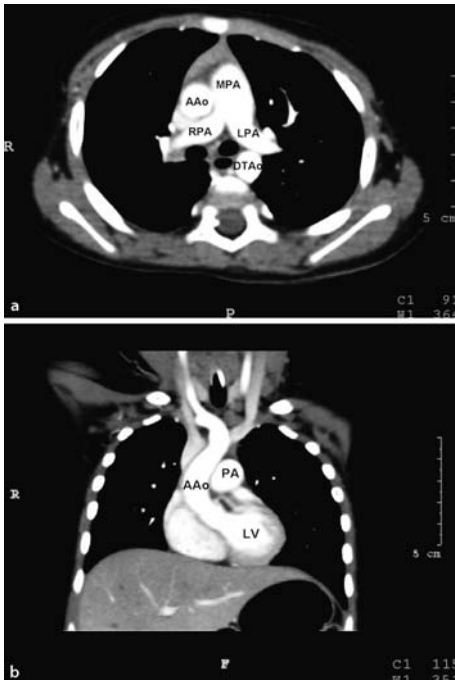
Fig. 3.0.1. CT scan of normal anatomy. **a** Axial section of a 2-dimensional study showing the relationship between the great arteries. **b** Para-coronal plan of a 2-dimensional study showing the relationship between the great arteries, in the presence of situs solitus, with the liver on the right side and the stomach on the left side (*AAo* ascending aorta, *DTAo* descending thoracic aorta, *LPA* left pulmonary artery, *MPA* main pulmonary artery, *RPA* right pulmonary artery, *LV* left ventricle, *PA* pulmonary artery)
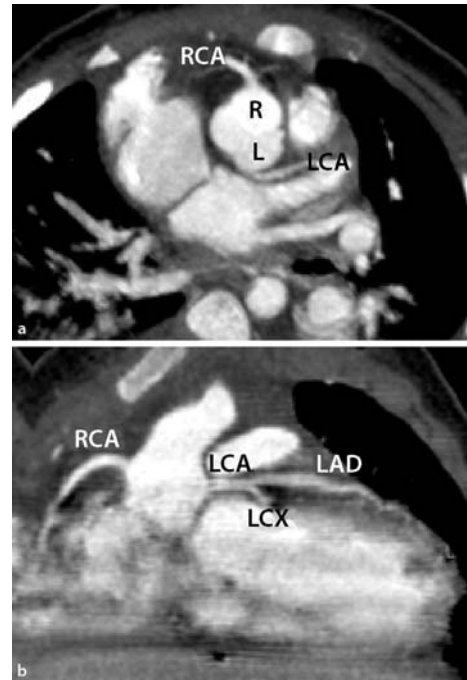
Fig. 3.0.2. CT scan of normal coronary arteries. CT angiography with axial (**a**) and coronal (**b**) projection showing the normal origin and course of right and left coronary arteries, respectively, from the right and left aortic sinus (*LAD* left anterior descending coronary artery, *LCA* left coronary artery, *LCX* left circumflex coronary artery, *RCA* right coronary artery) (reproduced with permission from Goo HW, Park IS, Ko JK, Kim YH, Seo DM, Yun TJ, Park JJ, Yoon CH (2003) CT of congenital heart disease: normal anatomy and typical pathologic conditions. Radiographics 23:S147–165)
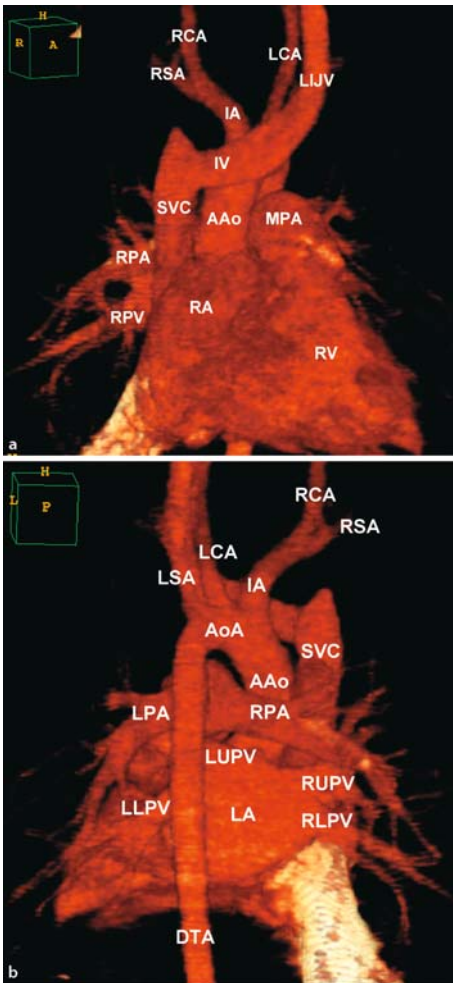
Fig. 3.0.3. CT scan of normal anatomy. **a** CT angiography with 3-dimensional reconstruction, oblique right anterior view of the normal cardiac anatomy. **b** CT angiography with 3-dimensional reconstruction, posterior view of the normal cardiac anatomy (*AAo* ascending aorta, *AoA* aortic arch, *DTA* descending thoracic aorta, *IA* innominate artery, *IV* innominate vein, *LA* left atrium, *LCA* left carotid artery, *LIJV* left internal jugular vein, *LLPV* left lower pulmonary vein, *LPA* left pulmonary artery, *LSA* left subclavian artery, *LUPV* left upper pulmonary vein, *MPA* main pulmonary artery, *RA* right atrium, *RCA* right carotid artery, *RLPV* right lower pulmonary vein, *RPA* right pulmonary artery, *RPV* right pulmonary veins, *RSA* right subclavian artery, *RUPV* right upper pulmonary vein, *RV* right ventricle, *SVC* superior vena cava)

and 3.0.2), and information regarding the 3-dimensional spatial relationship of anatomic structures is absent. Curved planar reconstructions are a variant of the routine multiplanar reconstructions, allowing curved or tortuous vessels such as the aorta and the pulmonary artery to be visualized in a single tomography volume.

▪ **Variable-thickness displays:** With this technique, CT images are acquired at their routine thickness section, and then combined in multiples ("slabs") to create a thicker image. This allows better visualization of smaller pulmonary vessels and airways.

▪ **3-Dimensional volume rendering:** Volume rendering has largely replaced other 3-dimensional reformatting techniques, because the use of a transfer function allows mapping of a CT number to brightness and color. This provides valuable information regarding the spatial relationship of anatomic structures, and it also allows the data to be displayed from an external or internal perspective. The volume-rendering technique is particularly useful for structures which are 3-dimensional and cannot be easily captured in a planar image (Fig. 3.0.3). The creation of volume-rendered images requires secondary processing, and the images can generally be produced in a few minutes.

Magnetic resonance imaging

▪ **General principles**

Cardiac MRI in the pediatric population is accompanied by a unique series of technical challenges superior to those encountered in imaging of adult patients: the anatomical structures are smaller, thus, demanding greater spatial resolution; the heart rates are generally higher, requiring a greater temporal resolution; and the pediatric patients can be either noncooperative or may require full sedation. Despite these technical difficulties,

cardiac MRI offers several characteristics favorable in comparison with the conventional imaging modalities, including soft tissue contrast, capacity for true 3-dimensional imaging, accurate flow measurements, freely selectable imaging planes, and lack of ionizing radiation. These advantages, in addition to continued advances in MRI hardware, software, and imaging techniques, are progressively increasing the widespread utilization of cardiac MRI in pediatric cardiology.

Through the use of several MRI techniques, examiners can obtain high-quality 3-dimensional images of the cardiovascular anatomy, accurately quantify volumes and mass of cardiac chambers, ejection fraction, stroke volumes, regurgitation volume and fraction, as well as regional left and right ventricular myocardial function. Therefore, MRI is ideal for noninvasive pre-operative evaluation of patients with complex intracardiac anatomy, anomalous connections of the systemic and pulmonary veins, anomalous pulmonary arteries, defects involving the aorta and its branches, single ventricles, systemic right ventricles and abnormally shaped left ventricles. MRI has also acquired a precise role in the postoperative evaluation of patients after complex surgery, such as, after repair of tetralogy of Fallot, univentricular type of circulation, and in the presence of abnormal blood flow dynamics.

The clinical indications for cardiac MRI are rapidly evolving due to recent considerable technical advances and potential benefits. In 2004, MRI clinical indications were published by a consensus panel composed of European and American cardiologists and radiologists with major input from members with additional established expertise in pediatric cardiology, nuclear cardiology, magnetic resonance physics and spectroscopy, as well as health economics (Table 3.0.2). Interestingly, cardiac MRI expertise is highly recommended in centers dedicated to the treatment of congenital heart defects. Moreover evaluation and follow-up of adults with congenital heart disease is considered as a Class I indication for a comprehensive cardiac

MRI investigation, since it is now possible to often answer anatomic and functional questions unresolved with other noninvasive investigations.

Cardiac MRI techniques are generally more operator dependent than other MRI techniques; however, some points should be highlighted: for a reliable study, a thorough understanding of the anatomic and functional principles, as well as the knowledge of the available interventional and surgical therapeutic options for congenital heart defects is nevertheless required. A comprehensive pathophysiological cardiac MRI evaluation, especially if dealing with complex congenital heart defects, requires a long time and may not be well tolerated by the patient. Therefore, accurate and detailed preparatory steps are required in planning the cardiac MRI investigation to precisely define the specific questions to be answered as some lesions may have already been well characterized by other diagnostic modalities. Hence the complete knowledge of all the details of the anatomic and functional findings derived from prior clinical, echocardiography or cardiac catheterization and angiographic studies, as well extensive communication with the referring physician are essential. Frequently, a direct review of previous echocardiography investigation is warranted to check some details of the myocardial function such as ventricular stroke volume in case of atrioventricular valve regurgitation. When dealing with patients with previous interventional and/or surgical procedures, direct access to the previous reports is extremely helpful, as well as the knowledge of the presence of implanted devices as potential sources of artifacts. Furthermore, excellent knowledge of the MRI techniques and physics is warranted to reach high accuracy both in terms of anatomical detail and, more importantly, functional information, often heavily determinant in view of the surgical indication. Thus, every cardiac MRI laboratory should strictly test their own interobserver reproducibility as well as a rigorous quality control of instruments.

Table 3.0.2. Indication for cardiac MRI in congenital heart defects (reproduced with permission from Pennell DJ, Sechtem UP, Higgins CB, Manning WJ, Pohost GM, Rademakers FE, van Rossum AC, Shaw LJ, Yucel EK (2004) Clinical indications for cardiovascular magnetic resonance (CMR): Consensus Panel Report. Eur Heart J 25(21):1940–1965. By permission of Oxford University Press)

Indication	Class
General indications	
1. Initial evaluation and follow-up of adult congenital heart disease	I
Specific indications	
1. Assessment of shunt size (Qp/Qs)	I
2. Anomalies of the viscero-atrial situs	
▪ Isolated situs anomalies	II
▪ Situs anomalies with complex congenital heart disease	I
3. Anomalies of the atria and venous return	
▪ Atrial septal defect (secundum and primum)	II
▪ Anomalous pulmonary venous return, especially in complex anomalies and cor triatriatum	I
▪ Anomalous systemic venous return	I
▪ Systemic or pulmonary venous obstruction following intra-atrial baffle repair or correction of anomalous pulmonary venous return	I
4. Anomalies of the atrioventricular valves	
▪ Anatomic anomalies of the mitral and tricuspid valves	II
▪ Functional valvular anomaly	II
▪ Ebstein's anomaly	II
▪ Atrioventricular septal defect	II
5. Anomalies of the ventricles	
▪ Isolated ventricular septal defect	III
▪ VSD associated with complex anomalies	I
▪ Ventricular aneurysms and diverticula	II
▪ Supracristal VSD	I
▪ Evaluation of right and left ventricular volumes, mass and function	I
6. Anomalies of the semilunar valves	
▪ Isolated valvular pulmonary stenosis and valvular dysplasia	III
▪ Supravalvular pulmonary stenosis	II
▪ Pulmonary regurgitation	I
▪ Isolated valvular aortic stenosis	III
▪ Subaortic stenosis	III
▪ Supravalvular aortic stenosis	I

Indication	Class
7. Anomalies of the arteries	
▪ Malpositions of the great arteries	II
▪ Postoperative follow-up of shunts	I
▪ Aortic (sinus Valsalva) aneurysm	I
▪ Aortic coarctation	I
▪ Vascular rings	I
▪ Patent ductus arteriosus	III
▪ Aortopulmonary window	I
▪ Coronary artery anomalies in infants	Inv
▪ Anomalous origin of coronary arteries in adults and children	I
▪ Pulmonary atresia	I
▪ Central pulmonary stenosis	I
▪ Peripheral pulmonary stenosis	Inv
▪ Systemic to pulmonary collaterals	I

▪ Methodology and technical aspects

To discuss the MRI technique is not the main aim of this chapter, however, we will give an overview on cardiac MRI methodology and technical aspects in order to make the readers more familiar with the technique.

The goals of a pre-operative cardiac MRI investigation in patients with congenital heart defects are the following:
- ▪ define the morphological characteristics and the location of the primary malformation and the potential presence of associated defects,
- ▪ evaluate and quantify the functional consequences of the primary malformation.

▪ **Morphological assessment:** Although there are several cardiac pulse sequences for MRI morphologic imaging, many with manufacturer-specific features, they can be grouped into three classes:
- ▪ *Black-blood imaging:* black-blood images are images with high signal-to-noise ratio, resolution and contrast. Most techniques use radiofrequency refocusing, making them robust to metal artifacts. This is important in the evaluation of postoperative patients where surgical clips would other-

wise cause local image voids and anatomic disruption. Black-blood techniques become very useful when the relationships between the airway and vessels must be elucidated. They are also extremely useful in characterizing the abdominal situs, the presence of masses, thrombi, hematomas or other soft tissue details as fatty infiltration as well as edema.

■ *White-blood cine imaging:* static pictures as black blood images can answer many questions in pediatric cardiology, but they incompletely characterize the details of the malformation. Any sonographer can relate to the difficulty of interpreting still-frames removed from their dynamic context. Although cine images in MRI can be prospective and retrospectively-gated (not real time), they offer the same physiologic context provided by echocardiography. In most instances the required spatial and temporal resolution makes it impossible to acquire a full series of images in a single heart beat. Instead, each image is assembled from data acquired during several heart beats (segmentation). Cine images represent the backbone of congenital cardiac MRI even though they have lower resolution and contrast than black-blood imaging. In recent years, steady-state free precession (sequences also known as balanced FFE, TrueFisp, and FIESTA) has practically replaced previously used spoiled gradient sequences. The steady-state free precession is extremely useful for imaging of the cardiac function because of its specific properties. Strong T2/T1-weighted and homogeneous contrast shows cavitary blood bright and myocardium with lower signal intensity. Contrast is virtually independent of inflow, imaging at consistent quality in all orientations, including horizontal and vertical long axes. The steady-state free precession sequences are also fast, allowing acquisition of a single slice heart phases in a breath-hold of a few seconds duration.

However, some disadvantages of the steady-state free precession have to be mentioned: the ultra-short TE produces lower flow sensitivity for vascular or valvular obstructions. Even more important steady-state free precession is troubled by flow artifacts near regions of rapid blood acceleration. These artifacts can be even more crippling in infants and young children since they have significantly greater blood acceleration than adult patients in the aorta and the great arteries. Local shimming improves but does not eliminate these artifacts. Another limit of steady-state free precession is that reducing the field of view and slice thickness can greatly prolong the echo and repetition times (this is done to reduce the absorbed radiofrequency power and gradient switching rates).

■ *3D gadolinium-enhanced angiography:* contrast-enhanced magnetic resonance angiography (CEMRA) is the most important 3-dimensional technique available for routine cardiac assessment. Since voxels are more isotropic than for 2-dimensional acquisitions, images collected by 3-dimensional sequences are ideally suited for multiplanar reformatting and volume rendering. CEMRA acquisitions are un-gated, so they are only useful for characterization of extracardiac structures. Despite short acquisition times, CEMRA has a high signal-to-noise ratio, allowing the highest resolution of any of the cardiac imaging sequences. Although large vessel disease may be well characterized by standard 2-dimensional imaging, CEMRA is absolutely essential to visualize small vessels such as in peripheral pulmonary stenosis or the presence of aortopulmonary collateral arteries. In fact, CEMRA offers comparable diagnostic accuracy as cardiac catheterization and angiography in evaluating the number and location of aortopulmonary collaterals in children and adults with pulmonary atresia.

■ **Functional assessment:** MRI provides unique functional information of major value related to ventricular function, flow as-

sessment, myocardial perfusion and viability. Information on function and flow is obtained from time-resolved series of gradient echo images (white blood), each time frame corresponding to a phase of the cardiac cycle.

▮ *Biventricular function:* one of the advantages of MRI over echocardiography in the assessment of ventricular volumes, ejection fraction and mass is its ability to reproducibly and accurately acquire parallel images in any orientation, eliminating geometrical assumptions. This advantage is especially important in congenital heart disease where the intracardiac morphology does not fit the usual shape assumptions. One example is the unique ability of cardiac MRI to determine ventricular function in patients with a single ventricle, either of right or left ventricular morphology. A single ventricle has an extremely variable and bizarre shape, difficult to mathematically model and which does not allow the geometric assumptions necessary to calculate mass, volume, or cardiac performance from a single image plane. Compared with other noninvasive imaging tools, cardiac MRI provides a precise assessment of the ventricular mass, volumes and function necessary for the early and late postoperative follow-up in these complex patients. The use of MRI has also been extensively validated for the quantification of the right ventricular function.

For measurement of ventricular volumes, a number of adjacent slices are acquired in the short-axis orientation covering them from apex to base. For each short-axis slice, a region of interest is defined by outlining the endocardial contour of the left or right ventricle on the end-systolic and end-diastolic images. For each slice, the area of the region of interest is multiplied by the slice thickness. Summation over all slices results in end-systolic and end-diastolic volume, respectively. The difference between the two volumes corresponds to the stroke volume. From these numbers the ejection fraction is calculated as ejection fraction = stroke volume/end-diastolic volume. Cardiac index is calculated as cardiac output per minute, normalized by the body surface area.

▮ *Velocity mapping:* quantification of blood flow is made using velocity-encoded cine MRI sequence, also called phase contrast velocity mapping (PVC-MRI), through planes transecting the targeted vessel (Fig. 3.0.4), which can provide information on blood flow in the major vessels, such as
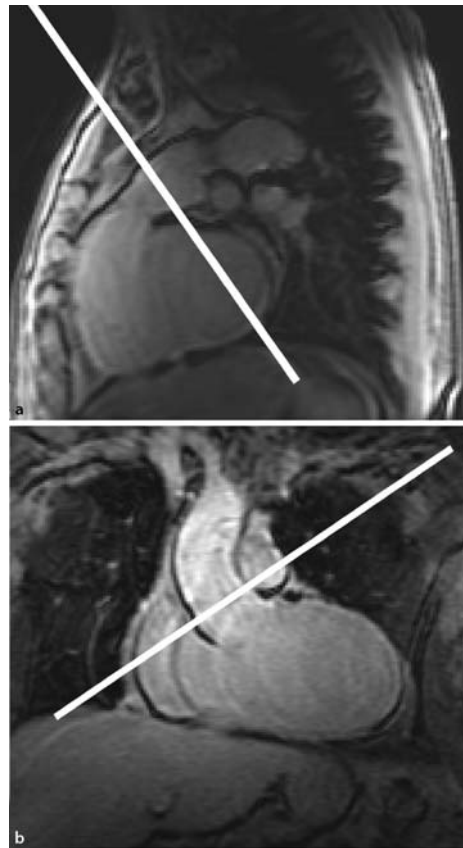
Fig. 3.0.4. MRI: measurement of blood flow. Coronal (**a**) and sagittal (**b**) projection to measure the aortic (*QS* systemic) and the pulmonary artery (*QP* pulmonary) blood flow (see Fig. 3.0.5)
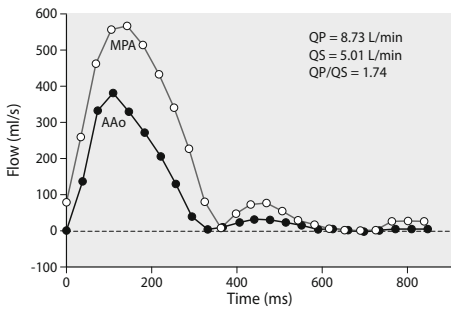
Fig. 3.0.5. MRI: measurement of blood flow. Graphic representation of the measurement of systemic (QS) and pulmonary (QP) blood flow, and calculation of the QP/QS

aorta, pulmonary arteries, central veins, and surgically implanted conduits. It represents a unique and unrivaled strength of MRI. The main clinical applications of PVC-MRI, very useful in the assessment of congenital heart defects before and after surgery, are the assessment of the systemic and pulmonary blood flow, the pulmonary to systemic flow ratio (QP/QS) (Fig. 3.0.5), valvular regurgitation, peak velocity measurement in stenotic vessels and valves, lung perfusion and flow dynamics. However, even when appropriate methods of acquisition have been used, there can be inaccuracies of flow measurement caused by background phase errors due to eddy current or uncorrected concomitant gradients. Furthermore for accurate measurements of aortic regurgitation or mitral valve inflow, motion tracking and velocity correction with respect to the cyclic displacements of the valves are needed, but few if any commercial systems provide this facility. Regarding the jet velocity, its measurement poses different challenges, mainly related to the voxel size and slice orientation relative to respectively a narrow jet and jet orientation. A recent application of MRI is to study the compliance of the wall of the great arteries (aorta and pulmonary artery) subjected to a chronic increase of the intravascular blood pressure.

▪ *Myocardial tagging:* myocardial tagging allows a more thorough investigation of the cardiac motion, providing detailed information on translation, rotation, and deformation, and allows calculation of measures, such as wall motion, regional wall thickening, and strain. This is obtained by destroying coherent magnetization periodically over space and subsequently performing a cine acquisition using a gradient echo sequence. Among other research applications, myocardial tagging has been used to investigate function in children and adult patients with single left ventricle and after heart transplant.

▪ *Myocardial perfusion and viability:* in adults with coronary artery disease contrast-enhanced MRI allows the identification of myocardial perfusion, extent and diffusion of myocardial ischemia, infarction, and viability. In patients with complex congenital heart disease, myocardial ischemia and fibrosis can also complicate the early and particularly the late follow-up after intracardiac surgery.

▪ *First pass perfusion:* the currently available MRI perfusion measurement techniques are all based on the dynamic imaging of the first-pass through the myocardium of gadolinium-based T1-shortening contrast agents. Adenosine is used as a coronary vasodilator to create a blood flow difference between the myocardial regions perfused by normal coronary arteries and those supplied by arteries with stenosis. As the contrast agent passes through the blood pool and myocardial tissue, the T1 is shortened, and the signal enhanced. Generally, 20 to 30 seconds are required for the first-pass of contrast agent through the myocardium from the time of injection. This time defines the length of the scan as images must be acquired throughout the passage of contrast agent through the myocardium. Ischemic regions with poor perfusion will not enhance at the same rate as normally perfused tissue and can be visualized as regions of transient dark signal.

Preliminary results demonstrate that MRI evaluation of myocardial perfusion and viability is feasible in pediatric patients with congenital and acquired heart disease, although so far there is a limited application of MRI perfusion imaging in the pediatric population. Cardiac MRI presents advantages in comparison with nuclear scintigraphy, including the lack of ionizing radiation, a very important factor when considering stress imaging in young patients who may require lifelong assessment of myocardial ischemia and function. In comparison with nuclear perfusion examination, which may require 2 to 6 hours, the cardiac MRI examination is generally completed in less than 1 hour. In addition the high spatial resolution of MRI is particularly helpful in pediatric patients because it allows even smaller perfusion defects to be detected. One all-inclusive study also provides complimentary data, such as regional wall motion abnormalities and delayed enhancement to evaluate viability. The diagnostic utility and clinical benefit in the pediatric population with congenital and acquired heart disease will be further addressed by future studies.

▪ *Delayed myocardial enhancement:* gadolinium-based MRI contrast agents in clinical use are all T1-shortening, extravascular, extracellular agents, rapidly diffusing out of the capillaries into the interstitial space. In adult patients, the areas of acute or chronic myocardial infarction provide a larger distribution volume for these agents when compared to viable tissue. T1-weighted, inversion recovery imaging can differentiate necrotic regions of delayed-enhancement from viable myocardium. The inversion time is set to null the signal from viable myocardium, to produce images in which necrotic tissue is bright by virtue of its shorter T1. In practice, the optimal T1 is based on the dose of contrast administered and the elapsed time between injection and imaging. The assessment of the transmural extent of viability by cardiac MRI is not available from other noninvasive imaging techniques. In adult patients with coronary artery disease, the late gadolinium-enhanced cardiac MRI is able to predict whether regions of abnormal ventricular contraction will improve after myocardial revascularization. At the moment, there is only limited experience with this technique in children, even if in infants with an anomalous left coronary artery from the pulmonary artery syndrome and severe left ventricular dysfunction, the impact of myocardial viability, utilizing delayed enhancement to detect ventricular infarct and myocardial fibrosis, has already been reported to direct the surgical choice between the two options of coronary artery reimplantation versus cardiac transplantation.

This technique of post-gadolinium myocardial-delayed enhancement is increasingly used in patients after repair of congenital heart defects to assess the presence and extent of area with myocardial fibrosis.

▪ Sedation and anesthesia

A comprehensive cardiac MRI investigation requires approximately 30 to 60 minutes with the patient in a still position in an uncomfortable environment; therefore, children under the age of 12 will commonly require anesthesia. The use of conscious sedation (such as pentobarbital or chloral hydrate), deep sedation (propofol), or general anesthesia varies tremendously among different hospitals depending upon local preferences and resources. Although general anesthesia with intubation and paralysis is frequently seen as excessively invasive, it is probably safer and more predictable than other strategies in young children. However it becomes highly preferable in patients with vulnerable airways or in infants.
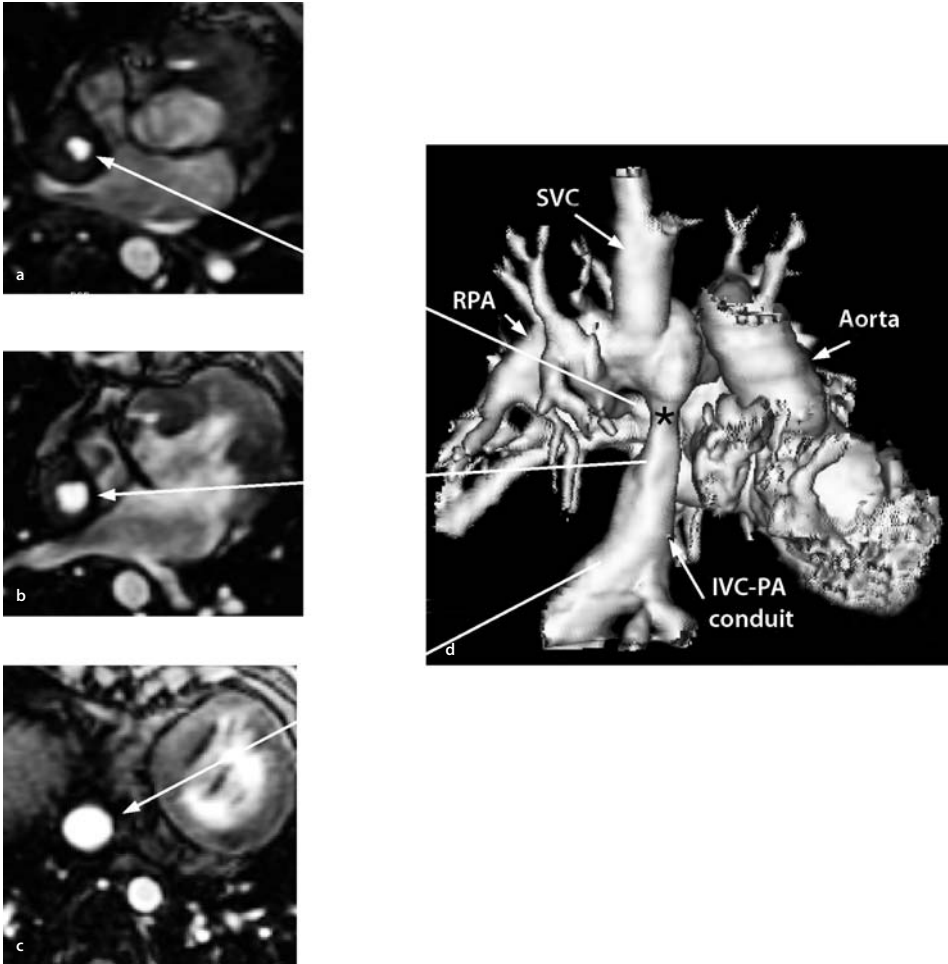
Fig. 3.0.6. Cardiac MRI. Axial time of flight images (**a**, **b**, and **c**) at different levels of the thorax in a patient after an extracardiac Fontan procedure. Arrows indicate the corresponding level to the *volume rendering reconstruction* (**d**) showing an unexpected narrowing of the extracardiac conduit between inferior vena cava and pulmonary artery (asterisk). Acquisition parameters were set as follows: flip angle 30°, trigger delay 400 ms; FOV 35×35 cm, fold over direction right-left in order to minimize respiratory artifacts, matrix: 256×160; slice thickness 3 mm; interpolated at 1.5 mm; NEX 2; TE 2.4 ms, TR 6.9 ms (*IVC* inferior vena cava, *PA* pulmonary artery, *RPA* right pulmonary artery, *SVC* superior vena cava)

▪ Appendix: Cardiac MRI protocols for the evaluation of congenital heart defects

Because the magnet performance changes depending on technical characteristics, manufacturer and type of release, it is worth mentioning that the cardiac protocols discussed in the present book were developed in the MRI laboratory of CNR (Massa-Pisa, Italy) equipped with a GE CVi HD 1.5 T, release software 12.0, coil elements 8 RF channels, slew rate 150 T/m/s, gradient field strength 50 mT/m. Each cardiac MRI investigation starts with a 3-plane localizer. This is a non-gating, free-breathing, white blood, fast acquisition in order to obtain a "pilot" representation of the heart and the mediastinum in three orthogonal planes. Furthermore, in

nearly all protocols a 2-dimensional axial "time of flight" acquisition prepared with a stack of thin (3 mm) axial intersected slices, covering the complete thorax from the aortic arch to the diaphragm, is prescribed. It is a quite long lasting, ECG-gated, free-breathing sequence, very useful for further sequences prescription, especially in the case of unusual heart anatomy, thanks to its possibility to be post-processed and reformatted in each plane of the space. Moreover, thanks to its high resolution and optimal visualization of mediastinal vessels, it can be used as an alternative to MR angiography without using contrast medium and any venous line (Fig. 3.0.6), a non-negligible advantage in children. After the heart and great vessels have been "localized", in nearly each cardiac MRI investigation, a series of cine acquisition from the axial view
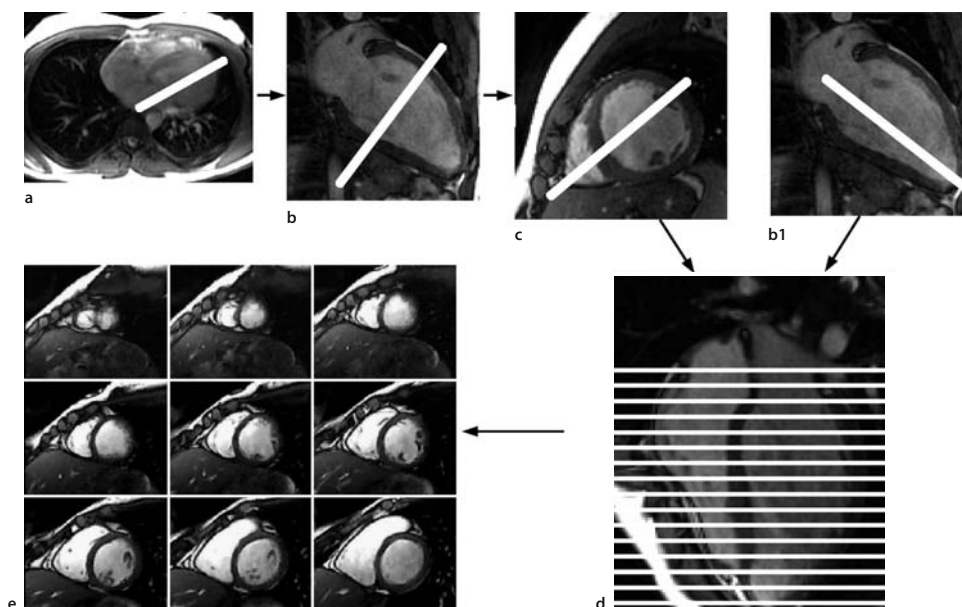
Fig. 3.0.7. Cardiac MRI. Steps to obtain the correct inclination for imaging in the cardiac axes: from a transverse or axial scout view at the level of the left ventricle (**a**), proceeding as shown, a 2-chamber view is obtained (**b**); from **b** is obtained a "localized short axis" (**c**). From the last two images (2-chamber and "localized short axis") a 4-chamber view (**d**) is obtained. A true short-axis plane stack can now be prescribed off the 4-chamber view perpendicular to the interventricular septum. The short-axis stack should cover the entirety of both ventricles from the atrioventricular valves to the apex

are prescribed in order to obtain a stack of ventricles short-axis slices ready to be post-processed and analyzed to assess both ventricles volumes, function and mass (Fig. 3.0.7).

■ References

Adams FH, Norman A, Bass D, Oku G (1978) Chromosome damage in infants and children after cardiac catheterization and angiocardiography. Pediatrics 2:312–316

Ait-Ali L, Foffa I, Andreassi MG (2007) Diagnostic and therapeutic radiation exposure in children: new evidence and perspectives from Biomarker approach. Pediatr Radiol 37:109–111

Amis ES, Butler PF, Applegate KE, Birnbaum SB, Brateman LF, Hevezi JM, Mettler FA, Morin RL, Pentecost MJ, Smith GG, Strauss KJ, Zeman RK (2007) American College of Radiology white paper on radiation dose in medicine. J Am Coll Radiol 4:272–284

Andreassi MG, Ait-Ali L, Botto N, Manfredi S, Mottola G, Picano E (2006) Cardiac catheterization and long-term chromosomal damage in children with congenital heart disease. Eur Heart J 27:2703–2708

Babu-Narayan SV, Kilner PJ, Gatzoulis MA (2003) When to order cardiovascular magnetic resonance in adults with congenital heart disease. Curr Cardiol Rep 5:324–330

Babu-Narayan SV, Gatzoulis MA, Kilner PJ (2007) Non-invasive imaging in adult congenital heart disease using cardiovascular magnetic resonance. J Cardiovasc Med 8:23–29

Beerbaum P, Korperich H, Barth P, Esdorn H, Gieseke J, Meyer H (2001) Noninvasive quantification of left-to-right shunt in pediatric patients: phase-contrast cine magnetic resonance imaging compared with invasive oximetry. Circulation 103:2476–2482

Beerbaum P, Korperich H, Gieseke J, Barth P, Peuster M, Meyer H (2003) Rapid left-to-right shunt quantification in children by phase-contrast magnetic resonance imaging combined with sensitivity encoding (SENSE). Circulation 108:1355–1361

BEIR VII Committee to Assess the Health Risks from Exposure to Low Levels of Ionizing Radiation, National Research Council (2005) Books.nap.edu/catalog/11340.html

Bell A, Muthurangu V, Hedge S, Schaeffer T, Razavi R (2007) MRI guided cardiac catheterization to assess pulmonary vascular resistance in the context of a left to right shunt: an illustration of clinical utility. J Cardiovasc Magn Reson 9:108–109

Boxt LM (2004) Magnetic resonance and computed tomographic evaluation of congenital heart disease. J Magn Reson Imaging 19:827–847

Cademartiri F, Marano R, Luccichenti G, Mollet N, Nieman K, De Feyter PJ, Krestin GP, Bonomo L (2004) Normal anatomy of the vessels of the heart with 16-row multislice computed tomography. Radiol Med 107:11–21

Chandran A, Fricker FJ, Schowengerdt KO, Cumming WA, Saidi A, Spencer CT, Paolillo J, Samyn MM (2005) An institutional review of the value of computed tomographic angiography in the diagnosis of congenital cardiac malformations. Cardiol Young 15:47–51

Chen SJ, Lee WJ, Wang JK, Wu MH, Chang CI, Liu KL, Chiu IS, Chen HY, Su CT, Li YW (2003) Usefulness of three-dimensional electron beam computed tomography for evaluating tracheobronchial anomalies in children with congenital heart disease. Am J Cardiol 92:483–486

Choi BW, Park YH, Choi JY, Choi BI, Kim MJ, Ryu SJ, Lee JK, Sul JH, Lee SK, Cho BK, Choe KO (2001) Using electron beam CT to evaluate conotruncal anomalies in pediatric and adult patients. Am J Roentgenol 177:1045–1049

Davlouros PA, Niwa K, Webb G, Gatzoulis MA (2006) The right ventricle in congenital heart disease. Heart 92 (Suppl 1):27–38

De la Pena E, Nguyen PK, Nayak KS, Yang PC, Rosenthal DN, Hu BS, Pauly JM, McConnell MV (2006) Real-time color-flow CMR in adults with congenital heart disease. J Cardiovasc Magn Reson 8:809–815

Didier D, Ratib O, Beghetti M, Oberhaensli I, Friedli B (1999) Morphologic and functional evaluation of congenital heart disease by magnetic resonance imaging. J Magn Reson Imaging 10:639–655

Diller GP, Dimopoulos K, Okonko D, Li W, Babu-Narayan SV, Broberg CS, Johansson B, Bouzas B, Mullen MJ, Poole-Wilson PA, Francis DP, Gatzoulis MA (2005) Exercise intolerance in adult congenital heart disease: comparative severity, correlates, and prognostic implications. Circulation 112:828–835

FDA Public Health Notification (2001) Reducing radiation risk from computed tomography for pediatric and small adult patient. November 2

Fitoz S, Unsal N, Tekin M, Tutar E (2007) Contrast-enhanced MR angiography of thoracic vascular malformations in children. Int J Cardiol 122:3–11

Fogel MA (2000) Assessment of cardiac function by magnetic resonance imaging. Pediatr Cardiol 21:59–69

Fogel MA, Wilson RD, Flake A, Johnson M, Cohen D, McNeal G, Tian ZY, Rychik J (2005) Preliminary investigations into a new method of functional assessment of the fetal heart using a novel application of "real-time" cardiac magnetic resonance imaging. Fetal Diagn Ther 20:475–480

Fogel MA (2006) Congenital heart disease. J Cardiovasc Magn Reson 8:569–571

Friedberg MK, Rosenthal DN (2005) New developments in echocardiographic methods to assess right ventricular function in congenital heart disease. Curr Opin Cardiol 20:84–88

Funabashi N, Asano M, Sekine T, Nakayama T, Komuro I (2006) Direction, location, and size of shunt flow in congenital heart disease evaluated by ECG-gated multislice computed tomography. Int J Cardiol 112:399–404

Geva T, Sahn DJ, Powell AJ (2003) Magnetic resonance imaging of congenital heart disease in adults. Prog Pediatr Cardiol 17:21–39

Geva T, Marshall AC (2006) Magnetic resonance imaging-guided catheter interventions in congenital heart disease. Circulation 113:1051–1052

Goo HW, Park IS, Ko JK, Kim YH, Seo DM, Yun TJ, Park JJ, Yoon CH (2003) CT of congenital heart disease: normal anatomy and typical pathologic conditions. Radiographics 23:S147–165

Goo HW, Park IS, Ko JK, Kim YH, Seo DM, Park JJ (2005) Computed tomography for the diagnosis of congenital heart disease in pediatric and adult patients. Int J Cardiovasc Imaging 21:347–365

Grothues F, Moon JC, Bellenger NG, Smith GS, Klein HU, Pennell DJ (2004) Interstudy reproducibility of right ventricular volumes, function, and mass with cardiovascular magnetic resonance. Am Heart J 147:218–223

Haber I, Metaxas DN, Geva T, Axel L (2005) Three-dimensional systolic kinematics of the right ventricle. Am J Physiol Heart Circ Physiol 289:H1826–1833

Harris MA, Weinberg PM, Whitehead KK, Fogel MA (2005) Usefulness of branch pulmonary artery regurgitant fraction to estimate the relative right and left pulmonary vascular resistances in congenital heart disease. Am J Cardiol 95:1514–1517

Helbing WA, Rebergen SA, Maliepaard C, Hansen B, Ottenkamp J, Reiber JH, de Roos A (1995) Quantification of right ventricular function with magnetic resonance imaging in children with normal hearts and with congenital heart disease. Am Heart J 130:828–837

Helbing WA, Mertens L, Sieverding L (2006) Recommendations from the Association for European Paediatric Cardiology for training in congenital cardiovascular magnetic resonance imaging. Cardiol Young 16:410–412

Kastler B, Livolsi A, Germain P, Zollner G, Willard D, Wackenheim A (1990) Magnetic resonance imaging in congenital heart disease of newborns: preliminary results in 23 patients. Eur J Radiol 10:109–117

Kellenberger CJ, Yoo SJ, Buchel ER (2007) Cardiovascular MR imaging in neonates and infants with congenital heart disease. Radiographics 27:5–18

Kilner PJ, Yang GZ, Wilkes AJ, Mohiaddin RH, Firmin DN, Yacoub MH (2000) Asymmetric redirection of flow through the heart. Nature 404:759–761

Ko SF, Liang CD, Huang CC, Ng SH, Hsieh MJ, Chang JP, Chen MC (2006) Clinical feasibility of free-breathing, gadolinium-enhanced magnetic resonance angiography for assessing extracardiac thoracic vascular abnormalities in young children with congenital heart disease. J Thorac Cardiovasc Surg 132:1092–1098

Korperich H, Gieseke J, Barth P, Hoogeveen R, Esdorn H, Peterschroder A, Meyer H, Beerbaum P (2004) Flow volume and shunt quantification in pediatric congenital heart disease by real-time magnetic resonance velocity mapping: a validation study. Circulation 109:1987–1993

Lambert V, Sigal-Cinqualbre A, Belli E, Planchè C, Roussin R, Serraf A, Bruniaux J, Angel C, Paul JF (2005) Preoperative and postoperative evaluation of airways compression in pediatric patients with 3-dimensional multislice computed tomographic scanning: effect on surgical management. J Thorac Cardiovasc Surg 129:1111–1118

Lee CI, Haims AH, Monico EP, Brink JA, Forman HP (2004) Diagnostic CT scans: assessment of patient, physician, and radiologist awareness of radiation dose and possible risks. Radiology 231:393–398

Leschka S, Oechslin E, Husmann L, Desbiolles L, Marincek B, Genoni M, Prêtre R, Jenni R, Wildermuth S, Alkadhi H (2007) Pre- and postoperative evaluation of congenital heart disease in children and adults with 64-section CT. Radiographics 27:829–846

Markle BM, Cross RR (2004) Cross-sectional imaging in congenital anomalies of the heart and great vessels: magnetic resonance imaging and computed tomography. Semin Roentgenol 39:234–262

Markl M, Pelc NJ (2004) On flow effects in balanced steady-state free precession imaging: pictorial description, parameter dependence, and clinical implications. J Magn Reson Imaging 20:697–705

McKie SJ, Hardwick DJ, Reid JH, Murchinson JT (2005) Features of cardiac disease demonstrated on CT pulmonary angiography. Clin Radiol 60:31–38

McLaughlin P, Benson L, Horlick E (2006) The role of cardiac catheterization in adult congenital heart disease. Cardiol Clin 24:531–556

Miquel ME, Hill DL, Baker EJ, Qureshi SA, Simon RD, Keevil SF, Razavi RS (2003) Three- and four-dimensional reconstruction of intra-cardiac anatomy from two-dimensional magnetic resonance images. Int J Cardiovasc Imaging 19:239–254

Mohrs OK, Petersen SE, Voigtlaender T, Peters J, Nowak B, Heinemann MK, Kauczor HU (2006) Time-resolved contrast-enhanced MR angiography of the thorax in adults with congenital heart disease. Am J Roentgenol 187:1107–1114

Moodie DS (2005) MRI and cardiac catheterization: seeing the heart in a new way. Catheter Cardiovasc Interv 66:9

Moore P (2005) MRI-guided congenital cardiac catheterization and intervention: the future? Catheter Cardiovasc Interv 66:1–8

Mostbeck GH, Caputo GR, Higgins CB (1992) MR measurement of blood flow in the cardiovascular system. Am J Roentgenol 159:453–461

Nicol ED, Gatzoulis M, Padley SP, Rubens M (2007) Assessment of adult congenital heart disease with multi-detector computed tomography: beyond coronary lumenography. Clin Radiol 62:518–527

Nield LE, Qi XL, Valsangiacomo ER, Macgowan CK, Wright GA, Hornberger LK, Yoo SJ (2005) In vivo MRI measurement of blood oxygen saturation in children with congenital heart disease. Pediatr Radiol 35:179–185

Niemann PS, Pinho L, Balbach T, Galuschky C, Blankenhagen M, Silberbach M, Broberg C, Jerosch-He-

rold M, Sahn DJ (2007) Anatomically oriented right ventricular volume measurements with dynamic three-dimensional echocardiography validated by 3-Tesla magnetic resonance imaging. J Am Coll Cardiol 50:1668–1676

Odegard KC, DiNardo JA, Tsai-Goodman B, Powell AJ, Geva T, Laussen PC (2004) Anaesthesia considerations for cardiac MRI in infants and small children. Paediatr Anaesth 14:471–476

Oosterhof T, Mulder BJ (2005) Magnetic resonance angiography for anatomical evaluation of the great arteries. Int J Cardiovasc Imaging 21:323–324

Ou P, Voisenet N, Billeau J, Girodon B, Lemoine T, Emond S, Brunelle F, Vouhé P, Sidi D, Bonnet D (2006) Multislice CT scan in congenital heart disease. Arch Mal Coeur Vaiss 99:497–502

Ou P, Celermajer DS, Calcagni G, Brunelle F, Bonnet D, Sidi D (2007) Three-dimensional CT scanning: a new diagnostic modality in congenital heart disease. Heart 93:908–913

Park JB, Hu BS, Conolly SM, Nayak KS, Nishimura DG (2006) Rapid cardiac-output measurement with ungated spiral phase contrast. Magn Reson Med 56:432–438

Pennell DJ, Sechtem UP, Higgins CB, Manning WJ, Pohost GM, Rademakers FE, van Rossum AC, Shaw LJ, Yucel EK (2004) Clinical indications for cardiovascular magnetic resonance (CMR): Consensus Panel report. J Cardiovasc Magn Reson 6:727–765

Picano E (2004) Informed consent and communication of risk from radiological and nuclear medicine examinations: how to escape from a communication inferno. BMJ 329:849–851

Powell AJ, Tsai-Goodman B, Prakash A, Greil GF, Geva T (2003) Comparison between phase-velocity cine magnetic resonance imaging and invasive oximetry for quantification of atrial shunts. Am J Cardiol 91:1523–1525

Prakash A, Powell AJ, Krishnamurthy R, Geva T (2004) Magnetic resonance imaging evaluation of myocardial perfusion and viability in congenital and acquired pediatric heart disease. Am J Cardiol 93:657–661

Razavi RS, Hill DL, Keevil SF, Miquel ME, Muthurangu V, Hedge S, Rhode K, Barnett M, van Vaals J, Hawkes DJ, Baker EJ (2003) Cardiac catheterisation guided by MRI in children and adults with congenital heart disease. Lancet 362:1877–1882

Rickers C, Seethamraju RT, Jerosch-Herold M, Wilke NM (2003) Magnetic resonance imaging guided cardiovascular interventions in congenital heart diseases. J Interv Cardiol 16:143–147

Rochitte CE, Ribiero FLR, Ikari NM, Bevenuti LA, Iwahashi ER, Andrade SS, Parga JR, Avila LF, Marcial MLB, Ramires JAF, Lopes AAB (2005) Magnetic resonance myocardial delayed enhancement in infants with anomalous origin of left main coronary artery from pulmonary artery. J Cardiovasc Magn Reson 7:74–75

Samyn MM (2004) A review of the complementary information available with cardiac magnetic resonance imaging and multi-slice computed tomography (CT) during the study of congenital heart disease. Int J Cardiovasc Imaging 20:569–578

Shellock FG, Valencerina S (2005) Septal repair implants: evaluation of magnetic resonance imaging safety at 3 T. Magn Reson Imaging 23:1021–1025

Shiraishi I, Yamamoto Y, Ozawa S, Kawakita A, Toiyama K, Tanaka T, Sakata K, Hayano T, Itoi T, Yamagishi M, Hamaoka K (2003) Application of helical computed tomographic angiography with differential color imaging three-dimensional reconstruction in the diagnosis of complicated congenital heart disease. J Thorac Cardiovasc Surg 125:36–39

Shiraishi I, Kajiyama Y, Yamagishi M, Hamaoka K (2006) Stereolithographic biomodeling of congenital heart disease by multislice computed tomography imaging. Circulation 113:e733–734

Siegel MJ (2003) Multiplanar and three-dimensional multi-detector row CT of thoracic vessels and airways in the pediatric population. Radiol 229:641–650

Siegel MJ, Bhalla S, Gutierrez FR, Billadello JB (2005) MDCT of postoperative anatomy and complications in adults with cyanotic heart disease. Am J Roentgenol 184:241–247

Simonetti OP, Cook S (2006) Technical aspects of pediatric CMR. J Cardiovasc Magn Reson 8:581–593

Sorensen TS, Korperich H, Greil GF, Eichhorn J, Barth P, Meyer H, Pedersen EM, Beerbaum P (2004) Operator-independent isotropic three-dimensional magnetic resonance imaging for morphology in congenital heart disease: a validation study. Circulation 110:163–169

Sorensen TS, Beerbaum P, Korperich H, Pedersen EM (2005) Three-dimensional, isotropic MRI: a unified approach to quantification and visualization in congenital heart disease. Int J Cardiovasc Imaging 21:283–292

Taylor AM, Dymarkowski S, De Meerler K, Hamaekers P, Gewillig M, Mertens L, Bogaert J (2005) Validation and application of single breath-hold cine cardiac MR for ventricular function assessment in children with congenital heart disease at rest and during adenosine stress. J Cardiovasc Magn Reson 7:743–751

Tsai SY, Wu MT, Lin YR, Hsieh KS, Lin CC, Huang TY, Chung HW, Pan JY, Huang YL, Pan HB, Yang CF (2006) Temporal correlation-based dynamic contrast-enhanced MR imaging improves assessment of complex pulmonary circulation in congenital heart disease. Magn Reson Med 56:517–526

Tsai IC, Lee T, Chen MC, Tsai WL, Lin PC, Liao WC (2007) Homogeneous enhancement in pediatric thoracic CT aortography using a novel and reproducible method: contrast-covering time. Am J Roentgenol 188:1131–1137

Tsai IC, Chen MC, Fu YC, Jan SL, Tsai WL, Wang CC (2007) Gradual pulmonary artery enhancement: new sign of septal defects on CT. Am J Roentgenol 188:1660–1664

Valsangiacomo Buchel ER, Di Bernardo S, Bauersfeld U, Berger F (2005) Contrast-enhanced magnetic resonance angiography of the great arteries in patients with congenital heart disease: an accurate tool for planning catheter-guided interventions. Int J Cardiovasc Imaging 21:313–322

Vick GW (2000) Three- and four-dimensional visualization of magnetic resonance imaging data sets in pediatric cardiology. Pediatr Cardiol 21:27–36

Wald RM, Powell AJ (2006) Simple congenital heart lesions. J Cardiovasc Magn Reson 8:619–631

Wang ZJ, Reddy GP, Gotway MB, Yeh BM, Higgins CB (2003) Cardiovascular shunts: MR imaging evaluation. Radiographics 23:S181–194

Wang J, Licht DJ, Silvestre DW, Detre JA (2006) Why perfusion in neonates with congenital heart defects is negative. Technical issues related to pulsed arterial spin labeling. Magn Reson Imaging 24:249–254

Weber OM, Higgins CB (2006) MR evaluation of cardiovascular physiology in congenital heart disease: flow and function. J Cardiovasc Magn Reson 8:607–617

Wood JC (2006) Anatomical assessment of congenital heart disease. J Cardiovasc Magn Reson 8:595–606

CHAPTER 3.1 Anomalous systemic venous connections

Definition

An anomalous systemic venous connection is present in 8 to 10% of patients with congenital heart defects. The most frequent congenital anomaly of systemic venous return is the presence of a *persistent left superior vena cava* (Figs. 3.1.1 and 3.1.2), in most of the cases connected to the coronary sinus, but sometimes draining into the left atrium. The persistent left superior vena cava can be associated with the *absence of the right superior vena cava* (Fig. 3.1.3). The strategy of cardiopulmonary bypass can be completely different if the persistent left superior vena cava is associated with the presence or the absence of the innominate vein and/or right superior vena cava.
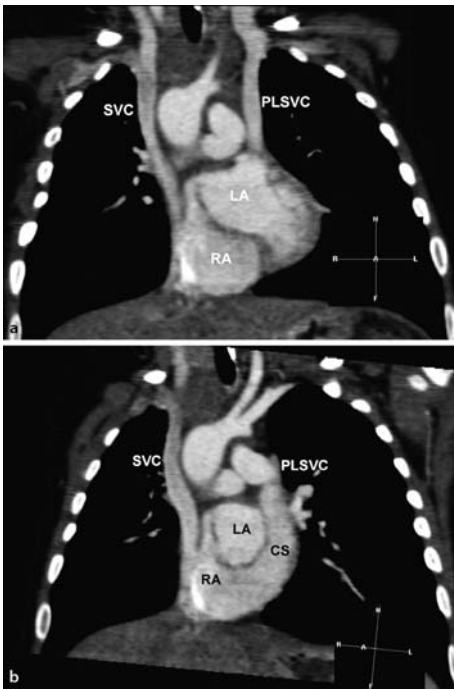
Fig. 3.1.1. Persistent left superior vena cava. **a** CT scan, coronal view, showing the presence of persistent left superior vena cava draining into the coronary sinus, with absent innominate vein. **b** CT scan of the same patient, coronal view, showing the drainage into the coronary sinus of the persistent left superior vena cava (*CS* coronary sinus, *LA* left atrium, *PLSVC* persistent left superior vena cava, *RA* right atrium, *SVC* superior vena cava) (photographs courtesy of Dr. Mohamed Tawil)
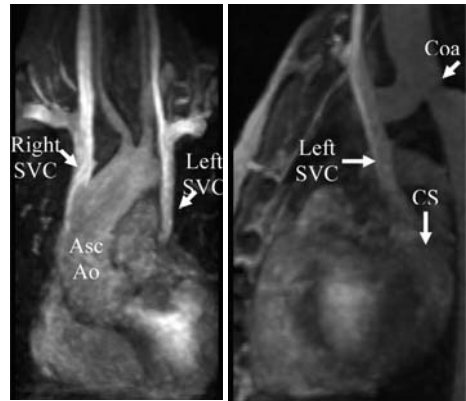
Fig. 3.1.2. Persistent left superior vena cava. MR angiography maximal intensity projection reconstruction in a patient with aortic coarctation and persistent left superior vena draining into a dilated coronary sinus and not communicated with the right superior vena cava (*Asc Ao* ascending aorta, *Coa* aortic coarctation, *CS* coronary sinus, *SVC* superior vena cava)

Another anomaly of the systemic venous return is the *interruption of the inferior vena cava* (Figs. 3.1.4 and 3.1.5) with the drainage of the inferior part of the body occurring through an "azygos continuation". If an open heart procedure is required, the presence of one or more of the above malformations will dictate not only the number and position of the venous cannulae, but also the strategy of cardiopulmonary bypass (continuous perfusion versus circulatory arrest).

Other more rare anomalous systemic venous connections (Figs. 3.1.6 and 3.1.7) must be taken into account before planning the surgical strategy.

Fig. 3.1.3. Persistent left superior vena cava with absent right superior vena cava. Gadolinium-enhanced 3-dimensional MR angiography with subvolume maximal intensity projection in the coronal plane demonstrating the absence of the right superior vena cava and persistent left superior vena cava draining in a dilated coronary sinus (*RA* right atrium, *RPA* right pulmonary artery, *SVC* superior vena cava)
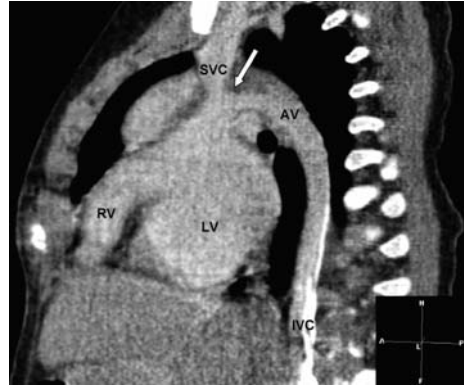
Fig. 3.1.4. Inferior vena cava interruption with azygos continuation. CT scan, sagittal projection, showing the azygos continuation of the inferior vena cava and the connection of the azygos vein to the superior vena cava (arrow) (*AV* azygos vein, *IVC* inferior vena cava, *LV* left ventricle, *RV* right ventricle, *SVC* superior vena cava) (photograph courtesy of Dr. Mohamed Tawil)
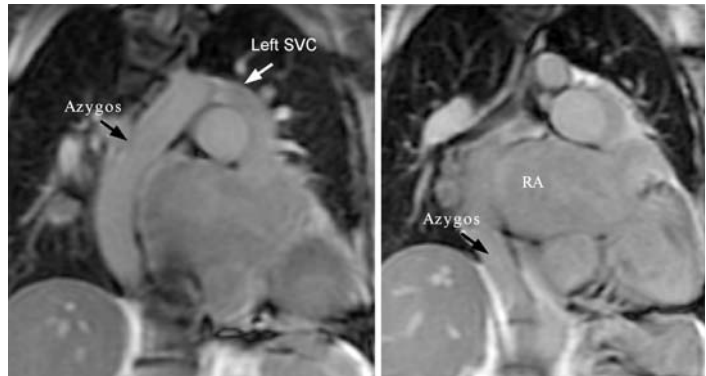
Fig. 3.1.5. Inferior vena cava interruption with azygos continuation. MRI with coronal localizer showing inferior vena cava azygos continuation in the left superior vena cava (*RA* right atrium, *SVC* superior vena cava)
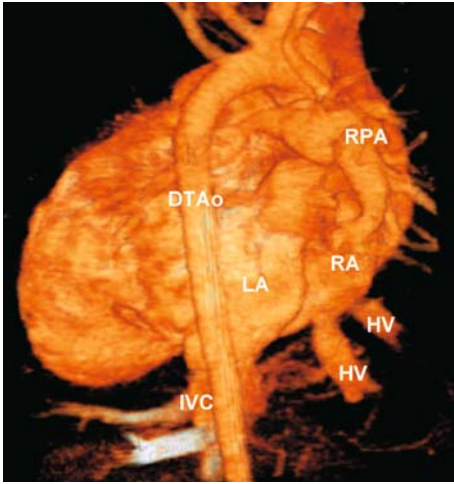
Fig. 3.1.6. Anomalous venous connections. CT scan, 3-dimensional reconstruction, right oblique projection showing the anomalous venous connection with the inferior vena cava, positioned on the left side of the descending thoracic aorta, connected to the left atrium, while the hepatic veins are connected to the right atrium (*DTAo* descending thoracic aorta, *HV* hepatic vein, *IVC* inferior vena cava, *LA* left atrium, *RA* right atrium, *RPA* right pulmonary artery) (photograph courtesy of Dr. Mohamed Tawil)

■ Surgical options

Once the problems related to the requirements of the cardiopulmonary bypass have been solved, with the choice of the most appropriate venous cannulation and the method of perfusion, the anomalous systemic venous connection has to be addressed.

■ **Persistent left superior vena cava:** The persistent left superior vena cava draining into the coronary sinus is generally left intact, unless the patient requires a superior vena cava to pulmonary artery connection (=bidirectional Glenn), and the innominate vein is absent; in this case, a bilateral bidirectional Glenn is performed. On the other hand, the presence of persistent left superior vena cava draining into the left atrium, with subsequent cyanosis, is different. In this case, the superior vena cava needs to be disconnected from the left atrium. There are
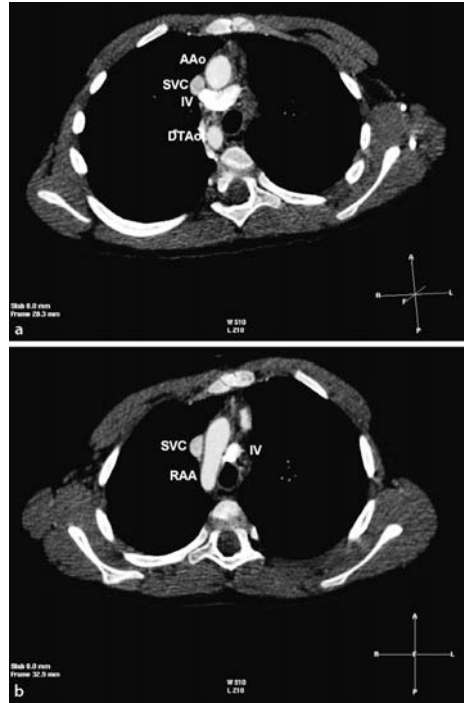
Fig. 3.1.7. Anomalous venous connections. **a** CT scan, axial projection showing the presence of an anomalous retro-aortic innominate vein, positioned posterior to the ascending aorta, and connected to the superior vena cava. The descending thoracic aorta is on the right side because of the presence of the right aortic arch. **b** CT scan of the same patient, axial projection showing the presence of an anomalous retro-aortic innominate vein in the presence of the right aortic arch (*AAo* ascending aorta, *DTAo* descending thoracic aorta, *IV* innominate vein, *RAA* right aortic arch, *SVC* superior vena cava) (photograph courtesy of Dr. Mohamed Tawil)

two options: a) in the simultaneous presence of innominate vein of adequate diameter, simple ligation of the persistent superior vena cava is sufficient; b) in the absence of innominate vein, the distal end of the persistent left superior vena cava needs to be divided and the vein connected either directly to the right auricular appendage or to the right superior vena cava.

■ **Interruption of the inferior vena cava:** The interruption of the inferior vena cava is im-
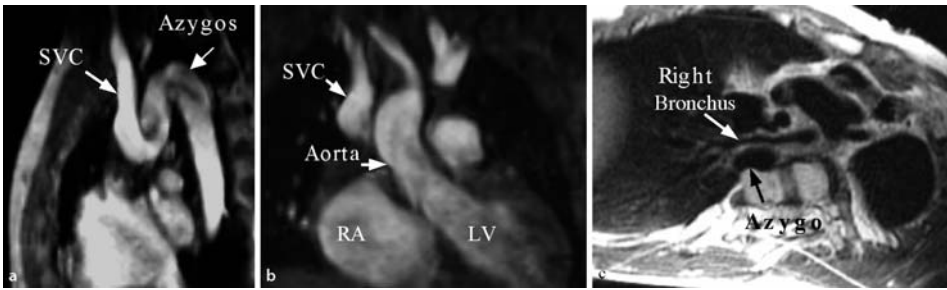
Fig. 3.1.8. Iatrogenic occlusion of the superior vena cava, status post closure of ventricular septal defect. Time of flight multiplanar reformatted MRI sagittal (**a**) and coronal (**b**) view of iatrogenic complete occlusion of the superior vena cava after surgical closure of the ventricular septal defect. Note the dilated azygos vein draining all the superior systemic venous return. Respiratory symptoms were due to right bronchial compression by the dilated azygos vein, as illustrated in the para-axial fast spin echo imaging (**c**) (*LV* left ventricle, *RA* right atrium, *SVC* superior vena cava)

portant whenever the patient requires a total cavopulmonary connection (= modified Fontan procedure). In these cases, the best surgical option is to perform a Kawashima procedure: connecting the superior vena cava (draining the total systemic venous return through the "azygos continuation") to the right pulmonary artery, like in the bidirectional Glenn, leaving the return of the hepatic vein into the right (or left) atrium (see chapter "Tricuspid atresia").

■ **Pre-operative information**

Echocardiography is generally limited in the evaluation of systemic venous return, while both CT and MRI 3-dimensional volume-rendered images give important insights for the assessment and location of anomalous systemic venous connections; CT and MRI allow also detection of systemic veins relationship to the surroundings structures and can evaluate potential associated congenital heart defects.

MRI can accurately evaluate systemic venous connections by gradient and spin echo and more recently by contrast-enhanced MR angiography. For the MRI assessment of the systemic venous connections a 2-dimensional axial Time of Flight (TOF) sequence prescribed from the neck to the liver (see "Introduction chapter") without using contrast agent provides a complete coverage of the thoracic systemic veins.

Obviously the entire CT or MRI investigations will be tailored to the potential presence of associated congenital heart disease.

■ **Potential complications**

Obstruction or total occlusion of the anomalous systemic venous connection.

■ **Post-operative follow-up**

CT scan and MRI could be helpful to identify or rule out potential obstructions or occlusions (Fig. 3.1.8) of the systemic venous connections after various procedures of cardiac surgery.

■ **References**

Bret-Zurita M, Pinilla I, Cuesta-Lopez E, Burgueros M (2008) Magnetic resonance imaging findings of persistent primitive hepatic venous plexus with complex congenital cardiac disease. Eur J Cardiothorac Surg 33:119–120

Burri H, Vuille C, Sierra J, Didier D, Lerch R, Kalangos A (2003) Drainage of the inferior vena cava to the left atrium. Echocardiography 20:185–189

Corno AF (2007) Systemic venous drainage: can we help Newton? Eur J Cardiothorac Surg 31:1044–1051

D'Aloia A, Faggiano P, Fiorina C, Vizzardi E, Bontempi L, Grazioli L, Dei Cas L (2003) Absence of inferior vena cava as a rare cause of deep venous thrombosis complicated by liver and lung embolism. Int J Cardiol 88:327–329

Eckart RE, Leitch WS, Shry EA, Krasuski RA, Lane MJ, Leclerc KM (2003) Utility of magnetic resonance imaging in cardiac venous anatomic variants. Cardiovasc Intervent Radiol 26:309–311

Eidsness WR, Benzmiller PG (2003) Dense coronary sinus: a sign of left superior vena cava on abdominopelvic CT. Am J Roentgenol 180:544

Ellis JH, Denham JS, Bies JR, Olson EW, Cory DA (1986) Magnetic resonance imaging of systemic venous anomalies. Comput Radiol 10:15–22

Erol I, Cetin II, Alehan F, Varan B, Ozkan S, Agildere AM, Tokel K (2006) Brain abscess associated with isolated left superior vena cava draining into the left atrium in the absence of coronary sinus and atrial septal defect. Cardiovasc Intervent Radiol 29:454–456

Fischer A, Long F, Feltes TF (2007) Hepatic necrosis following repair of totally anomalous pulmonary venous connection. Cardiol Young 17:435–437

Funabashi N, Asano M, Komuro I (2005) Constrictive pericarditis with persistent left superior vena cava flow into right atria through coronary sinus demonstrated by multislice computed tomography. Int J Cardiol 105:229–230

Gonzalez-Juanatey C, Testa A, Vidan J, Izquierdo R, Garcia-Castelo A, Daniel C, Armesto V (2004) Persistent left superior vena cava draining into the coronary sinus: report of 10 cases and literature review. Clin Cardiol 27:515–518

Greil GF, Powell AJ, Gildein HP, Geva T (2002) Gadolinium-enhanced three-dimensional magnetic resonance angiography of pulmonary and systemic venous anomalies. J Am Coll Cardiol 39:335–341

Hashmi ZA, Smaroff GG (2007) Dual inferior vena cava: two inferior vena cava filters. Ann Thorac Surg 84:661–663

Hosein RBM, Butler K, Miller P, Jones T, Brawn WJ, Barron DJ (2007) Innominate venous aneurysm presenting as a rapid expanding mediastinal mass. Ann Thorac Surg 84:640–642

Kabiri EH, Zidane A, Arsalane A, Atoini F (2007) Right diaphragmatic eventration associated with dextrocardia, hypoplasia of the right lower pulmonary lobe, and agenesis of the inferior vena cava. J Thorac Cardiovasc Surg 133:1380–1381

Karmazyn B, Dagan O, Vidne BA, Horev G, Kornreich L (2002) Neuroimaging findings in neonates and infants from superior vena cava obstruction after cardiac operation. Pediatr Radiol 32:806–810

Krasemann T, Kehl G, Vogt J, Asfour B (2003) Unusual systemic venous return with complete absence of the superior caval veins. Pediatr Cardiol 24:397–399

Marcu CB, Beek AM, van Rossum AC (2006) Unusual variation in upper-body venous anatomy found with cardiovascular MRI. CMAJ 175:27

Ou P, Calcagni G, Marini D, Le Bidois J, Gallo P, Brunelle F, Bonnet D (2007) Unusual systemic venous return with absence of superior caval veins. J Thorac Cardiovasc Surg 133:1368–1369

Puchalski MD, Williams RV, Minich LL (2003) An unusual variant of anomalous systemic venous return. Cardiol Young 13:563–564

Shiraishi I, Kajiyama Y, Yamagishi M, Hamaoka K (2006) Stereolithographic biomodeling of congenital heart disease by multislice computed tomography imaging. Circulation 113:e733–734

Uehara M, Funabashi N, Yasukawa K, Terai M, Komuro I (2007) Coarctation of the descending aorta, patent ductus arteriosus, deficiency of right superior vena cava, and persistent left superior vena cava in a five-month infant demonstrated by multislice computed tomography. Int J Cardiol 122:61–63

Vydt T, Cools F, Rademakers FE (2003) Absent right and persistent left superior vena cava. Acta Cardiol 58:421–423

Anomalous pulmonary venous connections

▍ Definition

▍ **Partial anomalous pulmonary venous connection:** One or more, but not all, of the pulmonary veins are connected to the right atrium or to one or more of its tributaries.

The commonest type of partial anomalous pulmonary venous connection is the sinus venosus defect: the right upper and middle lobe pulmonary veins (right superior pulmonary vein) attach to the low superior vena cava or the superior vena cava-right atrium junction (Figs. 3.2.1–3.2.3).

Anomalous left-sided pulmonary veins usually connect to the coronary sinus or left innominate vein (Fig. 3.2.4), while anomalous right pulmonary veins usually connect to the superior vena cava, inferior vena cava or right atrium.

Scimitar syndrome: all the right pulmonary veins (occasionally the middle and lower pulmonary veins) are connected to the inferior vena cava just above or below the diaphragm (Fig. 3.2.5); the orifice of the right pulmonary veins is usually very close to the orifices of the hepatic veins. Scimitar syndrome can also be associated with horseshoe lung (Fig. 3.2.6).

The left innominate vein is the usual site of anomalous connection of the left pulmonary veins via a derivative of the left cardinal system, called the anomalous vertical vein.

Bilateral partial anomalous pulmonary venous connection (= partial anomalous venous connection of both lungs) is very rare: the commonest variant is probably that in which the left superior pulmonary vein at-
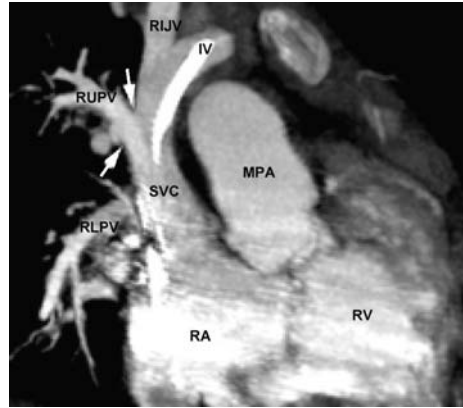
Fig. 3.2.1. Partial right anomalous pulmonary venous connection. CT scan, coronal projection, showing the anomalous connection of the right upper pulmonary veins to the superior vena cava (arrowheads) (*IV* innominate vein, *MPA* main pulmonary artery, *RA* right atrium, *RIJV* right internal jugular vein, *RLPV* right lower pulmonary vein, *RUPV* right upper pulmonary vein, *RV* right ventricle, *SVC* superior vena cava) (modified with permission from Goo HW, Park IS, Ko JK, Kim YH, Seo DM, Yun TJ, Park JJ, Yoon CH (2003) CT of congenital heart disease: normal anatomy and typical pathologic conditions. Radiographics 23:S147–165)

taches to the left innominate vein by way of an anomalous vertical vein, and the right superior pulmonary vein attaches to the superior vena cava-right atrial junction.

▍ **Total anomalous pulmonary venous connection:** All the pulmonary veins connect anomalously to the right atrium, either directly or via the coronary sinus, superior vena cava, or inferior vena cava; a patent foramen ovale or atrial septal defect allows
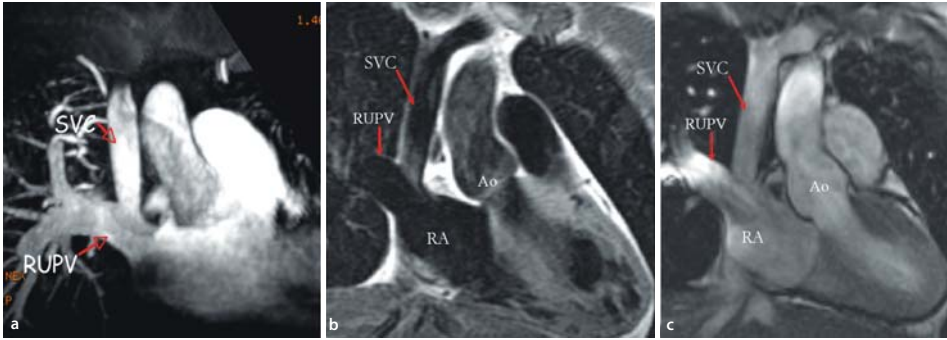
Fig. 3.2.2. Partial right anomalous pulmonary venous connection. Gadolinium-enhanced 3-dimensional MR angiography maximal intensity projection (**a**), fast spin echo (**b**) and cine steady-state free precession (**c**) in a patient with isolated anomalous connection of right upper pulmonary vein to the junction superior vena cava-right atrium, with abnormal rightward course of the superior vena cava (*Ao* aorta, *RA* right atrium, *RUPV* right upper pulmonary vein, *SVC* superior vena cava)

mixed blood in the right atrium to enter the left heart for systemic distribution; usually the confluence of the pulmonary veins is posterior to the left atrium, but separate from it.

There are four basic types:

▪ *supracardiac*: the anomalous connection is to an ascending vertical vein, usually on the left and connected to the left innominate vein; pulmonary venous obstruction is possible,

▪ *cardiac*: the pulmonary veins connect directly to the right atrium or (more frequently) to the coronary sinus; pulmonary venous obstruction is rare,

▪ *infracardiac*: (or infradiaphragmatic) the connection is to intraabdominal veins (more frequently to the portal vein); pulmonary venous obstruction is very frequent,

▪ *mixed*: the entire pulmonary venous drainage is through two (or more) of the above connections.

▪ Surgical options

▪ Partial anomalous pulmonary venous connection:

▪ *Anomalous right pulmonary vein(s) connected to the superior vena cava*

The right atrial incision depends on the position of the anomalous pulmonary vein(s).

Standard oblique atriotomy: the upper right pulmonary vein is deviated to the left atrium by means of a patch (synthetic or pericardial) sewn along the wall of the superior caval vein so as to include the anomalously connected vein(s); suturing of the patch is then carried down into the right atrium, and then sewn around an unrestricted interatrial communication (already present or surgically created) in the upper part of the interatrial septum. In this way, the anomalously connected right pulmonary vein(s) can drain through a tunnel, whose posterior wall is composed of the superior caval vein and whose anterior wall is composed of a patch through the atrial septal defect into the left atrium.

Posterior incision: another surgical option is the posterior incision of the right atrium, prolonged on the superior vena cava; this approach allows the plastic procedure of en-
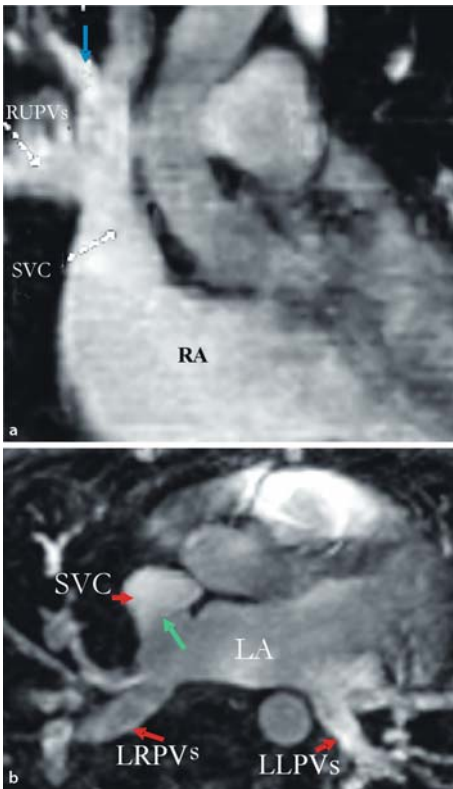
Fig. 3.2.3. Partial right anomalous pulmonary venous connection with sinus venosus atrial septal defect. Cardiac MR angiography with para-coronal (**a**) and axial (**b**) reformatted time of flight showing a sinus venous atrial septal defect (green arrow) with anomalous right upper pulmonary vein connected to the superior vena cava-right atrial junction. Note a small additional right upper pulmonary vein connected more distally to the superior vena cava (blue arrow) (*LA* left atrium, *LLPV* lower left pulmonary vein, *LRPV* lower right pulmonary vein, *RA* right atrium, *RUPV* right upper pulmonary vein, *SVC* superior vena cava)

larging the superior vena cava by a synthetic or pericardial gusset placed in the superior vena cava-right atrial junction.

■ *Anomalous right pulmonary vein(s) connected to the inferior vena cava*

Two surgical options are available: tunneling the anomalous right pulmonary vein(s) to the left atrium trough an atrial septal defect (like for the anomalous connection to the superior vena cava), or disconnection of the anomalous venous channel from the inferior vena cava and direct anastomosis to the left atrium.

■ *Anomalous left pulmonary vein(s)*

Different techniques have been reported to repair the anomalous left pulmonary vein(s), all use an end-to-side or side-to-side anastomosis between the left pulmonary vein(s) and the left auricular appendage.

■ *Scimitar syndrome:* correction of the scimitar syndrome may be technically demanding due to the infradiaphragmatic portion of the anomalous venous connection. Exposure of this portion of the vein is afforded by splitting the diaphragm to the veno-caval hiatus. In some patients, the repair may only require removal of the inferior vena cava cannula to expose the anomalous venous ostium during a brief period of deep hypothermic circulatory arrest. In this instance, an intraatrial baffle is used in much the same way as a partial anomalous venous connection with a sinus venosus defect. A final alternative technique consists of extracardiac reimplantation of the scimitar vein into the posterior wall of the right atrium followed by transposition of the atrial septum anterior to the new ostium, either directly or with a patch.

■ **Total anomalous pulmonary venous connection:**

■ *Supracardiac and infracardiac type:* a large anastomosis is created between the anterior wall of the common pulmonary venous sinus and the posterior wall of the left atrium, both opened wide to obtain an unrestrictive connection;

– the approach can be biatrial (right atriotomy, opening of the interatrial septum), posterior or superior (between aorta, right pulmonary artery and the roof of the left atrium),
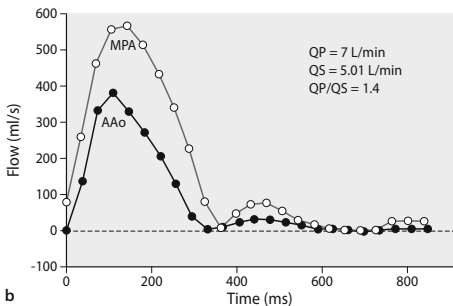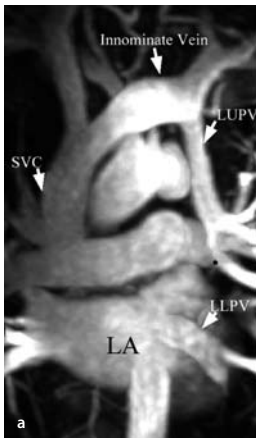
Fig. 3.2.4. Partial left anomalous pulmonary venous connection. Gadolinium-enhanced 3-dimensional MR angiography maximal intensity projection oblique plane (**a**) demonstrating the left upper pulmonary vein connected to the innominate vein with graphic pulmonary (QP) and aortic (QS) flows representations demonstrating a QP/QS = 1.4 (**b**) (*LA* left atrium, *LLPV* left lower pulmonary vein, *LUPV* left upper pulmonary vein, *SVC* superior vena cava)

– the ascending (or descending) vertical vein may be left open (to allow heart decompression), or ligated, or transected and opened longitudinally to be utilized to create a wider anastomosis,
– the patent foramen ovale may be closed or left (partially) open to allow heart decompression,
– the left atrium may be enlarged with a single or double patch technique to improve left ventricular filling.

■ *Cardiac type:* the total pulmonary venous return is deviated to the left atrium through an unrestricted (or surgically enlarged) interatrial communication by a patch; in the case of coronary sinus type, the roof of the coronary sinus in incised (or excised) to create an unrestricted connection.
■ *Mixed type:* surgical treatment must be individualized and based on the particular morphology.

■ Pre-operative information

■ **Partial anomalous pulmonary venous connection:** If a clinical doubt in the presence of partial anomalous venous connection cannot be solved with confidence by echocardiography, CT scan and MRI are the most appropriate additional diagnostic imaging tests. The acoustic properties of lung tissue makes it difficult using echocardiography to trace potential anomalous veins back into the lungs to confirm that they are pulmonary rather than systemic veins. This limitation is not encountered with CT scan and MRI.

The goals of CT scan MRI evaluation of partial anomalous pulmonary venous connection include precise delineation of the anatomy with location, size and connection site of the anomalous vein(s) by means of CT angiography with contrast material as well as gadolinium-enhanced 3-dimensional MR angiography (Figs. 3.2.1–3.2.5). The image dataset can be reformatted into any plane to illustrate spatial relationships and has sufficient resolution to detect vessels < 1 mm. For added confidence, additional MRI imaging of the vascular anatomy can be obtained using cine gradient echo or fast spin echo with blood signal nulling sequences (Fig. 3.2.2). Several studies assessing the accuracy and utility of gadolinium-enhanced 3-dimensional MRI have demonstrated a high level of agreement between findings on MR angiography compared with surgical inspection and X-ray angiography. MR angiography were uniformly more accu-
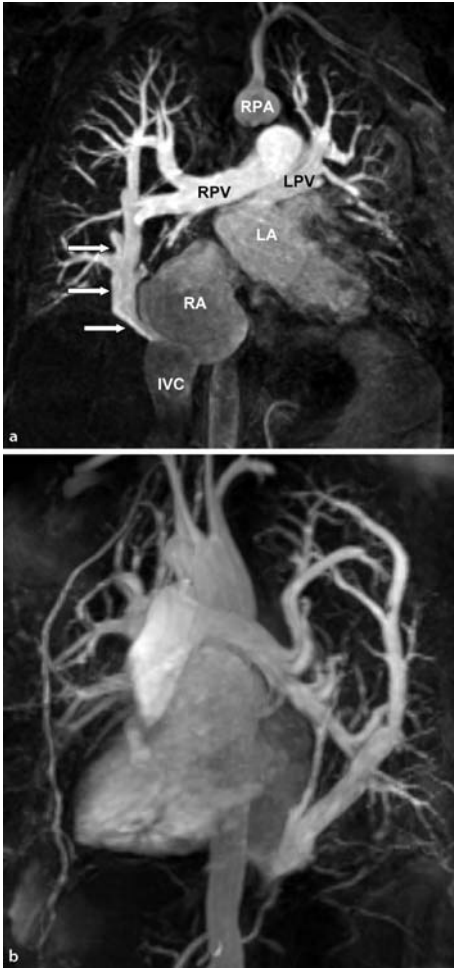
Fig. 3.2.5. Cardiac MRI, Gadolinium-enhanced 3D MR angiography maximal intensity projection anterior (**a**) and posterior (**b**) view showing the anomalous pulmonary venous connection to the inferior vena cava through "scimitar vein" (arrows)
(*IVC* inferior vena cava, *LA* left atrium, *LPA* left pulmonary artery, *LPV* left pulmonary vein, *RA* right atrium, *RPA* right pulmonary artery, *RPV* right pulmonary vein)

rate than transthoracic and transesophageal echocardiography. MRI investigations often diagnosed previously unknown presence of a partial anomalous pulmonary venous connection or added new clinically important information regarding anatomical details of the partial anomalous pulmonary venous connection.

Patients with a partial anomalous pulmonary venous connection should also have their ventricular dimensions and function measured using a stack of cine MRI oriented in the ventricular short-axis plane. Particular attention should be devoted to quantifying right ventricular end-diastolic volume as this should be related to the size of the left-to-right shunt. The shunt should also be measured directly by obtaining PVC MRI flow measurements in the main pulmonary artery (QP) and the ascending aorta (QS) (Fig. 3.2.4). It is worth noting that, in patients with partial anomalous pulmonary venous connection, QP/QS ratio measurements by oxymetric measurements in the catheterization laboratory are inherently inaccurate because of the difficulty in obtaining a reliable, representative mixed systemic venous saturation. Because blood flow is measured directly, these concerns do not apply to MRI measurements. In cases where there is a hypoplastic pulmonary artery or obstruction to the pulmonary venous return, it is also useful to calculate differential pulmonary blood flow by means of MRI measurements in the branch pulmonary arteries (Fig. 3.2.6 a).

In the presence of scimitar syndrome, the pre-operative CT scan and MRI, in addition to the visualization of the anomalous venous connection, are also useful to evaluate the degree of hypoplasia of the right lung, pulmonary artery and other associated anomalies (Figs. 3.2.5 and 3.2.6).

In case of a suspected anomalous pulmonary venous connection a comprehensive cardiovascular MRI investigation considers the following protocol:
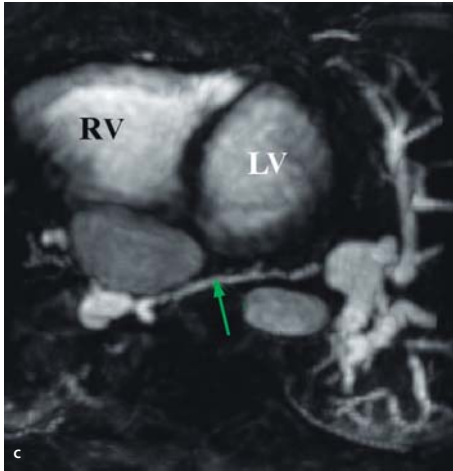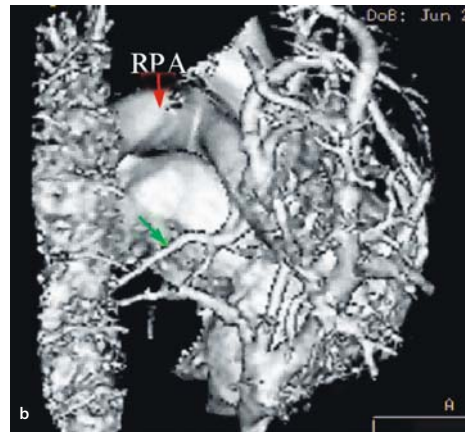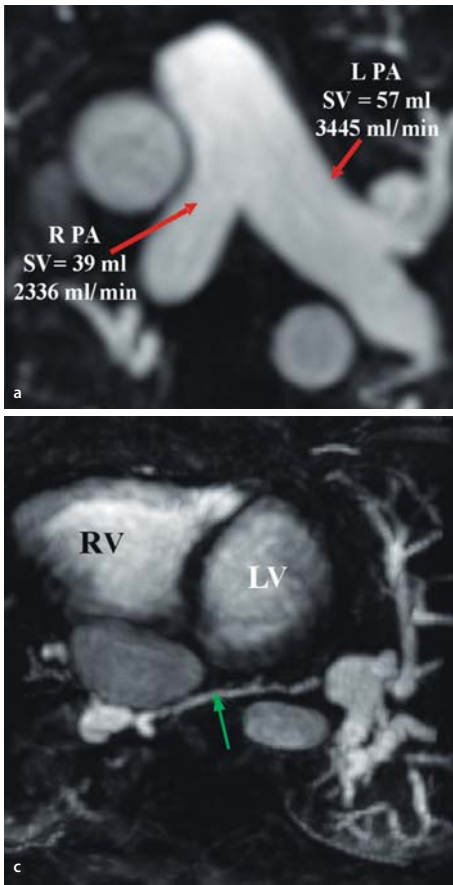
Fig. 3.2.6. Scimitar syndrome associated with horseshoe lung. (a) Gadolinium-enhanced 3-dimensional MR angiography maximal intensity projection of the pulmonary branches illustrating the mild hypoplasia and reduced flow of the right pulmonary artery, calculated with PVC. 3-dimensional MR angiography volume rendering reconstruction (b) and maximal intensity projection (c) showing a crossing small right pulmonary artery branch (green arrow) = horseshoe lung (*IVC* inferior vena cava, *LA* left atrium, *LPA* left pulmonary artery, *LV* left ventricle, *PA* pulmonary artery, *Pulm* pulmonary, *RA* right atrium, *RPA* right pulmonary artery, *RV* right ventricle)

- 3-plane localizing images,
- 2-dimensional axial Time-of-flight Angiography mainly to evaluate the pulmonary veins (see chapter 3.0) (Fig. 3.2.3),
- oblique axial and para-sagittal fast spin echo and segmented k-space cine steady-state free precession pulse sequences at the atrial level for anatomical detail of the atrial septal defect and the pulmonary veins connections and their relationship (Fig. 3.2.2),
- ECG-gated cine steady-state free precession sequences for quantitative assessment

of both ventricular dimensions and function, and stroke volumes.
- ECG-gated phase velocity contrast MRI sequences perpendicular to the main pulmonary artery, ascending aorta, pulmonary branches and pulmonary veins, to assess the QP/QS, the pulmonary arteries blood flow and pulmonary veins blood flow when needed,
- gadolinium-enhanced 3-dimensional MR angiography for the evaluation of pulmonary venous return (Figs. 3.2.2, 3.2.4 and 3.2.6).

Fig. 3.2.7. Obstructed supracardiac total anomalous pulmonary venous connection. CT scan, subvolume maximum intensity coronal projection, showing supracardiac total anomalous pulmonary venous connection with obstruction (arrowheads) of the vertical vein (asterisks) connecting the pulmonary venous connector to the innominate vein (*IV* innominate vein, *LLPV* left lower pulmonary vein, *LUPV* left upper pulmonary vein, *MPA* main pulmonary artery, *PVC* pulmonary venous connector, *RLPV* right lower pulmonary vein, *RPA* main pulmonary artery, *RUPV* right upper pulmonary vein, *SVC* superior vena cava) (modified with permission from Goo HW, Park IS, Ko JK, Kim YH, Seo DM, Yun TJ, Park JJ, Yoon CH (2003) CT of congenital heart disease: normal anatomy and typical pathologic conditions. Radiographics 23:S147–165)
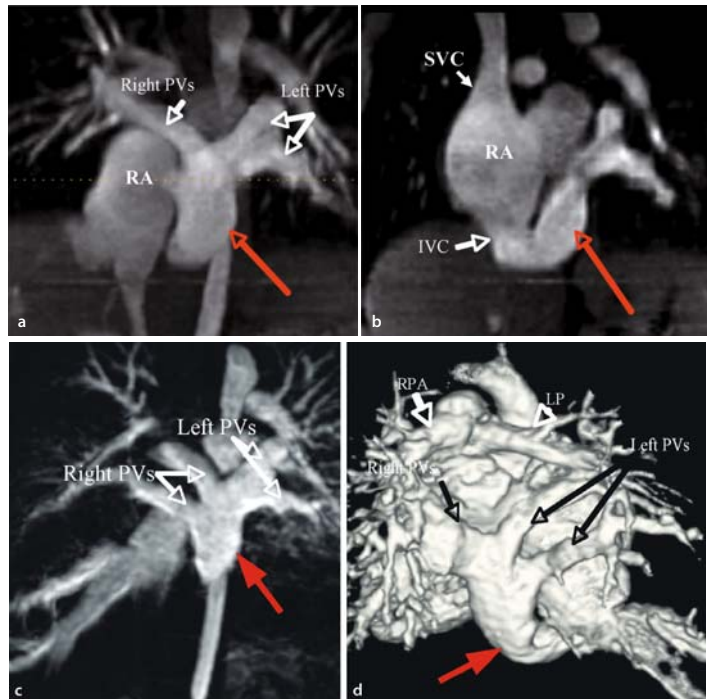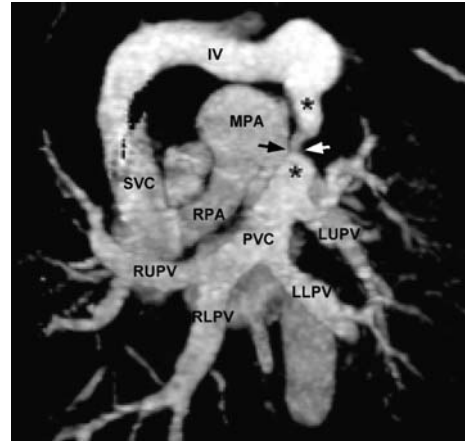
Fig. 3.2.8. Infra-cardiac total anomalous pulmonary venous connection. Gadolinium-enhanced 3-dimensional MR angiography showing unobstructed infracardiac total anomalous pulmonary venous connection. Maximal intensity projection (**a, b, c**) and 3-dimensional volume rendering reconstruction (**d**) showing all pulmonary veins connected to the inferior vena cava through an unobstructed pulmonary venous collector (red arrow) (*IVC* inferior vena cava, *LPA* left pulmonary artery, *PVs* pulmonary veins, *RA* right atrium, *RPA* right pulmonary artery, *SVC* superior vena cava)
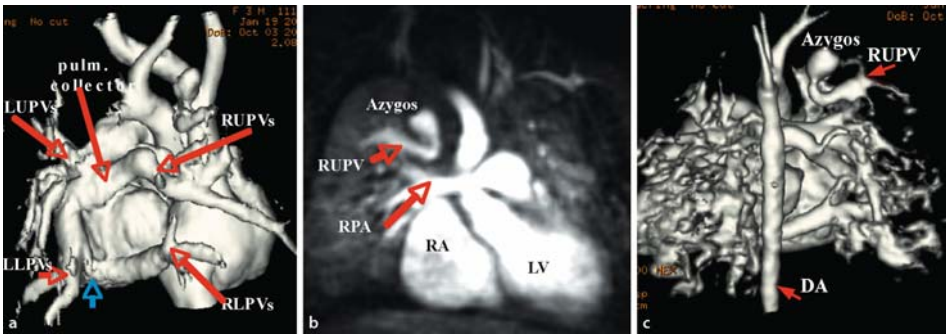
Fig. 3.2.9. Mixed total anomalous pulmonary venous connection. 3-dimensional MR angiography volume rendering (**a** and **c**) and gadolinium-enhanced angiography (**b**) showing a neonatal complex form of mixed total anomalous pulmonary venous connection, with the right pulmonary veins connected to the azygos vein, and into an odd shape pulmonary venous collector (blue arrow) (**a**), draining also the venous return from the left pulmonary veins (*DA* descending aorta, *LA* left atrium, *LLPV* left lower pulmonary veins, *LUPV* left upper pulmonary veins, *LV* left ventricle, *RA* right atrium, *RLPV* right lower pulmonary veins, *RPA* right pulmonary artery, *RUPV* right upper pulmonary veins)
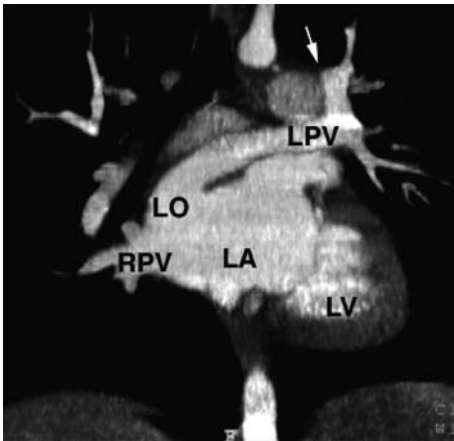
Fig. 3.2.10. Status post repair of anomalous pulmonary venous connection. CT scan angiogram showing 3-dimensional posterior multiplanar reconstruction of left atrium and left pulmonary venous drainage through a common vein, the legated levo-atrial cardinal vein (white arrow) (*LA* left atrium, *LO* levo-atrial cardinal vein opening, *LPV* left pulmonary vein, *LV* left ventricle, *RPV* right pulmonary vein)

■ **Total anomalous pulmonary venous connection:** Total anomalous pulmonary venous connection is clinically suspected early in life and echocardiography generally provides adequate information on the presence and location of anomalous pulmonary venous connections. However, if any doubt persists, mainly in cases with mixed or complex forms of total anomalous pulmonary venous connection, both 3-dimensional multi-planar volume-rendered CT images and MRI contrast angiography can be extremely useful to delineate the connection of each pulmonary vein (Figs. 3.2.7–3.2.9).

■ **Potential complications**

Residual or recurrent intraatrial shunt, air embolism (early), acute pulmonary edema, pulmonary arterial hypertensive crisis, phrenic nerve damage, supraventricular arrhythmias, pulmonary venous obstruction, systemic venous obstruction, anastomotic obstruction, systemic and pulmonary thromboembolism (late).
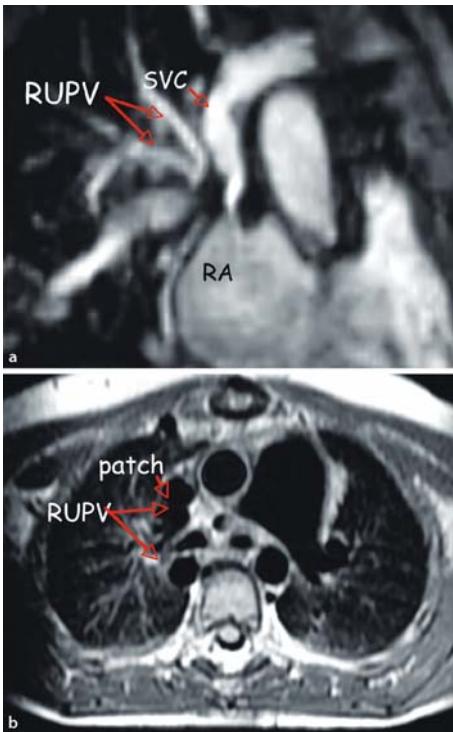
Fig. 3.2.11. Status post repair of partial anomalous right pulmonary venous connection. MRI confirmed the severe obstruction of the superior vena cava just above its junction to the right atrium, as showed in the gadolinium-enhanced main intensity projection coronal plane (**a**); MRI also highlighted an unsuspected right upper pulmonary vein obstruction as illustrated in the fast spin echo axial plane (**b**) as well, probably caused by the surgical baffle (*RA* right atrium, *RUPV* right upper pulmonary veins, *SVC* superior vena cava)
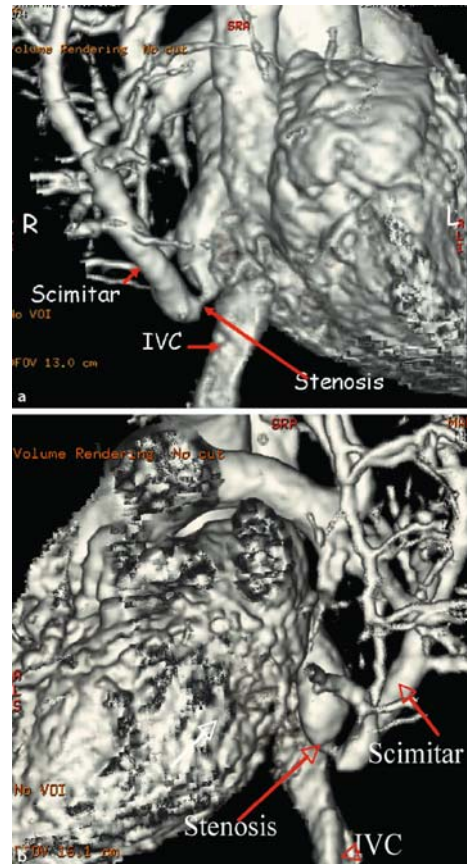
Fig. 3.2.12. Status post repair of scimitar syndrome. MRI with gadolinium-enhancement volume rendering anterior (**a**) and posterior view (**b**) showing a significant obstruction of the proximal channel scimitar-to-left atrium (*IVC* inferior vena cava)

■ Post-operative follow-up

In the postoperative setting, CT scan and MRI are very useful tools to rule out potential residual defects (Figs. 3.2.10–3.2.13)

MRI is particularly important when the following residual complications are suspected: intraatrial shunts, systemic and/or pulmonary venous obstructions, leak and/or obstruction of the intraatrial baffle.

As for the pre-operative evaluation, in addition to the possibility of assessing the ventricular volumes and quantifying the residual shunts, each pulmonary and systemic vein can be optimally visualized by 3-dimensional MR angiography. Moreover in some cases it is possible to study the anomalous flow pattern of obstructed veins by means of PVC-MRI.

Fig 3.2.13. Status post repair of scimitar syndrome. MRI with gadolinium-enhancement volume rendering oblique plane (**a** = anterior view, **b** = posterior view) showing a significant narrowing of the inferior vena cava due to the intraatrial PTFE baffle, as later confirmed at re-operation to relieve the obstruction. The inferior systemic venous return drains principally into the superior vena cava through a dilated azygos and hemiazygos veins 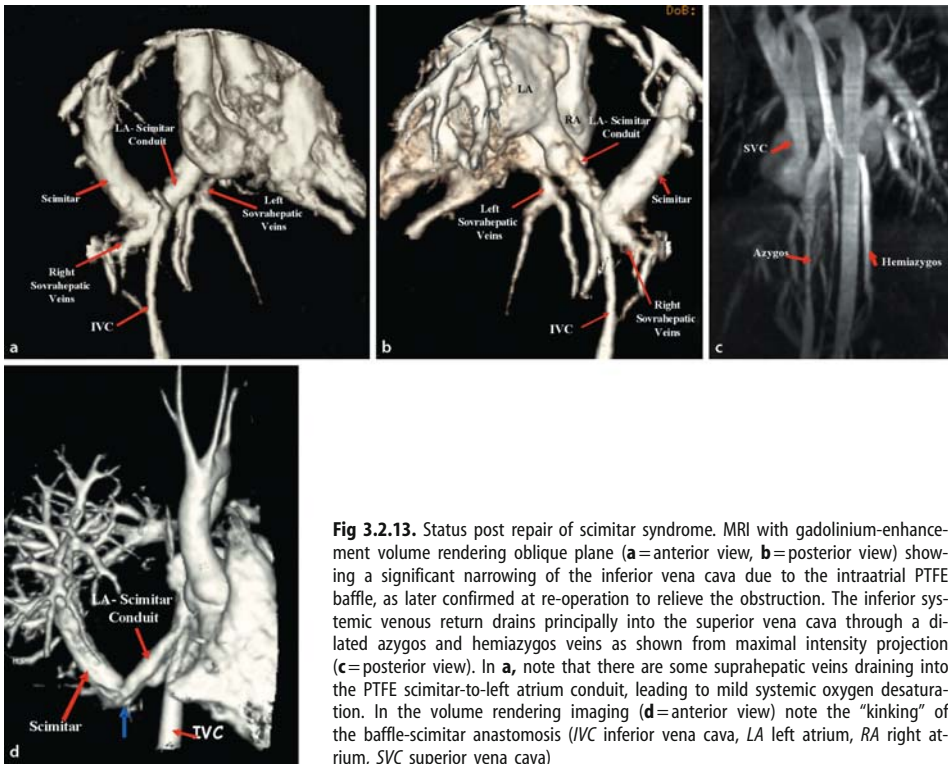as shown from maximal intensity projection (**c** = posterior view). In **a**, note that there are some suprahepatic veins draining into the PTFE scimitar-to-left atrium conduit, leading to mild systemic oxygen desaturation. In the volume rendering imaging (**d** = anterior view) note the "kinking" of the baffle-scimitar anastomosis (*IVC* inferior vena cava, *LA* left atrium, *RA* right atrium, *SVC* superior vena cava)

■ References

Amodeo A, Corno AF, Marino B, Carta MG, Marcelletti C (1990) Combined repair of transposed arteries and total anomalous pulmonary venous connecion. Ann Thorac Surg 50:820–821

Balci NC, Yalcin Y, Tunaci A, Balci Y (2003) Assessment of the anomalous pulmonary circulation by dynamic contrast-enhanced MR angiography in under four seconds. Magn Reson Imaging 21:1–7

Beerbaum P, Korperich H, Barth P, Esdorn H, Gieseke J, Meyer H (2001) Noninvasive quantification of left-to-right shunt in pediatric patients: phase-contrast cine magnetic resonance imaging compared with invasive oximetry. Circulation 103:2476–2482

Chang YC, Li YW, Liu HM, Wang JK, Wu MH, Wu CY, Su CT, Tsang YM, Hsu JC (1994) Findings of anomalous venous return using MRI. J Formos Med Assoc 93:462–468

Cohen M, Hartnell G, Finn J (1994) Magnetic resonance angiography of congenital pulmonary veins anomalies. Am Heart J 127:954–955

Corno AF, Giamberti A, Carotti A, Giannico S, Marino B, Marcelletti C (1990) Total anomalous pulmonary venous connection: surgical repair with a "double patch" technique. Ann Thorac Surg 49:492–494

Corno AF, Rosti L, Machado I (1995) Horshoe lung associated with anomalous pulmonary venous connection without pulmonary hypoplasia. Cardiol Young 5:91

Corno AF (1996) Bilateral partial anomalous pulmonary venous connection with intact atrial septum. Asian Cardiovasc Ann 4:181

Corno AF (1997) An unusual type of total anomalous pulmonary venous connection. Ann Thorac Surg 64:1218

Da Cruz E, Milella L, Corno AF (1998) Left isomerism with tetralogy of Fallot and anomalous systemic and pulmonary venous connections. Cardiol Young 8: 131–133

Dikensoy O, Kervancioglu R, Bayram NG, Elbek O, Uyar M, Ekinci E (2006) Horseshoe lung associated with scimitar syndrome and pleural lipoma. J Thorac Imaging 21:73–75

Douglas YL, van den Broek SAJ, Wijkstra PJ, Wolf RFE, Timens W, DeRuiter MC, Ebels T (2007) Clinical-

pathologic conference in surgery for congenital and acquired cardiovascular disease: unilateral pulmonary vein stenosis with a contralateral pulmonary varix. J Thorac Cardiovasc Surg 134:496–501

Drozd J, Tomaszewski A, Czekajska-Chehab E, Drop A, Widomska-Czekajska T (2004) Partial anomalous pulmonary venous drainage with atrial septal defect of the sinus venosus type. Diagnostic role of multislice spiral computerised tomography – a case report. Kardiol Pol 60:591–594

Dyme JL, Prakash A, Printz BF, Kaur A, Parness IA, Nielsen JC (2006) Physiology of isolated anomalous pulmonary venous connection of a single pulmonary vein as determined by cardiac magnetic resonance imaging. Am J Cardiol 98:107–110

Ferrari VA, Scott CH, Holland GA, Axel L, St John Sutton M (2001) Ultrafast three-dimensional contrast-enhanced magnetic resonance angiography and imaging in the diagnosis of partial anomalous pulmonary venous drainage. J Am Coll Cardiol 37: 1120–1128

Festa P, Ait-Ali L, Murzi B, Bini MR (2005) Tetralogy of Fallot with left heart hypoplasia, total anomalous pulmonary venous return, and right lung hypoplasia: role of magnetic resonance imaging. Pediatr Cardiol 26:467–469

Festa P, Ait-Ali L, Cerillo AG, De Marchi D, Murzi B (2006) Magnetic resonance imaging is the diagnostic tool of choice in the preoperative evaluation of patients with partial anomalous pulmonary venous return. Int J Cardiovasc Imaging 22:685–693

Geva T, Sahn DJ, Powell AJ (2003) Magnetic resonance imaging of congenital heart disease in adults. Prog Pediatr Cardiol 17:21–39

Goo HW, Park IS, Ko JK, Kim YH, Seo DM, Yun TJ, Park JJ, Yoon CH (2003) CT of congenital heart disease: normal anatomy and typical pathologic conditions. Radiographics 23:S147–165

Gorincour G, Lapierre C, Miro J, Garel L, Guerin R (2006) The role of cardiac magnetic resonance in the diagnosis of anomalous pulmonary venous return with subsequent Amplatzer device treatment. J Cardiovasc Magn Reson 8:499–502

Greil GF, Powell AJ, Gildein HP, Geva T (2002) Gadolinium-enhanced three-dimensional magnetic resonance angiography of pulmonary and systemic venous anomalies. J Am Coll Cardiol 39:335–341

Grosse-Wortmann L, Al-Otay A, Goo HW, Macgowan CK, Coles JG, Benson LN, Redington AN, Yoo SJ (2007) Anatomical and functional evaluation of pulmonary veins in children by magnetic resonance imaging. J Am Coll Cardiol 49:993–1002

Gulati G, Sharma S (2003) A rare form of supracardiac total anomalous pulmonary venous drainage: evaluation by computed tomography and magnetic resonance imaging. Clin Radiol 58:172–175

Haramati LB, Moche IE, Rivera VT, Patel PV, Heyneman L, McAdams HP, Issenberg HJ, White CS (2003) Computed tomography of partial anomalous pulmonary venous connection in adults. J Comput Assist Tomogr 27:743–749

Hernandez RJ, Aisen AM, Foo TK, Beekman RH (1993) Thoracic cardiovascular anomalies in children: evaluation with a fast gradient-recalled-echo sequence with cardiac-triggered segmented acquisition. Radiology 188:775–780

Kafka H, Mohiaddin R (2007) Undiagnosed cause of right ventricular enlargement: value of cardiovascular magnetic resonance for the detection of sinus venosus defect and partial anomalous pulmonary venous connection. J Cardiovasc Magn Reson 9:105

Kaster B, Livolsi A, Germain P, Gangi A, klinkert A, Dietemann JL, Willard D, Wackenheim A (1992) Contribution of MRI in supracardiac total anomalous pulmonary venous drainage. Pediatr Radiol 22:262–263

Kim TH, Kim YM, Suh CH, Cho DJ, Park IS, Kim WH, Lee YT (2000) Helical CT angiography and three-dimensional reconstruction of total anomalous pulmonary venous connections in neonates and infants. Am J Roentgenol 175:1381–1386

Livolsi A, Kastler B, Marcellin L, Casanova R, Bintner M, Haddad J (1991) MR diagnosis of subdiaphragmatic anomalous pulmonary venous drainage in a newborn. J Comput Assist Tomogr 15:1051–1053

Masui T, Seelos K, Kersting-Sommerhoff B, Higgins C (1991) Abnormalities of the pulmonary veins. Evaluation with MR imaging and comparison with cardiac angiography and echocardiography. Radiology 181:645–649

Otsuka M, Itoh A, Haze K (2004) Sinus venosus type of atrial septal defect with partial anomalous pulmonary venous return evaluated by multislice CT. Heart 90:901

Ou P, Celermajer DS, Stos B, Marijon E, Vouhé P, Brunelle F, Bonnet D, Sidi D (2006) Images in cardiovascular medicine. Definitive diagnosis of obstructed total anomalous pulmonary venous drainage in a critically ill newborn with high-resolution computed tomography. Circulation 114:e646–647

Powell AJ, Maier SE, Chung T, Geva T (2000) Phase-velocity cine magnetic resonance imaging measurement of pulsatile blood flow in children and young adults: in vitro and in vivo validation. Pediatr Cardiol 21:104–110

Powell AJ, Tsai-Goodman B, Prakash A, grail GF, Geva T (2003) Comparison between phase-velocity cine magnetic resonance imaging and invasive oximetry for quantification of atrial shunts. Am J Cardiol 91:1523–1525

Prasad SK, Soukias N, Hornung T, Khan M, Pennell DJ, Gatzoulis MA, Mohiaddin RH (2004) Role of magnetic resonance angiography in the diagnosis of major aortopulmonary collateral arteries and partial anomalous pulmonary venous drainage. Circulation 109:207–214

Rebergen SA, de Roos A (2000) Congenital heart disease. Evaluation of anatomy and function by MRI. Herz 25:365–383

Shiraishi I, Kato Y, Todoroki H, Satoh H, Hamaoka K (2000) Images in cardiovascular medicine. Differential color imaging technique of helical CT angiogra-

phy in the diagnosis of total anomalous pulmonary venous drainage. Circulation 101:2017–2018

Sridhar PG, Kalyanpur A, Suresh PV, John C, Sharma R, Maheshwari S (2003) Total anomalous pulmonary venous connection: helical computed tomography as an alternative to angiography. Indian Heart J 55: 624–627

Valente AM, Sena L, Powell AJ, Del Nido PJ, Geva T (2007) Cardiac magnetic resonance imaging evaluation of sinus venosus defects: comparison to surgical findings. Pediatr Cardiol 28:51–56

Valsangiacomo ER, Levasseur S, McCrindle BW, Mac-Donald C, Smallhorn JF, Yoo SJ (2003) Contrast-enhanced MR angiography of pulmonary venous abnormalities in children. Pediatr Radiol 33:92–98

Wald RM, Powell AJ (2006) Simple congenital heart lesions. J Cardiovasc Magn Reson 8:619–631

White C, Baffa J, Haney P, Campbell A, Nessaiver M (1998) Anomalies of pulmonary veins: usefulness of spin-echo and gradient-echo MR images. Am J Roentgenol 170:1365–1368

Definition

To understand the anatomy determining the presence of shunts between the atrial chambers, it is crucial to appreciate the difference between a defect of the atrial septum and an interatrial communication.

- *True atrial septal defects*: defects existing within the floor of the fossa ovalis; they can be produced by an insufficient or perforated flap valve; defects within the fossa (so-called "ostium secundum" defects) must be distinguished from probe-patency of the fossa, in which the flap valve overlaps, but does not seal anatomically, the rim.
- *Sinus venosus:* interatrial communications in the mouth of usually the superior, but sometimes the inferior, vena cava; they are outside the floor of the fossa ovalis. Their anatomical feature is overriding of the superior or posterior margin by the mouth of the superior or inferior vena cava, respectively.
- *Coronary sinus*: defects existing through the mouth of the sinus when there is a wide fenestration between the wall of the sinus and the left atrium. Usually, but not always, the left superior vena cava drains to the roof of the left atrium (see chapter "Unroofed coronary sinus").
- *Ostium primum*: defects between the leading edge of the atrial septum and the upper margin of the ventricular septum. They are atrioventricular septal defects and have a common atrioventricular junction (see chapter "Atrioventricular septal defects").

Atrial septal defects within the fossa ovalis may coexist with nearly all varieties of congenital heart disease, but such cases are not considered the primary lesion unless the left-to-right shunt at the atrial level is the dominant hemodynamic lesion. Partial anomalous pulmonary venous connection (virtually always present in patients with sinus venosus defect), mitral valvar prolapse, ventricular septal defect, patent ductus arteriosus, pulmonary valvar stenosis, peripheral pulmonary arterial stenosis, and persistence of the left superior vena cava are the lesions which are more frequently found secondary to interatrial communications.

Surgical options

The percutaneous closure with a device implanted using an interventional cardiac procedure is nowadays considered whenever possible.

In all other cases, the defect is surgically approached through a right atriotomy on cardiopulmonary bypass. True atrial septal defects are closed by direct suture or patch closure of the defect (depending on the size and shape of the defect).

Sinus venosus atrial septal defects are treated by patch closure of the defect, leaving the right pulmonary veins on the left side of the patch, with unrestricted communication with the left atrium, and avoiding damage to the sinus node (and the sinus node artery) by the suture line (see chapter "Partial anomalous pulmonary venous connection").

■ Pre-operative information

Ostium secundum atrial septal defect is usually sufficiently evaluated, mainly in children, by transthoracic echocardiography for diagnosis and indication to management, even if percutaneous transcatheter occlusion of secundum atrial septal defects has increased the need for accurate anatomic information of the defect size, morphology, and spatial relationships.

However, a few recent reports proposed evaluating the ostium secundum atrial septal defect by MRI prior to attempting percutaneous closure to correctly identify those patients not suitable for such a procedure due to anatomical problems. This approach can result in the avoidance of unneeded invasive and radiologic ionizing procedures or transesophageal echocardiography which, although more accurate but semi-invasive, is not well tolerated and needs general anesthesia in children.

The anatomical evaluation of the atrial septum by MRI includes location, size and number of the atrial septal defects by both cine MRI sequences and "black blood" static images performed with breath-holding and ECG-gating (Fig. 3.3.1).

Optimal images are necessary to avoid overestimation of the defect's size. It has been reported that the spin-echo measurements resulted in significantly larger defect sizes compared with the reference standards, and the discrepancy was attributed to "signal dropout" in the thin portion of the septum. Therefore, in some studies defect size and rim measurements were assessed using velocity encoded cine MRI oriented in the plane of the atrial septum for *en face* visualization and in orthogonal planes for the distance from adjacent structures.
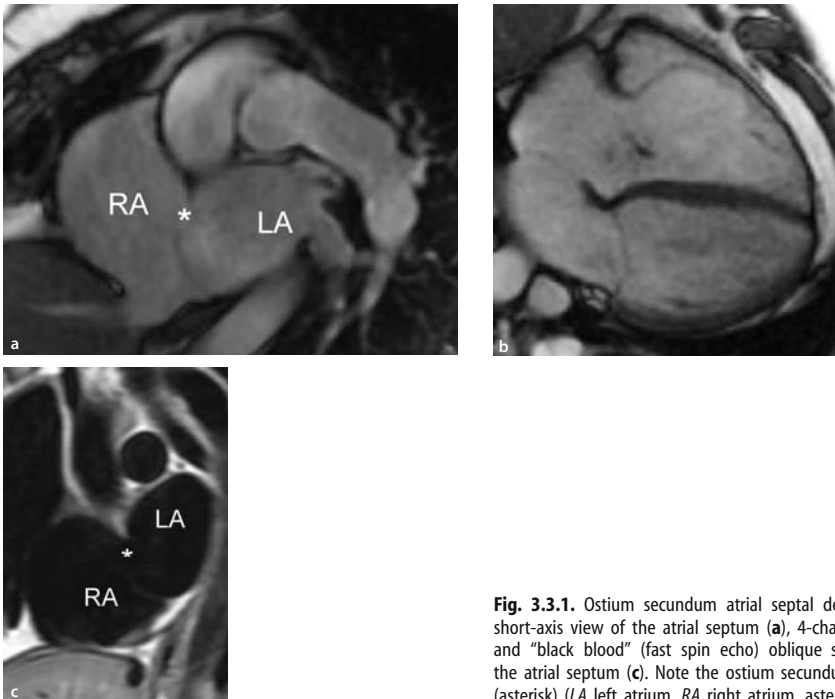
Fig. 3.3.1. Ostium secundum atrial septal defect. Cine MRI short-axis view of the atrial septum (**a**), 4-chamber view (**b**), and "black blood" (fast spin echo) oblique sagittal plan of the atrial septum (**c**). Note the ostium secundum atrial defect (asterisk) (*LA* left atrium, *RA* right atrium, asterisk = defect)

In order to quantify the shunt, a commercially available gradient-echo phase velocity mapping ECG-triggered sequence is used for the blood flow determination at the pulmonary and aortic levels (for calculation of the pulmonary-to-systemic flow ratio = QP/QS). QP/QS can also be derived from the right and left ventricular stroke volumes calculated from the short-axis cine stack of the ventricles, paying close attention to consider the potential presence of atrioventricular valve regurgitation. This image series can also help to obtain a qualitative estimate of right ventricular systolic pressure based on the configuration of the ventricular septum.

Cardiac MRI is particularly indicated in patients with echocardiographic diagnosis of suspected ostium primum atrial septal defect (Fig. 3.3.2) and sinus venous atrial septal defect (Fig. 3.3.3), in order to visualize both the defect and the pulmonary venous return in detail as well as to correctly quantify the left to right shunt and the volume overload imposed to the right heart. Moreover as a first-line diagnostic tool for the evaluation of the pulmonary veins, MRI is particularly useful in patients with right ventricular volume overload in whom transthoracic echocardiography cannot clarify its cause.

In patients with atrial septal defect, a comprehensive cardiovascular MRI investigation considers the following protocol:

■ 3-plane localizing images,
■ 2-dimensional axial Time-of-flight Angiography mainly to evaluate the pulmonary veins (see appendix in "Introduction"),
■ oblique axial and para-sagittal fast spin echo and segmented k-space cine steady-state free precession pulse sequences at the atria level for anatomical detail of atrial septal defect and pulmonary venous connections and their relationship,
■ ECG-gated phase contrast velocity mapping MRI sequence parallel to the atrial septum plane in order to better delineate the size, shape and rims of the defect,
■ ECG-gated cine steady-state free precession sequences for quantitative assessment
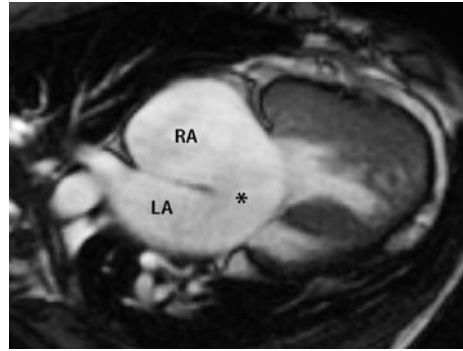
Fig. 3.3.2. Ostium primum atrial septal defect. Axial cine MRI 4-chamber view showing a large ostium primum atrial septal defect (asterisk) (*LA* left atrium, *RA* right atrium, asterisk = defect)
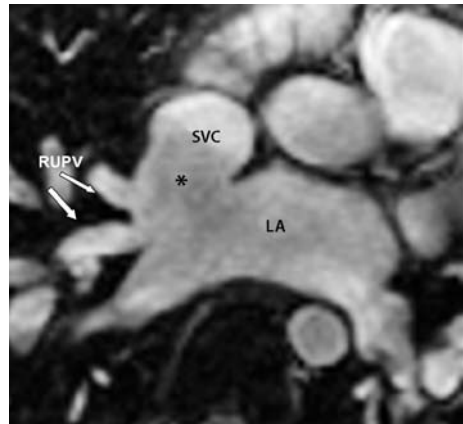
Fig. 3.3.3. Sinus venosus atrial septal defect. Axial cine MRI showing the sinus venous atrial septal defect (asterisk) as a lack of septation between the superior vena cava and the pulmonary veins. Note the right upper pulmonary veins draining to the superior vena cava at the right atrium junction level (*LA* left atrium, *RUPV* right upper pulmonary veins, *SVC* superior vena cava)

of both ventricular dimensions and functions, and stroke volumes,
■ ECG-gated phase contrast velocity mapping MRI sequences perpendicular to the main pulmonary artery, ascending aorta, pulmonary branches, to assess QP/QS,

■ gadolinium-enhanced 3-dimensional MR angiography for the evaluation of pulmonary venous return.

■ Potential complications

Residual or recurrent atrial septal defect, air embolism (early), systemic and pulmonary thromboembolism (late), supraventricular arrhythmias (particularly in adult patients), pericardial effusion (frequent).

■ Post-operative follow-up

Current MRI techniques are inferior to trans-oesophageal echocardiography for detection of residual left-to-right and through the atrial septum after device closure of interatrial communications.

In patients post transcatheter closure of an atrial septal defect (Fig. 3.3.4), MRI can rule out device malposition, interference with the atrioventricular valves and venous blood flow, thrombus formation.

After surgical repair of sinus venosus atrial septal defect, cardiac MRI could be helpful to rule out iatrogenic obstruction of the systemic or pulmonary venous return.
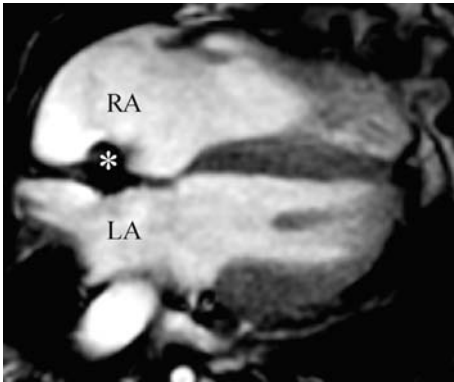
Fig. 3.3.4. Post transcatheter closure of ostium secundum atrial septal defect. 4-chamber view cine steady-state free precession MRI showing the good position of the Amplatzer device (asterisk) (*LA* left atrium, *RA* right atrium)

■ References

Beerbaum P, Korperich H, Barth P, Esdorn H, Gieseke J, Meyer H (2001) Noninvasive quantification of left-to-right shunt in pediatric patients: phase-contrast cine magnetic resonance imaging compared with invasive oximetry. Circulation 103:2476–2482

Beerbaum P, Korperich H, Esdorn H, Blanz U, Barth P, Gieseke J, Meyer H (2003) Atrial septal defects in pediatric patients: noninvasive sizing with cardiovascular MR imaging. Radiology 228:361–369

Bolz D, Lacina T, Buser P, Buser M, Guenthard J (2005) Long-term outcome after surgical closure of atrial septal defect in childhood with extensive assessment including MRI measurement of the ventricles. Pediatr Cardiol 26:614–621

Brenner LD, Caputo GR, Mostbeck G, Steiman D, Dulce M, Cheitlin MD, O'Sullivan M, Higgins CB (1992) Quantification of left to right atrial shunts with velocity-encoded cine nuclear magnetic resonance imaging. J Am Coll Cardiol 20:1246–1250

Corno AF, Chassot PG, Horisberger J, Tozzi P, von Segesser LK (2002) Interatrial communication: mini-invasive surgical approach. Forum Med Suisse 8:40S

Diethelm L, Dery R, Lipton MJ, Higgins CB (1987) Atrial-level shunts: sensitivity and specificity of MR in diagnosis. Radiology 162:181–186

Dinsmore RE, Wismer GL, Guyer D, Thompson R, Liu P, Stratemeier E, Miller S, Okada R, Brady T (1985) Magnetic resonance imaging of the interatrial septum and atrial septal defects. Am J Roentgenol 145:697–703

Drozd J, Tomaszewski A, Czekajska-Chehab E, Drop A, Widomska-Czekajska T (2004) Partial anomalous pulmonary venous drainage with atrial septal defect of the sinus venosus type. Diagnostic role of multislice spiral computerised tomography – a case report. Kardiol Pol 60:591–594

Durongpisitkul K, Tang NL, Soongswang J, Laohaprasitiporn D, Nanal A (2004) Predictors of successful transcatheter closure of atrial septal defect by cardiac magnetic resonance imaging. Pediatr Cardiol 25:124–130

Ferrari VA, Scott CH, Holland GA, Axel L, Sutton MS (2001) Ultrafast three-dimensional contrast-enhanced magnetic resonance angiography and imaging in the diagnosis of partial anomalous pulmonary venous drainage. J Am Coll Cardiol 37:1120–1128

Festa P, Ait-Ali L, Cerillo AG, De Marchi D, Murzi B (2006) Magnetic resonance imaging is the diagnostic tool of choice in the preoperative evaluation of patients with partial anomalous pulmonary venous return. Int J Cardiovasc Imaging 22:685–693

Greil GF, Powell AJ, Gildein HP, Geva T (2002) Gadolinium-enhanced three-dimensional magnetic resonance angiography of pulmonary and systemic venous anomalies. J Am Coll Cardiol 39:335–341

Henk PT, Grampp S, Linnau KF, Thurnher MM, Czerny C, Herold CJ, Mostbeck GH (2003) Suspected pulmonary embolism enhancement of pulmonary ar-

teries at deep-inspiration CT angiography: influence of patent foramen ovale and atrial septal defect. Radiology 226:749–755

Holmvang G, Palacios IF, Vlahakes GJ, Dinsmore RE, Miller SW, Liberthson RR, Block PC, Ballen B, Brady TJ, Kantor HL (1995) Imaging and sizing of atrial septal defects by magnetic resonance. Circulation 92:3473–3480

Kadiyala M, Beasley HS, Dua A (2007) A rare case of anomalous left anterior descending artery with a large interatrial communication: an invasive and CT angiographic study. J Invasive Cardiol 19:E69–72

Kafka H, Mohiaddin R (2007) Undiagnosed cause of right ventricular enlargement: value of cardiovascular magnetic resonance for the detection of sinus venosus defect and partial anomalous pulmonary venous connection. J Cardiovasc Magn Reson 9:105

Lapierre C, Raboisson MJ, Miro J, Dahdah N, Guerin R (2003) Evaluation of a large atrial septal occluder with cardiac MR imaging. Radiographics 23:S51–58

Lilje C, Weiss F, Weil J (2005) Non-invasive follow up of an atrial septal defect device occlusion. Heart 91:464

Mohrs OK, Petersen SE, Erkapic D, Rubel C, Schrader R, Nowak B, Fach WA, Kauczor HU, Voigtlaender T (2005) Diagnosis of patent foramen ovale using contrast-enhanced dynamic MRI: a pilot study. Am J Roentgenol 184:234–240

Mohrs OK, Petersen SE, Erkapic D, Victor A, Schlosser T, Nowak B, Kauffmann G, Voigtlaender T, Kauczor HU (2007) Dynamic contrast-enhanced MRI before and after transcatheter occlusion of patent foramen ovale. Am J Roentgenol 188:844–849

Nusser T, Hoher M, Merkle N, Grebe OC, Spiess J, Kestler HA, Rasche V, Kochs M, Hombach V, Wohrle J (2006) Cardiac magnetic resonance imaging and transesophageal echocardiography in patients with transcatheter closure of patent foramen ovale. J Am Coll Cardiol 48:322–329

Otsuka M, Itoh A, Haze K (2004) Sinus venosus type of atrial septal defect with partial anomalous pulmonary venous return evaluated by multislice CT. Heart 90:901

Piaw CS, Kiam OT, Rapaee A, Khoon LC, Bang LH, Ling CW, Samion H, Hian SK (2006) Use of non-invasive phase contrast magnetic resonance imaging for estimation of atrial septal defect size and morphology: a comparison with transesophageal echo. Cardiovasc Intervent Radiol 29:230–234

Powell AJ, Tsai-Goodman B, Prakash A, Grail GF, Geva T (2003) Comparison between phase-velocity cine magnetic resonance imaging and invasive oximetry for quantification of atrial shunts. Am J Cardiol 91:1523–1525

Puvaneswary M, Singham T, Bastian B (2003) Atrial septal aneurysm: MRI and echocardiography correlation. Australas Radiol 47:468–471

Rickers C, Jerosch-Herold M, Hu X, Murthy N, Wang X, Kong H, Seethamtaju RT, Weil J, Wilke NM (2003) Magnetic resonance image-guided transcatheter closure of atrial septal defects. Circulation 107:132–138

Sakakibara M, Kobayashi S, Imai H, Watanabe S, Masuda Y, Inagaki Y (1987) Diagnosis of atrial septal defect using magnetic resonance imaging. J Cardiol 17:817–829

Schalla S, Saeed M, Higgins CB, Martin A, Weber O, Moore P (2003) Magnetic resonance-guided cardiac catheterization in a swine model of atrial septal defect. Circulation 108:1865–1870

Schalla S, Saeed M, Higgins CB, Weber O, Martin A, Moore P (2005) Balloon sizing and transcatheter closure of acute atrial septal defects guided by magnetic resonance fluoroscopy: assessment and validation in a large animal model. J Magn Reson Imaging 21:204–211

Schoen SP, Kittner T, Bohl S, Braun MU, Simonis G, Schmeisser A, Strasser RH (2006) Transcatheter closure of atrial septal defects improves right ventricular volume, mass, function, pulmonary pressure, and functional class: a magnetic resonance imaging study. Heart 92:821–826

Shellock FG, Valencerina S (2005) Septal repair implants: evaluation of magnetic resonance imaging safety at 3 T. Magn Reson Imaging 23:1021–1025

Valente AM, Sena L, Powell AJ, Del Nido PJ, Geva T (2007) Cardiac magnetic resonance imaging evaluation of sinus venosus defects: comparison to surgical findings. Pediatr Cardiol 28:51–56

Wald RM, Powell AJ (2006) Simple congenital heart lesions. J Cardiovasc Magn Reson 8:619–631

Weber C, Dill T, Mommert I, Hofmann T, Adam G (2002) The role of MRI for the evaluation of atrial septal defects before and after percutaneous occlusion with the Amplatzer septal occluder®. Röfo 174:1387–1394

Weber OM, Higgins CB (2006) MR evaluation of cardiovascular physiology in congenital heart disease: flow and function. J Cardiovasc Magn Reson 8:607–617

Weber M, Dill T, Deetjen A, Neumann T, Ekinci O, Hansel J, Elsaesser A, Mitrovic V, Hamm C (2006) Left ventricular adaptation after atrial septal defect closure assessed by increased concentrations of N-terminal pro-brain natriuretic peptide and cardiac magnetic resonance imaging in adult patients. Heart 92:671–675

Wittram C (2003) Pulmonary artery enhancement at CT pulmonary angiography. Radiology 229:932–933

Chapter 3.4 Unroofed coronary sinus

Definition

Complete form: the common wall between the coronary sinus and the left atrium (roof of the coronary sinus) is totally absent.

Partial form: an opening is present in the mid-portion of the wall between the coronary sinus and the left atrium (also called biatrial opening of coronary sinus or coronary sinus to left atrial fenestration).

Associated cardiac anomalies: persistent left superior vena cava (very frequent), atrial septal defect, common atrium, partial or complete atrioventricular septal defect, mitral stenosis, mitral atresia, tricuspid atresia, tetralogy of Fallot, atrial isomerism.

Surgical options

Surgical repair can be accomplished with two techniques:

- complete excision of the entire atrial septum except for a rim of the anterior limbus, in order to preserve the conduction system, followed by suture of a pericardial or synthetic patch as a repositioned atrial septum, leaving all three caval vein orifices on the right site of the patch;
- re-routing the coronary sinus to the roof of the left atrium, by using the incised atrial septum, and then reconstructing an atrial septum with a pericardial or synthetic patch.

Alternative surgical techniques consist of transection of the persistent left superior vena cava and its anastomosis to the right
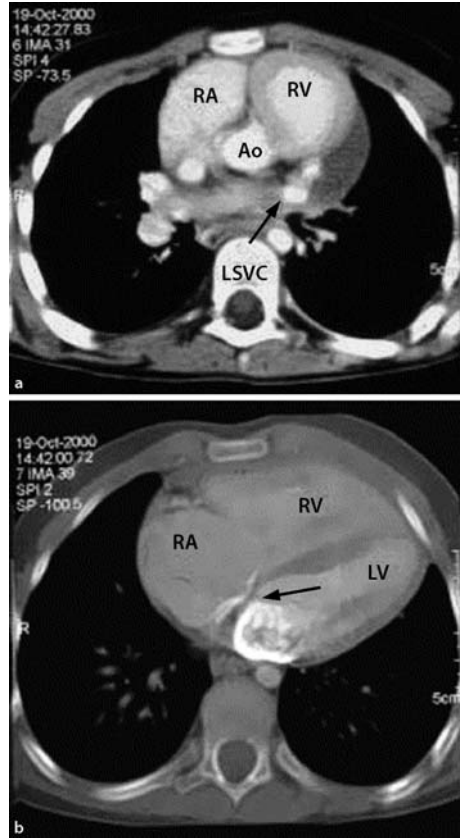
Fig. 3.4.1. Unroofed coronary sinus. CT scan, contrast angiography, axial views showing the persistent left superior vena cava (**a**) and the unroofed coronary sinus (**b**, arrow) (*Ao* aorta, *LSVC* persistent left superior vena cava, *LV* left ventricle, *RA* right atrium, *RV* right ventricle) (reproduced with permission from Brancaccio G, Miraldi F, Ventriglia F, Michielon G, di Donato RM, de Santis M (2003) Multidetector-row helical computed tomography imaging of unroofed coronary sinus. Int J Cardiol 91:251–253

superior vena cava, to the right auricular appendage, or directly to the left pulmonary artery.

■ Pre-operative information

The anatomy of the coronary sinus and its tributary veins can be evaluated using CT. The most frequent observation (63% of the cases) is the separate insertion of the coronary sinus and the small cardiac vein in the right atrium. The second most frequent appearance (29%) is the continuity of the anterior and posterior venous system at the crux cordis. Less frequent (8%) is the absence of a connection between the posterior interventricular vein and the coronary sinus.

When the presence of persistent left superior vena cava is diagnosed, especially if associated with situs abnormalities, an unroofed coronary sinus always has to be ruled out and this could be a difficult task with echocardiography. In these cases, CT scan (Fig. 3.4.1) and MRI (Fig. 3.4.2) should be considered as the first-line diagnostic tools due to the high resolution images, independent of body size and the location of the targeted structure. A few reports have been published regarding CT and MRI diagnosis of unroofed coronary sinus, generally associated with complex congenital heart disease. However, unroofed coronary sinus is often an intraoperative finding.
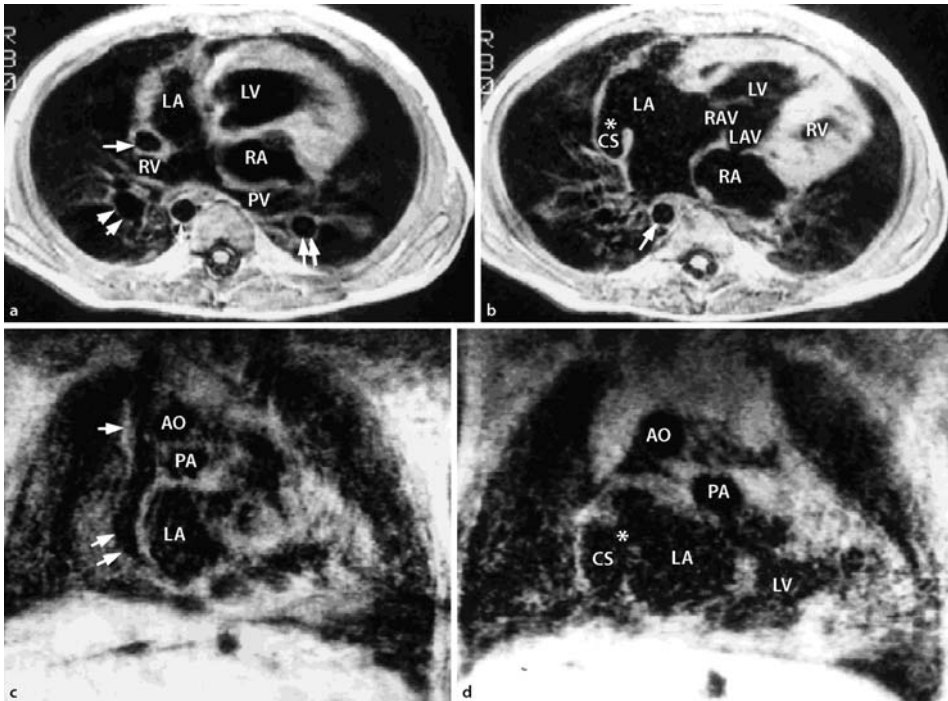
Fig. 3.4.2. Unroofed coronary sinus (reproduced with permission from Hahm JK, Park YW, Lee JK, Choi JY, Sul JH, Lee SK, Cho BK, Choe KO (2000) Magnetic resonance imaging of unroofed coronary sinus: three cases. Pediatr Cardiol 21:382–387)
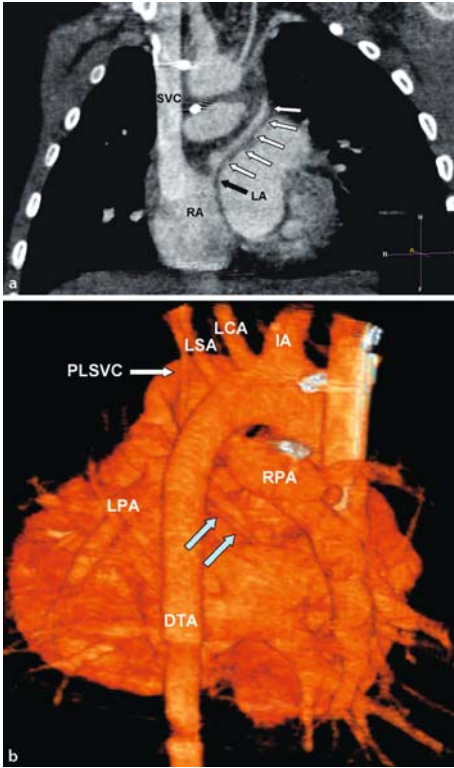
Fig. 3.4.3. Status post repair of unroofed coronary sinus. **a** CT scan, contrast angiography, coronal projection showing the reconstruction of the unroofed coronary sinus with a patch creating a tunnel inside the left atrial chamber (white arrows) to deviate the venous return of the persistent left superior vena cava to a new connection with the right atrium (black arrow). **b** CT scan in the same patient, with 3-dimensional reconstruction contrast angiography, posterior coronal projection showing the reconstruction of the unroofed coronary sinus with a patch creating a tunnel inside the left atrial chamber (blue arrows) to deviate the venous return of the persistent left superior vena cava to the right atrium (*DTA* descending thoracic aorta, *IA* innominate artery, *LA* left atrium, *LCA* left carotid artery, *LPA* left pulmonary artery, *LSA* left subclavian artery, *PLSVC* persistent left superior vena cava, *RA* right atrium, *RPA* right pulmonary artery, *SVC* superior vena cava) (photographs courtesy of Dr. Mohamed Tawil)
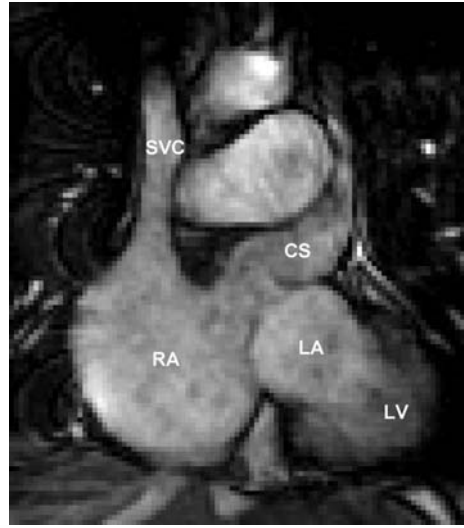
Fig. 3.4.4. Unroofed coronary sinus, status post repair. MR angiography with maximal intensity projection reconstruction showing the coronary sinus re-routing to the right atrium (*CS* coronary sinus, *LA* left atrium, *LV* left ventricle, *RA* right atrium, *SVC* superior vena cava)

■ Potential complications

Obstruction of the persistent left superior vena cava and/or of the left pulmonary veins, residual or recurrent atrial septal defect, air embolism, supraventricular arrhythmias.

■ Post-operative follow-up

CT scan (Fig. 3.4.3) and MRI (Fig. 3.4.4) can be useful to visualize the surgical reconstruction with the deviation of the venous return from the persistent left superior vena cava to the right atrium, and to rule out the presence of residual obstructions and/or intracardiac shunts.

■ References

Brancaccio G, Miraldi F, Ventriglia F, Michielon G, di Donato RM, de Santis M (2003) Multidetector-row helical computed tomography imaging of unroofed coronary sinus. Int J Cardiol 91:251–253

Hahm JK, Park YW, Lee JK, Choi JY, Sul JH, Lee SK, Cho BK, Choe KO (2000) Magnetic resonance imaging of unroofed coronary sinus: three cases. Pediatr Cardiol 21:382–387

Jongbloed MR, Lamb HJ, Bax JJ, Schuijf JD, de Roos A, van der Wall EE, Schalij MJ (2005) Noninvasive visualization of the cardiac venous system using multislice computed tomography. J Am Coll Cardiol 45:749–753

Nakatani S, Katsuki K, Miyatake K (2002) Images in cardiology: unroofed coronary sinus. Heart 87:278

Raghib G, Ruttenberger HD, Anderson RC, Amplatz K, Adams P, Edwards JE (1965) Termination of the left superior vena cava in left atrium, atrial septal defect, and absence of coronary sinus. A developmental complex. Circulation 31:906–918

▌ Definition

Types of atrioventricular septal defect accordingly with the Anderson classification:

▐ *Separate atrioventricular orifices, shunting at the atrial level*: ostium primum defect, three leaflet left atrioventricular valve (so-called mitral valve with cleft anterior leaflet).

▐ *Separate atrioventricular orifices, shunting at the atrial and ventricular levels*: ostium primum defect, space between superior and inferior bridging leaflets of the left atrioventricular valve, inlet ventricular septal defect partially or almost completely closed by fibrous tissue of the atrioventricular valve.

▐ *Common atrioventricular orifice, shunting at atrial and ventricular levels*: ostium primum defect, common atrioventricular valve, unrestrictive inlet ventricular septal defect (Fig. 3.5.1).

Associated anomalies

Patent ductus arteriosus, tetralogy of Fallot or double outlet right ventricle with ventriculo-arterial concordance (more frequent in Down's syndrome), left ventricular outflow tract obstruction (more frequent in patients with separate atrioventricular orifices and those without Down's syndrome), unbalanced ventricles (right ventricular dominance more frequent in patients without Down's syndrome), persistent left superior vena cava with or without unroofed coronary sinus, additional muscular ventricular septal defects, accessory left atrioventricular valve, single papillary muscle in the left ventricle.

▌ Surgical options

In the presence of a complex anatomical situation, like right or left ventricular dominance, or associated cardiac malformations (e.g., aortic coarctation or aortic arch interruption) or in patients very ill because of repeated infections and/or associated noncardiac malformations, the palliative approach with pulmonary artery banding can be considered as an alternative. Pulmonary artery banding can be accomplished with the conventional technique of implanting a tape around the main pulmonary artery or with a telemetrically adjustable device (FloWatch®, EndoArt, Lausanne, Switzerland).

In all cases the surgical approach for repair is from a right atriotomy. In the case of the double patch technique, a prosthetic patch (PTFE, Dacron, Teflon) is used for the ventricular component and a biological patch (autologous or heterologous pericardium) for the atrial component. In the case of the single patch technique, either a prosthetic or biological patch is used according to the surgical preferences.

▐ *Separate atrioventricular orifices, shunting at the atrial level:* patch closure of ostium primum ± suture of the space between the bridging leaflets ("cleft").

▐ *Separate atrioventricular orifices, shunting at atrial and ventricular levels:* as above with patch closure of the ventricular septal defect.
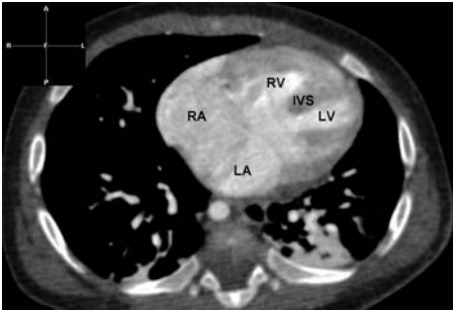
Fig. 3.5.1. Atrioventricular septal defect. CT scan, 4-chamber view, showing the complete atrioventricular septal defect (*IVS* inter-ventricular septum, *LA* left atrium, *LV* left ventricle, *RA* right atrium, *RV* right ventricle) (photograph courtesy of Dr. Mohamed Tawil)

■ *Common atrioventricular orifice, shunting at atrial and ventricular levels:*
single patch closure of atrial and ventricular septal defects, division of the bridging leaflets and resuspension to the patch, with or without suture of the so-called "cleft"
or:
double patch closure of atrial and ventricular septal defects, bridging leaflets "sandwiched" between atrial and ventricular patches, with or without suture of the so-called "cleft".

In both techniques: test the competence of the left atrioventricular valve with injection of saline solution under pression in the left ventricle; in case of significant regurgitation, adjust the repair by shifting the valvular leaflets with additional sutures; caution should be used to avoid creating left atrioventricular valvular stenosis or subvalvular aortic stenosis.

■ **Pre-operative information**

Pre-operative echocardiographic evaluation of patients with atrioventricular septal defect generally provides enough information for the decision-making process without the requirement for other investigations, unless associated cardiac malformations or the presence of elevated pulmonary vascular resistance are suspected.

Cardiac MRI could be useful in case of isomerism, not rare in such patients, in order to delineate systemic and pulmonary venous connections, and whenever more anatomical details are requested, such as in other congenital heart defects. The goal of MRI, therefore, is to visualize the systemic and pulmonary venous connections, quantify the ventricular volumes and functions particularly in unbalanced ventricular chambers, visualize the left ventricular outflow tract, and determine the precise relationship between the ventricular septal defect and the ventricular outflow tract.

To achieve these goals we propose the following cardiac MRI protocol:
■ 3-plane localizing images,
2-dimensional axial Time-of-flight Angiography (see the appendix in the "Introduction"),
■ ECG-gated cine steady-state free precession sequences in the 2-chamber and 4-chamber planes, and ventricular short axis for the quantitative assessment of both the ventricular dimensions, function and stroke volume (Fig. 3.5.2), as illustrated in the appendix of the "Introduction",
■ ECG-gated cine steady-state free precession and static fast spin echo sequences on additional planes are often required to better determine the anatomy of the ostium primum defect (Figs. 3.5.2 and 3.5.3), the location of the coronary sinus, the anatomy of the ventricular septal defect (Fig. 3.5.4) and its relationship with the great arteries,
■ ECG-gated cine steady-state free precession double-oblique sequences on two perpendicular planes to visualize the left ventricular outflow tract (Fig. 3.5.2),
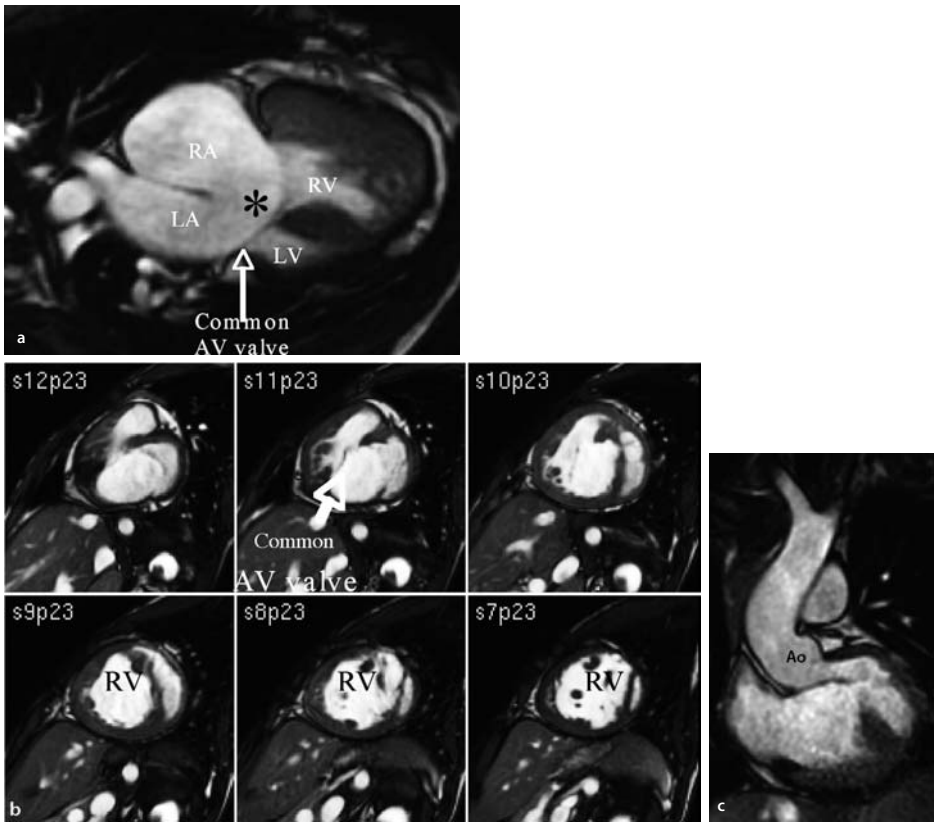
Fig. 3.5.2. Atrioventricular septal defect with common atrioventricular orifice and hypoplastic left ventricle. MRI cine steady-state free precession 4-chamber view (**a**) and ventricular short-axis view (**b**) showing the ostium primum defect (asterisk) and the presence of hypoplastic left ventricle; cine steady-state free precession double-oblique sequences of left ventricular outflow tract showing the typical goose-neck appearance of the left ventricular outflow tract (**c**) (*Ao* aorta, *LA* left atrium, *LV* left ventricle, *RA* right atrium, *RV* right ventricle)
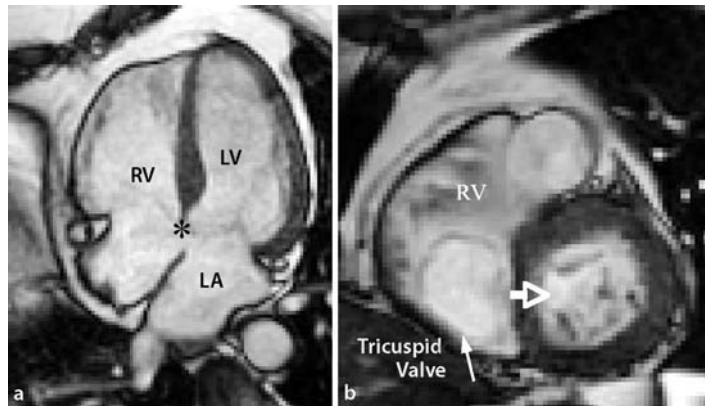
Fig. 3.5.3. Atrioventricular septal defect with two separate atrioventricular valves orifice. MRI cine steady-state free precession 4-chamber view (**a**) and ventricular short-axis view (**b**) showing an atrioventricular septal defect with separate atrioventricular orifices without ventricular component, ostium primum atrial septal defect (asterisk) and cleft of the mitral valve (arrow) (*LA* left atrium, *LV* left ventricle, *RV* right ventricle)
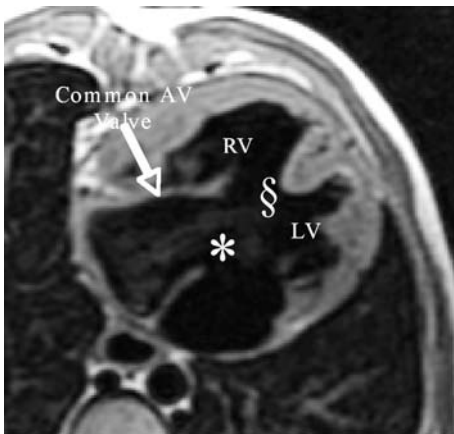
Fig. 3.5.4. Atrioventricular septal defect with single atrioventricular orifice. MRI fast spin echo 4-chamber view showing the common atrioventricular valve, a large ostium primum defect (asterisk) and a huge ventricular septal component (§) (*LV* left ventricle, *RV* right ventricle)

■ ECG-gated phase velocity contrast MRI sequences perpendicular to the main pulmonary artery and ascending aorta to calculate the QP/QS,

■ Gadolinium-enhanced 3-dimensional MRA for the evaluation of pulmonary and systemic venous connections if required.

■ Potential complications

Residual or recurrent atrial and/or ventricular septal defect, complete atrioventricular block, left atrioventricular valvar regurgitation and/or stenosis, left ventricular outflow tract obstruction, pulmonary arterial hypertensive crisis.

■ Post-operative follow-up

Post-operative echocardiography after repair of atrioventricular septal defect generally provides all the required information on the adequacy of the surgical procedure.

MRI could be useful in the presence of residual intracardiac defect to quantitate the residual intracardiac shunt, to evaluate resid-
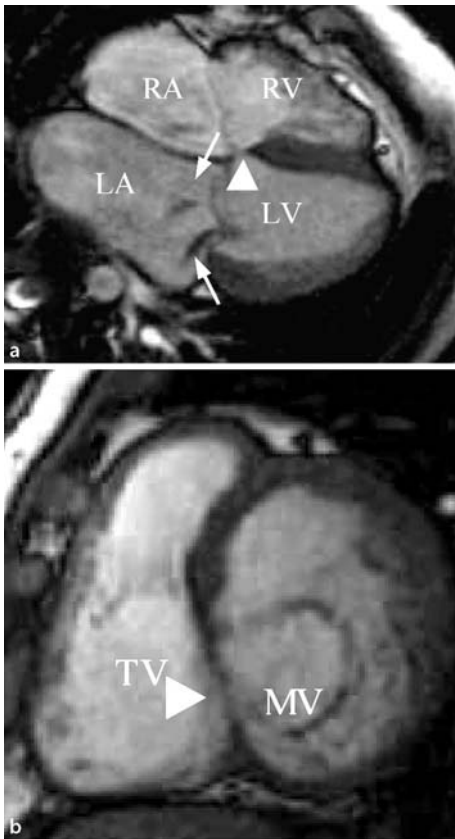
Fig. 3.5.5. Status post repair of atrioventricular septal defect with common atrioventricular valve. MRI cine steady-state free precession 4-chamber view in systole (**a**) and short axis at the atrioventricular valve level in diastole (**b**). Note the surgical patch (arrowhead) separating the mitral and tricuspid valves, and also two systolic jets of mitral valve regurgitation in the left atrium (arrow) (*LA* left atrium, *LV* left ventricle, *MV* mitral valve, *RA* right atrium, *RV* right ventricle, *TV* tricuspid valve)

ual atrioventricular valve regurgitation (Fig. 3.5.5), to visualize the left ventricular outflow tract and to quantify the ventricular volumes and functions particularly in unbalanced ventricular chambers.

■ References

Backer CL, Stewart RD, Mavroudis C (2007) Overview: history, anatomy, timing, and results of complete atrioventricular canal. Semin Thorac Cardiovasc Surg Pediatr Card Surg Ann 10:3–10

Beerbaum P, Korperich H, Barth P, Esdorn H, Gieseke J, Meyer H (2001) Noninvasive quantification of left-to-right shunt in pediatric patients: phase-contrast cine magnetic resonance imaging compared with invasive oximetry. Circulation 103:2476–2482

Bonnet D, Corno AF, Sidi D, Sekarski N, Beghetti M, Schulze-Neick I, Fasnacht M, Le Bret E, Kalangos A, Vouhé PR, von Segesser LK (2004) Early clinical results of telemetric adjustable pulmonary artery banding FloWatch®-PAB. Circulation 110:II-158–163

Cohen GA, Stevenson JG (2007) Intraoperative echocardiography for atrioventricular canal: decision-making for surgeons. Semin Thorac Cardiovasc Surg Pediatr Card Surg Ann 10:47–50

Corno AF, Marino B, Catena G, Marcelletti C (1988) Atrioventricular septal defects with severe left ventricular hypoplasia. Staged palliation. J Thorac Cardiovasc Surg 96:249–252

Corno AF, Sekarski N, Bernath MA, Payot M, Tozzi P, von Segesser LK (2003) Pulmonary artery banding: long-term telemetric adjustment. Eur J Cardiothorac Surg 23:317–322

Corno AF, Bonnet D, Sekarski N, Sidi D, Vouhé P, von Segesser LK (2003) Remote control of pulmonary blood flow: initial clinical experience. J Thorac Cardiovasc Surg 126:1775–1780

Corno AF, Prosi M, Fridez P, Zunino P, Quarteroni A, von Segesser LK (2006) The non-circular shape of FloWatch-PAB prevents the need for pulmonary artery reconstruction after banding. Computational fluid dynamics and clinical correlations. Eur J Cardiothorac Surg 29:93–99

Corno AF, Ladusans EJ, Pozzi M, Kerr S (2007) FloWatch® versus conventional pulmonary artery banding. J Thorac Cardiovasc Surg 134:1413–1419

Crawford FA, Stroud MR (2001) Surgical repair of complete atrioventricular septal defect. Ann Thorac Surg 72:1621–1628

Goo HW, Park IS, Ko JK, Kim YH, Seo DM, Yun TJ, Park JJ, Yoon CH (2003) CT of congenital heart disease: normal anatomy and typical pathologic conditions. Radiographics 23:S147–165

Marino B, Vairo U, Corno AF, Nava S, Guccione P, Calabrò R, Marcelletti C (1990) Atrioventricular canal in Down syndrome. Am J Dis Child 144:1120–1122

▮ Definition

▮ *Perimembranous ventricular septal defect:* the membranous septum is very small, therefore, ventricular septal defects usually extend into the surrounding muscle septum, and this is called perimembranous ventricular septal defect;
this type of ventricular septal defect is the most common after infancy, accounting for 75% of all ventricular septal defects; defect surrounding the membranous septum, at the meeting point of the three right ventricular components (inlet, apical trabecular and outlet); the diagnostic feature is fibrous continuity between the leaflets of the aortic and tricuspid valves; can extend to open mostly to the inlet or outlet of the right ventricle, or can be confluent,
juxta-crux ventricular septal defect: particular posterior perimembranous defect associated with straddling and overriding of the tricuspid valve; diagnostic feature is malalignment between the atrial and ventricular septum.

▮ *Muscular ventricular septal defect:* this is the second most common type of ventricular septal defect after infancy; in infancy, muscular ventricular septal defect is the most frequent type, but most of them, very small in size, undergo complete spontaneous closure; a defect, which has completely muscular rims, can be situated anywhere within the septum, but can be subdivided into those opening to the inlet, trabecular or outlet components of the right ventricle.

▮ *Doubly committed juxtaarterial ventricular septal defect:* defect limited superiorly by fibrous continuity between the leaflets of the pulmonary and aortic valves, because of absence of the outlet septum and the septal component of the subpulmonary infundibulum; can have a muscular posterior rim or can extend to become perimembranous.

▮ *Multiple ventricular septal defects*: combination of multiple muscular defects or of one or more muscular defect(s) co-existing with perimembranous or juxtaarterial defects.

▮ *Inlet ventricular septal defects*: (see chapter "Atrioventricular septal defects")

A ventricular septal defect may coexist with nearly all varieties of congenital heart disease, but the interventricular communication is only considered the primary lesion when the left-to-right shunt at the ventricular level is the dominant hemodynamic lesion.

Atrial septal defect, partial (or total) anomalous pulmonary venous connection, infundibular or pulmonary valvular stenosis, double-chambered right ventricle, mitral stenosis, discrete (fibrous) subvalvar aortic stenosis, aortic valvular regurgitation (Laubry-Pezzi syndrome), aneurysm of the sinuses of Valsalva (right coronary sinus is the most common), patent ductus arteriosus, aortic coarctation, aortic arch hypoplasia or interruption are the commonest lesions which complicate ventricular septal defect seen as the primary lesion.

￭ Surgical options

In the presence of complex anatomical situations (e.g., like multiple ventricular septal defects), associated cardiac malformations (e.g., aortic coarctation or aortic arch interruption) or in patients very ill because of repeated infections and/or associated non-cardiac malformations, the palliative approach with pulmonary artery banding can be considered as an alternative. Pulmonary artery banding can be accomplished with the conventional technique of implanting a tape around the main pulmonary artery or with a telemetrically adjustable device (FloWatch®, EndoArt, Lausanne, Switzerland).

For the surgical repair, the defect is generally closed with a patch (heterologous pericardium, PTFE, Dacron, Teflon) sutured with interrupted or running sutures, according to the surgeon's preferences. Direct closure with pledgeted interrupted sutures (reinforced) is used only for very small defects.

￭ *Perimembranous ventricular septal defect:*
 – patch closure of the defect through a right atriotomy with tricuspid valve retraction (or rarely disinsertion),
 – patch closure through right ventriculotomy in case of associated infundibular obstruction requiring right ventriculotomy for relief.

￭ *Muscular ventricular septal defect:*
 – patch closure of the defect through a right atriotomy with tricuspid valve retraction,
 – more rarely through a right ventriculotomy,
 – very rarely through an apical left ventriculotomy.

￭ *Doubly committed juxtaarterial ventricular septal defect:* patch closure of the defect through a right atriotomy with tricuspid retraction or through an aortotomy or through an incision of the main pulmonary artery, based on the position of the defect and its relationship with the semilunar valves, with the need for treatment of prolapsed aortic leaflet or of a right ventricular outflow tract enlarge-

ment, and with the size of the ascending aorta.

￭ *Multiple ventricular septal defects:*
 – multiple or large single patch closure of the defects through a right atriotomy,
 – more rarely through a right ventriculotomy,
 – very rarely through an apical left ventriculotomy.

￭ Preoperative information

Transthoracic echocardiography is the primary diagnostic imaging modality in patients with suspected or known ventricular septal defects, in order to provide information on the location and extent of the defect, and on the potential presence of associated cardiac malformations. Echocardiography is usually also sufficient for the decision-making process related to the patient's management.

MRI and CT scan can be useful in defining the location of the ventricular septal defect in order to distinguish between perimembranous ventricular septal defect (Fig. 3.6.1), muscular (Fig. 3.6.2), doubly committed juxtaarterial, and inlet type of ventricular septal defect.
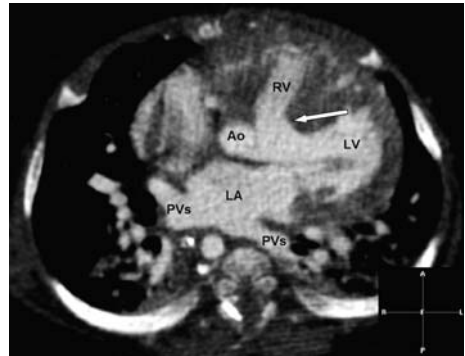
Fig. 3.6.1. Ventricular septal defect. CT scan, axial view, showing a large perimembranous subaortic ventricular septal defect (arrow) (*Ao* aorta, *LA* left atrium, *LV* left ventricle, *PVs* pulmonary veins, *RV* right ventricle)
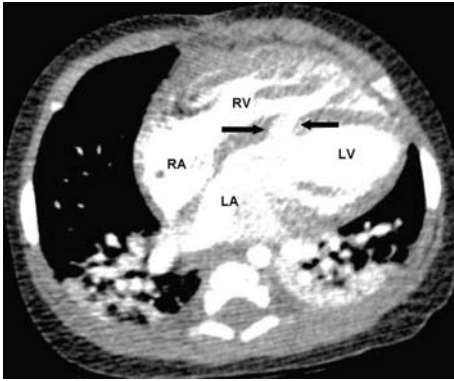
Fig. 3.6.2. Ventricular septal defect. CT scan, axial 4-chamber view, showing a midmuscular ventricular septal defect (arrows) (*LA* left atrium, *LV* left ventricle, *RA* right atrium, *RV* right ventricle)

MRI is useful to noninvasively quantify the intracardiac shunt, specially in the presence of small ventricular septal defects with borderline indications for repair, as well as in patients with a poor acoustic window for echocardiography.

MRI in fact, thanks to its capability to 3-dimensionally image the intracardiac anatomy with high resolution, can also provide useful anatomical details on the ventricular septal defect, particularly related to its position as well as its relationship to adjacent key structures, such as atrioventricular or semilunar valves, and the potential association of intracardiac lesions, such as prolapsed aortic valve leaflets. This can be particularly useful for the decision-making process with respect to the choice of the technique to close the ventricular septal defect,
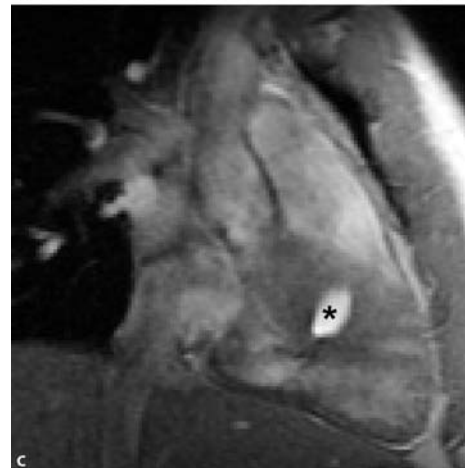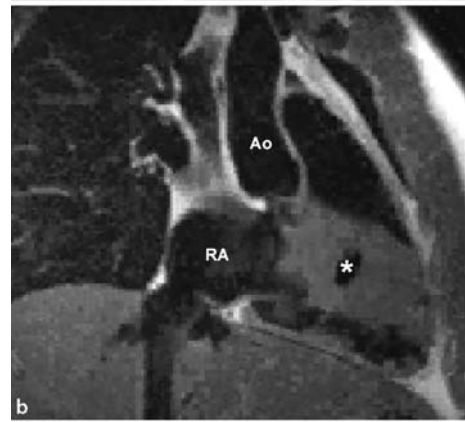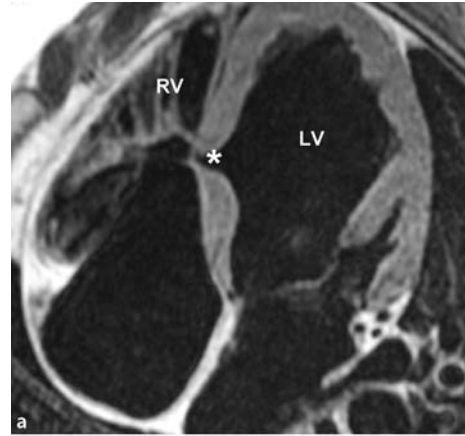
Fig. 3.6.3. Muscular ventricular septal defect. MRI fast spin echo 4-chamber view (**a**) showing a small muscular ventricular septal defect (asterisk); the same defect viewed *en face* from the right ventricular aspect in fast spin echo (**b**) and cine steady-state free precession (**c**). The left-to-right shunt (QP/QS) evaluated by phase velocity mapping at the aortic and pulmonary artery level was 1.4:1. This defect was scheduled for percutaneous interventional closure (*Ao* aorta, *LV* left ventricle, *RA* right atrium, *RV* right ventricle)

percutaneous interventional or surgical technique, or in case of complex anatomy.

To achieve these goals the cardiac MRI protocol is the following:

■ 3-plane localizing images,

■ 2-dimensional axial Time-of-flight Angiography (see appendix in the "Introduction"),

■ ECG-gated cine steady-state free precession sequences for quantitative assessment of both ventricular dimensions and func-

tion, and for calculation of stroke volumes, following the steps as indicated in the "Introduction",

■ ECG-gated cine steady-state free precession and fast spin echo sequences on additional planes are often required to better
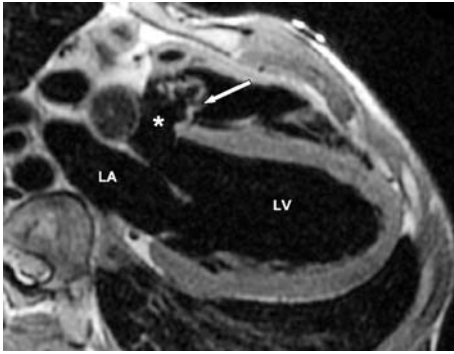
Fig. 3.6.4. Perimembranous ventricular septal defect. MRI fast spin echo 3-chamber view of perimembranous septal defect (asterisk), partially closed by fibrous accessory tissue (arrow). The left-to-right shunt (QP/QS) evaluated by phase velocity mapping was 1.2:1. The left ventricular volume was in the normal range (Z-value in diastole = +1) (LA left atrium, LV left ventricle)
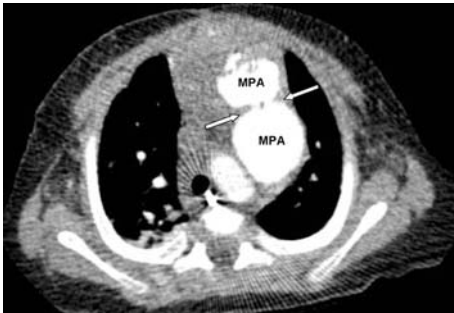
Fig. 3.6.5. Ventricular septal defect, status post pulmonary artery banding. CT scan, axial projection, showing the indentation of the pulmonary artery banding on the main pulmonary artery (arrows)

Fig. 3.6.6. Multiple ventricular septal defect, status post pulmonary artery banding. Cine steady-state free precession right ventricular outflow tract MRI showing a narrow pulmonary banding (asterisk) (RV right ventricle)
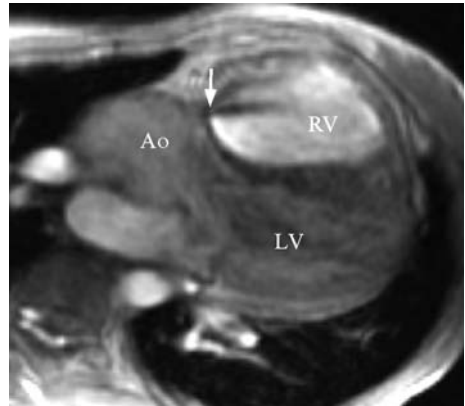
Fig. 3.6.7. Small residual ventricular septal defect. Cine gradient MRI 3-chamber view showing a narrow jet (arrow) through a small residual leak around the patch used to close the ventricular septal defect. The left-to-right shunt (QP/QS) evaluated by phase velocity mapping was 1.45:1 (Ao aorta, LV left ventricle, RV right ventricle)
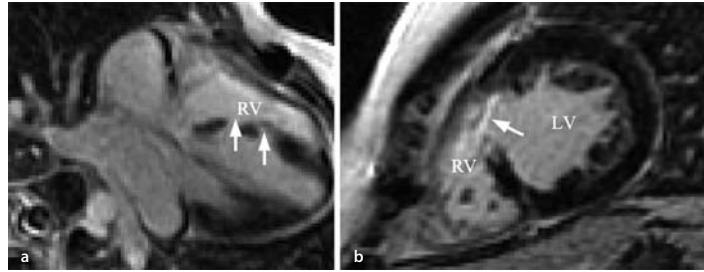
Fig. 3.6.8. Ventricular septal necrosis, status post closure of ventricular septal defect. Post gadolinium delayed enhancement MRI after surgical closure of a ventricular septal defect, showing a large area of transmural fibrosis (**a, b**) in the anterior part of the interventricular septum (arrows) corresponding to a dyskinetic area at the cine sequence (*LV* left ventricle, *RV* right ventricle)
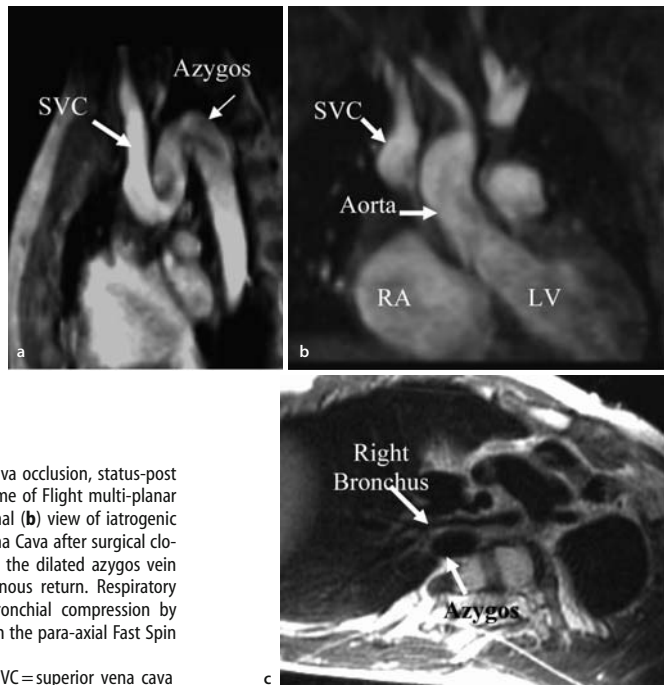
Fig. 3.6.9. Iatrogenic superior vena cava occlusion, status-post closure of ventricular septal defect. Time of Flight multi-planar reformatted MRI sagittal (**a**) and coronal (**b**) view of iatrogenic complete occlusion of the Superior Vena Cava after surgical closure of ventricular septal defect. Note the dilated azygos vein draining all the superior systemic venous return. Respiratory symptoms were due to the right bronchial compression by the dilated azygos vein, as illustrated in the para-axial Fast Spin Echo imaging (**c**).
LV = left ventricle, RA = right atrium, SVC = superior vena cava

define the anatomy of the ventricular septal defect along its axis and *en face* as well as its relationship with the great arteries, the atrioventricular valves and the adjacent structures; however very small defects may be difficult to resolve. In these cases, since turbulent high velocity flow is always present, it can be useful to use gradient echo enhanced sequences (instead of steady-state free precession), provided that the echo time is long enough to allow for sufficient spin de-phasing,

- ECG-gated double-oblique cine steady-state free precession and fast spin echo sequences on two perpendicular planes can visualize the left ventricular outflow tract and provide details of perimembranous ventricular septal defect (Figs. 3.6.3 and 3.6.4),
- ECG-gated phase velocity contrast MRI sequences perpendicular to the main pulmonary artery and ascending aorta to assess the QP/QS, and the potential presence of aortic valve regurgitation,

▪ Potential complications

Residual or recurrent ventricular septal defect, complete atrioventricular block, pulmonary arterial hypertensive crisis, residual or recurrent aortic valve regurgitation.

▪ Postoperative follow-up

Clinical and echocardiographic evaluations are usually sufficient in the postoperative follow-up of ventricular septal defects. CT scan and particularly cardiac MRI could be useful to show the result of palliation with pulmonary artery banding (Figs. 3.6.5 and 3.6.6), to quantify a residual intracardiac shunt (Fig. 3.6.7), to demonstrate the presence and quantify a residual/recurrent aortic regurgitation, and in case of unusual iatrogenic postoperative complications (Figs. 3.6.8 and 3.6.9).

▪ References

Baker EJ, Ayton V, Smith MA, Parsons JM, Ladusans EJ, Anderson RH, Maisey MN, Tynan M, Fagg NL, Deverall PB (1989) Magnetic resonance imaging at high field strength of ventricular septal defects in infants. Br Heart J 62:305–310

Beerbaum P, Korperich H, Barth P, Esdorn H, Gieseke J, Meyer H (2001) Noninvasive quantification of left-to-right shunt in pediatric patients: phase-contrast cine magnetic resonance imaging compared with invasive oximetry. Circulation 103:2476–2482

Bonnet D, Corno AF, Sidi D, Sekarski N, Beghetti M, Schulze-Neick I, Fasnacht M, Le Bret E, Kalangos A, Vouhé PR, von Segesser LK (2004) Early clinical results of telemetric adjustable pulmonary artery banding FloWatch®-PAB. Circulation 110:II-158–163

Cicini MP, Giannico S, Marino B, Iorio FS, Corno AF, Marcelletti C (1992) "Acquired" subvalvular aortic stenosis after repair of a ventricular septal defect. Chest 101:115–118

Corno AF, Sekarski N, Bernath MA, Payot M, Tozzi P, von Segesser LK (2003) Pulmonary artery banding: long-term telemetric adjustment. Eur J Cardiothorac Surg 23:317–322

Corno AF, Bonnet D, Sekarski N, Sidi D, Vouhé P, von Segesser LK (2003) Remote control of pulmonary blood flow: initial clinical experience. J Thorac Cardiovasc Surg 126:1775–1780

Corno AF, Prosi M, Fridez P, Zunino P, Quarteroni A, von Segesser LK (2006) The non-circular shape of FloWatch-PAB prevents the need for pulmonary artery reconstruction after banding. Computational fluid dynamics and clinical correlations. Eur J Cardiothorac Surg 29:93–99

Corno AF, Ladusans EJ, Pozzi M, Kerr S (2007) FloWatch® versus conventional pulmonary artery banding. J Thorac Cardiovasc Surg 134:1413–1419

Funabashi N, Rubin GD (2000) Qualitative blood flow differentiation: depiction of a left to right cardiac shunt across a ventricular septal defect using electron-beam computed tomography. Jpn Circ J 64:901–903

Goo HW, Park IS, Ko JK, Kim YH, Seo DM, Yun TJ, Park JJ, Yoon CH (2003) CT of congenital heart disease: normal anatomy and typical pathologic conditions. Radiographics 23:S147–165

Harris MA, Johnson TR, Weinberg PM, Fogel MA (2007) Delayed-enhancement cardiovascular magnetic resonance identifies fibrous tissue in children after surgery for congenital heart disease. J Thorac Cardiovasc Surg 133:676–681

Khanna A, Litt HI (2004) ECG-gated MDCT of left-to-right shunt flow through a ventricular septal defect. Am J Roentgenol 183:1838

Kilner PJ, Sievers B, Meyer GP, Ho SY (2002) Double-chambered right ventricle or sub-infundibular stenosis assessed by cardiovascular magnetic resonance. J Cardiovasc Magn Reson 4:373–379

Marino B, Papa M, Guccione P, Corno AF, Marasini M, Calabrò R (1990) Ventricular septal defect in Down syndrome: anatomic types and associated malformations. Am J Dis Child 144:544–545

Marino B, Corno AF, Guccione P, Marcelletti C (1991) Ventricular septal defect and Down's syndrome. Lancet 337:245–246

Papa M, Santoro F, Corno AF (1993) Spontaneous closure of inlet ventricular septal defect in an infant with Down's syndrome and aortic coarctation. Chest 104:620–622

Ropers D, Regenfus M, Wasmeier G, Rost C, Ropers U, Achenbach S, Daniel WG (2007) Ventricular septum defect: imaging using computer tomography, mag-

netic resonance tomography and color Doppler echocardiography. Dtsch Med Wochenschr 132:769–770

Stauder NI, Miller S, Scheule AM, Ziemer G, Claussen CD (2001) MRI diagnosis of a previously undiagnosed large trabecular ventricular septal defect in an adult after multiple catheterizations and angiocardiograms. Br J Radiol 74:280

Trusler GA, Mustard WT (1972) A method of banding the pulmonary artery for large isolated ventricular septal defect with and without transposition of the great arteries. Ann Thorac Surg 13:351

Verhoye JP, Levin JM, Ihnken K, Miller DC (2004) Computed tomography angiographic demonstration of a ventricular septal defect. Eur J Cardiothorac Surg 26:1037

Wald RM, Powell AJ (2006) Simple congenital heart lesions. J Cardiovasc Magn Reson 8:619–631

Weber OM, Higgins CB (2006) MR evaluation of cardiovascular physiology in congenital heart disease: flow and function. J Cardiovasc Magn Reson 8:607–617

CHAPTER 3.7 Tetralogy of Fallot

▉ Definition

In anatomic terms, the malformation is characterized by four constant features: subpulmonary infundibular stenosis, ventricular septal defect, rightward deviation of the aortic valve with a biventricular origin of its leaflets, and right ventricular hypertrophy.

Although all hearts have comparable features, the malformation represents a morphological spectrum, with one morphological hallmark which unifies the overall entity: the anterocephalad deviation of the infundibular septum, the muscular structure separating the subaortic and pulmonary outlets, relative to the rest of the muscular septum.

Although unified in the sense of the septal malalignment, the patients with tetralogy of Fallot have significant variations in the precise anatomy of the ventricular septal defect, the nature of pulmonary infundibular and valvular stenosis, and the degree of aortic override, which account for the differences in hemodynamic consequences.

The ventricular septal defect is located in the membranous septum; it is subaortic and sometimes extends to the subpulmonic valve area. The ventricular septal defect is large, at least as large as the aortic valve, causing equalization of left and right ventricular pressures. The right ventricular outflow tract is hypoplastic and almost always obstructive. Occasionally at birth the right ventricular outflow tract shows no significant obstruction and results in the so-called "pink" tetralogy of Fallot. The pulmonary valve annulus is typically small in tetralogy of Fallot and the leaflets are deformed. In contrast to pulmonary valvular stenosis, the main pulmonary artery and the branch pulmonary arteries are small. There might be branch pulmonary artery stenosis as well as peripheral pulmonary artery stenosis in addition to the right ventricular outflow tract and pulmonary valvular stenosis. Bronchial arterial collaterals which connect to the peripheral pulmonary arteries are sometimes present. The main pulmonary artery is occasionally atretic and the pulmonary arteries are fed either by patent ductus arteriosus or collateral vessels. The aortic valve is typically large.

The most frequently associated anomalies are atrial septal defect or patent foramen ovale (40% of the patients), right aortic arch (25%), anomalous coronary arteries (10%), persistent left superior vena cava (8%), and major aortopulmonary collateral arteries with an extremely variable incidence, mostly correlated with the degree and duration of the cyanosis. Other associated malformations rarely reported are anomalous pulmonary venous connection, supravalvular mitral stenosis, cor triatriatum, atrioventricular septal defect, multiple ventricular septal defects, restrictive ventricular septal defect, hypoplastic or absent infundibular septum, fibromuscular subaortic stenosis, valvular aortic stenosis, valvular aortic regurgitation, aortopulmonary window, patent ductus arteriosus, aortic coarctation, vascular ring, non-confluent pulmonary arteries, and anomalous origin of the left subclavian artery.

■ Surgical options

■ **Palliative treatment:** systemic-to-pulmonary artery shunt, consisting in a classical (nowadays almost abandoned) or modified Blalock-Taussig anastomosis with interposition of a PTFE tubular prosthesis between the subclavian artery and the ipsilateral pulmonary artery.

■ **Repair:** consists of two main steps: a) patch closure of the ventricular septal defect from a transatrial-transpulmonary or from transventricular approach with longitudinal ventriculotomy; b) right ventricular outflow tract reconstruction. This can be performed with different techniques:

■ from the right atrium and/or from the pulmonary artery (transatrial-transpulmonary approach) or from the right ventricle (transventricular approach): incision with resection of the heavy trabeculations that bind the infundibular septum to the anterior right ventricular wall,

■ infundibular (pericardial or synthetic) patch enlargement (transventricular approach),

■ transannular (pericardial or synthetic, with or without monocusp) patch enlargement (transatrial-transpulmonary and transventricular approach) in case of inadequate size of the pulmonary valve annulus, measured with Hegar dilators, after pulmonary valvotomy performed from the pulmonary artery (transatrial-transpulmonary approach) or from the right ventricle (transventricular approach),

■ pulmonary arteries enlargement in case of inadequate size (measured with Hegar dilators), with prolongation of the transannular patch in case of an inadequate left pulmonary artery, with a separate patch in case of inadequate right pulmonary artery,

■ valved conduit, generally biologic, interposed between the right ventriculotomy and the pulmonary artery bifurcation, to bypass an anomalous coronary artery.

■ Pre-operative information

In addition to the demographic and clinical data, the following morphologic information is required in order to plan surgical *repair*:

■ size and morphology of entire right ventricular outflow tract, the pulmonary valve and annulus, the main pulmonary artery and its branches (Figs. 3.7.1 and 3.7.2),

■ the origin and course of the main coronary arteries (Fig. 3.7.3), particularly the presence of a major branch crossing the infundibulum,

■ the end-diastolic volume of the left ventricle.

To better plan a *palliative procedure*, generally a modified Blalock-Taussig shunt, the following information is required:

■ the side of the aortic arch (Fig. 3.7.2 c),

■ presence of an anomalous subclavian artery,

■ size and morphology of the pulmonary arteries, and in particular the presence of stenotic origin of one of them (Figs. 3.7.2 c and 3.7.4).

Fig. 3.7.1. Tetralogy of Fallot. CT scan, sagittal projection, showing severe obstruction of the right ventricular outflow tract, with practically pulmonary atresia (arrow); the size of the main pulmonary artery has been adequately maintained (diameter = 9.9 mm) by the presence of functioning modified Blalock-Taussig shunt (*LV* left ventricle, *RV* right ventricle) (photograph courtesy of Dr. Mohamed Tawil)
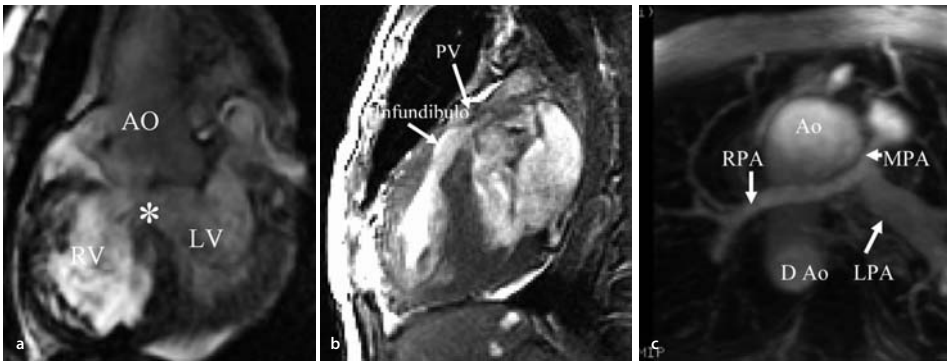
Fig. 3.7.2. Tetralogy of Fallot. Cardiac MRI with steady-state free precession showing (**a**) oblique projection with the aorta overriding a malalignment ventricular septal defect (asterisk), (**b**) sagittal projection with severe infundibular and pulmonary valve stenosis, and (**c**) 3-dimensional MR angiography, axial view, with severe hypoplasia of the main and right pulmonary artery, and the presence of right aortic arch (*AO* aorta, *DAo* descending aorta, *LPA* left pulmonary artery, *LV* left ventricle, *MPA* main pulmonary artery, *PV* pulmonary valve, *RPA* right pulmonary artery, *RV* right ventricle, *VSD* ventricular septal defect)
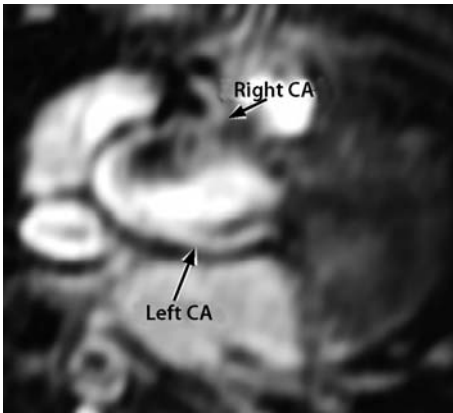

Fig. 3.7.3. Tetralogy of Fallot with normal coronary arteries. Cardiac MRI multiplanar reformatted time of flight acquisition showing normal origin and pattern of the coronary arteries in an infant with tetralogy of Fallot. Note the origin of the right coronary artery with anterior and leftward rotation (*CA* coronary artery)

While in infants echocardiography generally provides all the necessary diagnostic information for surgical palliation or repair, its role is limited in children and adolescents with tetralogy of Fallot, in whom the acoustic windows are frequently limited; CT scan and cardiac MRI are useful in both pre-operative and post-operative assessment of tetralogy of Fallot, with the focus of the investigations being different.

The CT scan and MRI can provide full visualization of the pulmonary arteries, particularly of the proximal segment of the left pulmonary artery, a frequent blind spot for both transthoracic and transesophageal echocardiography.

In most patients with tetralogy of Fallot, the central questions are to delineate all the sources of pulmonary blood flow (pulmonary arteries, aortopulmonary collaterals and ductus arteriosus) and the origin and course of the main coronary arteries (Fig. 3.7.3). Spin echo and 2-dimensional gradient echo cine MRI techniques provide excellent imaging of the central pulmonary arteries and major aortopulmonary collaterals. However, these MRI techniques require relatively long scan times for complete anatomical coverage, and small arteries (diameter less than 2 mm) may not be identified. Furthermore, these 2-dimensional techniques are suboptimal for imaging long and tortuous blood arteries, some of which arise from the brachiocephalic arteries or from the abdominal aorta. Con-
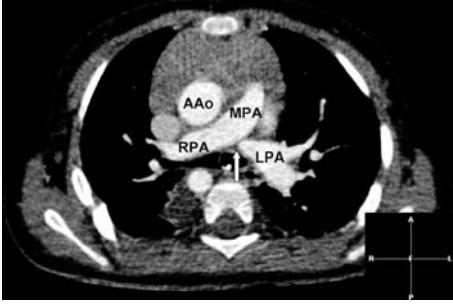
Fig. 3.7.4. Tetralogy of Fallot with stenotic origin of the left pulmonary artery. CT scan, axial projection, showing the severe stenosis at the origin of the left pulmonary artery (arrow) (*AAo* ascending aorta, *LPA* left pulmonary artery, *MPA* main pulmonary artery, *RPA* right pulmonary artery) (photograph courtesy of Dr. Mohamed Tawil)

trast CT scan and gadolinium-enhanced 3-dimensional MRI are ideally suited to image these arteries as well as the aortic arch sidedness and the subclavian artery for the pre-palliation evaluation (Fig. 3.7.2 c). Compared with conventional angiography, MRI have proved to be highly accurate in depicting all sources of pulmonary blood flow in patients with complex pulmonary stenosis or atresia, including infants with multiple small aortopulmonary collaterals.

When the origin and proximal course of the left and right coronary arteries are not known from other previous imaging studies, they should be imaged either by a gradient echo sequence designed for coronary imaging or by a fast spin echo sequence. Particular attention should be paid to rule out the presence of a major coronary artery crossing the right ventricular outflow tract.

The cardiac MRI protocol currently used in patients with tetralogy of Fallot is the following:
▪ 3-plane localizing images,
▪ 2-dimensional axial Time-of-flight Angiography (see the appendix in the "Introduction"),
▪ ECG-gated cine steady-state free precession sequences in 2-chamber, 4-chamber planes, and ventricular short axis for the

quantitative assessment of both ventricular dimensions, function and stroke volume, as illustrated in the appendix of the "Introduction",
▪ ECG-gated cine steady-state free precession and static fast spin echo sequences on additional planes to better delineate the morphology of the right ventricular outflow tract,
▪ ECG-gated static isotropic 3-dimensional steady-state free precession for the evaluation of origin and proximal course of the coronary arteries,
▪ Gadolinium-enhanced 3-dimensional MRI for the evaluation of the pulmonary arteries, as well as the side of the aortic arch and any abnormal source of pulmonary blood flow.

▪ Potential complications

▪ **Palliation (systemic-to-pulmonary artery shunt):** inadequate pulmonary blood flow (insufficient, excessive or nonhomogeneous), pulmonary artery distortion, inadequate growth of the pulmonary arteries, acquired pulmonary atresia.

▪ **Repair:** residual or recurrent ventricular septal defect (patch dehiscence or separate defect), residual or recurrent right ventricular outflow tract obstruction, complete atrioventricular block, arrhythmias, aneurysm of right ventricular outflow patch, pulmonary valve insufficiency.

Late complications after repair:
▪ *pulmonary valve regurgitation*: long standing pulmonary valve regurgitation, particularly after repair with transannular patch enlargement, can determine right ventricular dilatation and failure, with or without subsequent tricuspid valve regurgitation, requiring re-operation to insert a valve or a biological valve conduit in pulmonary valve position,
▪ *arrhythmias*: supraventricular and ventricular arrhythmias can occur years after repair, requiring treatment.

■ Post-operative follow-up

■ **After palliation:** Because the course of tortuous arteries of variable caliber can be seen in a single image, multidetector row CT or cardiac MRI with multiplanar and 3D volume rendering images are valuable to facilitate the identification of surgically created systemic-to-pulmonary artery shunts and the relationships of the shunts to the heart and to the pulmonary arteries (Fig. 3.7.5), and the presence of stenosis or kinking along the tubular prosthesis (Figs. 3.7.6 and 3.7.7).

Post-operative CT or MRI can demonstrate the presence of a false aneurysm at the level of the subclavian artery origin of a modified Blalock-Taussig shunt.

In the presence of a perigraft seroma (sterile collection of fluid in a nonsecretory wall surrounding the tubular prosthesis used for a modified Blalock-Taussig shunt), the conventional radiographic investigations show an opacification of the lung on the ipsilateral side of the modified Blalock-Taussig shunt, indistinguishable from lung atelectasis or infection, and a widening of the superior
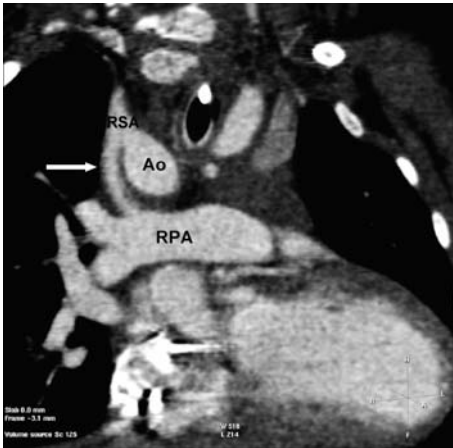
Fig. 3.7.5. Modified right Blalock-Taussig shunt. CT scan, right oblique anterior projection, showing the modified right Blalock-Taussig shunt (arrow) (*Ao* aorta, *RPA* right pulmonary artery, *RSA* right subclavian artery) (photograph courtesy of Dr. Mohamed Tawil)
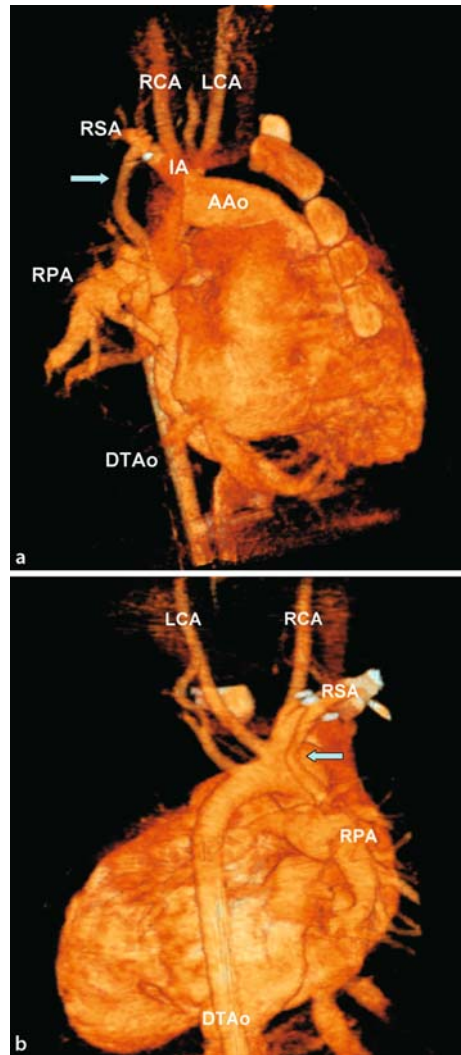
Fig. 3.7.6. a Modified Blalock-Taussig shunt. CT scan, 3-dimensional reconstruction, with right oblique view showing the modified Blalock-Taussig shunt, with a narrowing of the tubular prosthesis (arrow) implanted between the right subclavian and the right pulmonary artery. **b** CT scan, 3-dimensional reconstruction, with left oblique projection showing the modified Blalock-Taussig shunt, with a kinking of the tubular prosthesis (arrow) implanted between the right subclavian and the right pulmonary artery (*AAo* ascending aorta, *DTAo* descending thoracic aorta, *IA* innominate artery, *LCA* left carotid artery, *RCA* right carotid artery, *RPA* right pulmonary artery, *RSA* right subclavian artery) (photographs courtesy of Dr. Mohamed Tawil)
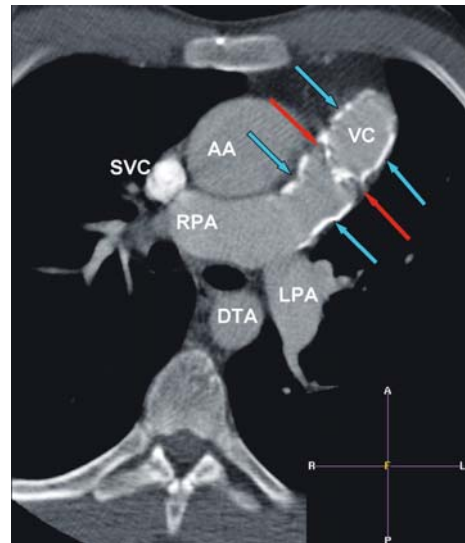
mediastinum. CT investigation instead can show a fluid collection of intermediate intensity surrounding or adjacent to the tubular prosthesis. After the administration of I.V. contrast medium, the capsule of the perigraft seroma shows slight enhancement, and the tubular prosthesis itself can be seen as a hyperdense structure adjacent to or transversing the perigraft seroma.

■ **After repair:** CT scan in the post-operative period can investigate the presence, the location and the extent of stenosis of the pulmonary arteries and also show the presence of an aneurysm of the right ventricular outflow tract, calcifications either in the right ventricular outflow tract or in the biological conduit used to reconstruct the continuity between the right ventricle and the pulmonary artery (Fig. 3.7.8).

Cardiac MRI is extensively used to assess patients of all ages after repair of tetralogy of Fallot, but its greatest clinical utility is in older children, adolescents and adults. Quantitative assessment of right and left ventricular dimensions and function is a key element of cardiac MRI evaluation in these patients. The presence and degree of right ventricular dysfunction is an important de-

Fig. 3.7.7. Modified right Blalock-Taussig shunt. MRI oblique fast spin echo (**a**) and volume rendering 3-dimensional gadolinium enhancement angiography (**b**) showing the modified right Blalock-Taussig shunt with severe stenosis of the right pulmonary artery at the level of the distal anastomosis of the shunt, good size left pulmonary artery with a mild kinking at its origin, and right aortic arch (*Ao* aorta, *BT* Blalock-Taussig, *LA* left atrium, *LPA* left pulmonary artery, *LV* left ventricle, *RPA* right pulmonary artery)

Fig. 3.7.8. Tetralogy of Fallot, status post repair with valved conduit. CT scan, axial projection showing the right ventricle to pulmonary artery valved conduit, with evident calcification on the wall (blue arrows) and on the valve (red arrows) (*AA* ascending aorta, *DTA* descending thoracic aorta, *LPA* left pulmonary artery, *RPA* right pulmonary artery, *SVC* superior vena cava, *VC* valved conduit)

terminant of clinical status late after repair of tetralogy of Fallot, and right ventricular dysfunction is also closely correlated with left ventricular dysfunction, likely through ventricular-ventricular interactions. The degree of pulmonary valve regurgitation measured by PVC-MRI (Fig. 3.7.9) is closely correlated with the degree of right ventricular dilation. Another factor affecting right ventricular function is the presence and extent of an aneurysm in the right ventricular outflow tract (Figs. 3.7.10–3.7.12).

Another technique increasingly used in these patients is post-gadolinium myocardial delayed enhancement for assessment of myocardial fibrosis (Fig. 3.7.13). The clinical significance of positive myocardial delayed enhancement in patients after repair of tetralogy of Fallot still requires further studies.

The goals of the cardiac MRI examination, therefore, include the following: quantitative assessment of left and right ventricular volumes, mass, stroke volumes, and ejection fraction; imaging of the morphology of the right ventricular outflow tract, pulmonary arteries, aorta, and aortopulmonary collaterals; quantification of pulmonary valve regurgitation, tricuspid regurgitation, pulmonary-to-systemic flow ratio (QP/QS) if there is a residual intracardiac shunt, and finally distribution of the pulmonary blood flow.

In patients after surgery for tetralogy of Fallot, the following cardiac MRI protocol is used:

- 3-plane localizing images,
- 2-dimensional axial Time-of-flight Angiography (see the appendix of the "Introduction"),
- ECG-gated cine steady-state free precession sequences in 2-chamber, 4-chamber planes, and ventricular short axis for the quantitative assessment of both ventricular dimensions, function and stroke volume as illustrated in the appendix of the "Introduction",
- ECG-gated cine steady-state free precession sequence on both frontal and sagittal view to evaluate the right ventricular outflow tract,
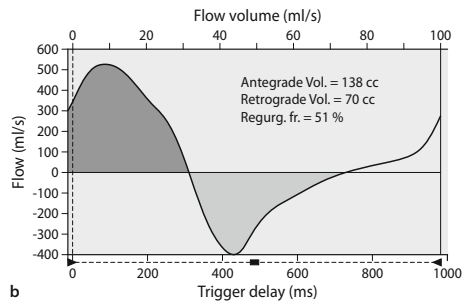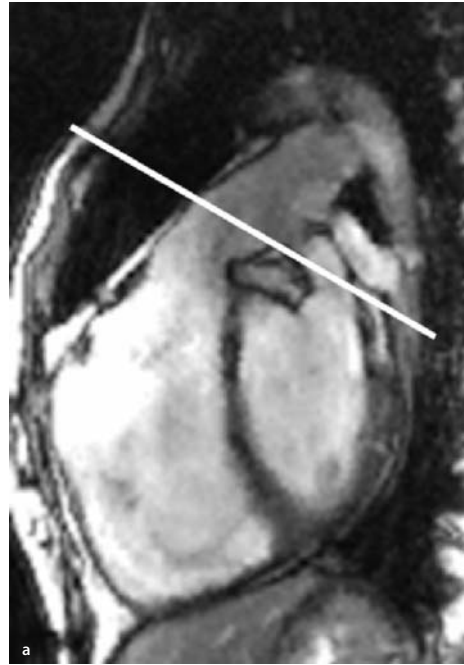
Fig. 3.7.9. Tetralogy of Fallot, status-post repair, pulmonary valve regurgitation. MRI quantification of the pulmonary valve regurgitation. **a** Sagittal projection, steady-state free precession of right outflow tract. A PVC MRI is prescribed perpendicular to the right outflow tract (white line). **b** Flow volume curve shows severe pulmonary valve regurgitation, with pulmonary regurgitation fraction = 51%
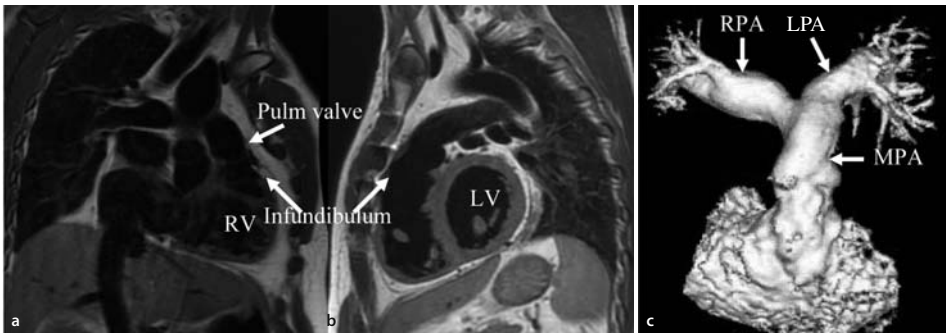
Fig. 3.7.10. Tetralogy of Fallot, status post repair with a transannular patch. MRI fast spin echo (black blood), para-coronal (**a**) and para-sagittal (**b**) projections showing the right ventricular outflow tract. **c** 3-dimensional volume rendering MR angiography showing right ventricular outflow tract and pulmonary arteries with adequate size and morphology (*LPA* left pulmonary artery, *LV* left ventricle, *MPA* main pulmonary artery, *RPA* right pulmonary artery, *RV* right ventricle)
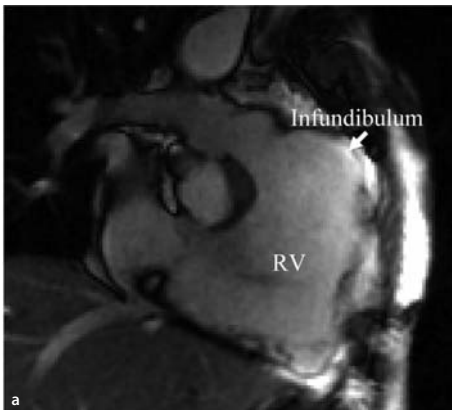
Fig. 3.7.11. Tetralogy of Fallot, status post repair with transannular patch. MRI steady-state free precession para-coronal right ventricular outflow tract (**a**) and main intensity projection MR angiography (**b**) showing a dilated infundibulum (*RV* right ventricle)
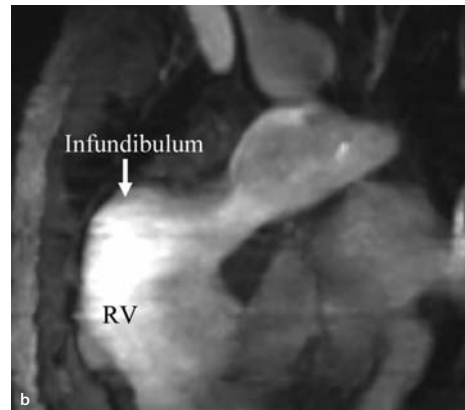
- ECG-gated cine steady-state free precession sequence along the long axis of both pulmonary arteries,
- ECG-gated cine steady-state free precession sequence double oblique 3-chambers for the evaluation of the left ventricle outflow tract and aortic root,
- Gadolinium-enhanced 3-dimensional MRI mainly for the right ventricular outflow tract and pulmonary arteries anatomy (Fig. 3.7.14), as well as for the assessment of any aortopulmonary collateral artery,
- ECG-gated PVC-MRI sequences perpendicular to the main, right and left pulmonary arteries and ascending aorta, and atrioventricular valves in order to assess flow patterns,
- Post-gadolinium delayed myocardial enhancement may be used to evaluate the presence of scar tissue (Fig. 3.7.13).
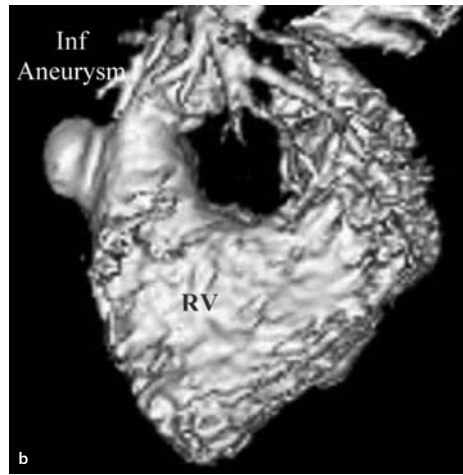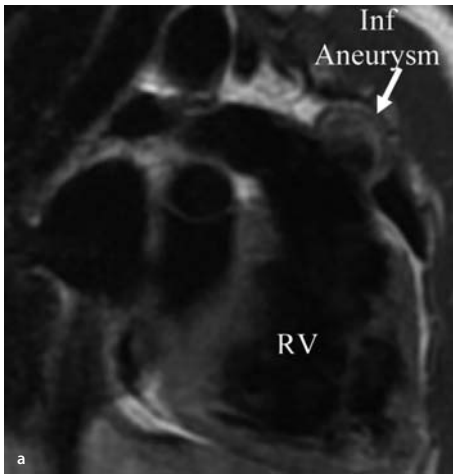
Fig. 3.7.12. Tetralogy of Fallot, status post repair, infundibular aneurysm. MRI with fast spin echo (black blood) para-coronal right ventricular outflow tract (**a**) and 3-dimensional volume rendering angiography (**b**) showing an aneurysm of the infundibular patch (arrow) (*Inf* infundibular, *RV* right ventricle)
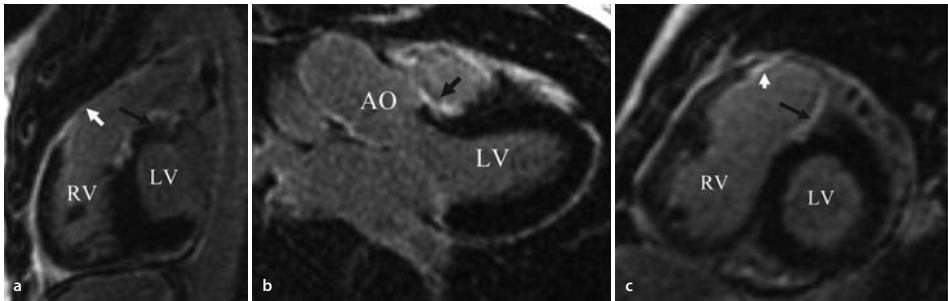
Fig. 3.7.13. Tetralogy of Fallot, status post repair. MRI sagittal projection (**a**), 3-chamber view (**b**) and ventricular short axis (**c**) showing the white strip appearance of the infundibular patch (white arrow) and of the patch for ventricular septal defect closure (black arrow), demonstrating delayed enhancement (*AO* aorta, *LV* left ventricle, *RV* right ventricle)

The timing of re-operation for reconstruction of right ventricular outflow tract in patients with previous repair of tetralogy of Fallot is still a matter of debate: ideally the indication should be not too late because of the risk of irreversible right ventricular dysfunction and fatal arrhythmias, but not too early because of the limited durability of any biological device used for right ventricular outflow tract reconstruction, particularly in young children.

Thanks to the use of cardiac MRI in a subset of patients, some cut-off points related to the indexed right ventricular volumes and ejection fractions are emerging for the indication to implant a pulmonary valve in the right ventricular outflow tract. However, the end-points of these cut-offs are generally based on the complete post-operative recovery of the right ventricular size to the normal value; this is not a suitable goal, when by dealing with patients who have un-
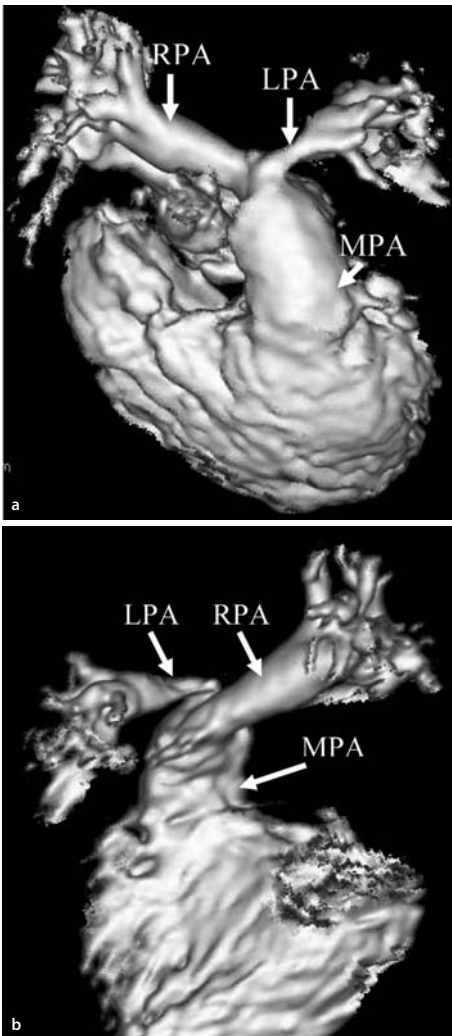
Fig. 3.7.14. Tetralogy of Fallot, status post repair, left pulmonary artery stenosis. MRI gadolinium angiography volume rendering 3-dimensional reconstruction, anterior (**a**) and posterior (**b**) view, showing severe stenosis at the origin of the left pulmonary artery (*LPA* left pulmonary artery, *MPA* main pulmonary artery, *RPA* right pulmonary artery)

dergone repair of tetralogy of Fallot, who had patch closure of the ventricular septal defect and another patch to enlarge the infundibulum. Moreover many other variables should be taken into consideration, such as right ventricular outflow tract with transannular patch extension with or without aneurysm, tricuspid valve regurgitation, elevated right ventricular systolic and/or diastolic pressure, and left ventricular function as well their evolution over time and other clinical and electrophysiological variables.

Thus, due to the accuracy of parameters and information obtained by cardiac MRI (some of which are not available by any other diagnostic investigation), nowadays it is inconceivable to make any decision on patients operated on for repair of tetralogy of Fallot without a previous targeted cardiac MRI investigation.

▪ References

Azevedo CF, Hadlich MS, Albuquerque DC, Moll JN (2006) Images in cardiovascular medicine. Untreated tetralogy of Fallot with pulmonary atresia: giant aneurysm of an aortopulmonary collateral artery demonstrated by magnetic resonance imaging. Circulation 113:293–294

Babu-Narayan SV, Kilner PJ, Li W, Moon JC, Goktekin O, Davlouros PA, Khan M, Ho SY, Pennell DJ, Gatzoulis MA (2006) Ventricular fibrosis suggested by cardiovascular magnetic resonance in adults with repaired tetralogy of Fallot and its relationship to adverse markers of clinical outcome. Circulation 113:405–413

Beekman RP, Beek FJ, Meijboom EJ (1997) Usefulness of MRI for the pre-operative evaluation of the pulmonary arteries in Tetralogy of Fallot. Magn Reson Imaging 15:1005–1015

Bernardes RJ, Marchiori E, Bernardes PM, Monzo Gonzaga MB, Simoes LC (2006) A comparison of magnetic resonance angiography with conventional angiography in the diagnosis of tetralogy of Fallot. Cardiol Young 16:281–288

Boechat MI, Ratib O, Williams PL, Gomes AS, Child JS, Allada V (2005) Cardiac MR imaging and MR angiography for assessment of complex tetralogy of Fallot and pulmonary atresia. Radiographics 25:1535–1546

Buechel ER, Dave HH, Kellenberger CJ, Dodge-Khatami A, Prêtre R, Berger F, Bauersfeld U (2005) Remodelling of the right ventricle after early pulmonary valve replacement in children with repaired tetralogy of Fallot: assessment by cardiovascular magnetic resonance. Eur Heart J 26:2721–2727

Chen SJ, Chang CI, Chiu IS, Wang JK, Lin CD, Chen HY, Lue HC, Li YW (2001) Preoperative diagnosis by electron beam computed tomography and perioperative management of primary tracheal anomalies in tetralogy of Fallot. J Formos Med Assoc 100:26–31

Choi BW, Park YH, Choi JY, Choi BI, Kim MJ, Ryu SJ, Lee JK, Sul JH, Lee SK, Cho BK, Choe KO (2001) Using electron beam CT to evaluate conotruncal anomalies in pediatric and adult patients. Am J Roentgenol 177:1045–1049

Choi BW, Park YH, Lee JK, Kim MJ, Kim DJ, Ryu SJ, Cho BK, Choe KO (2003) Evaluation of the postshunt status with electron beam computed tomography in cyanotic congenital heart disease. Yonsei Med J 44:249–258

Chowdhury UK, Pradeep KK, Patel CD, Singh R, Kumar AS, Airan B, Gulati GS, Kothari SS, Saxena A, Kalaivani M, Venugopal P (2006) Noninvasive assessment of repaired tetralogy of Fallot by magnetic resonance imaging and dynamic radionuclide studies. Ann Thorac Surg 81:1436–1442

Corno AF, Hurni M, Griffin H, Galal OM, Payot M, Sekarski N, Tozzi P, von Segesser LK (2002) Bovine jugular vein as right ventricle-to-pulmonary artery valved conduit. J Heart Valve Dis 11:242–247

Corno AF, Qanadli SD, Sekarski N, Artemisia S, Hurni M, Tozzi P, von Segesser LK (2004) Bovine valved xenograft in pulmonary position: medium-term follow-up with excellent hemodynamics and freedom from calcifications. Ann Thorac Surg 78:1382–1388

Davlouros PA, Kilner PJ, Hornung TS, Li W, Francis JM, Moon JC, Smith GC, Tat T, Pennell DJ, Gatzoulis MA (2002) Right ventricular function in adults with repaired tetralogy of Fallot assessed with cardiovascular magnetic resonance imaging: detrimental role of right ventricular outflow aneurism or akinesia and adverse right-to-left ventricular interaction. J Am Coll Cardiol 40:2044–2052

Dodge-Khatami A, Buechel ER, Knirsch W, Kadner A, Rousson V, Dave HH, Bauersfeld U, Prêtre R (2006) Brain natriuretic peptide and magnetic resonance imaging in tetralogy with right ventricular dilatation. Ann Thorac Surg 82:983–988

Dorfman AL, Geva T (2006) Magnetic resonance imaging evaluation of congenital heart disease: conotruncal anomalies. J Cardiovasc Magn Reson 8:645–659

Eichhorn J, Schoenberg S, Ulmer HE (2003) Cardiacgated multislice computerised tomographic angiography in the preoperative evaluation of an infant with tetralogy of Fallot and pulmonary atresia. Cardiol Young 13:466–468

Festa P, Ait-Ali L, Murzi B, Bini MR (2005) Tetralogy of Fallot with left heart hypoplasia, total anomalous pulmonary venous return, and right lung hypoplasia: role of magnetic resonance imaging. Pediatr Cardiol 26:467–469

Geva T, Greil GF, Marshall AC, Landzberg M, Powell AJ (2002) Gadolinium-enhanced three-dimensional magnetic resonance angiography of pulmonary blood supply in patients with complex pulmonary stenosis or atresia: comparison with X-ray angiography. Circulation 106:473–478

Geva T, Sahn DJ, Powell AJ (2003) Magnetic resonance imaging of congenital heart disease in adults. Progress in Pediatric Cardiology 17:21–39

Geva T, Sandweiss BM, Gauvreau K, Lock JE, Powell AJ (2004) Factors associated with impaired clinical status in long-term survivors of tetralogy of Fallot repair evaluated by magnetic resonance imaging. J Am Coll Cardiol 43:1068–1074

Gulati GS, Singh C, Kothari SS, Sharma S (2006) An unusual coronary artery anomaly in tetralogy of Fallot shown on MDCT. Am J Roentgenol 186:1192–1193

Halt M, Kastler B, Livolsi A, Mardini M, Willard D, Wackenheim A (1991) Tetralogy of Fallot: a pre- and post-operative study using magnetic resonance tomography. Röfo 154:111–113

Harris MA, Johnson TR, Weinberg PM, Fogel MA (2007) Delayed-enhancement cardiovascular magnetic resonance identifies fibrous tissue in children after surgery for congenital heart disease. J Thorac Cardiovasc Surg 133:676–681

Helbing WA, de Roos A (2000) Clinical applications of cardiac magnetic resonance imaging after repair of tetralogy of Fallot. Pediatr Cardiol 21:70–79

Holmqvist C, Hochbergs P, Bjorkhem G, Brockstedt S, Laurin S (2001) Pre-operative evaluation with MR in tetralogy of Fallot and pulmonary atresia with ventricular septal defect. Acta Radiol 42:63–69

Kang IS, Redington AN, Bensol LN, Macgowan C, Valsangiacomo ER, Roman K, Kellenberger CJ, Yoo SJ (2003) Differential regurgitation in branch pulmonary arteries after repair of tetralogy of Fallot: a phase-contrast cine magnetic resonance study. Circulation 107:2938–2943

Kastler B, Livolsi A, Germain P, Zollner G, Dietemann JL (1991) Evaluation of Blalock-Taussig shunts in newborns: value of oblique MRI planes. Int J Card Imaging 7:1–5

Lajos PS, White C, Cardarelli M (2006) Multislice computed tomographic angiography: valuable tool in the diagnosis and planning of complex cardiac surgery. Ann Thorac Surg 81:2317

Li W, Davlouros PA, Kilner PJ, Pennell DJ, Gibson D, Henein MY, Gatzoulis MA (2004) Doppler-echocardiographic assessment of pulmonary regurgitation in adults with repaired tetralogy of Fallot: comparison with cardiovascular magnetic resonance imaging. Am Heart J 147:165–172

Menteer J, Wienberg PM, Fofel MA (2005) Quantifying regional right ventricular in tetralogy of Fallot. J Cardiovasc Magn Reson 7:753–761

Nieman K, Roos-Hesselink JW, de Feyter PJ (2003) Coronary anomaly imaging by multislice computed

tomography in corrected tetralogy of Fallot. Heart 89:664

Norton KI, Tong C, Glass RB, Nielsen JC (2006) Cardiac MR imaging assessment following tetralogy of Fallot repair. Radiographics 26:197–211

Oosterhof T, Mulder BJ, Vliegen HW, de Roos A (2005) Corrected tetralogy of Fallot: delayed enhancement in right ventricular outflow tract. Radiology 237: 868–871

Oosterhof T, Mulder BJ, Vliegen HW, de Roos A (2006) Cardiovascular magnetic resonance in the follow-up of patients with corrected tetralogy of Fallot: a review. Am Heart J 151:265–272

Oosterhof T, Tulevski II, Vliegen HW, Spijkerboer AM, Mulder BJ (2006) Effects of volume and/or pressure overload secondary to congenital heart disease (tetralogy of Fallot or pulmonary stenosis) on right ventricular function using cardiovascular magnetic resonance and B-type natriuretic peptide levels. Am J Cardiol 97:1051–1055

Oosterhof T, van Straten A, Vliegen HW, Meijboom FJ, van Dijk AP, Spijkerboer AM, Bouma BJ, Zwinderman AH, Hazekamp MG, de Roos A, Mulder BJ (2007) Preoperative thresholds for pulmonary valve replacement in patients with corrected tetralogy of Fallot using cardiovascular magnetic resonance. Circulation 116:545–551

Niezen RA, Helbing WA, van der Wall EE, van der Geest RJ, Vliegen HW, de Roos A (1999) Left ventricular function in adults with mild pulmonary insufficiency late after Fallot repair. Heart 82:697–703

Prakash A, Powell AJ, Krishnamurthy R, Geva T (2004) Magnetic resonance imaging evaluation of myocardial perfusion and viability in congenital and acquired pediatric heart disease. Am J Cardiol 93:657–661

Powell AJ, Chung T, Landzberg MJ, Geva T (2000) Accuracy of MRI evaluation of pulmonary blood supply in patients with complex pulmonary stenosis or atresia. Int J Card Imaging 16:169–174

Puderbach M, Eichhorn J, Fink C, Kauczor HU (2004) Images in cardiovascular medicine. Untreated tetralogy of Fallot with pulmomary atresia in a 55-year-old woman: findings from magnetic resonance imaging. Circulation 110:e461–462

Raman SV, Cook SC, McCarthy B, Ferketich AK (2005) Usefulness of multidetector row computed tomography to quantify right ventricular size and function in adults with either tetralogy of Fallot or transposition of the great arteries. Am J Cardiol 95:683–686

Rebergen SA, Chin AJ, Ottenkamp J, van der Wall EE, de Roos A (1993) Pulmonary regurgitation in the late postoperative follow-up of tetralogy of Fallot. Volumetric quantitation by nuclear magnetic resonance velocity mapping. Circulation 88:2257–2266

Redington AN (2006) Determinants and assessment of pulmonary regurgitation in tetralogy of Fallot: practice and pitfalls. Cardiol Clin 24:631–639

Rodrigo Carbonero D, Cabreara Duro A, Martinez Corrales P, Rios Altolaguirre G, Alcibar Villa J, Aramendi

Gallardo J, Barrera Portillo MC, Pastor Menchaca E, Cabrera Zubizarreta A (2004) Magnetic resonance imaging and lung perfusion scintigraphy in tetralogy of Fallot following surgery. An Pediatr 60:153–160

Roest AA, Helbing WA, Kunz P, van den Aardweg JG, Lamb HJ,Vliegen HW, van der Wall EE, de Roos A (2002) Exercise MR imaging in the assessment of pulmonary regurgitation and biventricular function in patients after tetralogy of Fallot repair. Radiology 223:204–211

Roest AA, de Roos A, Lamb HJ, Helbing WA, van den Aardweg JG, Doornbos J, van der Wall EE, Kunz P (2003) Tetralogy of Fallot: postoperative delayed recovery of left ventricular stroke volume after physical exercise assessment with fast MR imaging. Radiology 226:278–284

Schievano S, Migliavacca F, Coats L, Khambadkone S, Carminati M, Wilson N, Deanfield JE, Bonhoeffer P, Taylor AM (2007) Percutaneous pulmonary valve implantation based on rapid prototyping of right ventricular outflow tract and pulmonary trunk from MR data. Radiology 242:490–497

Therrien J, Provost Y, Merchant N, Williams W, Colman J, Webb G (2005) Optimal timing for pulmonary valve replacement in adults after tetralogy of Fallot repair. Am J Cardiol 95:779–782

Tsai SK, Chang CI, Wang MJ, Chen SJ, Chiu IS, Chen YS, Lue HC (2001) The assessment of the proximal left pulmonary artery by transoesophageal echocardiography and computed tomography in neonates and infants: a case series. Anesth Analg 93:594–597

Van den Berg J, Wielopolski PA, Meijboom FJ, Witsenburg M, Bogers AJ, Pattynama PM, Helbing WA (2007) Diastolic function in repaired tetralogy of Fallot at rest and during stress: assessment with MR imaging. Radiology 243:212–219

Van Straten A, Vliegen HW, Lamb HJ, Roes SD, van der Wall EE, Hazekamp MG, de Roos A (2005) Time course of diastolic and systolic function improvement after pulmonary valve replacement in adult patients with tetralogy of Fallot. J Am Coll Cardiol 46:1559–1564

Vick GW 3rd, Wendt RE 3rd, Rokey R (1994) Comparison of gradient echo with spin echo magnetic resonance imaging and echocardiography in the evaluation of major aortopulmonary collateral arteries. Am Heart J 127:1341–1347

Vliegen HW, van Straten A, de Ross A, Roest AA, Schoof PH, Zwinderman AH, Ottenkamp J, van der Wal EE, Hazekamp MG (2002) Magnetic resonance imaging to assess the hemodynamic effects of pulmonary valve replacement in adults late after repair of tetralogy of Fallot. Circulaton 106:1703–1707

Wu MT, Huang YL, Hsieh KS, Huang JT, Peng NJ, Pan JY, Huang JS, Yang TL (2007) Influence of pulmonary regurgitation inequality on differential perfusion of the lungs in tetralogy of Fallot after repair. A phase-contrast magnetic resonance imaging and perfusion scintigraphy study. J Am Coll Cardiol 49: 1880–1886

Tetralogy of Fallot with absent pulmonary valve

▌ Definition

This is an uncommon variation of tetralogy of Fallot with a ring-like and usually stenotic malformation (rather than absence) of the pulmonary valve, with failure of the development of valve cusps. The central pulmonary arteries are usually hugely dilated or aneurysmal. The pulmonary artery dilatation may extend beyond what is expected from severe pulmonary regurgitation to several generations of pulmonary arteries causing tracheobronchial compression; this often results in either hyperexpansion from air trapping or collapse of lobes, or even an entire lung. The ductus arteriosus is generally absent. The intracardiac anatomy generally presents with the same characteristics of tetralogy of Fallot (see chapter "Tetralogy of Fallot") except that the right ventricular outflow tract is not excessively restrictive.

Associated anomalies

Atrial septal defect, common atrioventricular valve (rare), tricuspid atresia (rare), intact ventricular septum (rare), transposition of the great arteries (rare), agenesis of the ductus arteriosus, branch pulmonary arteries anomalies (non-confluent pulmonary arteries), right aortic arch (frequent), anomalous coronary arteries, dextrocardia and situs inversus (very rare).

▌ Surgical options

The surgical repair consists of the following steps. Excision of the main pulmonary artery, with transection of its proximal end just above the pulmonary valve annulus and of its distal end at the level of the bifurcation. Resection and plication of the aneurysmal pulmonary arteries, extended laterally to the hilum, with or without including the plication of the posterior wall of both pulmonary arteries. Transannular longitudinal right ventriculotomy. Patch closure of ventricular septal defect from longitudinal right ventriculotomy. Valved conduit (homograft or heterograft) interposition between the right ventricle and the reconstructed pulmonary arteries bifurcation.

▌ Pre-operative information

Pre-operative information in patients with tetralogy of Fallot with absent pulmonary valve is similar to that required in patients with tetralogy of Fallot (see relative chapter), with particular attention focused on potential airway obstruction due to dilated pulmonary artery branches and the frequent association of the right aortic arch. Both CT scan (Fig. 3.8.1) and MRI can provide clear imaging of the dilated pulmonary arteries and their relationship with the airways.
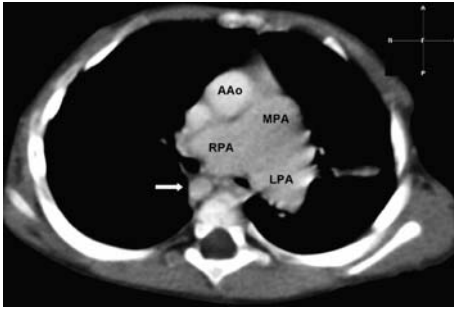
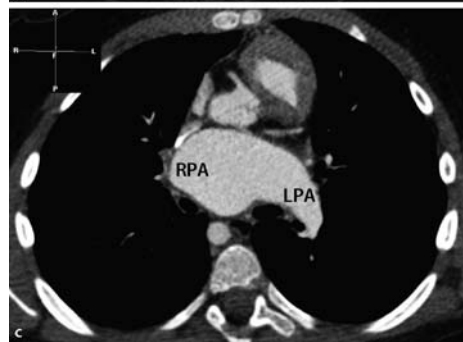**Fig. 3.8.1.** Tetralogy of Fallot with absent pulmonary valve. CT scan, contrast angiography, axial projection showing the huge dilatation of the main pulmonary artery and its branches, and the right aortic arch (arrow) (*AAo* ascending aorta, *LPA* left pulmonary artery, *MPA* main pulmonary artery, *RPA* right pulmonary artery) (photograph courtesy of Dr. Mohamed Tawil)

■ Potential complications

Residual or recurrent ventricular septal defect (patch dehiscence or separate defect), residual or recurrent right ventricular outflow tract obstruction, complete atrioventricular block, arrhythmias, airway compression, respiratory insufficiency.

■ Post-operative follow-up

As for the pre-operative information, in patients with tetralogy of Fallot with absent pulmonary valve the goals of the post-operative investigations are similar to the ones required in patients with tetralogy of Fallot (see relative chapter), again with particular attention focused on potential airway obstruction due to the dilated pulmonary arteries branches and the surgical technique utilized. Again both CT scan (Fig. 3.8.2) and MRI (Fig. 3.8.3) are able to evaluate the results of the different surgical techniques.
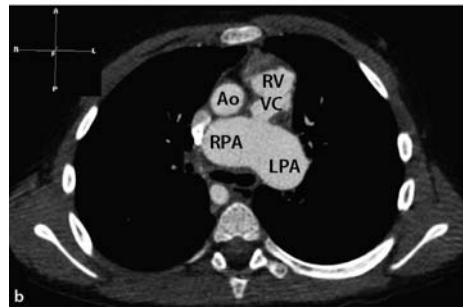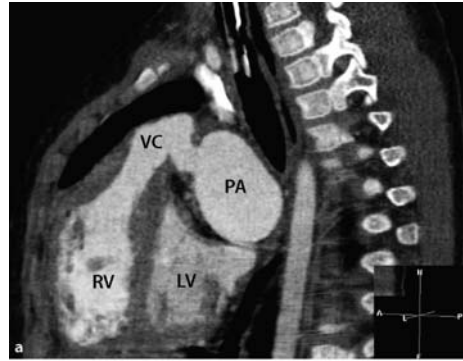
Fig. 3.8.2. Tetralogy of Fallot with absent pulmonary valve, status post repair. CT scan, contrast angiography, sagittal (**a**) and axial projections (**b**, **c**), showing the tortuous right ventricle to pulmonary artery conduit and the aneurismatic dilatation of the pulmonary artery, not resected at the time of surgery (*Ao* aorta, *LPA* left pulmonary artery, *LV* left ventricle, *PA* pulmonary artery, *RPA* right pulmonary artery, *RV* right ventricle, *VC* valved conduit) (photographs courtesy of Dr. Mohamed Tawil)
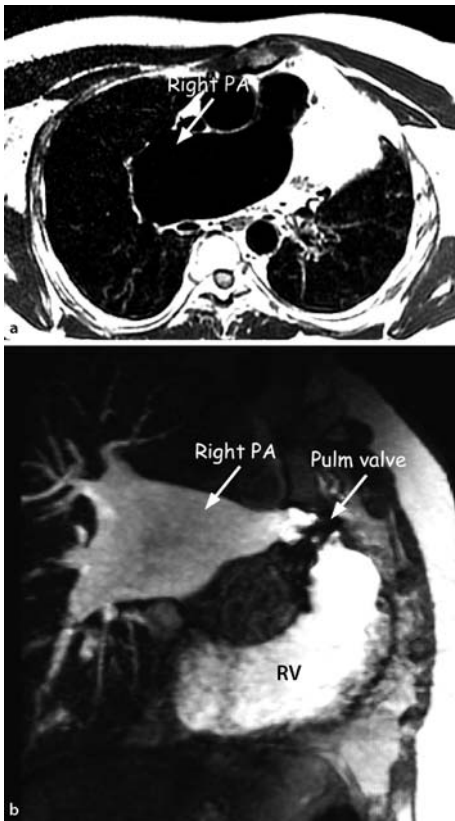
Fig. 3.8.3. Tetralogy of Fallot with absent pulmonary valve, status post repair, right pulmonary artery aneurysm. MRI axial fast spin echo (black blood) (**a**) and maximal intensity projection angiography (**b**) showing right pulmonary artery aneurysm after right ventricular outflow tract reconstruction with implantation of a mechanical valve in the pulmonary position (*PA* pulmonary artery, *RV* right ventricle)

■ References

Alsoufi B, Williams WG, Zhondong H, Cai S, Karamlou T, Chan CC, Coles JG, van Arsdell GS, Caldarone CA (2007) Surgical outcomes in the treatment of patients with tetralogy of Fallot and absent pulmonary valve. Eur J Cardiothorac Surg 31:354–359

Brown JW, Ruzmetov M, Vijay P, Rodefeld MD, Turrentine MW (2006) Surgical treatment of absent pulmonary valve syndrome associated with bronchial obstruction. Ann Thorac Surg 82:2221–2226

Corno AF, Picardo S, Ballerini L, Gugliantini P, Marcelletti C (1985) Bronchial compression by dilated pulmonary artery: surgical treatment. J Thorac Cardiovasc Surg 90:706–720

Hew CC, Daebritz SH, Zurakowski D, del Nido PI, Mayer JE, Jonas RA (2002) Valved homograft replacement of aneurysmal pulmonary arteries for severely symptomatic absent pulmonary valve syndrome. Ann Thorac Surg 73:1778–1785

Hiraishi S, Bargeron LM, Isabel-Jones JB, Emmanouilides GC, Friedman WF, Jarmakani JM (1983) Ventricular and pulmonary artery volumes in patients with absent pulmonary valve. Factors affecting the natural course. Circulation 67:183

Hraska V, Kantorova A, Kunovsky P, Haviar D (2002) Intermediate results with correction of tetralogy of Fallot with absent pulmonary valve using a new approach. Eur J Cardiothorac Surg 21:711–714

Kim YM, Yoo SJ, Kim TH, Park IS, Kim WH, Lee JY, Han MY (2002) Three-dimensional computed tomography in children with compression of the central airways complicating congenital heart disease. Cardiol Young 12:44–50

Knauth AL, Marshall AC, Geva T, Jonas RA, Marx GR (2004) Respiratory symptoms secondary to aortopulmonary collateral vessels in tetralogy of Fallot absent pulmonary valve syndrome. Am J Cardiol 93:503–505

Nolke L, Azakie A, Anagnostopulos PV, Alphonso N, Karl TR (2006) The Lecompte maneuver for relief of airway compression in absent pulmonary valve syndrome. Ann Thorac Surg 81:1802–1807

Snir E, de Leval MR, Elliott MJ, Stark J (1991) Current surgical technique to repair Fallot's tetralogy with absent pulmonary valve syndrome. Ann Thorac Surg 51:979

Stellin G, Jonas RA, Goh TH, Brawn WJ, Venables AW, Mee RBB (1983) Surgical treatment of absent pulmonay valve syndrome in infants: relief of bronchial obstruction. Ann Thorac Surg 36:468–475

Sung SC, Chang YH, Woo JS (2007) Anterior translocation of pulmonary artery without aortic transection in repair of tetralogy of Fallot with absent pulmonary valve. Eur J Cardiothorac Surg 31:742–743

▮ Definition

The pulmonary valve annulus is generally small, rarely hypoplastic, and the pulmonary valve leaflets are generally well formed but fused. The main pulmonary artery is small but rarely is atretic as seen with pulmonary atresia and ventricular septal defect. The patent ductus arteriosus is usually small because it carries blood from the aorta to the pulmonary arteries in utero and not the other way around as in normal fetuses; therefore, much less blood travels through the patent ductus arteriosus in utero.

The right ventricle might present with one of the following morphologies:
- *Type I*: tripartite,
- *Type II*: bipartite (atretic body),
- *Type III*: unipartite (atretic body and infundibulum).

The tricuspid valve might be malformed and stenotic. Other congenital heart defects are rarely associated. The origin and distribution of the coronary arteries may exhibit the same variability as the normal heart, including the presence of coronary artery stenosis. Ventriculocoronary sinusoids are frequent from the right ventricular cavity to the myocardium and from the myocardium to the coronary arteries.

▮ Surgical options

The right ventricular size and function dictate the possibility of surgical management with respect to biventricular or univentricular type of repair, or one-and-half ventricular repair. Surgical pulmonary valvotomy can be performed with or without a systemic-to-pulmonary arterial shunt depending upon the right ventricular size and function. If the right ventricle is small, a systemic-to-pulmonary arterial shunt is necessary to provide pulmonary blood flow until antegrade flow through the pulmonary valve becomes adequate. However, if the pulmonary arteries are not small, then pulmonary valvotomy alone may be adequate, with or without a postoperative period with maintained prostaglandin E infusion. Decompression of the right ventricle by pulmonary valvotomy may cause reversal of flow in the coronary arteries to sinusoids, leading to poor myocardial perfusion. This is especially true in the presence of right ventricular dependent coronary circulation, particularly in the presence of coronary artery stenosis. Therefore, right ventricular decompression should not be performed if coronary artery stenoses are demonstrated with sinusoids. In patients with small pulmonary arteries treated with a systemic-to-pulmonary artery shunt, if the right ventricle continues to be small and inadequate, then a cavopulmonary connection may be required. Patients with severe right ventricle-to-coronary arteries sinusoids may require cardiac transplantation. Sinusoids are typically not present in patients with severe tricuspid insufficiency and a normal right ventricular size. In patients with significant tricuspid valve regurgitation and low right ventricular pressure, pulmonary valvotomy may not result in effective forward flow through the right ventricle because of tricuspid valve regurgitation.

■ Pre-operative information

The information required to make the decision about surgical treatment include the size, morphology and function of the right ventricular cavity, the tricuspid size and function, the presence and extension of myocardial sinusoids, the size and shape of the patent ductus arteriosus as the only source of pulmonary blood flow, and the morphology of the pulmonary arteries (Figs. 3.9.1–3.9.3). Transthoracic echocardiography is generally exhaustive for preoperative evaluation of neonates with pulmonary atresia with intact ventricular septum. Conventional angiography could be indicated in case of suspected myocardial sinusoids not seen with echocardiography.
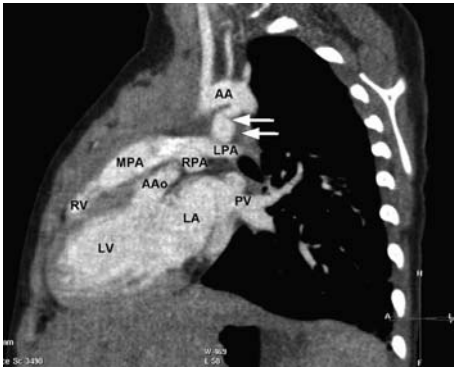
Fig. 3.9.1. Pulmonary atresia with intact ventricular septum. CT scan, sagittal oblique, showing the hypoplastic right ventricle and the confluent pulmonary arteries with long and tortuous patent ductus arteriosus (arrows) (*AA* aortic arch, *AAo* ascending aorta, *LA* left atrium, *LPA* left pulmonary artery, *LV* left ventricle, *MPA* main pulmonary artery, *PV* pulmonary veins, *RPA* right pulmonary artery, *RV* right ventricle) (photograph courtesy of Dr. Mohamed Tawil)
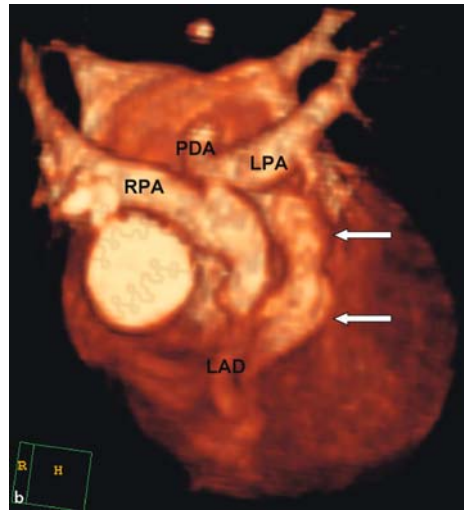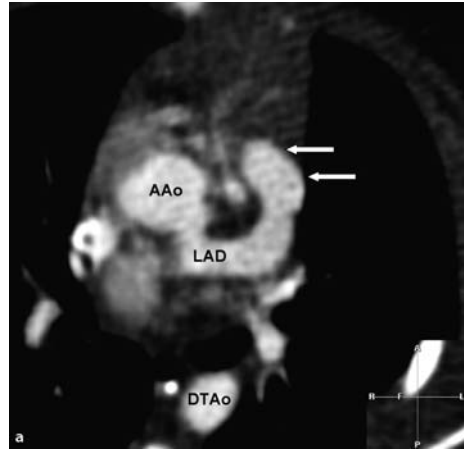
Fig. 3.9.2. Pulmonary atresia with intact ventricular septum. **a** CT contrast angiography, axial view, showing a major myocardial sinusoid (arrows) coming from the hypoplastic right ventricle and reaching the left anterior descending coronary artery. **b** CT scan of the same neonate with 3-dimensional reconstruction, showing the major myocardial sinusoid (arrows) coming from the hypoplastic right ventricle and reaching the left anterior descending coronary artery (*AAo* ascending aorta, *DTAo* descending thoracic aorta, *LAD* left anterior descending coronary artery, *LPA* left pulmonary artery, *PDA* patent ductus arteriosus, *RPA* right pulmonary artery) (photographs courtesy of Dr. Mohamed Tawil)
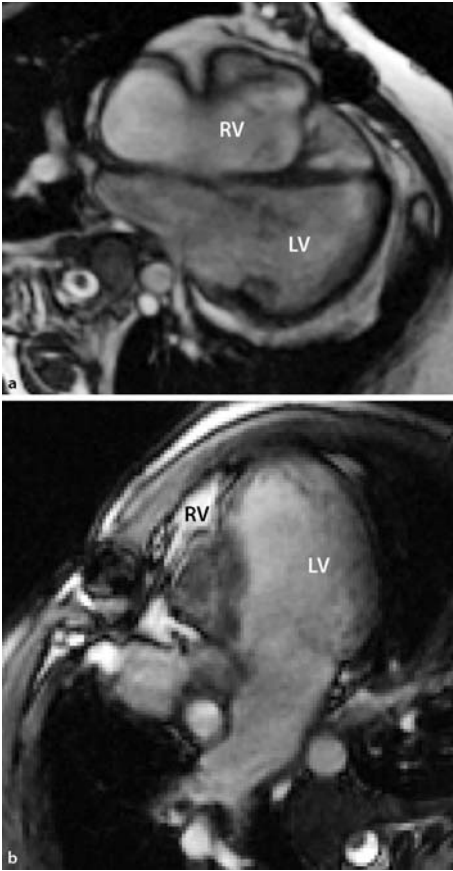
Fig. 3.9.3. Pulmonary atresia with intact ventricular septum. **a** MRI cine steady-state free precession 4-chamber view in a patient after biventricular type of repair. Note the adequate size of the right ventricular cavity. **b** MRI with cine steady-state free precession 4-chamber view in a patient with after univentricular type of repair due to the severe hypoplasia of the right ventricle (*LV* left ventricle, *RV* right ventricle)

■ Potential complications

Inadequate or inhomogeneous pulmonary blood flow, poor myocardial perfusion, myocardial infarction, residual tricuspid valve regurgitation, right heart failure.

■ Post-operative follow-up

Patients with pulmonary atresia with intact ventricular septum after the first stage of treatment (pulmonary valvotomy and/or systemic-to-pulmonary shunt), depending on the morphology and function of the right heart (tricuspid valve, right ventricle, pulmonary valve and arteries) are candidate for univentricular or biventricular or one-and-half ventricular repair. In borderline cases MRI can be useful in the decision-making process by evaluating the right ventricular volume and function, pulmonary blood flow and degree of residual pulmonary valve regurgitation.

After one-and-half ventricular repair, in addition to the previous goals and to the evaluation of the cavopulmonary anastomosis, MR angiography can identify potential veno-venous collaterals between superior and inferior vena cava and even quantify them by means of phase contrast velocity acquisition at both inferior and superior vena cava level (Fig. 3.9.6).

The evaluation of univentricular repair has already been described in the relative chapter (see "Single ventricle").

The following protocol is used for post-operative evaluation in these patients:

- 3-plane localizing images,
- 2-dimensional axial Time-of-flight Angiography (see the appendix of the "Introduction"),
- ECG-gated cine steady-state free precession sequences in 2-chamber, 4-chamber planes, and ventricular short axis for the quantitative assessment of both ventricular dimensions, function and stroke volume as illustrated in the appendix of the "Introduction" (Fig. 3.9.4),
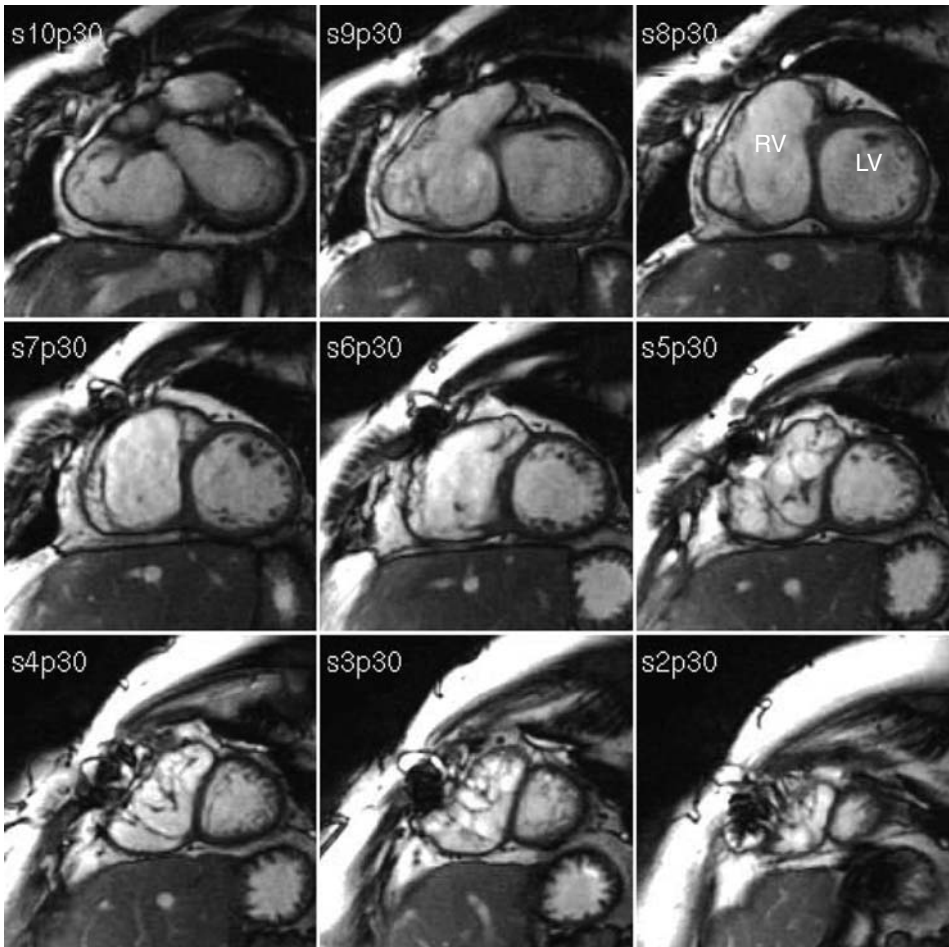
Fig. 3.9.4. Pulmonary atresia with intact ventricular septum, status post one-and-half ventricular repair. MRI cine steady-state free precession ventricular short-axis projection showing a very trabeculated and mildly dilated (100 mL/m^2 B.S.A.) right ventricle (*LV* left ventricle, *RV* right ventricle)
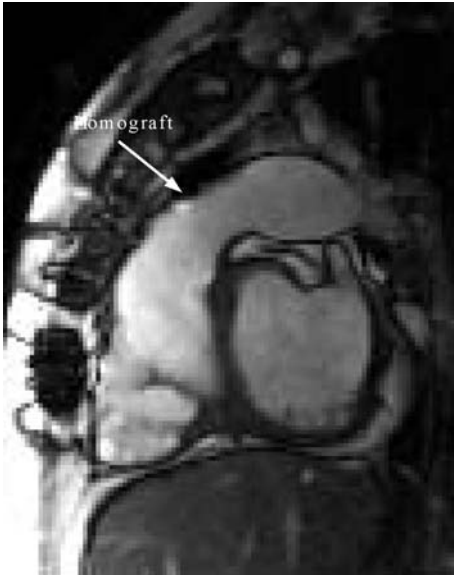
Fig. 3.9.5. Pulmonary atresia with intact ventricular septum, status post one-and-half ventricular repair. Cine MRI right ventricular outflow tract steady-state free precession showing the pulmonary homograft

■ ECG-gated cine steady-state free precession sequence for right ventricle 2-chamber view,

■ ECG-gated cine steady-state free precession sequence on sagittal view to evaluate the right ventricular outflow tract (Fig. 3.9.5),

■ ECG-gated cine steady-state free precession and fast spin echo sequence to visualize the cavopulmonary anastomosis,

■ gadolinium-enhanced 3-dimensional MRA of the right ventricular outflow tract and pulmonary arteries morphology, as well as for the assessment of veno-venous collateral and cavopulmonary anastomosis (Figs. 3.9.6 and 3.9.7),

■ ECG-gated PVC-MRI sequences perpendicular to the main pulmonary artery (also to quantify the pulmonary valve regurgitation), ascending aorta, superior and inferior vena cava,
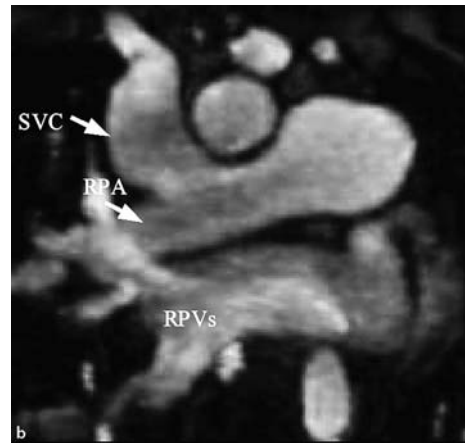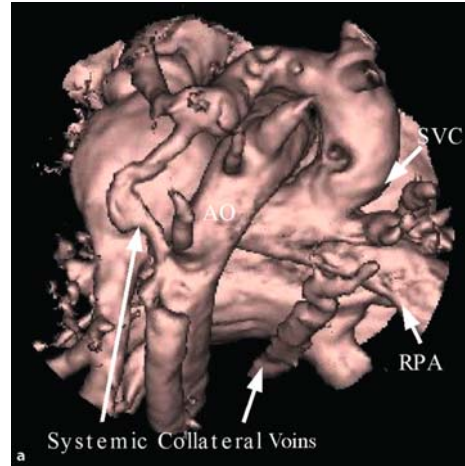
Fig. 3.9.6. Pulmonary atresia with intact ventricular septum, status post one-and-half ventricular type of repair. MR angiography volume rendering posterior view (**a**); maximal intensity projection reconstruction showing a good size of cavopulmonary anastomosis (**b**) (*RPA* right pulmonary artery, *RPVs* right pulmonary veins, *SVC* superior vena cava)
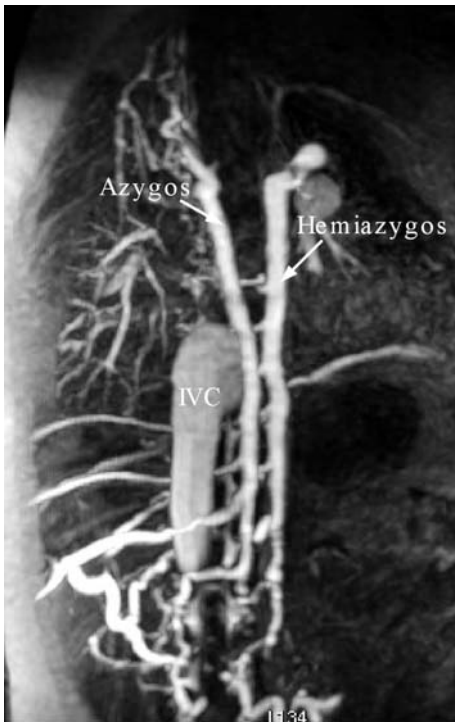
Fig. 3.9.7. Pulmonary atresia with intact ventricular septum, status post one-and-half ventricular type of repair. MR angiography maximal intensity projection showing dilated azygos, hemiazygos and inferior vena cava (*IVC* inferior vena cava)

▮ post-gadolinium delayed myocardial enhancement may be used to evaluate the presence of myocardial scar tissue.

▮ References

Adachi I, Yagihara T, Kagisaki K, Hagino I, Ishizaka T, Kobayashi J, Kitamura S, Uemura H (2007) Preoperative small pulmonary artery did not affect the midterm results of Fontan operation. Eur J Cardiothorac Surg 32:156–162

Choi BW, Park YH, Lee JK, Kim MJ, Kim DJ, Ryu SJ, Cho BK, Choe KO (2003) Evaluation of the post-shunt status with electron beam computed tomography in cyanotic congenital heart disease. Yonsei Med J 44:249–258

Corno AF, Mazzera E, Marino B, Parisi F, Marcelletti C (1986) Simultaneous patency of ductus arteriosus and surgical shunt in pulmonary atresia with intact ventricular septum. A cause of acute myocardial failure? Scand J Thorac Cardiovasc Surg 20:123–127

De Leval MR, Bull C, Stark J, Anderson RH, Taylor JFN, Macartney FJ (1982) Pulmonary atresia and intact ventricular septum: surgical management based on a revised classification. Circulation 66:272–280

Freedom RM (1983) The morphological variations of pulmonary atresia with intact ventricular septum: guidelines for surgical intervention. Pediatr Cardiol 4:183–188

Geva T, Greil GF, Marshall AC, Landzberg M, Powell AJ (2002) Gadolinium-enhanced three-dimensional magnetic resonance angiography of pulmonary blood supply in patients with complex pulmonary stenosis or atresia: comparison with X-ray angiography. Circulation 106:473–478

Giannico S, Corno AF, Marino B, Cicini MP, Gagliardi MG, Amodeo A, Picardo S, Marcelletti C (1992) Total extracardiac right heart bypass. Circulation 86(Suppl2):110–117

Giannico S, Hammad F, Amodeo A, Michielon G, Drago F, Turchetta A, di Donato R, Sanders SP (2006) Clinical outcome of 193 extracardiac Fontan patients. J Am Coll Cardiol 47:2065–2073

Gray RG, Altmann K, Mosca RS, Prakash A, Williams IA, Quaegebeur JM, Chen JM (2007) Persistent antegrade pulmonary blood flow post-Glenn does not alter early post-Fontan outcomes in single-ventricle patients. Ann Thorac Surg 84:888–893

Hirata Y, Chen JM, Quaegebeur JM, Hellenbrand WE, Mosca RS (2007) Pulmonary atresia with intact ventricular septum: limitations of catheter-based intervention. Ann Thorac Surg 84:574–580

Hosein RBM, Clarke AJB, McGuirk SP, Griselli M, Stumper O, De Giovanni JV, Barron DJ, Brawn WJ (2007) Factors influencing early and late outcome following the Fontan procedure in the current era. The "Two Commandments"? Eur J Cardiothorac Surg 31:344–353

Marcelletti C, Corno AF, Giannico S, Marino B (1990) Inferior vena cava to pulmonary artery extracardiac conduit: a new form of right heart bypass. J Thorac Cardiovasc Surg 100:228–232

Qureshi SA (2001) Collaborative approach in the management of pulmonary atresia with intact ventricular septum. J Interv Cardiol 14:377–384

Zhang H, Li SJ, Li YQ, Wang H, Hu SS (2007) Hybrid procedure for the neonatal management of pulmonary atresia with intact ventricular septum. J Thorac Cardiovasc Surg 133:1654–1656

Chapter 3.10 Ebstein's anomaly

▊ Definition

Ebstein's anomaly is a congenital malformation of the tricuspid valve and right ventricle characterized by several features, each of which can exhibit a spectrum of malformations relevant to the surgical management of the condition:

▊ displacement of the septal and posterior leaflets of the tricuspid valve towards the apex of the right ventricle, with adherence to the myocardium,

▊ anterior leaflet attached to the appropriate level of the tricuspid valve annulus, however, redundant, larger than normal and with multiple fenestrations and chordal attachments to the ventricular wall,

▊ segment of the right ventricle from the level of true tricuspid annulus to the level of attachment of the septal and posterior leaflets unusually thin and dysplastic, and described as "atrialized"; right atrio-ventricular junction (being the true tricuspid valvular annulus) and right atrium extremely dilated,

▊ cavity of the right ventricle, beyond the atrialized portion, reduced in size, usually with lack of an inlet chamber, and with a small trabecular component,

▊ infundibulum often obstructed by the redundant tissue of the anterior leaflet as well as by the chordal attachments of the anterior leaflet to the infundibulum,

▊ variable type and degree of ventricular dysfunction.

Each heart with Ebstein's malformation is different, and there is an infinite variability that can occur with the above mentioned characteristics.

Carpentier classified four clinical variants with progressively increasing severity:

▊ *Type A*: the volume of the true right ventricle is adequate,

▊ *Type B*: the volume of the right ventricle is small, and there is a large atrialized portion of the right ventricle,

▊ *Type C*: the volume of the right ventricle is small, with right ventricular outflow tract obstruction,

▊ *Type D*: there is almost complete atrialization of the right ventricle with the exception of a small infundibular component, and the only communication between the atrialized ventricle and the infundibulum is through the anteroseptal commissura of the tricuspid valve.

The most common associated anomaly is atrial septal defect, occurring in about 50% of cases, often causing cyanosis due to right-to-left shunt at the atrial level. There is a variable degree of right ventricular outflow tract obstruction. A Wolff-Parkinson-White type of accessory pathway, often with associated pre-excitation, is present in about 10% of cases. In symptomatic neonates, survival is dependent on the presence of a patent ductus arteriosus. Rare associated anomalies are abnormality of the ventriculoarterial connection or double discordance (atrioventricular and ventriculoarterial), atrioventricular septal defect, ventricular septal defect, tetralogy of Fallot, and aortic coarctation.

❚ Surgical options

The surgical repair includes:
❚ closure of the atrial septal defect,
❚ plication of the atrialized portion of the right ventricle,
❚ repair or replacement of the tricuspid valve.

As tricuspid repair is based predominantly on a satisfactory arrangement of the anterior leaflet, its feasibility and result mainly depends on the presence of a mobile and free leading edge of the anterior leaflet. In patients with reduced size or function of the right ventricle, a one-and-half ventricular repair is performed, with end-to-side anastomosis of the superior vena cava to the right pulmonary artery in addition to intracardiac repair, in order to reduce the volume overload of the small/malfunctioning right ventricle. Exceptionally, a total cavopulmonary connection (univentricular repair) is required for patients with an extremely small or malfunctioning right ventricle. Pre-operative electrophysiology for bypass pathways is necessary in order to perform intraoperative ablation. When ventricular pacing is required, it should be done through epicardial leads rather intravenously, since the tricuspid valve function is already compromised.

❚ Pre-operative information

Echocardiography is generally sufficient for diagnosis and evaluation of Ebstein's anomaly. However, there are aspects that need to be considered:
❚ it is remarkably difficult to understand from 2-dimensional echocardiography alone the arrangement of the tricuspid leaflets and their tension apparatus (mainly for the surgical implications). However 3-dimensional echocardiography offers new insight into the morphology and function of a malformed tricuspid valve and allows elucidation of all the features mentioned above. In our opinion as this technique will gain widespread diffu-

sion it will become the best tool in the selection of patients for surgery and in planning the surgical approach.
❚ both right and/or left myocardial dysfunction can be present; thus, assessment of ventricular function by 2-dimensional echocardiography, albeit of crucial importance in some cases, can be inaccurate, due to unusual right ventricular anatomy and septal displacement. Therefore, as an alternative cardiac MRI is useful to estimate right and left ventricular volume, function and potential myocardial thinning, in addition to visualizing the interatrial septum and measuring the right atrial volume.

The cardiovascular MRI protocol currently used in Ebstein's anomaly is the following:
❚ 3-plane localizing images,
❚ ECG-gated cine steady-state free precession sequences in 2-chamber, 4-chamber planes (Fig. 3.10.1), and ventricular short axis for the quantitative assessment of both ventricular dimensions, function, stroke volume (as illustrated in the appendix in the "Introduction") and potential right ventricle myocardial thinning,
❚ ECG-gated cine steady-state free precession and static fast spin echo sequences on additional planes to better determine the anatomy of the right ventricular outflow tract,
❚ ECG-gated cine steady-state free precession and fast spin echo in axial and coronal plane for the evaluation of the tricuspid valve (Fig. 3.10.2), the posterior leaflet being better imaged in a coronal or oblique-coronal orientation,
❚ ECG-gated cine steady-state free precession and fast spin echo in oblique-sagittal orientation at the fossa ovalis level to better delineate the potential atrial communication,
❚ ECG-gated phase velocity contrast MRI sequences perpendicular to the main pulmonary artery, ascending aorta, to assess QP/QP and particularly the right-to-left shunt.
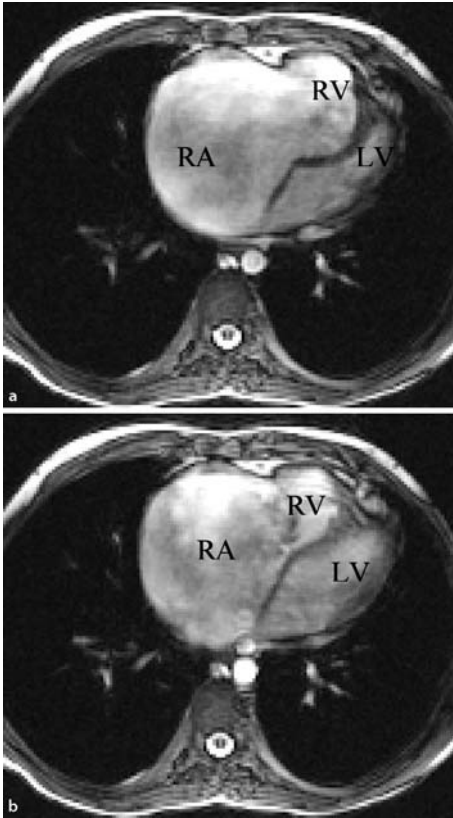
Fig. 3.10.1. Ebstein's anomaly. Cine MRI 4-chamber view, in systole (**a**) and diastole (**b**) showing a severe right atrial dilatation (*LV* left ventricle, *RA* right atrium, *RV* right ventricle) (reproduced with permission from Festa P (2004) Congenital heart disease. In: Lombardi M (ed) MRI of the heart and vessels (chapter 7.7). Springer Italia, Milan)

■ Potential complications

Residual or recurrent atrial septal defect, residual or recurrent (or surgically induced) tricuspid valve stenosis or insufficiency, complete atrioventricular block, right coronary artery obstruction during the process of plication, right ventricular dysfunction, left ventricular dysfunction.
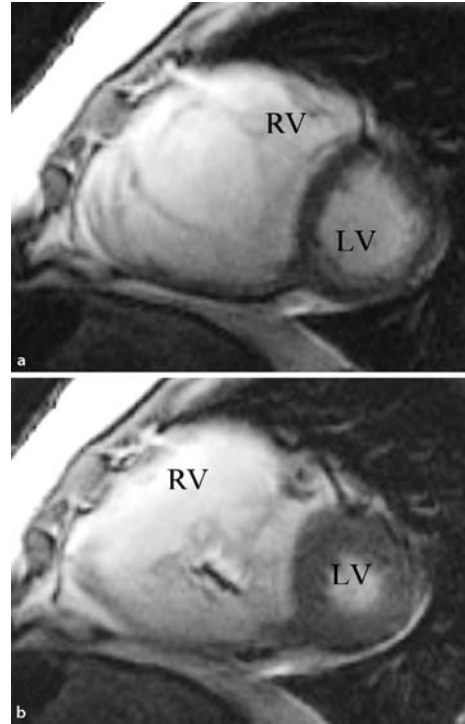
Fig. 3.10.2. Ebstein's anomaly. Cine steady-state free precession short axis of the tricuspid valve in systole (**a**) and in diastole (**b**) showing a significant lack of coaptation (*LV* left ventricle, *RV* right ventricle)

■ Post-operative follow-up

Right and left ventricular end-diastolic and end-systolic volume indexes can be measured and compared with the pre-operative values, as well as the tricuspid valve function.

■ References

Barnard CN, Schrire V (1963) Surgical correction of Ebstein's malformation with a prosthetic tricuspid valve. Surgery 54:302

Beerepoot JP, Woodard PK (2004) Case 71: Ebstein anomaly. Radiology 231:747–751

Carpentier A, Chauvaud S, Macé L, Relland J, Mihaileanu S, Marino JP, Abry B, Guibourt P (1988) A new reconstructive operation for Ebstein's anomaly of the tricuspid valve. J Thorac Cardiovasc Surg 96:92

Chauvaud SM, Hernigou AC, Mousseaux ER, Sidi D, Hébert JL (2006) Ventricular volumes in Ebstein's anomaly: X-ray multislice computed tomography before and after repair. Ann Thorac Surg 81:1443–1449

Choi YH, Park YK, Choe YH (1994) MR imaging of Ebstein's anomaly of the tricuspid valve. Am J Roentgenol 163:359

Corno AF, Chassot PG, Payot M, Sekarski N, Tozzi P, von Segesser LK (2002) Ebstein's anomaly: one and half ventricular repair. Swiss Med Weekly 132:485–488

Corno AF, Schreiber C, Augustin N (2007) Ebstein's anomaly. In: Yuh DD, Vricella LA, Baumgartner WA (eds) The John Hopkins manual of cardiothoracic surgery. McGraw-Hill, New York, pp 1353–1365

Da Silva JP, Baumgratz JF, da Fonseca L, Franchi SM, Lopes LM, Tavares GM, Soares AM, Moreira LF, Barbero-MArcial M (2007) The cone reconstruction of the tricuspid valve in Ebstein's anomaly. The operation: early and midterm results. Thorac Cardiovasc Surg 133:215–223

Goo HW, Park IS, Ko JK, Kim YH, Seo DM, Yun TJ, Park JJ, Yoon CH (2003) CT of congenital heart disease: normal anatomy and typical pathologic conditions. Radiographics 23:S147–165

Kastler B, Livolsi A, Zhu H, Roy E, Zollner G, Dietemann JL (1990) Potential role of MR imaging in the diagnostic management of Ebstein anomaly in a newborn. J Comput Assist Tomogr 14:825–827

Knott-Craig CJ, Goldberg SP, Overholt ED, Colvin EV, Kirklin JK (2007) Repair of neonates and young infants with Ebstein's anomaly and related disorders. Ann Thorac Surg 84:587–593

Quinonez LG, Dearani JA, Puga FJ, O'Leary PW, Driscoll DJ, Connolly HM, Danielson GK (2007) Results of the 1.5-ventricle repair for Ebstein anomaly and the failing right ventricle. J Thorac Cardiovasc Surg 133:1303–1310

Sarris GE, Giannopoulos NM, Tsoutsinos AJ, Chatzis AK, Kirvassilis G, Brawn WJ, Comas JV, Corno AF, Di Carlo D, Fragata J, Hraska V, Jacobs JP, Krupianko S, Sairanen H, Stellin G, Urban A, Ziemer G (2006) Results of surgery for Ebstein anomaly: a multicenter study from the European Congenital Surgeons Association. J Thorac Cardiovasc Surg 132: 50–57

Stulak JM, Dearani JA, Danielson GK (2007) Surgical management of Ebstein's anomaly. Semin Thorac Cardiovasc Surg Pediatr Card Surg Ann 10:105–111

Yun TJ, Lee SH, Ko JK (2006) Neonatal stenotic Ebstein's anomaly: a novel technique of right ventricular exclusion. J Thorac Cardiovasc Surg 131: 469–471

Wu Q, Huang Z (2001) Anatomic correction of Ebstein anomaly. J Thorac Cardiovasc Surg 122:1237–1238

CHAPTER **3.11 P**atent ductus arteriosus

▊ Definition

The ductus arteriosus connects the aortic arch opposite the left subclavian artery to the left pulmonary artery. Patent ductus arteriosus, when it closes, usually does so beginning from the pulmonary artery end, leaving a diverticulum on the aortic side (Kommerel diverticulum) which eventually closes. The patent ductus arteriosus is connected to the left pulmonary artery even in the presence of a right aortic arch. Rarely, however, it connects to the right pulmonary artery. Bilateral patent ductus arteriosus has very rarely been observed.

Associated anomalies

Atrial septal defect, atrioventricular septal defect, ventricular septal defect, aortic coarctation, tetralogy of Fallot, transposition of the great arteries and the group of ductus-dependent congenital heart defects: hypoplastic left heart, aortic arch interruption, pulmonary atresia with intact ventricular septum.

▊ Surgical options

The surgical procedure is performed through a left posterolateral thoracotomy without cardiopulmonary bypass; occasionally, in adults with large hypertensive patent ductus arteriosus with calcification on the ductal wall, cardiopulmonary bypass may be utilized.

In the case of repair of associated lesions with cardiopulmonary bypass from the median sternotomy, the repair of patent ductus arteriosus is performed through a transmediastinal approach. In this case, the ductus is exposed by dissecting along the superior aspect of the pulmonary artery bifurcation and is closed at the beginning of cardiopulmonary bypass. After careful dissection from the adjacent tissues, closure of the patent ductus can be obtained by means of ligature or surgical division between two vascular clamps and anastomosis of the two ductal stumps.

In premature neonates, due to the extreme friability of the ductal tissue, extensive dissection in the area of the patent ductus is avoided and closure is accomplished with a metal clip.

▊ Pre-operative information

Isolated patent ductus arteriosus is generally fully diagnosed by echocardiography and is considered a Class III indication for CT scan or MRI, mainly in neonates and infants. However both CT and MRI can provide more precise anatomical and morphologic details of the patent ductus arteriosus (Figs. 3.11.1 and 3.11.2). Using multiplanar CT reformations, the location, caliber, length and morphology of the patent ductus arteriosus can be assessed in isolated defects as well in complex malformations.

In adult patients, the presence and degree of calcifications of the wall of patent ductus arteriosus can be shown.

MRI is useful particularly in the case of aneurysm formation (Fig. 3.11.3) or in association with a potential co-existing great ar-
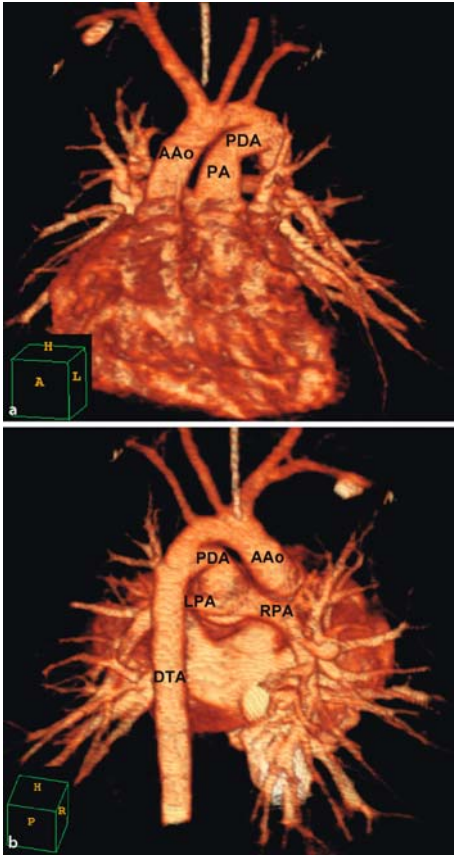
Fig. 3.11.1. Patent ductus arteriosus. CT scan in a patient with transposition of the great arteries, 3-dimensional oblique sagittal (**a**) and posterior (**b**) view showing the patent ductus arteriosus (*AAo* ascending aorta, *LPA* left pulmonary artery, *PA* pulmonary artery, *PDA* patent ductus arteriosus, *RPA* right pulmonary artery) (photographs courtesy of Dr. Mohammed Tawil)
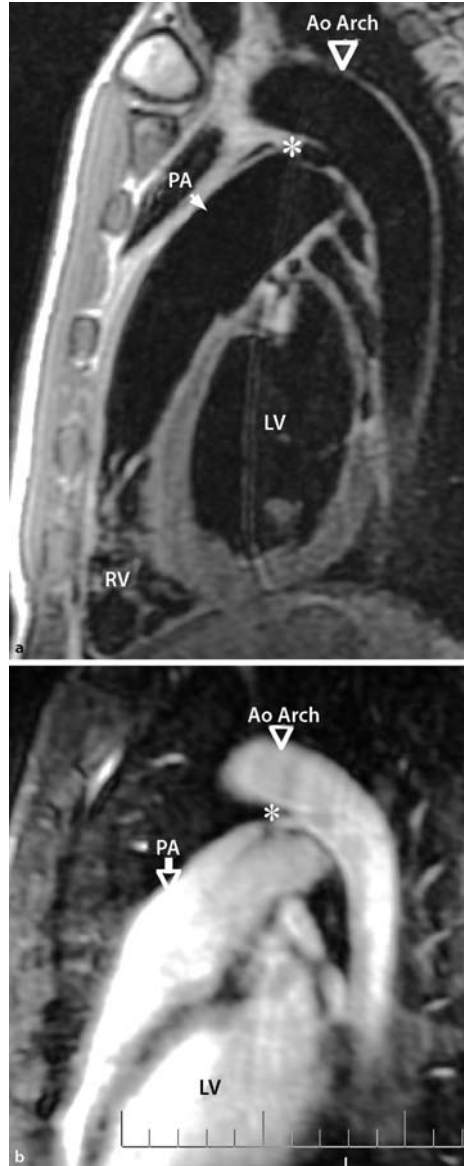
Fig. 3.11.2. Patent ductus arteriosus. MRI oblique sagittal fast spin echo (**a**) and gadolinium-enhanced 3-dimensional angiography (maximal intensity projection) (**b**) showing a small patent ductus arteriosus (*) (*Ao* aorta, *LV* left ventricle, *PA* pulmonary artery, *RV* right ventricle)
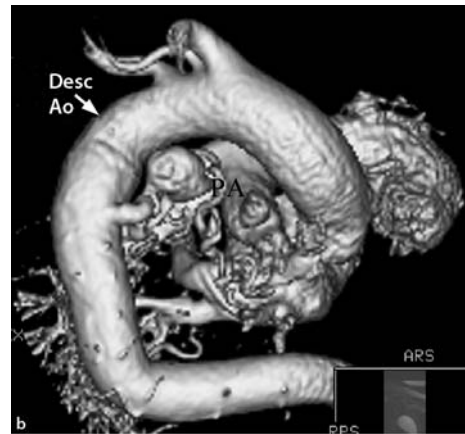
Fig. 3.11.3. Patent ductus arteriosus aneurysm. Gadolinium-enhanced 3D MR angiography (**a**) maximal intensity projection and (**b**) volume rendering showing an aneurysm (*) of patent ductus arteriosus (*Desc. Ao* descending aorta, *PA* pulmonary artery)
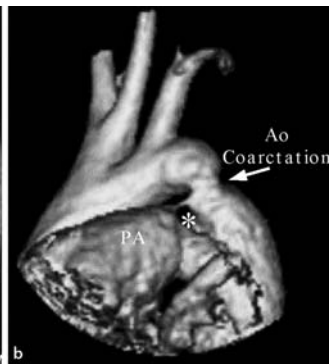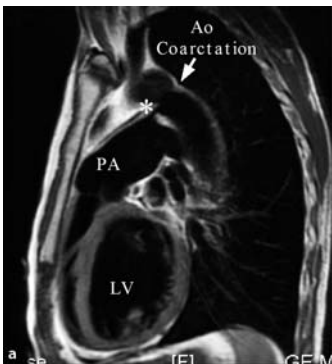
Fig. 3.11.4. Patent ductus arteriosus and aortic coarctation. Oblique sagittal fast spin echo (**a**), gadolinium-enhanced 3-dimensional MR angiography volume rendering (**b**) and cine MRI (**c**) showing a very small patent ductus arteriosus (*) associated with aortic coarctation (*Ao* aorta, *LV* left ventricle, *PA* pulmonary artery)

tery anomaly (Fig. 3.11.4). Cine MRI and MRI-PVC acquisitions can respectively visualize the flow jet into the main pulmonary artery (Fig. 3.11.4) and assess the amount of shunt, knowing that in the presence of patent ductus arteriosus without other shunting lesions, the systemic blood flow (QS) is equal to the main pulmonary artery flow, and pulmonary blood flow (QP) is equal to the ascending aorta flow.

In the presence of patent ductus arteriosus, we suggest the following MRI protocol:

- 3-plane localizing images,
- 2-dimensional axial Time-of-flight Angiography (see the appendix in the "Introduction"),
- ECG-gated cine steady-state free precession and fast spin echo sequences in the para-sagittal oblique and axial view at the level of the patent ductus arteriosus and great arteries (Fig. 3.11.2),
- ECG-gated phase velocity contrast MRI sequences perpendicular to the main pulmonary artery and ascending aorta, to assess the QP/QS,
- gadolinium-enhanced 3-dimensional MR angiography for the evaluation of the aortic arch and patent ductus arteriosus (Fig. 3.11.3).

▌ Potential complications

Residual or recurrent patency (after ligature, not after division), hemorrhage, paradoxical arterial hypertension (in neonates), chylothorax, recurrent laryngeal nerve lesion. A late complication, extremely rare, is the formation of an aneurysm.

▌ Post-operative follow-up

CT scan and MRI are very rarely indicated in the post-operative evaluation, unless an aneurysm at the site of the ductus arteriosus is suspected.

▌ References

Beerbaum P, Korperich H, Barth P, Esdorn H, Gieseke J, Meyer H (2001) Noninvasive quantification of left-to-right shunt in pediatric patients: phase-contrast cine magnetic resonance imaging compared with invasive oximetry. Circulation 103:2476–2482

Goitein O, Fuhrman CR, Lacomis JM (2005) Incidental finding on MDCT of patent ductus arteriosus: use of CT and MRI to assess clinical importance. Am J Roentgenol 184:1924–1931

Goo HW, Park IS, Ko JK, Kim YH, Seo DM, Yun TJ, Park JJ, Yoon CH (2003) CT of congenital heart disease: normal anatomy and typical pathologic conditions. Radiographics 23:S147–165

Lankipalli RS, Lax K, Keane MG, Toca FM, Bavaria JE, Milas BL, Ferrari VA, Charagundla SR, Silvestry FE (2005) Images in cardiovascular medicine. Infected patent ductus arteriosus. Circulation 112:364–365

Lee TY, Ng SH, Liang CD, Hsieh MJ, Ko SF (2006) Dissection of Kommerell's aneurysm mimicking aortic arch dissection on echocardiography: multislice computed tomographic diagnosis. J Thorac Cardiovasc Surg 132:1228–1230

Morgan-Hughes GJ, Marshall AJ, Roobottom C (2003) Morphologic assessment of patent ductus arteriosus in adults using retrospectively ECG-gated multidetector CT. Am J Roentgenol 181:749–754

Salvana EM (2006) Images in clinical medicine. Patent ductus arteriosus in an elderly man. N Engl J Med 354:2484

Tomaszewski A, Czekajska-Chehab E, Wojcik M, Drop A (2004) Patent ductus arteriosus (PDA) in adults evaluated in echocardiography and multi-slice computed tomography (MSCT). Ann Univ Mariae Curie Sklodowska 59:339–345

Wald RM, Powell AJ (2006) Simple congenital heart lesions. J Cardiovasc Magn Reson 8:619-631

Weber OM, Higgins CB (2006) MR evaluation of cardiovascular physiology in congenital heart disease: flow and function. J Cardiovasc Magn Reson 8:607–617

Left ventricular outflow tract obstruction

Valvular

▮ Definition

The commissurae of the aortic valve may be fused, and the ring is occasionally small. The orifice of the aortic valve can be eccentric. The valve is commonly bicuspid in aortic stenosis and the leaflets are asymmetric in 40% of cases. There is occasionally more than one level of obstruction in the left ventricular outflow tract together with aortic valvular stenosis. About 10% of patients with aortic valvular stenosis have subvalvar aortic stenosis. Supravalvar aortic stenosis is rarely associated with aortic stenosis. In 50% of valvular aortic stenosis patients, a certain degree of aortic insufficiency is associated. Aortic valvular stenosis is not always the result of a bicuspid aortic valve, since bicuspid aortic valve is 10–20 times as common as aortic stenosis. Thus, a small number of bicuspid valves leads to aortic stenosis, but the majority will not develop into aortic stenosis. Right-to-left commissures have a worse prognosis in bicuspid aortic than anteroposterior commissures in developing aortic stenosis. Also eccentric orifices have a worse prognosis than central orifices in developing aortic stenosis.

Associated anomalies

Subvalvular and/or supravalvular obstruction, hypoplastic aortic annulus, hypoplastic aortic arch, aortic coarctation, mitral stenosis, mitral regurgitation, atrial septal defect, ventricular septal defect, patent ductus arteriosus. In neonates, the association of left ventricular hypoplasia or fibroelastosis is relatively frequent.

▮ Surgical options

Surgical *aortic valvotomy* is performed accordingly with the aortic valve morphology: the fused commissurae are opened by careful incision, but without reaching the aortic wall. The obtained opening is controlled with Hegar dilators and compared with the normal size for the age and body weight.

Aortic valve replacement, where required, can be performed using conventional surgical techniques, even if in infants and children the preferred surgical option is a *Ross operation* (autotransplantation of the native pulmonary valve in the aortic position and right ventricle to pulmonary artery continuity obtained with a valved homograft or heterograft).

If the size of the aortic annulus is small, the *enlargement of the aortic annulus* can be performed with one of the following techniques:

▮ *Posterior annular enlargement*
- *Nicks*: aortotomy extended through the noncoronary sinus and the anterior leaflet of the mitral valve; enlargement obtained with prosthetic patch,
- *Managouian*: aortotomy extended through the left and noncoronary sinuses and the anterior leaflet of the mitral valve; enlargement obtained with prosthetic patch.

▍ *Aortoventriculoplasty*
  – *Konno-Rastan*: aortotomy extended through the right ventricular outflow tract, aortic annulus divided between the right and left cusps, interventricular septum incised; enlargement obtained with one patch to enlarge interventricular septum, aortic annulus and aortic root, one to enlarge the right ventricular outflow tract,
  – *Clarke*: aortoventriculoplasty performed using an aortic homograft instead of an artificial valve; the septal leaflet of the mitral valve of the homograft is used as a patch for the incised interventricular septum,
  – *Ross-Konno*: aortoventriculoplasty performed using a pulmonary autograft.

▍ Pre-operative information

The transthoracic and, when required, transesophageal echocardiography are generally able to accurately evaluate the anatomy and functioning of the malformed aortic valve, as well as to provide information useful for the decision-making and the timing for intervention.

According to the guidelines of the Society of Cardiac MRI, cardiac MRI is not indicated in case of isolated aortic valve stenosis. However, aortic insufficiency, due to MRI's ability to accurately evaluate left ventricular volume and function, to identify the potential presence of fibrosis, as well as to quantify the degree of aortic valve regurgitation, is considered a class II indication. In adult patients with a bicuspid aortic valve, MRI and CT are useful to assess the size of the ascending aorta and its progressive dilatation over time. Moreover new insights on bicuspid aortic valves are coming from cardiac MRI studies, mainly focused on the abnormal mechanical proprieties of the aortic wall in such subjects. CT scan can be also indicated for calcium detection and quantification.

The following is the cardiac MRI protocol suggested to evaluate the left ventricular outflow tract and aortic obstructions:
▍ 3-plane localizing images,
▍ 2-dimensional axial Time-of-flight Angiography (see the appendix in the "Introduction")
▍ ECG-gated cine steady-state free precession sequences in 2-chamber, 4-chamber planes, and ventricular short axis for the quantitative assessment of ventricular dimensions, function, mass and stroke volume, as illustrated in the appendix of the "Introduction",
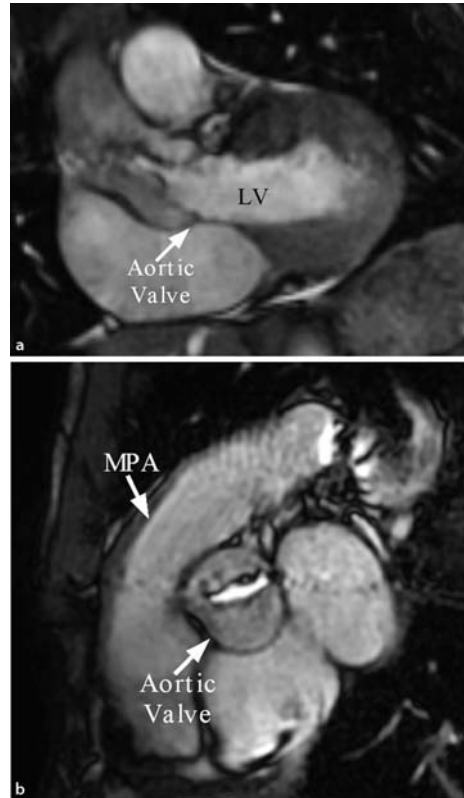
Fig. 3.12.1. Bicuspid aortic valve stenosis. Cine MRI steady-state free precession of long axis (**a**) and short axis (**b**) showing a bicuspid aortic valve. Note the reduced opening of the aortic leaflets (*LV* left ventricle, *MPA* main pulmonary artery)
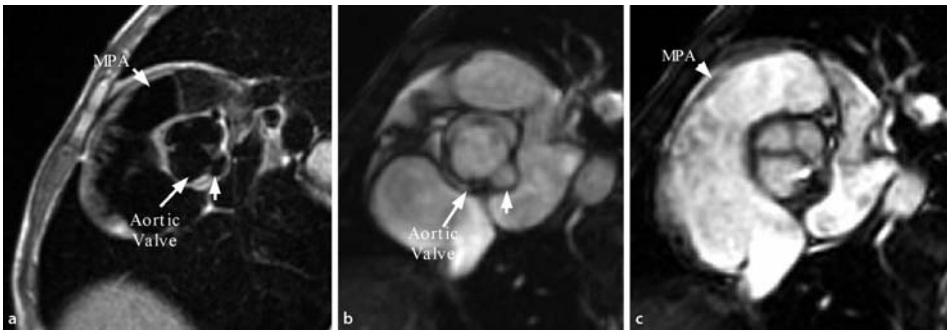
Fig. 3.12.2. Bicuspid aortic valve stenosis. MRI showing the aneurysm of noncoronary sinus of Valsalva in a steno-insufficient bicuspid aortic valve (headarrow): static fast spin echo imaging (**a**); cine MRI steady-state free precession (**b, c**) (*MPA* main pulmonary artery)

▪ ECG-gated cine steady-state free precession para-sagittal sequence to visualize the left ventricular outflow tract, ascending aorta, and the aortic arch,

▪ ECG-gated cine steady-state free precession 3-chamber view, and others planes if required to visualize the left ventricular outflow tract,

▪ ECG-gated cine steady-state free precession and, when needed, fast echo short axis of the aortic valve and ascending aorta to evaluate the morphology, and the leaflet opening and coaptation (Figs. 3.12.1 and 3.12.2), and the wall of the proximal ascending aorta,

▪ ECG-gated phase velocity contrast MRI sequences perpendicular to the aortic valve and ascending aorta to estimate the degree of aortic valve regurgitation and the flow maximum velocity,

▪ gadolinium-enhanced 3-dimensional MRI if required for the evaluation of the aortic arch and the brachiocephalic vessels,

▪ post-gadolinium delayed myocardial enhancement may be used to evaluate the presence of fibrotic tissue.

▪ Potential complications

Residual or recurrent aortic valve stenosis, aortic valve regurgitation, complete atrioventricular block.

▪ Post-operative follow-up

Regardless of the type of surgery, echocardiography is obviously the first diagnostic tool for the post-operative evaluation. Cardiac MRI could be required, mainly in adult patients, when echocardiography is not exhaustive or when it contradicts the clinical picture, or when more insight is required on the status of the ascending aorta, degree of aortic valve regurgitation, left ventricular function, myocardial fibrosis or in case of associated anomalies.

The MRI protocol in the post-operative follow-up is the same as in the pre-operative evaluation.

Post-operative investigations after the Ross operation are addressed to both the left and the right ventricular outflow tracts (Fig. 3.12.3). With regard to the newly constructed *left* ventricular outflow tract, the following information is increasingly being incorporated into the clinical imaging protocol in patients after Ross operation:

▪ the adequate reconstruction of the new aortic root with the position of the pulmonary autograft;

▪ the transplanted orifices of the coronary arteries on the pulmonary autograft (if the root replacement technique was used), with absence of kinking, twisting, compression or distortion;
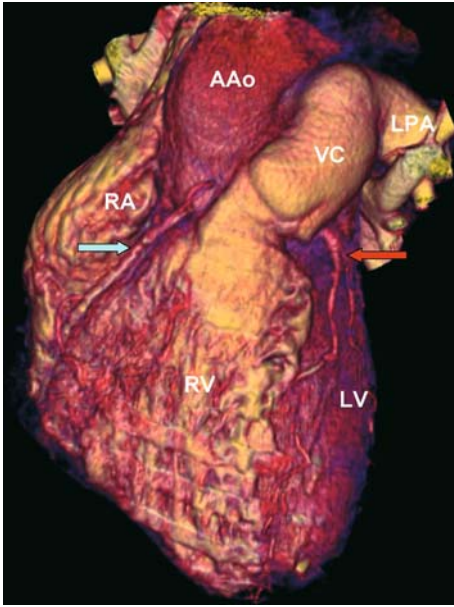
Fig. 3.12.3. Status post Ross operation. CT scan with contrast angiography, volume rendering technique, showing the autotransplantation of the pulmonary valve in the aortic position, the reimplanted right (blue arrow) and left (red arrow) coronary artery, and the biological valve conduit used to reconstruct the continuity right ventricle to the pulmonary artery (*AAo* ascending aorta, *LPA* main pulmonary artery, *LV* left ventricle, *RA* right atrium, *RV* right ventricle, *VC* valved conduit)

▮ the size of the aortic root and ascending aorta, and their potential progressive dilatation over time, in the cases that required size adaptation of the ascending aorta because of the presence of pre-operative dilatation, like for severe aortic valve regurgitation;

▮ the function of the "new" aortic valve;

▮ imaging of the coronary arteries for evaluation of proximal stenosis of the coronary arteries.

With regard to the newly constructed *right* ventricular outflow tract by means of either a homograft or a heterograft, the following can be determined:

▮ the adequate reconstruction of the new right ventricular outflow tract without narrowing at various levels: proximal anastomosis on the right ventricle, biological valved conduit itself or distal anastomosis on the pulmonary artery;

▮ the absence of extrinsic compression, kinking or twisting of the biological valved conduit;

▮ the "new" pulmonary valve function at late follow-up.

Subvalvular

▮ Definition

The subaortic obstruction can be determined by the following different morphological types:

▮ posterior malalignment of the outlet septum,

▮ asymmetric septal hypertrophy or hypertrophic cardiomyopathy,

▮ discrete fibromuscular diaphragm or ridge, generally close to the aortic valve,

▮ extensive fibromuscular tunnel with involvement of the mitral valve,

▮ the combination of the above.

The aortic annulus can be normal or hypoplastic.

Associated anomalies

Coarctation of the aorta, aortic arch interruption, mitral stenosis, ventricular septal defect, atrioventricular septal defect, double chamber right ventricle, univentricular heart.

▮ Surgical options

The discrete fibromuscular diaphragm is treated by diaphragm dissection/resection with septal myotomy/myectomy. In the presence of malalignment between the left ventricular outflow tract and the ascending aorta, septal myectomy is needed in order to obtain a straight outflow and prevent recurrences.

An extensive fibromuscular tunnel is treated with one of two different techniques, depending on the size of the aortic annulus:

- *Small annulus*: aortoventriculoplasty (see above for aortic valve replacement),
- *Normal annulus*: ventricular septoplasty, generally called partial Konno-Rastan procedure, despite it being described for the first time by Cooley in 1986; the right ventricular outflow tract and the interventricular septum are incised, without incising the aortic annulus; relief of subaortic obstruction is obtained with a prosthetic patch to enlarge the interventricular septum; a second patch is required to enlarge the incised right ventricular outflow tract.

▪ Pre-operative information

Even more than for valvular obstruction, the transthoracic and, when required, transesophageal echocardiography, are generally exhaustive to accurately evaluate the morphology of the left ventricular outflow tract and the degree of obstruction, as well as to provide information useful for the decision-making and the timing for intervention.

Thus, CT scan and MRI (Fig. 3.12.4) are rarely used in the pre-operative evaluation of subaortic obstruction, with the exception of
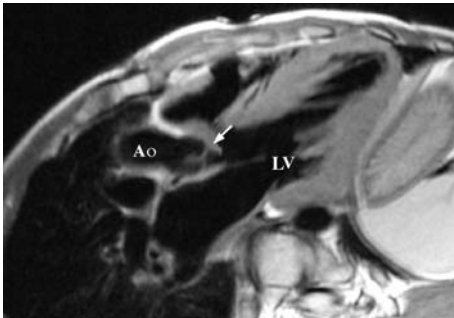
Fig. 3.12.4. Subvalvular aortic obstruction. MRI fast spin echo 3-chamber view parallel to the left ventricular outflow tract showing a severe subaortic stenosis due to the posterior infundibular deviation (arrow) (*Ao* aorta, *LV* left ventricle)

hypertrophic cardiopulmonary, where MRI can provide useful prognostic data, as recently reported.

▪ Potential complications

Residual or recurrent left ventricular outflow tract obstruction, residual or recurrent aortic valve regurgitation, mitral valve lesion, creation of ventricular septal defect, complete atrioventricular block.

▪ Post-operative follow-up

For the post-operative follow-up, echocardiography also provides sufficient information.

Supravalvular

▪ Definition

Supravalvular aortic stenosis may be localized or diffuse:

- *Localized:* usually there is an externally apparent waisting of the supravalvular area of aorta, just above or at the upper level of attachments of the valve leaflets; hourglass appearance in association with some dilatation of the sinuses of Valsalva. There is a variable amount of intimal thickening with an internal shelf which substantially increases the obstruction and may cause severe stenosis or even a complete occlusion of the origin of the left main coronary artery.
- *Diffuse:* less frequently the supravalvular narrowing is diffuse with extension through the entire ascending aorta, even beyond into the aortic arch and the origin of the brachiocephalic arteries.

Associated anomalies

One-third of all cases have Williams-Beuren syndrome.

Thickened aortic valve leaflets but without a true valvular stenosis (30%), rarely hypo-

plastic aortic annulus or subvalvular obstruction, hypoplastic pulmonary arteries (30%), coarctation of the aorta (15%), stenosis at the origin of the subclavian and carotid arteries or renal artery stenosis (5%), very rarely ventricular septal defect. Obstruction of the left main coronary artery origin is more frequent, but it can occur also in the right. In the absence of obstruction at the origin, the coronary arteries are exposed to high pressure and as a consequence they present with dilatations, tortuosities and medial hypertrophy.

∎ Surgical options

∎ Localized type
∎ *Classical technique*: the aorta is opened above the valve and the incision is prolonged into the right coronary sinus or into the noncoronary sinus or into both the right and noncoronary sinuses. After inspection of the origin of the coronary arteries, the intimal shelf is resected. Aortic enlargement is then obtained with either a diamond-shaped (in the case of a single incision in one of the sinuses of Valsalva) or with an inverted-Y (in the case of incision extending into both the right and noncoronary sinuses) prosthetic patch.
∎ *Brom technique*: the aorta is completely transected just above the supravalvular stenosis, all sinuses of Valsalva are incised and enlarged with three separate prosthetic patches; the ascending aorta is then reconstructed with end-to-end anastomosis.

Fig. 3.12.5. Supravalvular aortic stenosis. MRI images: anteroposterior (**a**) and lateral (**b**) projections showing moderate to severe degree of supravalvular aortic stenosis, with mild to moderate degree of aortic arch hypoplasia; the aortic wall appears thickened, and this extends around the arch and into the neck vessels. **c** 3-dimensional contrast-enhanced MRI, lateral view, showing moderate to severe degree of supravalvular aortic stenosis, with mild to moderate degree of aortic arch hypoplasia (photographs courtesy of Dr. Philipp Beerbaum and Dr. Rob Johnson)
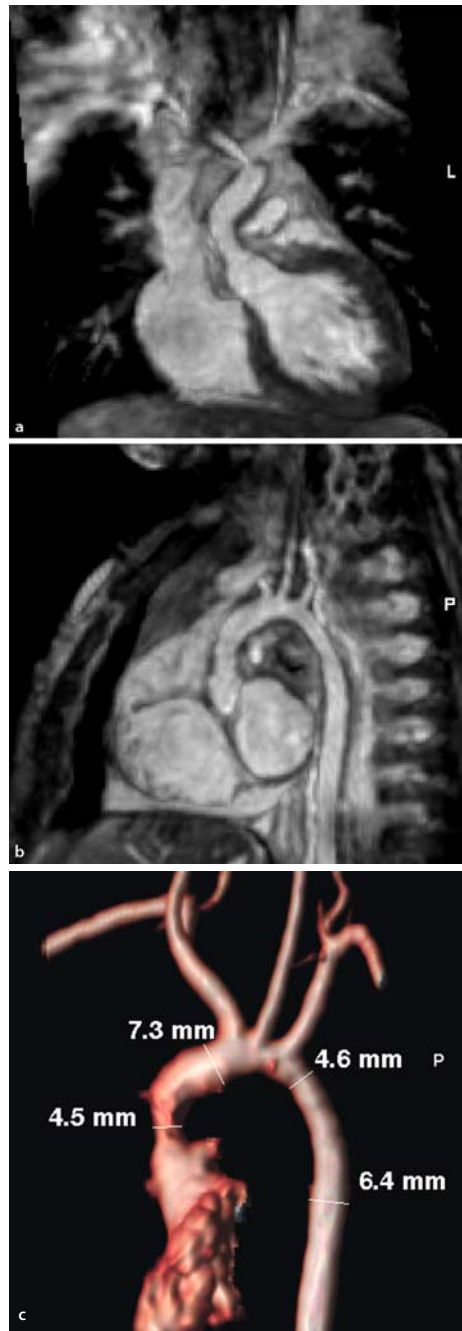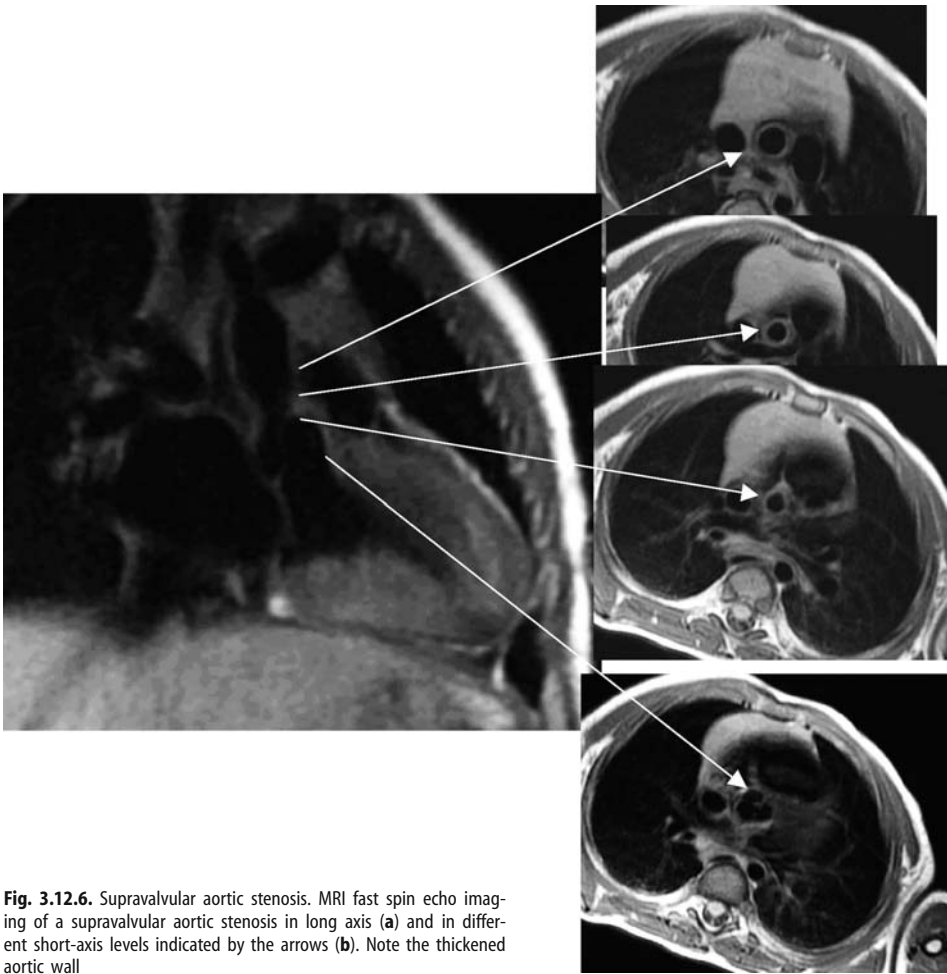
Fig. 3.12.6. Supravalvular aortic stenosis. MRI fast spin echo imaging of a supravalvular aortic stenosis in long axis (**a**) and in different short-axis levels indicated by the arrows (**b**). Note the thickened aortic wall

■ **Diffuse type:** Deep hypothermia and circulatory arrest are generally required. The incision corresponding to the supravalvular obstruction is prolonged through the ascending aorta and aortic arch, until reaching a normal diameter of the aorta. Enlargement is obtained with a prosthetic patch or with an aortic homograft.

■ **Pre-operative information**

Especially in patients with Williams's syndrome, CT scan (Fig. 3.12.5 a) and MRI (Figs. 3.12.5 b and 3.12.6) are very helpful to visualize the entire aorta and the peripheral pulmonary arteries. In these cases, in addition to the MRI protocol described above, MR angiography targeted to both the pulmonary and systemic circulation is necessary.
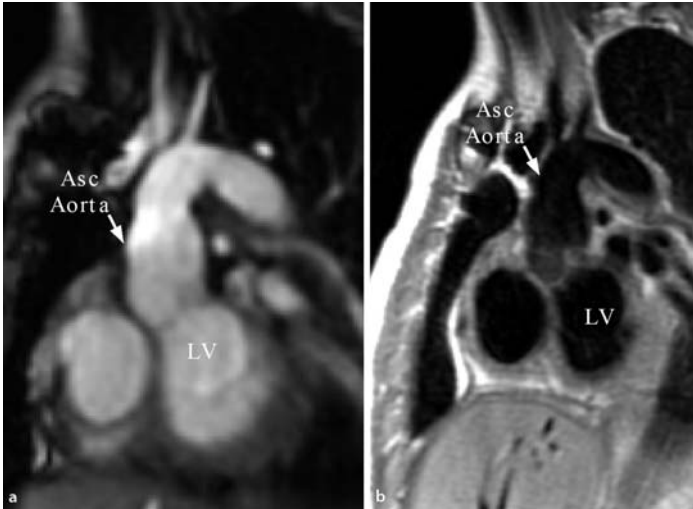
Fig. 3.12.7. Supravalvular aortic stenosis, status post repair. MRI post-operative imaging of the ascending aorta after surgical repair. **a** MR angiography maximal intensity projection reconstruction; **b** fast spin echo imaging in the para-sagittal plane (*Asc. aorta* ascending aorta, *LV* left ventricle)
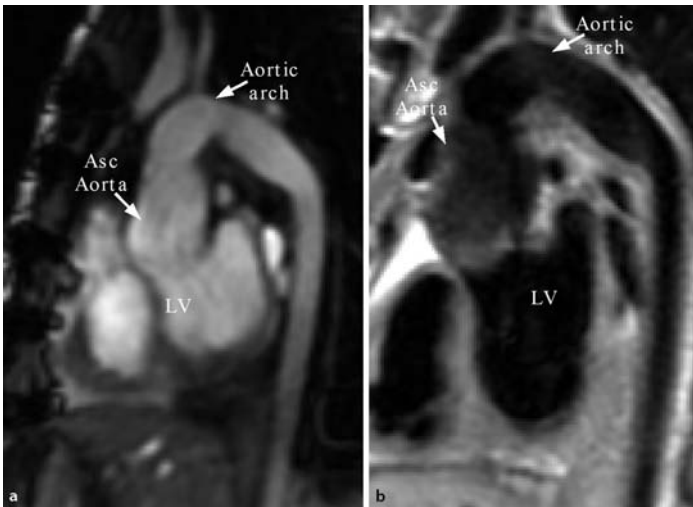
Fig. 3.12.8. Supravalvular aortic stenosis, status-post repair. MRI with post-operative imaging of the ascending aorta after surgical repair of supravalvular aortic stenosis and aortic coarctation. **a** MR angiography maximal intensity projection reconstruction; **b** fast spin echo imaging in the para-sagittal plane (*Asc. aorta* ascending aorta, *LV* left ventricle)

■ Potential complications

Residual or recurrent supravalvular stenosis, aortic valve regurgitation, coronary artery lesion.

■ Post-operative follow-up

As for the pre-operative investigation, CT scan and MRI (Figs. 3.12.7 and 3.12.8) are very useful to visualize the entire aorta and to show the result of the surgical reconstruction.

■ References

Adabag AS, Maron BJ, Appelbaum E, Harrigan CJ, Buros JL, Gibson CM, Lesser JR, Hanna CA, Udelson JE, Manning WJ, Maron MS (2008) Occurrence and frequency of arrhythmias in hypertrophic cardiomyopathy in relation to delayed enhancement on cardiovascular magnetic resonance. J Am Coll Cardiol 51: 1369–1374

Ait-Ali L, Aquaro G, Bernabei M, Chiappino D, Farneti A, Kull S, Mariani M, Festa P (2007) MRI evaluation of biophysical proprieties of ascending aorta in bicuspid aortic valve. J Cardiovasc Med 8(Suppl 2):37

Arai AE, Epstein FH, Bove KE, Wolff SD (1999) Visualization of aortic valve leaflets using black blood MRI. J Magn Reson Imaging 10:771–777

Cicini MP, Giannico S, Marino B, Iorio FS, Corno AF, Marcelletti C (1992) "Acquired" subvalvular aortic stenosis after repair of a ventricular septal defect. Chest 101:115–118

Corno AF, Hurni M, Griffin H, Jeanrenaud X, von Segesser LK (2001) Glutaraldehyde-fixed bovine jugular vein as a substitute for the pulmonary valve in the Ross operation. J Thorac Cardiovasc Surg 122: 493–494

Corno AF, Chassot PG, Jeanrenaud X, Tozzi P, Wicky S, von Segesser LK (2002) Aortic valve disease: is the Ross operation the solution? Med Cardiovasc 5 (Suppl 4):46S

Corno AF, von Segesser LK (2003) The stealth Ross operation. Asian Cardiovasc Thorac Ann 11:186

Corno AF, Qanadli SD, Sekarski N, Artemisia S, Hurni M, Tozzi P, von Segesser LK (2004) Bovine valved xenograft in pulmonary position: medium-term follow-up with excellent hemodynamics and freedom from calcifications. Ann Thorac Surg 78:1382–1388

Davtyan HG, Corno AF, Drinkwater DC, George B, Laks H (1986) Valve replacement for congenital heart disease. Circulation 74:II-250

Grotenhuis HB, Ottenkamp J, Westenberg JJ, Bax JJ, Kroft LJ, de Roos A (2007) Reduced aortic elasticity and dilatation are associated with aortic regurgitation and left ventricular hypertrophy in nonstenotic bicuspid aortic valve patients. J Am Coll Cardiol 49:1660–1665

Konno S, Imai Y, Iida Y, Nakajima M, Tatsuno K (1975) A new method for prosthetic valve replacement in congenital aortic stenosis associated with hypoplasia of the aortic valve ring. J Thorac Cardiovasc Surg 70:909

Pierli C, Marino B, Picardo S, Corno AF, Pasquini L, Marcelletti C (1989) Discrete subaortic stenosis: surgery in children based on two dimensional and Doppler echocardiography. Chest 96:325–328

Rastan H, Koncz J (1976) Aortoventriculoplasty. A new technique for the treatment of left ventricular outflow tract obstruction. J Thorac Cardiovasc Surg 71:920

Ross DN (1967) Replacement of aortic and mitral valve with a pulmonary autograft. Lancet 2:956

Sebastià C, Quiroga S, Boyé R, Perez-Lafuente M, Castellà E, Alvarez-Castells A (2003) Aortic stenosis: spectrum of diseases depicted at multisection CT. Radiographics 23:S79–S91

Shone JD, Sellers RD, Anderson RC, Adams P, Lillehei CW, Edwards JE (1963) The developmental complex of parachute mitral valve, supravalvular ring of left atrium, subaortic stenosis and coarctation of the aorta. Am J Cardiol 11:714–725

Stolzmann P, Scheffel H, Bettex D, Karlo C, Frauenfelder T, Prêtre R, Marincek B, Alkadhi H (2007) Subvalvular aortic stenosis: comprehensive cardiac evaluation with dual-source computed tomography. J Thorac Cardiovasc Surg 134:240–242

Wang IJ, Chen SJ, Wang JK, Chang CI, Wu MH (2003) Electron beam computed tomography appearance of endocardial fibroelastosis. Int J Cardiovasc Imaging 19:85–90

Williams JCP, Barrat-Boyes BG, Lowe JB (1961) Supravalvular aortic stenosis. Circulation 24:1311

Chapter 3.13 Aortic coarctation
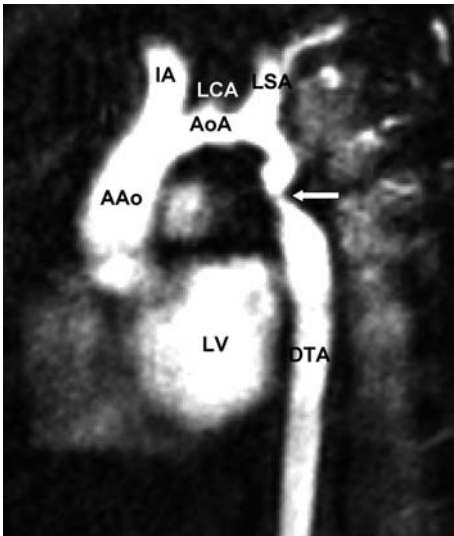
▊ Definition

Aortic coarctation is a congenital narrowing of the aortic lumen, usually situated between the origin of the left subclavian artery proximally and the junction of the aorta and the ductus arteriosus distally. When the coarctation is an isolated finding, the wall of the aorta is pinched in a waist-like fashion, the ascending and descending portions of the arch tending to expand above and below the

Fig. 3.13.1. Aortic coarctation. MR angiography, sagittal view, showing severe aortic coarctation (arrow) (*AAo* ascending aorta, *AoA* aortic arch, *DTA* descending thoracic aorta, *IA* innominate artery, *LCA* left carotid artery, *LSA* left subclavian artery, *LV* left ventricle)

site of coarctation. The narrowing may consist of an elongated and diffuse tract, proximally to the ductus arteriosus (Fig. 3.13.1), or of a sharp constriction in the area of aortic insertion of the arterial duct, with a diaphragmatic shelf of fibrous tissue protruding into the lumen, often with a pin-hole orifice representing the only communication between the ascending and descending aortic segments (Fig. 3.13.2). Aortic arch hypoplasia of mild or severe degree may also be present (Figs. 3.13.3–3.13.5). Collateral circulation between the aorta proximal and distal to the aortic coarctation increases in size and extensiveness as the patient ages (Fig. 3.13.6).

Occasionally the aorta may be redundant and severely kinked opposite the ligamentum arteriosum, without any pressure gradient or with a mild gradient, so-called pseudo-coarctation (Fig. 3.13.7).

Associated anomalies

Patent ductus arteriosus, atrial septal defect, atrioventricular septal defect, ventricular septal defect, double inlet ventricle (with or without actual or potential systemic outlet obstruction), supravalvular or valvular mitral stenosis, valvular or subvalvular aortic stenosis (frequently with bicuspid aortic valve), multiple stenotic lesions of the left heart (=Shone's syndrome), transposition of the great arteries (usually with ventricular septal defect, with or without actual or potential systemic outlet obstruction), double-outlet right ventricle (usually with ventricular septal defect, with or without actual or potential systemic outlet obstruction), trun-

Fig. 3.13.2. Aortic coarctation. Fast spin echo MRI acquisition showing different types of aortic coarctation: "discrete" shelf (arrow) clearly seen at the isthmus level (**a**) and an elongate type of aortic coarctation (arrow) (**b**) (*Coa* aortic coarctation)
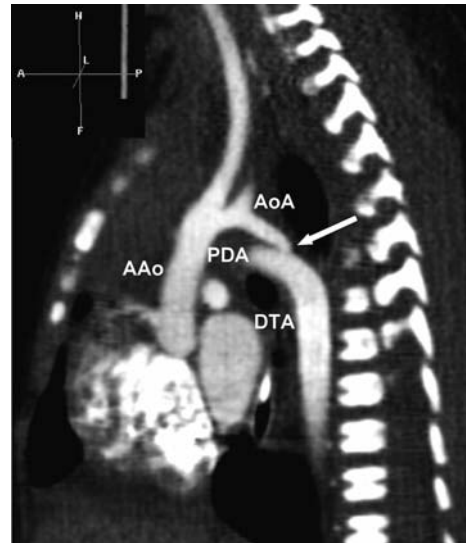
Fig. 3.13.3. Aortic coarctation with hypoplastic aortic arch. CT scan, sagittal projection, contrast angiography showing the diffuse narrowing of the hypoplastic distal transverse aortic arch with severe aortic coarctation (arrow), and the distal systemic circulation perfused by a patent ductus arteriosus (*AAo* ascending aorta, *AoA* aortic arch, *DTA* descending thoracic aorta, *PDA* patent ductus arteriosus) (photograph courtesy of Dr. Mohamed Tawil)
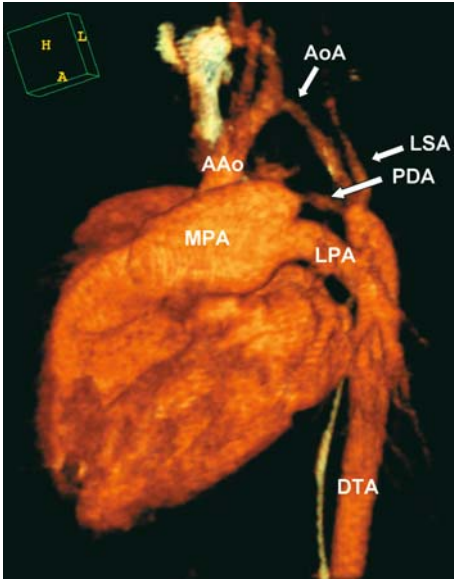
Fig. 3.13.4. Aortic coarctation with hypoplastic aortic arch. CT angiography in a neonate with 3-dimensional reconstruction, sagittal projection, showing severe hypoplasia of the aortic arch and anomalous origin of the left subclavian artery (*AAo* ascending aorta, *AoA* aortic arch, *DTA* descending thoracic aorta, *LPA* left pulmonary artery, *LSA* left subclavian artery, *MPA* main pulmonary artery, *PDA* patent ductus arteriosus) (photograph courtesy of Dr. Mohamed Tawil)
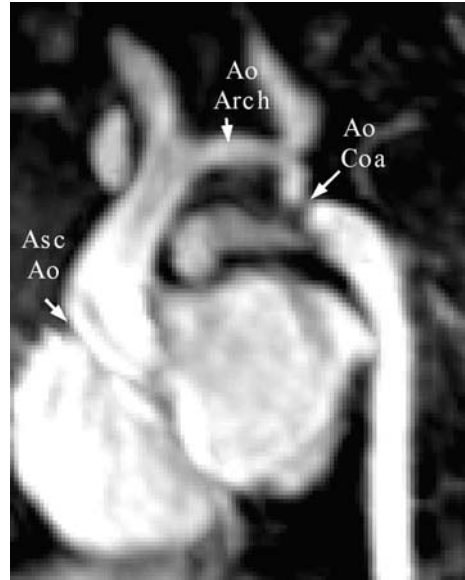
Fig. 3.13.5. Aortic coarctation with hypoplastic aortic arch. MR angiography maximal intensity projection reconstruction showing severe aortic coarctation with hypoplastic aortic arch (*Ao* aorta, *Asc Ao* ascending aorta, *Ao Coa* aortic coarctation)

cus arteriosus, double discordance, hypoplastic left heart, anomalous origin of coronary arteries, anomalous right subclavian artery, intracranial aneurysms, very rarely tetralogy of Fallot.

∎ Surgical options

All the following procedures are performed through a left posterolateral thoracotomy without cardiopulmonary bypass. If present, the patent ductus arteriosus is ligated and divided. Occasionally, in adults with complex anatomy or recurrent coarctation, a temporary bypass (from the ascending aorta or from the left atrium to the descending thoracic aorta) may be utilized.

In the case of repair of associated lesions with cardiopulmonary bypass from median sternotomy, the repair of aortic coarctation is performed through a transmediastinal approach.

∎ *Resection and end-to-end anastomosis*:
   – this is the standard procedure for discrete aortic coarctation,
   – in neonates and infants with aortic arch hypoplasia this can be *extended* to the aortic arch,
   – in adults, due to poor mobilization of the aortic stumps, *conduit interposition* may (rarely) be necessary after aortic resection in order to avoid excessive tension of the anastomosis.
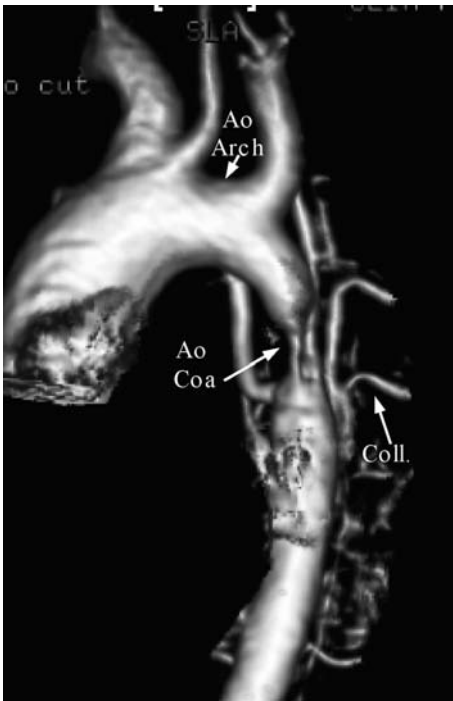
Fig. 3.13.6. Aortic coarctation with huge collateral circulation. MR angiography volume rendering reconstruction showing extensive collateral arteries (*Ao Arch* aortic arch, *Ao Coa* aortic coarctation, *Coll* = collateral arteries)

3.13.7. Aortic pseudo-coarctation. MR angiography maximal intensity projection reconstruction of the aortic arch showing the aorta stretched with mild "kinking", but without obstruction (*Ao Arch* aortic arch, *Asc Ao* ascending aorta)

■ *Subclavian flap aortoplasty*:
 – the aortic enlargement is obtained by utilizing the left subclavian artery, opened longitudinally and brought down and sutured to enlarge the aortic isthmus,
 – this can be modified in *reverse subclavian flap* to enlarge a hypoplastic aortic arch.
■ *Patch aortoplasty*:
 A biological (rarely) or synthetic (frequently) patch is implanted to enlarge the narrow aortic isthmus, opened with a longitudinal incision. However, this technique is nowadays virtually abandoned because of the frequent reports of aneurysm formation in the area of the prosthetic patch. An acceptable alternative option, particularly in infants, is aortoplasty using the enlarged base of the transected left subclavian artery.
■ *Aortic bypass*:
 Rarely, in case of complex or recurrent coarctation or in case of pseudo-coarctation (aortic kinking, without collateral circulation), a synthetic tubular prosthesis may be inserted between the ascending aorta (through an extended left or a right thoracotomy) or the left subclavian artery (left thoracotomy) and the distal descending thoracic aorta.
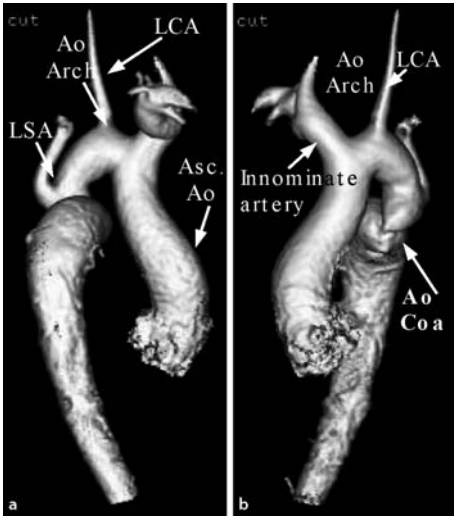
■ Pre-operative information

In infants, transthoracic echocardiography is generally sufficient to correctly diagnose aortic coarctation. However, in children and adults, as the anatomy of the arch can be

difficult to assess by echocardiography (Fig. 3.13.8), CT scan and MRI can provide excellent anatomic details of the aortic arch and are very helpful for the decision-making process to decide between interventional and surgical treatment. The advantages and disadvantages of CT and MRI have already been discussed in the "Introduction".

The preoperative informations required in suspected aortic coarctation are the following:

■ anatomy of the aortic arch and isthmus, including cross-sectional diameters and relationship to brachiocephalic vessels. The aortic arch diameter accepted as normal in neonates and infants is ≥1 mm/kg of body weight; however some consider the aortic arch as hypoplastic if the ratio aortic arch/descending aorta diameter at the level of the diaphragm is <0.9,

■ potential associated anomalies: bicuspid aortic valve, patent ductus arteriosus, anomalous right subclavian artery (Fig. 3.13.9),

■ severity of the obstruction and hemodynamics,

■ left ventricular volume, mass and function.

Classically, the severity of aortic coarctation is evaluated by measuring the pressure gradient as assessed by cardiac catheterization. Echo Doppler can assess the pressure gradient as well, even if some inaccuracies have been reported due to the fact that the utilized mathematical model (Bernoulli) cannot equally fit depending upon the severity of the stenosis. Recently a model using MRI to

Fig. 3.13.8. Complex aortic coarctation. MR angiography volume rendering reconstruction in a young adult showing the complex anatomy of native aortic coarctation (**a** and **b**) not fully delineate by echocardiography (*Ao Arch* aortic arch, *Asc Ao* ascending aorta, *Ao Coa* aortic coarctation, *LCA* left carotid artery, *LSA* left subclavian artery)
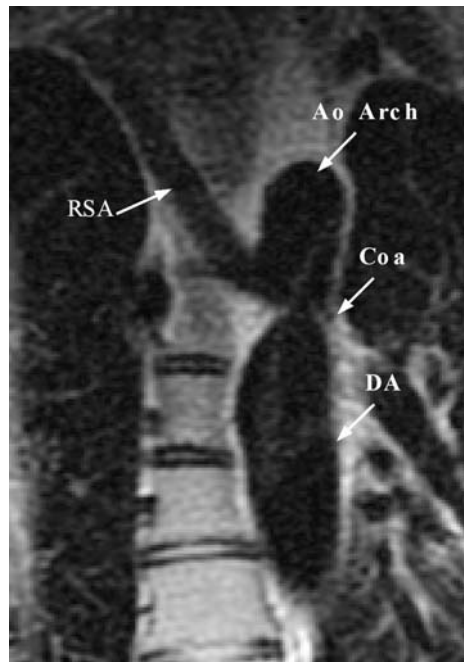
Fig. 3.13.9. Aortic coarctation with anomalous right subclavian artery. Fast spin echo MRI showing aortic coarctation with anomalous right subclavian artery (*Ao Arch* aortic arch, *Coa* aortic coarctation, *DA* descending thoracic aorta, *RSA* right subclavian artery)

predict the probability of a hemodynamically significant aortic coarctation pressure gradient (defined as ≥20 mmHg measured during cardiac catheterization) was developed at Boston Children's Hospital. A combination of the smallest cross-sectional area of the aorta (measured from the gadolinium-enhanced 3-dimensional MR angiography) and the heart rate-adjusted mean deceleration of flow in the descending aorta (measured by PVC-MRI distal to the aortic coarctation) was able to predict a gradient ≥20 mmHg with 95% sensitivity and 82% specificity, 90% positive and negative predictive values. Other investigators performed MRI flow measurements in the ascending and descending aorta distal to the aortic coarctation; compared to controls, patients with aortic coarctation had a significantly lower descending to ascending aorta flow ratio as well as a smaller, more blunted descending aortic flow profile. In aortic coarctation, severe obstruction is suggested by the presence of increased collateral flow; higher collateral flow is expected to decrease the likelihood of spinal cord ischemic injury during surgical treatment involving interruption of aortic blood flow during cross clamping. If little collateral flow is found, the surgeon may consider performing left heart bypass to the descending aorta during the surgical repair.

The following cardiac MRI protocol is used in the evaluation of aortic coarctation:

▌ 3-plane localizing images,
▌ 2-dimensional axial Time-of-flight Angiography (see appendix in the "Introduction"),
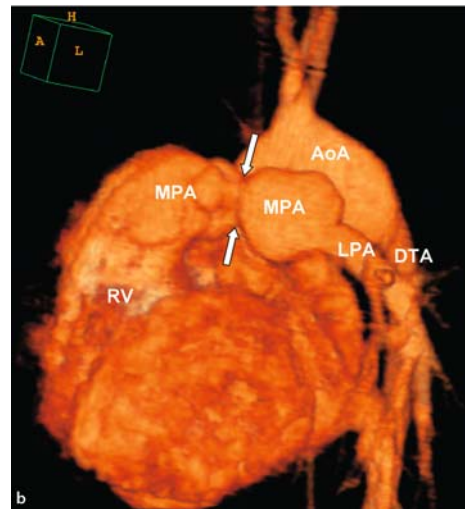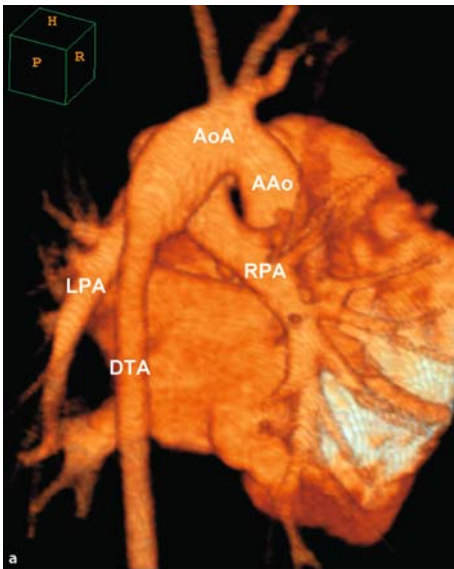
Fig. 3.13.10. Status post repair of aortic coarctation with hypoplastic aortic arch. **a** 3-dimensional reconstruction of a postoperative CT in the same patient of Fig. 3.13.4 with contrast angiography, posterior coronal view, showing the reconstructed aortic arch; the anomalous left subclavian artery has been sacrificed. **b** 3-dimensional reconstruction of a postoperative CT in the same patient of Fig. 3.13.4 with contrast angiography, oblique sagittal projection, showing the reconstructed aortic arch and a pulmonary artery banding (arrows) associated because of the presence of multiple ventricular septal defects (*AAo* ascending aorta, *AoA* aortic arch, *DTA* descending thoracic aorta, *LPA* left pulmonary artery, *MPA* main pulmonary artery, *RPA* right pulmonary artery, *RV* right ventricle) (photographs courtesy of Dr. Mohamed Tawil)

■ ECG-gated cine steady-state free precession and static fast spin echo on the parasagittal plane to visualize the aortic arch and the aortic coarctation site. Quite often the arch is distorted in patients with aortic coarctation, so it does not lie on a single plane; thus, additional planes are required to fully delineate the aortic arch and isthmus,

■ ECG-gated cine steady-state free precession sequences in 2-chamber, 4-chamber planes, and ventricular short axis for the quantitative assessment of ventricular dimensions, function, mass and stroke volume (as illustrated in appendix of the "Introduction"),

■ ECG-gated cine steady-state free precession sequence to visualize the left ventricular outflow tract and the aortic valve,

■ ECG-gated phase velocity contrast MRI sequences perpendicular to the ascending aorta, aortic arch, isthmus, proximal and distal descending aorta, to assess the aortic coarctation flow pattern and the collateral flow,
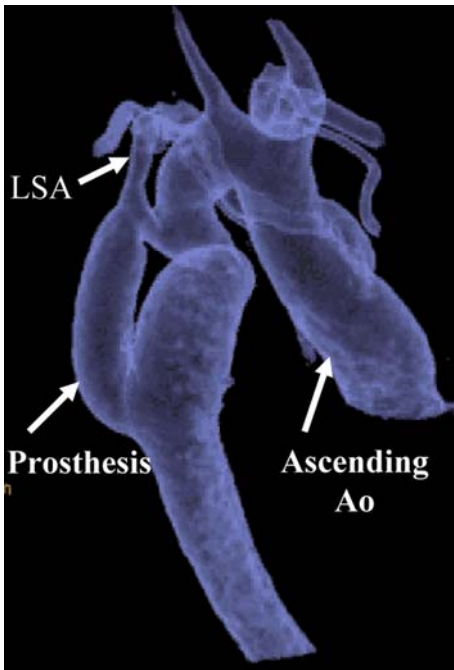
Fig. 3.13.11. Complex aortic coarctation, status post repair with implantation of a tubular prosthesis. MR angiography volume rendering reconstruction in the same patient of Fig. 3.13.8 showing the tubular prosthesis interposed between the left subclavian artery and the descending thoracic aorta. This technique was chosen to bypass the narrowing due to the adult age and the complex anatomy of the native aortic coarctation (*Ao* aorta, *LSA* left subclavian artery)

Fig. 3.13.12. Recurrent aortic coarctation. **a** MR angiography volume rendering reconstruction showing significant aortic re-coarctation. **b** The flow pattern at the coarctation site shows the typical flow profile of significant aortic coarctation: prolonged deceleration with increased antegrade diastolic flow (*Ao Coa* aortic coarctation, *LCA* left carotid artery, *LSA* left subclavian artery)

■ gadolinium-enhanced 3-dimensional MRI for the evaluation of the aortic arch and brachiocephalic vessels and collaterals (Fig. 3.13.6).

■ Potential complications

Residual or recurrent aortic coarctation, hemorrhage, paraplegia, paradoxical arterial hypertension, abdominal pain, mesentery (necrotising) vasculitis, chylothorax, aneurysm (after patch aortoplasty), left upper arm ischemia (after subclavian flap), recurrent nerve lesion.

■ Post-operative follow-up

CT angiography and MRI with 3-dimensional reconstructions represent reliable noninvasive techniques to replace diagnostic cardiac catheterization with angiography in the postoperative follow-up for aortic coarctation and provide valuable information concerning the need for interventional procedures or re-operations without further invasive investigations (Figs. 3.13.10 and 3.13.11).
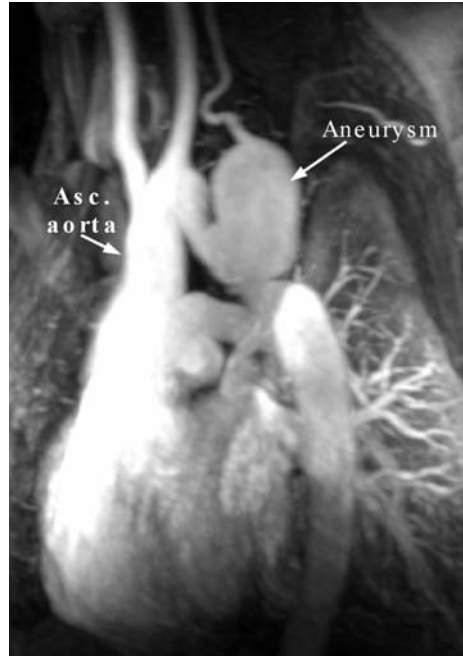
Fig. 3.13.13. Aortic arch aneurysm after repair of the aortic arch. MR angiography maximal intensity projection reconstruction showing a huge aortic arch aneurysm (*Asc. Ao* ascending aorta)
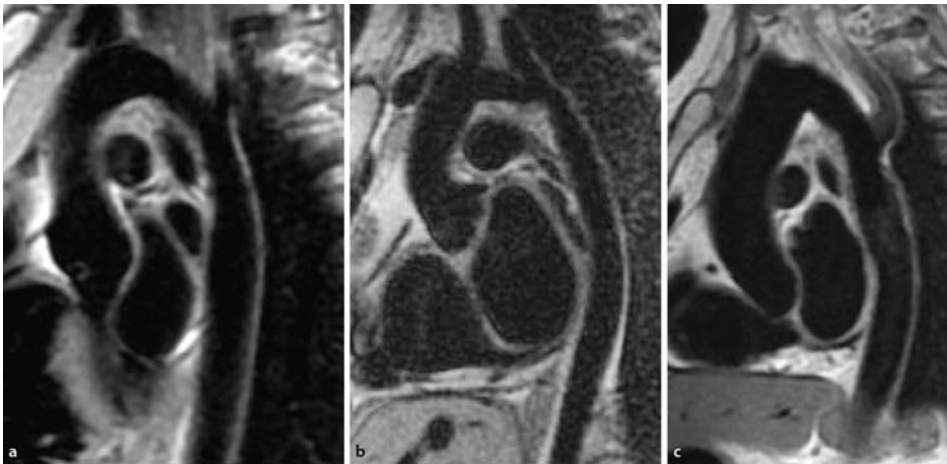
Fig. 3.13.14. Different postoperative aortic arch morphology. MRI fast spin echo para-sagittal acquisition showing the three possible postoperative aspects of the aortic arch: **a** Romanesque, **b** Crenel, **c** Gothic
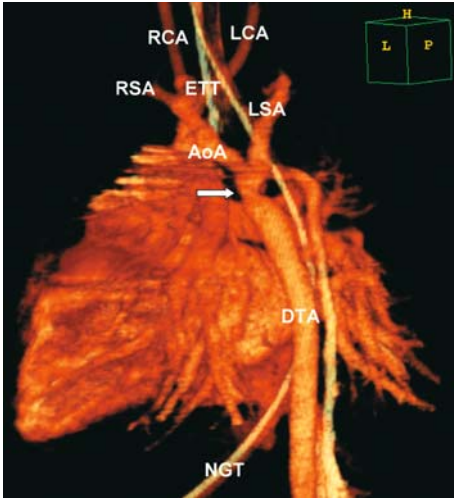
Fig. 3.13.15. Aortic coarctation, status post balloon dilatation. CT scan in a neonate, contrast angiography, oblique sagittal projection, showing the relatively hypoplastic aortic arch with aortic coarctation (arrow), after successful balloon dilatation of the aortic coarctation (*AoA* aortic arch, *DTA* descending thoracic aorta, *ETT* endotracheal tube, *LCA* left carotid artery, *LSA* left subclavian artery, *NGT* naso-gastric tube, *RCA* right carotid artery, *RSA* right subclavian artery) (photograph courtesy of Dr. Mohamed Tawil)
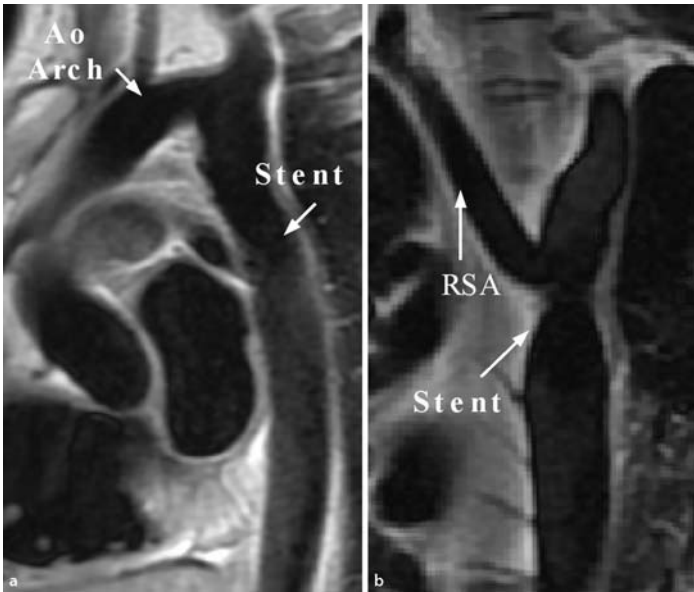
Fig. 3.13.16. Aortic coarctation and anomalous right subclavian artery, status post stent implantation. Aortic coarctation and aberrant subclavian artery in the same patient of Fig. 3.13.9 successfully treated with a stent as illustrated by fast spin echo MRI showing the good position of the stent (**a**) and the patent right subclavian artery (**b**) (*Ao Arch* aortic arch, *RSA* right subclavian artery)

Both techniques can provide morphometric and morphologic findings such as different aortic diameters, presence of residual or recurrent stenosis (Fig. 3.13.12), aneurysms (Fig. 3.13.13), intimal flaps, circumscribed pouches, and arteriosclerotic plaques. Indication for re-operation after coarctectomy can be established based on the CT or MRI demonstration of residual or recurrent distal aortic arch obstruction, depending also on the aortic arch geometry. Three types of geometry have been described (Fig. 3.13.14):

a) gothic arch with angular geometry and increase height/width ratio,
b) crenel arch with a rectangular shape,
c) normal arch with smooth rounded shape (= Romanesque).

The gothic arch is associated with high risk of hypertension in young adult life.

Localized dilatation of aorta late after repair with patch aortoplasty is primarily due to the use of a large synthetic patch, and partly to increased aortic wall growth. Serial investigations are indicated to monitor the aortic wall growth and the potential occurrence of aneurysm in association with the aortoplasty.

After interventional procedures of balloon dilatation (Fig. 3.13.15) and stenting (Fig. 3.13.16) to treat native or recurrent coarctation, volume-rendered images also may provide valuable insight regarding the endovascular stent position, its relationship to the origin of the great arteries, and potential aortic wall complications, such as aneurysm and dissection.

The MRI protocol is the same as preoperative evaluation. The fast spin echo sequences are particularly useful in case of stent dilatation because they present fewer metallic artifacts.

■ References

Almeida de Oliveira S, Lisboa LA, Dallan LA, Abreu FCA, Rochitte CE, de Souza JM (2003) Extraanatomic aortic bypass for repair of aortic arch coarctation via sternotomy: midterm clinical and magnetic resonance imaging results. Ann Thorac Surg 76:1962–1966

Araoz PA, Reddy GP, Tarnoff H, Roge CL, Higgins CB (2003) MR findings of collateral circulation are more accurate measures of hemodynamic significance than arm-leg blood pressure gradient after repair of coarctation of the aorta. J Magn Reson Imaging 17:177–183

Augustin N, Kaemmerer H, Porner M, Meinhardt G, Hess J, Lange R (2006) Images in cardiovascular medicine. Giant aortic aneurysm after patch repair of coarctation. Circulation 113:e297–298

Baum U, Anders K, Ropers D, Noemayr A, Schmid A, Seeliger T, Singer H, Daniel WG, Bautz W, Achenbach S (2005) Multi-slice spiral CT imaging after surgical treatment of aortic coarctation. Eur Radiol 15:353–355

Becker C, Soppa C, Fink U, Haubner M, Muller-Lisse U, Englmeier KH, Buhlmeyer K, Reiser M (1997) Spiral CT angiography and 3D reconstruction in patients with aortic coarctation. Eur Radiol 7:1473–1477

Bogaert J, Kuzo R, Dymarkowski S, Janssen L, Celis I, Budts W, Gewillig M (2000) Follow-up of patients with previous treatment for coarctation of the thoracic aorta: comparison between contrast-enhanced MR angiography and fast spin-echo MR imaging. Eur Radiol 10:1847–1854

Cademartiri F, van Geuns RJ, Nieman K, Meijboom E, de Feyter PJ (2004) Images in cardiovascular medicine. Multislice computed tomography for the evaluation and follow-up of stenting of aortic coarctation. Circulation 109:e176

Cademartiri F, Mollet N, Nieman K, Alfieri O, Krestin GP (2004) Images in cardiovascular medicine. Motion-free ECG-gated 16-row multislice computed tomography in the follow-up of aortic coarctation with three-dimensional volume rendering. Ital Heart J 5:167–168

Chernoff DM, Derugin N, Rajasinghe HA, Hanley FL, Higgins CB, Gooding CA (1997) Measurement of collateral blood flow in a porcine model of aortic coarctation by velocity-encoded cine MRI. Magn Reson Imaging 7:557–563

Choi BW, Choe KO, Kim YJ (2004) Magnetic resonance angiography of pseudocoarctation. Heart 90:1213

Connolly HM, Huston J, Brown RD, Warnes CA, Ammash NM, Tajik AJ (2003) Intracranial aneurysms in patients with coarctation of the aorta: a prospective magnetic resonance angiographic study of 100 patients. Mayo Clin Proc 78:1491–1499

Corno AF, Marcelletti C (1990) Bypass grafts for complex aortic coarctation: simplified approach. J Thorac Cardiovasc Surg 99:945–946

Corno AF, Botta U, Hurni M, Payot M, Sekarski N, Tozzi P, von Segesser LK (2001) Surgery for aortic coarctation: a 30 years experience. Eur J Cardiothorac Surg 20:1202–1206

Didier D, Saint-Martin C, Lapierre C, Trindade PT, Lahlaidi N, Vallee JP, Kalangos A, Friedli B, Beghetti M (2006) Coarctation of the aorta: pre- and postoperative evaluation with MRI and MR angiography; correlation with echocardiography and surgery. Int J Cardiovasc Imaging 22:457–475

Eichhorn JG, Fink C, Delorme S, Hagl S, Kauczor HU, Ulmer HE (2006) Magnetic resonance blood flow measurements in the follow-up of pediatric patients with aortic coarctation. A re-evaluation. Int J Cardiol 113:291–298

Elkington AG, Thorne S, Mohiaddin RH (2003) False aortic aneurysm at site of previous coarctation repair: the role of cardiovascular magnetic resonance. J Cardiovasc Magn Res 5:501–504

Fiocca L, Zumbo F, Montenero AS, Tesoro-Tess JD (2004) Magnetic resonance angiography in an adult with aortic coarctation associated with subclavian stenosis. Heart 90:424

Frydrychowicz A, Schlensak C, Stalder A, Russe M, Siepe M, Beyersdorf F, Langer M, Hennig J, Markl M (2007) Ascending-descending aortic bypass surgery in aortic arch coarctation: four-dimensional magnetic resonance flow analysis. J Thorac Cardiovasc Surg 133:260–262

Godart F, Labrot G, Devos P, McFadden E, Rey C, Beregi JP (2002) Coarctation of the aorta: comparison of aortic dimensions between conventional MR imaging, 3D MR angiography, and conventional angiography. Eur Radiol 12:2034–2039

Goo HW, Park IS, Ko JK, Kim YH, Seo DM, Yun TJ, Park JJ, Yoon CH (2003) CT of congenital heart disease: normal anatomy and typical pathologic conditions. Radiographics 23:S147–165

Gutberlet M, Hosten N, Vogel M, Abdul-Khaliq H, Ehrenstein T, Amthauer H, Hoffmann T, Teichgraber U, Berger F, Lange P, Felix R (2001) Quantification of morphologic and hemodynamic severity of coarctation of the aorta by magnetic resonance imaging. Cardiol Young 11:512–520

Hager A, Kaemmerer H, Leppert A, Prokop M, Blucher S, Stern H, Hess J (2004) Follow-up of adults with coarctation of the aorta: comparison of helical CT and MRI, and impact on assessing diameter changes. Chest 126:1169–1176

Hager A, Kaemmerer H, Hess J (2005) Comparison of helical CT scanning and MRI in the follow-up of adults with coarctation of the aorta. Chest 127:2296

Henk CB, Grampp S, Koller J, Schoder M, Frank H, Klaar U, Gomischek G, Mostbeck GH (2002) Elimination of errors caused by first-order aliasing in velocity encoded cine-MR measurements of postoperative jets after aortic coarctation: in vitro and in vivo validation. Eur Radiol 12:1523–1531

Ho VB, Bakalov VK, Cooley M, Van PL, Hood MN, Burklow TR, Bondy CA (2004) Major vascular anomalies in Turner syndrome: prevalence and magnetic resonance angiographic features. Circulation 110:1694–1700

Holmqvist C, Stahlberg F, Hanseus K, Hochbergs P, Sandstrom S, Larsson EM, Laurin S (2002) Collateral flow in coarctation of the aorta with magnetic resonance velocity mapping: correlation to morphological imaging of collateral vessels. J Magn Reson Imaging 15:39–46

Ilyas M, Chu C, Ettles D, Mathew V, Atkin S (2006) Evaluation by magnetic resonance imaging of aortic dilatation and coarctation in adult Turner syndrome patients. Clin Endocrinol (Oxf) 65:154–157

Ismat FA, Weinberg PM, Rychik J, Karl TR, Fogel MA (2006) Right aortic arch and coarctation: a rare association. Congenit Heart Dis 1:217-223

Johnson TR, Goldmuntz E, McDonald-McGinn DM, Zackai EH, Fogel MA (2005) Cardiac magnetic resonance imaging for accurate diagnosis of aortic arch anomalies in patients with 22q11.2 deletion. Am J Cardiol 96:1726–1730

Konen E, Merchant N, Provost Y, McLaughlin PR, Crossin J, Paul NS (2004) Coarctation of the aorta before and after correction: the role of cardiovascular MRI. Am J Roentgenol 182:1333–1339

Kramer U, Greil G, Damman F, Schick F, Miller S, Fenchel M, Sieverding L, Claussen CD (2004) Clinical implication of parameter-optimized 3D-FISP MR angiography (MRA) in children with aortic coarctation: comparison with catheter angiography. Rofo 176:1458–1465

Krueger JJ, Ewert P, Yilmaz S, Gelernter D, Peters B, Pietzner K, Bornstedt A, Schnackenburg B, Abdul-Khaliq H, Fleck E, Nagel E, Berger F, Kuehne T (2006) Magnetic resonance imaging-guided balloon angioplasty of coarctation of the aorta: a pilot study. Circulation 113:1093–1100

Larsen TH, Taxt AM, Aslaksen A, Segadal L, Norgard G, Roksund OD, Greve G (2003) Magnetic resonance imaging of patients with increased blood pressure and altered blood pressure response to exercise after coarctation repair. Scand Cardiovasc J 37:98–103

Lembcke A, Dohmen P, Rodenwaldt J, Kopka L, Mews J, Rogalla P (2003) Images in cardiovascular medicine. Recoarctation of the aorta associated with ascending aortic aneurysm demonstrated by ECG-gated multislice CT. Circulation 107:e80–81

Leschka S, Alkadhi H, Wildermuth S (2005) Images in cardiology. Collateral circulation in aortic coarctation shown by 64 channel multislice computed tomography angiography. Heart 91:1422

Masiello P, Santoro G, Franzesi E, De Lillo L, Fittipaldi O, Di Benedetto G (1999) Aortic pseudo-coarctation: spiral volumetric computed tomography imaging. Ann Thorac Surg 68:1421

Mulder BJ, van der Wall EE (2006) Optimal imaging protocol for evaluation of aortic coarcta(tion) time for a reappraisal. Int J Cardiovasc Imaging 22:695–697

Nielsen JC, Powell AJ, Gauvreau K, Marcus EN, Prakash A, Geva T (2005) Magnetic resonance imaging predictors of coarctation severity. Circulation 111:622–628

Oshinski JN, Parks WJ, Markou CP, Bergman HL, Larson BE, Ku DN, Mukundan S, Pettigrew RI (1996) Improved measurement of pressure gradients in aortic coarctation by magnetic resonance imaging. J Am Coll Cardiol 28:1818–1826

Ou P, Mousseaux E, Celermajer DS, Pedroni E, Vouhé P, Sidi D, Bonnet D (2006) Aortic arch shape deformation after coarctation surgery: effect on blood pressure response. J Thorac Cardiovasc Surg 132:1105–1111

Papavero R, Kastler B, Clair C, Litzler J, Delabrousse E, Livolsi A, Schneider P, Site O, Bernard Y (2001) Thoracic aortic coarctation: MRI evaluation and follow-up. J Radiol 82:555–561

Pinilla I, Bret M, Cuesta E, Borches D, Oliver JM, Gomez-Leon N (2006) Role of computed tomography and magnetic resonance imaging in aortobronchial fistula diagnosis following aortic coarctation reparative surgery. Report of two cases. J Cardiovasc Surg 47:221–227

Pujadas S, Reddy GP, Weber O, Tan C, Moore P, Higgins CB (2006) Phase contrast MR imaging to measure changes in collateral blood flow after stenting of recurrent aortic coarctation: initial experience. J Magn Reson Imaging 24:72–76

Quenot JP, Boichot C, Petit A, Falcon-Eicher S, d'Athis P, Bonnet C, Wolf JE, Louis P, Brunotte F (2005) Usefulness of MRI in the follow-up of patients with repaired aortic coarctation and bicuspid aortic valve. Int J Cardiol 103:312–316

Rakvit A, Meyerrose G, Jenkins LA, Harris J, Sanchez R, Lane Cox S, Kurdi J, Gunder A (2002) Coarctation of the aorta demonstrated by a radionuclide first-pass flow study using tc-99m tetrofosmin. Clin Nucl Med 27:822–823

Raval AN, Telep JD, Guttman MA, Ozturk C, Jones M, Thompson RB, Wright VJ, Schenke WH, DeSilva R, Aviles RJ, Raman VK, Slack MC, Lederman RJ (2005) Real-time magnetic resonance imaging-guided stenting of aortic coarctation with commercially available catheter devices in Swine. Circulation 112:699–706

Riehle TJ, Oshinski JN, Brummer ME, Favaloro-Sabatier J, Mahle WT, Fyfe DA, Kanter KR, Parks WJ (2006) Velocity-encoded magnetic resonance image assessment of regional aortic flow in coarctation patients. Ann Thorac Surg 81:1002–1007

Robles P, Olmedilla P, Jimenez JJ (2006) Aneurysm formation following stent implantation for aortic coarctation detected by multidetector computed cardiac tomography. Eur Heart J 27:2774

Ruiz A, Texier N, Bertrand P, Sirinelli D (2005) Aortic diameter measurements on MRI follow-up of coarctation. J Radiol 86:1705–1709

Saeed M, Henk CB, Weber O, Martin A, Wilson M, Shunk K, Saloner D, Higgins CB (2006) Delivery and assessment of endovascular stents to repair aortic coarctation using MR and X-ray imaging. J Magn Reson Imaging 24:371–378

Salanitri GC (2007) Intercostal artery aneurysm complicating thoracic aortic coarctation: diagnosis with magnetic resonance angiography. Australas Radiol 51:78–82

Schaffer GJ, Sorantin E, Groell R, Gamillscheg A, Maier E, Schoellnast H, Fotter R (2000) Helical CT angiography with maximum intensity projection in the assessment of aortic coarctation after surgery. Am J Roentgenol 175:1041–1045

Shebani SO, Khan MD, Keal R (2005) Anatomical imaging of severe coarctation in childhood. Cardiol Young 15:666

Shih MC, Tholpady A, Kramer CM, Sydnor MK, Hagspiel KD (2006) Surgical and endovascular repair of aortic coarctation: normal findings and appearance of complications on CT angiography and MR angiography. Am J Roentgenol 187:W302–312

Smith Maia MM, Cortes TM, Parga JR, De Avila LF, Aiello VD, Barbero-Marcial M, Ebaid M (2004) Evolutional aspects of children and adolescents with surgically corrected aortic coarctation: clinical, echocardiographic, and magnetic resonance image analysis of 113 patients. J Thorac Cardiovasc Surg 127:712–720

Snider AR, Enderlein MA, Teitel DF, Juster RP (1984) Two-dimensional echocardiographic determination of aortic and pulmonary artery sizes from infancy to adulthood in normal subjects. Am J Cardiol 53:218–224

Tanju S, Ustuner E, Erden I, Aytac SK (2007) Right cervical aortic arch and pseudocoarctation of the aorta associated with aneurysms and steal phenomena: US, CTA, and MRA findings. Cardiovasc Intervent Radiol 30:146–149

Uehara M, Funabashi N, Yasukawa K, Terai M, Komuro I (2007) Coarctation of the descending aorta, patent ductus arteriosus, deficiency of right superior vena cava, and persistent left superior vena cava in a five-month infant demonstrated by multislice computed tomography. Int J Cardiol 122:61–63

Vriend JW, Lam J, Mulder BJ (2004) Complete aortic arch obstruction: interruption or aortic coarctation? Int J Cardiovasc Imaging 20:393–396

Vriend JW, Oosterhof T, Mulder BJ (2005) Noninvasive imaging for the postoperative assessment of aortic coarctation patients. Chest 127:2295

Yildiz A, Ozturk S, Cagirci G (2006) Images in cardiology. Double coarctation and double grafts: role of computed tomographic angiography in diagnosis of a clinic mistery. Heart 92:581

Yoshioka K, Niinuma H, Ogino Y, Muranaka K, Kawazoe K, Ehara S (2006) Three-dimensional demonstration of the collateral circulation to the artery of Adamkiewicz with 16-row multislice computed tomography. Ann Thorac Surg 81:749

Wald RM, Powell AJ (2006) Simple congenital heart lesions. J Cardiovasc Magn Reson 8:619-631

Definition

The aortic arch is described as three segments: proximal, distal and isthmus. The proximal component extends from the take-off of the innominate artery to the left common carotid artery. The distal component extends from the left common carotid artery to take-off of the left subclavian artery. The segment of the aorta connecting the distal aortic arch to the juxtaductal region of the descending aorta is termed the isthmus. This complex composite of segments introduces a risk of developmental anomalies in the form of interruptions at the various junction points. Aortic arch interruption is characterized by complete lack of anatomic continuity between the aortic arch or isthmus and the descending thoracic aorta. In aortic arch atresia, with identical pathophysiology and hemodynamics, there is anatomic continuity between the two segments, represented by an imperforate fibrous strand of various lengths. Three anatomic types of aortic arch interruption have been described:

- *Type A*: the interruption is distal to the left subclavian artery.
- *Type B*: the interruption is between the left common carotid artery and the left subclavian artery.
- *Type C*: the interruption is between the innominate artery and the left common carotid artery.

Associated anomalies

Patent ductus arteriosus, ventricular septal defect, actual or potential systemic left ventricular outflow tract obstruction, bicuspid aortic valve, double outlet right ventricle, univentricular heart with discordant ventriculoarterial connection, aortopulmonary window, truncus arteriosus, atrial isomerism. Patent ductus arteriosus is always present. The ventricular septal defect is nearly always present, in the majority of cases of malalignment-type, subpulmonic, because of posterior malalignment of the ventricular septum. Subaortic stenosis is also generally present, due to the posterior malalignment of the ventricular septum.

Surgical options

Two surgical approaches are available:

- *two stages*, with repair of the interrupted aortic arch and pulmonary artery banding, followed by later closure of the ventricular septal defect;
- *single stage*, with simultaneous repair of the interrupted aortic arch and a patch closure of the ventricular septal defect.

In the absence of associated lesions other than patent ductus arteriosus and ventricular septal defect, primary repair by direct anastomosis of the arch with closure of the ventricular septal defect is the preferred surgical approach. The main reason is that pulmonary artery banding might promote or aggravate subaortic stenosis in patients with a malalignment ventricular septal defect. Although the primary repair is physiologically corrective, it should not be viewed as fully curative due to the high incidence of significant late obstruction of the left ventricular outflow tract.

Left ventricular outflow tract obstruction: The morphology of left ventricular outflow tract obstruction with interrupted aortic arch varies, and therefore, surgical management also varies according to the specific circumstances.

▪ Pre-operative information

CT and MRI investigations (Figs. 3.14.1 and 3.14.2) allow the precise identification of aortic arch interruption type, distance between proximal and distal segments, size of the patent ductus arteriosus, narrowest dimension of the left ventricular outflow tract, and association o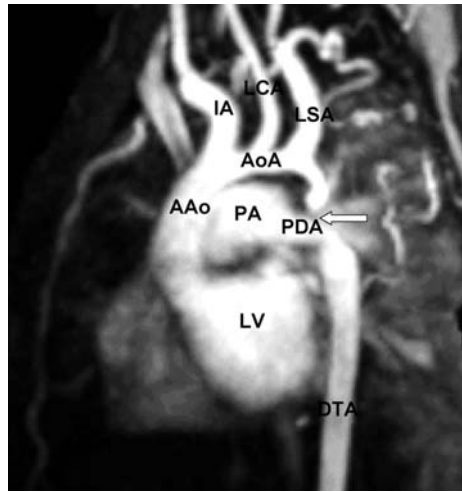f other malformations potentially interfering with the surgical planning, such as intracardiac defects, the presence of an anomalous retro-esophageal right subclavian artery, the presence of a right aortic arch.

The cardiac MRI protocol used for the evaluation of infants with aortic arch interruption is the following:

▪ 3-plane localizing images,
▪ 2-dimensional axial Time-of-flight Angiography (see appendix in the "Introduction"),
▪ ECG-gated cine steady-state free precession sequences in 2-chamber, 4-chamber planes, and ventricular short axis for the quantitative assessment of ventricular dimensions, function, mass and stroke volume, as illustrated in the appendix of the "Introduction",
▪ ECG-gated cine steady-state free precession sequence to visualize the left ventricular outflow tract and the aortic valve,
▪ gadolinium-enhanced 3-dimensional MRI for the evaluation of the aortic arch, brachiocephalic arteries and patent ductus arteriosus.

Fig. 3.14.1. Aortic arch interruption. CT scan posterior coronal view, volume rendering imaging, showing type A aortic arch interruption, distal to the left subclavian artery, in a neonate with anomalous origin of the right pulmonary artery from the right subclavian artery (*AAo* ascending aorta, *DTA* descending thoracic aorta, *LA* left atrium, *LCA* left carotid artery, *LSA* left subclavian artery, *RCA* right carotid artery, *RPA* right pulmonary artery, *RSA* right subclavian artery) (photograph courtesy of Dr. Mohammed Tawil)

Fig. 3.14.2. Aortic arch interruption. MR angiography showing the aortic arch interruption (arrow), with the distal systemic circulation perfused through a patent ductus arteriosus (*AAo* ascending aorta, *AoA* aortic arch, *DTA* descending thoracic aorta, *IA* innominate artery, *LCA* left carotid artery, *LSA* left subclavian artery, *LV* left ventricle, *PA* pulmonary artery, *PDA* patent ductus arteriosus)
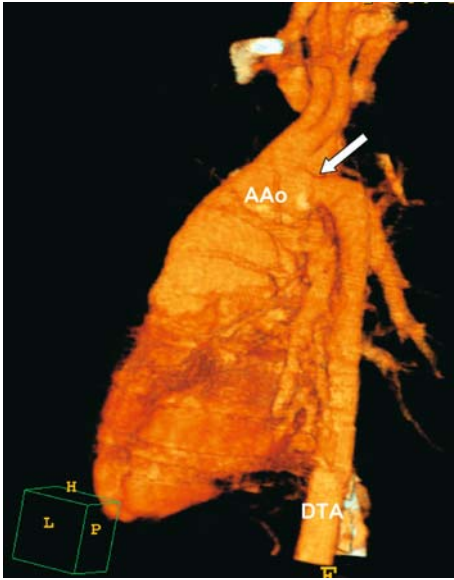
Fig. 3.14.3. Aortic arch interruption: status post repair. CT scan in the same patient of Fig. 3.14.1 with left oblique posterior sagittal view, volume rendering imaging, showing the end-to-side anastomosis (arrow) used to reconstruct the aortic arch continuity one year after surgery (*AAo* ascending aorta, *DTA* descending thoracic aorta) (photograph courtesy of Dr. Mohammed Tawil)
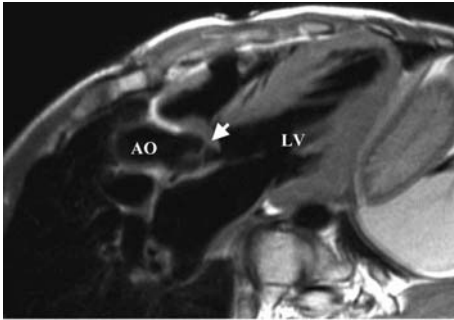
Fig. 3.14.4. Aortic arch interruption with ventricular septal defect, status post repair. MRI fast spin echo 3-chamber view parallel to the left ventricular outflow tract. Note the severe subaortic stenosis due to posterior infundibular deviation (arrow) (*Ao* aorta, *LV* left ventricle)
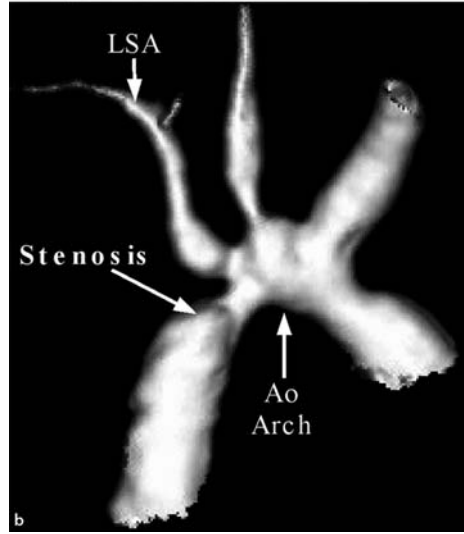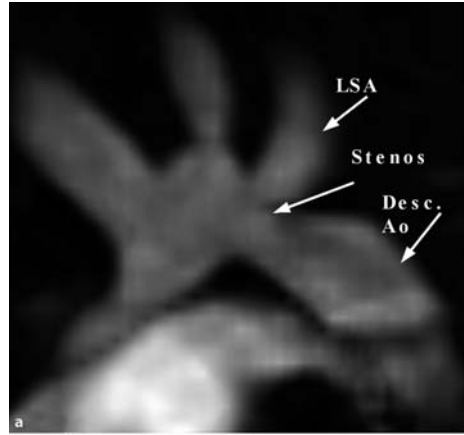
Fig. 3.14.5. Aortic arch interruption, status post surgery with direct anastomosis. MR angiography maximal intensity projection reconstruction (**a**) and volume rendering reconstruction (**b**) showing normal brachiocephalic arteries and significant aortic isthmus narrowing (*Ao Arch* aortic arch, *Desc Ao* descending thoracic aorta, *LSA* left subclavian artery)

■ Potential complications

Residual pressure gradient at the level of the aortic arch anastomosis and/or at the left ventricular outflow tract, residual ventricular septal defect, complete atrioventricular block, left bronchial obstruction.

Left bronchial obstruction: The left main bronchus passes under the aortic arch. If a direct anastomosis is performed without adequate mobilization of the ascending and descending aorta, a bowstring effect over the left main bronchus may result. This is manifested by air trapping in the left lung with hyperexpansion, as seen on chest radiography and confirmed by bronchoscopy. Surgical management may require an ascending-to-descending aortic conduit after division of the arch.

■ Post-operative follow-up

The role of CT scan (Fig. 3.14.3) and MRI after surgery for aortic arch interruption is to evaluate residual or recurrent anatomic and hemodynamic problems, such as aortic arch obstruction or aneurysm formation. However, other abnormalities (e.g., left ventricular outflow tract obstruction, aortic valve stenosis or regurgitation, residual ventricular septal defect, left ventricular size and function) should be examined as well. CT scan and MRI are also useful in case of suspected post-operative left bronchial compression.

The following protocol is suggested in the post-operative evaluation of patients with arch interruption:

■ 3-plane localizing images,
■ 2-dimensional axial Time-of-flight Angiography (see appendix in the "Introduction"),
■ ECG-gated cine steady-state free precession and fast spin echo para-sagittal,
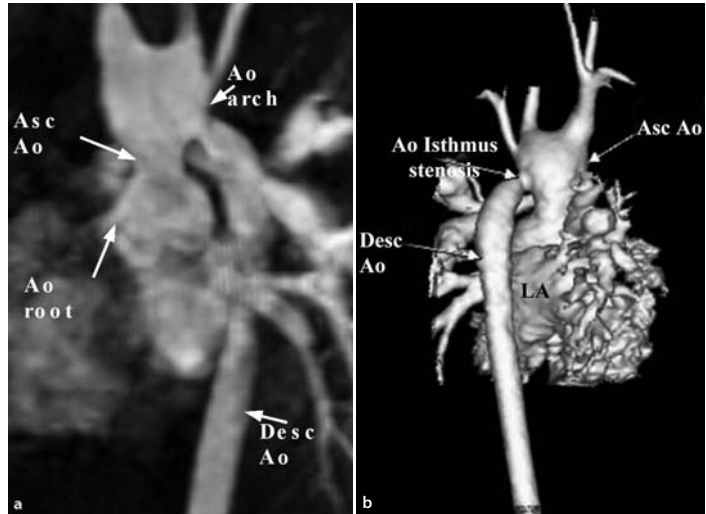
Fig. 3.14.6. Truncus arteriosus and aortic arch interruption, status post repair. MR angiography MIP reconstruction (**a**) and volume rendering reconstruction (**b**) showing an aortic arch aneurysm, mild ascending aorta stenosis and significant aortic isthmus obstruction (*Asc Ao* ascending aorta, *Ao arch* aortic arch, *Ao root* aortic root, *Desc Ao* descending thoracic aorta, *LA* left atrium)

coronal and additional oblique plane (if needed) to visualize the aortic arch,

▌ ECG-gated cine steady-state free precession sequences in 2-chamber, 4-chamber planes, and ventricular short axis for the quantitative assessment of ventricular dimensions, function, mass and stroke volume as illustrated in the appendix of the "Introduction",

▌ ECG-gated cine steady-state free precession and fast spin echo sequence parallel to the left ventricular outflow tract (Fig. 3.14.4),

▌ ECG-gated phase velocity contrast (PVC-MRI) sequences perpendicular to the ascending aorta, aortic arch, isthmus, proximal and distal descending aorta. Additional flow measurements, based on clinical relevance, such as assessment of potential aortic valve regurgitation or to quantitate the intracardiac shunt in case of suspected residual ventricular septal defect, are sometime required as well,

▌ gadolinium-enhanced 3-dimensional MRI for the evaluation of the aortic arch and brachiocephalic arteries (Figs. 3.14.5 and 3.14.6).

▌ References

Akdemir R, Ozhan H, Erbilen E, Yazici M, Gunduz H, Uyan C (2004) Isolated interrupted aortic arch: a case report and review of the literature. Int J Cardiovasc Imaging 20:389–392

Cinar A, Haliloglu M, Karagoz T, Karcaaltincaba M, Celiker A, Tekinalp G (2004) Interrupted aortic arch in a neonate: multidetector CT diagnosis. Pediatr Radiol 34:901–903

Corno AF, Lam J, Becker AE, Marcelletti C (1981) Aortic arch interruption. G Ital Cardiol 11:679–685

Davotoglu V, Soydinc S, Sirikci A, Dinckal H, Akdemir I (2004) Interrupted aortic arch in an adolescent male. Can J Cardiol 20:1367–1368

Dorfman AL, Geva T (2006) Magnetic resonance imaging evaluation of congenital heart disease: conotruncal anomalies. J Cardiovasc Magn Reson 8:645–659

Goo HW, Park IS, Ko JK, Kim YH, Seo DM, Yun TJ, Park JJ, Yoon CH (2003) CT of congenital heart disease: normal anatomy and typical pathologic conditions. Radiographics 23:S147–S165

Johnson TR, Goldmuntz E, McDonald-McGinn DM, Zackai EH, Fogel MA (2005) Cardiac magnetic resonance imaging for accurate diagnosis of aortic arch anomalies in patients with 22q11.2 deletion. Am J Cardiol 96:1726–1730

Maier JM, Scheffold N, Cyran J (2005) Primary diagnosis of an interrupted aortic arch in a 65-year old woman with hypertension. Dtsch Med Wochenschr 130:2893–2895

Morriss J, Moreland J, Burkhart H, Kao S (2007) Presurgical evaluation of interrupted aortic arch with 3-dimensional reconstruction of CT images. Ann Thorac Surg 84:299

Taylor AM, Jones R, Derrick G (2006) Post-mortem magnetic resonance imaging provides the diagnosis following aortic rupture in an infant with treated aortic interruption. Cardiol Young 16:81–83

Vriend JW, Lam J, Mulder BJ (2004) Complete aortic arch obstruction: interruption or aortic coarctation? Int J Cardiovasc Imaging 20:393–396

Yoo SJ, Choi HY, Park IS, Hong MG, Kim SH (1991) Distal aortopulmonary window with aortic origin of the right pulmonary artery and interruption of the aortic arch (Berry syndrome): diagnosis by MR imaging. Am J Roentgenol 157:835–836

Wong MN, Chang LG, Sim KH (2007) Interrupted aortic arch and aortopulmonary window demonstrated on 64-slice multidetector computed tomography angiography. Heart 93:95

CHAPTER **3.15** **C**omplete transposition of the great arteries

▍ Definition

Transposition of the great arteries is an abnormality of ventriculoarterial connection, with the aorta originating from the morphologically right ventricle and the pulmonary artery from the morphologically left ventricle. The aorta is anterior and slightly to the right of the main pulmonary artery. The aortic valve is to the right of the pulmonary valve but still anterior to it. The main pulmonary artery is in a position, with respect to the left ventricle, such that there is direct flow into the right pulmonary artery; as a consequence the right pulmonary artery becomes larger, with more flow to the right lung.

There are four major subgroups of complete transposition of the great arteries:

▍ *Transposition of the great arteries with intact ventricular septum or with restrictive ventricular septal defect (60% of the cases):* one-third of patients with complete transposition of the great arteries and ventricular septal defect will have closure of the ventricular septal defect in the first year of life.

▍ *Transposition of the great arteries with unrestrictive ventricular septal defect (20%):* the most common position of ventricular septal defects in transposition of the great arteries is the infundibular septum, with or without malalignment, followed by defects in the membranous septum.

▍ *Transposition of the great arteries with ventricular septal defect and left ventricular outflow tract obstruction (15%):* pulmonary stenosis (left ventricular outflow tract obstruction) in patients with transposition of the great arteries is due to the leftward bowing of the ventricular septum due to the elevated (systemic) right ventricular pressure, and to the close proximity of the mitral valve to the ventricular septum, leading to dynamic obstruction. Anatomical valvular and subvalvular pulmonary stenoses are more rare, and mainly due to tissue tags, aneurysm of the membranous septum, straddling of the atrioventricular valve, pulmonary valve stenosis.

▍ *Transposition of the great arteries with intact ventricular septum and left ventricular outflow tract obstruction (5%):* most infants with complete transposition of the great arteries have patent foramen ovale and a patent ductus arteriosus.

Coronary arteries: In 60% of patients, the right coronary artery originates from the right coronary sinus and the left coronary artery, whereby the circumflex and left anterior descending arteries originate, from the left coronary sinus. In 10% of patients, the right coronary artery and the circumflex originate from the right coronary sinus with the left anterior descending artery originating from the left coronary sinus. In these cases the circumflex is located posterior to the pulmonary artery. In another 10% of patients, the circumflex originates from the right coronary sinus, and the right coronary artery and left anterior descending artery originate from the left coronary sinus. In these cases the right coronary artery is located rightwards anterior to the aorta. In an-

other 10% of patients, the right coronary artery originates from the right coronary sinus and gives origin to the right coronary artery and the left coronary artery; in these cases the left coronary artery is located between the aorta and the pulmonary artery and gives origin to the circumflex and the left anterior descending branches. In 5% of patients, there is a single origin of all the coronary arteries, either from the right or from the left sinus, and this anomaly can complicate the surgical technique of arterial switch. The most troublesome coronary anomaly in view of arterial switch is an intramural coronary artery (3–5%): in this situation the first portion of a coronary artery, generally the left, is located within the aortic wall, before assuming epicardial distribution.

Associated anomalies

Right aortic arch is seen in 4% of patients with an intact ventricular septum and in 8% of patients with a ventricular septal defect. A right aortic arch is more common (10%) in patients with transposition of the great arteries with pulmonary stenosis or pulmonary atresia. Other associated anomalies include the following: aortic coarctation (5%), left juxtaposition of the auricular appendages (2–4%), malformations of the tricuspid (including Ebstein's anomaly) or the mitral valve, right or left ventricular hypoplasia, superoinferior ventricles, subaortic stenosis.

❚ Surgical options

❚ **Atrioseptectomy:** The original procedure of atrioseptectomy (Blalock-Hanlon) is nowadays virtually abandoned, replaced by balloon atrioseptostomy (Rashkind) performed with venous access by the interventional cardiologists.

❚ **Atrial rerouting:** *Mustard procedure and Senning procedure:* In these two different surgical techniques of intraatrial rerouting, the oxygenated blood of the pulmonary venous returns is channeled towards the tricuspid valve, and therefore to the right ventricle and the aorta, while the desaturated blood of the systemic venous returns is channeled towards the mitral valve, and therefore to the left ventricle and the pulmonary artery.

❚ **Arterial switch (Jatene operation):** The aorta and pulmonary artery are divided above the sinuses. The coronary arteries are excised from the aortic root with a button of aorta and implanted in the new aortic root (old pulmonary artery). The pulmonary artery bifurcation is brought anterior to the aorta (Lecompte maneuver) and the ascending aorta is anastomosed to the new aortic root. A portion of pericardium is utilized to close the defects created in the neopulmonary root (old aorta) by the excision of the coronary arteries, and the pulmonary artery bifurcation is anastomosed to the new pulmonary artery root.

❚ **Rastelli operation:** After right ventriculotomy, the ventricular septal defect is closed with a prosthetic patch (generally PTFE) by creating a tunnel which connects the left ventricle to the aorta, and continuity between the right ventricle and the pulmonary artery is obtained with a biological valved conduit.

❚ **Lecompte procedure (or REV = Réparation à l'Etage Ventriculaire):** After right ventriculotomy and infundibular resection, the left ventricle is connected to the aorta by closure of the ventricular septal defect with a straight patch. After transection and shortening of the ascending aorta and transfer of the pulmonary artery bifurcation anterior to the aorta (Lecompte maneuver), the right ventricle-to-pulmonary artery continuity is obtained with reimplantation of the transected pulmonary artery directly on the right ventricle for its posterior wall, while the anterior aspect is connected to the rest of the right ventriculotomy with a monocusp pericardial patch.

▪ **Damms-Kaye-Stansel procedure:** The pulmonary artery is transected proximal to the bifurcation and end-to-side anastomosed to the ascending aorta, diverting the left ventricular outflow to the systemic circulation; the ventricular septal defect is closed with a prosthetic patch. The continuity between the right ventricle and the pulmonary artery is obtained with a biological valved conduit implanted between the right ventriculotomy and the pulmonary artery bifurcation.

▪ **Bex-Nikaidoh procedure (aortic translocation):** The aortic root is completely harvested, with or without excision of the coronary arteries, as well as the pulmonary valve. After the incision of the infundubular septum and the transfer of the pulmonary artery bifurcation anterior to the aorta (Lecompte maneuver), the aortic root is connected to the posterior left ventricle, with or without reimplantation of the buttons of the excised coronary arteries, closing the ventricular septal defect at the same time. The pulmonary artery is then connected to the anterior right ventricle.

▪ Pre-operative information

The diagnostic criterion of complete transposition of the great arteries is the presence of a discordant ventriculoarterial connection (Fig. 3.15.1). Detailed images of the spatial relationship between the two great arteries and their size discrepancy, the presence of associated malformations, in particular a ventricular septal defect and left ventricular outflow tract obstruction, as well as origin and course of the coronary arteries, are crucial insights for the decision-making process among the various available surgical options.

In the presence of systemic obstructions, particularly aortic coarctation with hypoplastic aortic arch or aortic arch interruption, a more accurate representation of the morphology of the great arteries is required for better surgical planning. In case of indi-
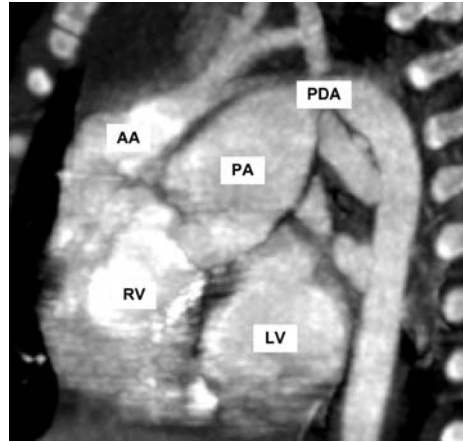
Fig. 3.15.1. Transposition of the great arteries. CT scan, sagittal projection, contrast angiography showing the ventriculoarterial discordance (*AA* ascending aorta, *LV* left ventricle, *PA* pulmonary artery, *PDA* patent ductus arteriosus, *RV* right ventricle) (modified with permission from Goo HW, Park IS, Ko JK, Kim YH, Seo DM, Yun TJ, Park JJ, Yoon CH (2003) CT of congenital heart disease: normal anatomy and typical pathologic conditions. Radiographics 23:S147–165)

cation for atrial re-routing (Mustard or Senning), it is also mandatory to assess the morphology and position of the auricular appendages (Fig. 3.15.2). In case of complete transposition of the great arteries with intact ventricular septum, an arterial switch is feasible only in the first few weeks of life. For later referral, it is crucial to estimate the left ventricular mass in order to evaluate the possibility of the morphologic left ventricle to function as the systemic ventricle after an arterial switch operation. In patients with ventricular septal defect and left ventricular outflow tract obstruction, a detailed definition of the intracardiac anatomy is useful to decide between the available options: Rastelli, Lecompte (REV) or Bex-Nikaidoh procedures. In all the above situations, echocardiography and cardiac catheterization with angiography can provide most of the required information. However, in some complex cases, more sophisticated imaging tools could provide some anatomical details that
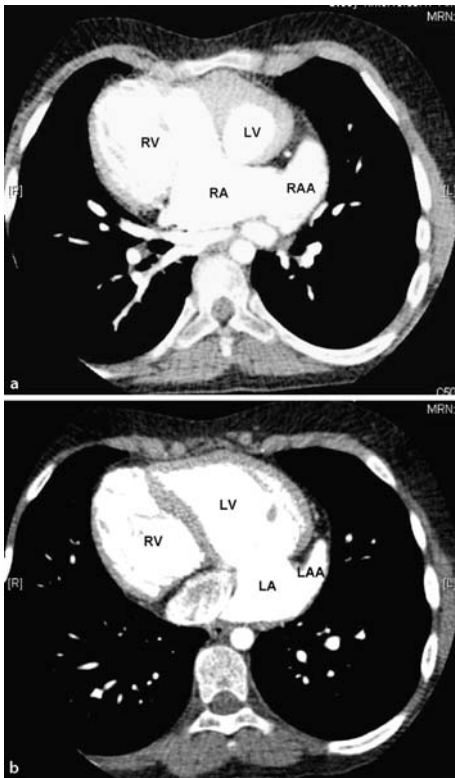
Fig. 3.15.2. Transposition of the great arteries, left juxtaposition of the auricular appendages. **a** CT scan, axial projection, contrast angiography showing dextrocardia and the right auricular appendage on the left side. **b** CT scan of the same patient, axial projection, contrast angiography showing dextrocardia and the left auricular appendage on the left side (*LAA* left auricular appendage, *LA* left atrium, *LV* left ventricle, *RV* right ventricle, *RAA* right auricular appendage, *RA* right atrium)

are not available with traditional diagnostic investigations. Particularly attractive is the development of a stereolithographic model derived from a standard CT scan or MRI to create accurate and realistic models of complex congenital defects for pre-operative assessment and intraoperative orientation; a virtual incision-making tool that allows arbitrary incisions to be made in a 3-dimensional reconstruction of the MRI data has been developed.

In summary, CT scan and MRI are seldom required for pre-operative assessment of infants with transposition of the great arteries. However the development of new acquisition and MRI techniques able to display high-resolution 3-dimensional heart images, ready to be post-processed, could greatly help surgeons planning surgical repair particularly in the case of intraventricular rerouting.

▪ Potential complications

▪ *Atrioseptostomy/atriospectectomy:* supraventricular arrhytmias, inadequate *mixing* at the atrial level,

▪ *Atrial rerouting:* arrhytmias, tricuspid valve regurgitation, right (systemic) ventricular dysfunction, residual or recurrent obstruction of the pulmonary or the systemic venous return because of stenosis of the new caval or pulmonary venous channels,

▪ *Arterial switch (Jatene operation):* residual or recurrent coronary arteries stenosis because of the coronary artery reimplantation, residual or recurrent obstruction of the new right ventricular outflow tract (more frequent) or the new left ventricular outflow tract (much more rare), aortic valve regurgitation,

▪ *Rastelli operation:* residual or recurrent ventricular septal defect, residual or recurrent obstruction of the new left ventricular outflow tract, obstruction of the right ventricle-to-pulmonary artery valved conduit, complete atrioventricular block,

▪ *Lecompte procedure (or REV = Réparation à l'Etage Ventriculaire):* residual or recurrent ventricular septal defect, residual or recurrent obstruction of the new right ventricle outflow tract, complete atrioventricular block, pulmonary artery stenosis due to pulmonary arteries stretching,

▪ *Damus-Kaye-Stansel procedure:* residual or recurrent ventricular septal defect, residual or recurrent obstruction of the new left ventricular outflow tract, late regurgitation of the systemic (aortic or pulmonary) valves, obstruction of the right ventricle-

to-pulmonary artery valved conduit, complete atrioventricular block,

■ *Bex-Nikaidoh procedure:* residual or recurrent ventricular septal defect, residual or recurrent obstruction of the new left ventricular outflow tract, residual or recurrent coronary arteries stenosis because of the coronary artery reimplantation, regurgitation of the aortic valve, obstruction of the right ventricle-to-pulmonary artery connection, complete atrioventricular block.
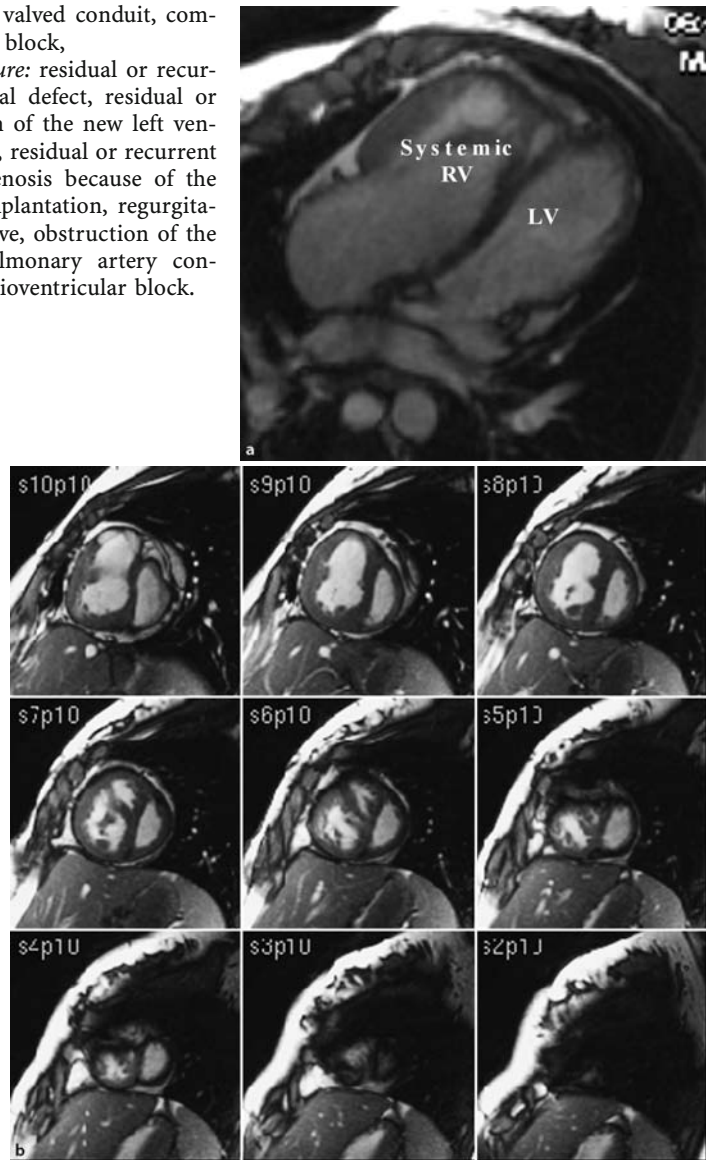
Fig. 3.15.3. Transposition of the great arteries, status post atrial rerouting (Mustard). MRI cine steady-state free precession 4-chamber view (**a**) and ventricular short axis (**b**) showing the hypertrophic systemic right ventricle. The ventricular septum is shifted towards the left ventricle (*LV* left ventricle, *RV* right ventricle)
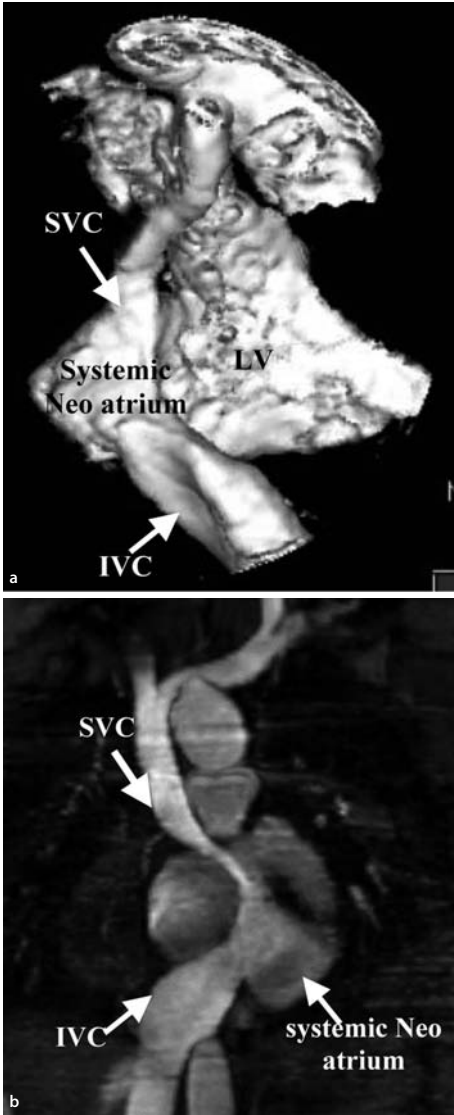
Fig. 3.15.4. Transposition of the great arteries, status post atrial rerouting (Mustard). MRI 2-dimensional time of flight volume rendering reconstruction (**a**), and maximal intensity projection reconstruction (**b**) showing significant baffle obstruction of the superior vena cava (*IVC* inferior vena cava, *LV* left ventricle, *SVC* superior vena cava)
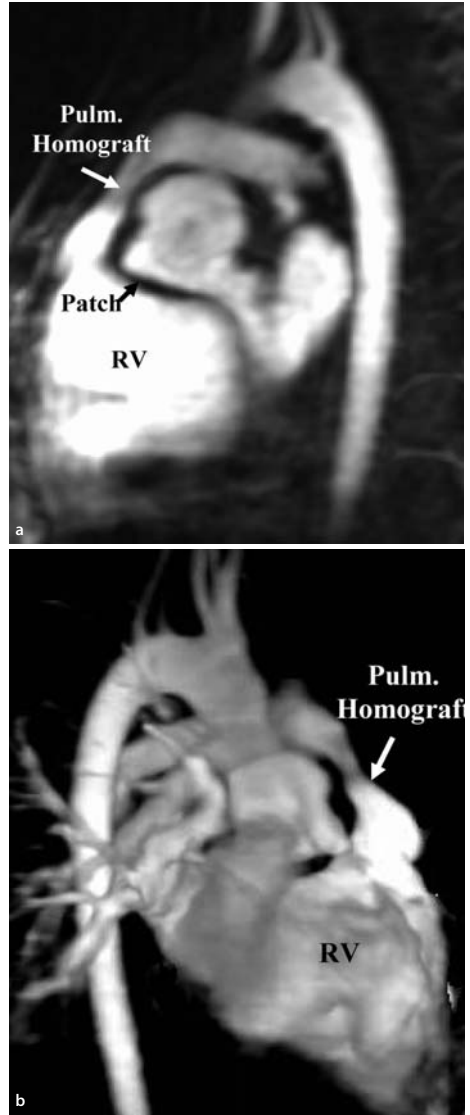
Fig. 3.15.5. Transposition of the great arteries, ventricular septal defect and pulmonary stenosis, status post Rastelli procedure. MR angiography maximal intensity projection reconstruction (**a**) and volume rendering reconstruction (**b**) showing a stenosis of the pulmonary homograft. Note the anterior location of the pulmonary artery bifurcation because of the Lecompte maneuver (*Pulm* pulmonary, *RV* right ventricle)

▪ Post-operative follow-up

In the post-operative evaluation of patients with transposition of the great arteries, cardiac MRI is assuming an increasing role due to its ability to noninvasively evaluate most clinically relevant issues. The goals of evaluation of post-operative atrial switch (Mustard or Senning) include:

- quantitative evaluation of the size and function of the systemic right ventricle (Fig. 3.15.3),
- imaging of the systemic and pulmonary venous pathways to rule out obstructions and/or baffle leaks (Fig. 3.15.4),
- assessment of tricuspid (systemic) valve regurgitation,
- evaluation of the left and right ventricular outflow tracts,
- detection of aortopulmonary collateral arteries and other associated anomalies.

In patients with right (systemic) ventricular dysfunction, post-gadolinium delayed myocardial enhancement can be used to detect myocardial fibrosis. The response of the systemic right ventricle to pharmacological stress (dobutamine) or to exercise can be tested by cardiac MRI. However the clinical utility of these informations requires further studies.

The long-term follow-up of patients after arterial switch, Rastelli, Lecompte (REV) or Bex-Nikaidoh procedures mainly focuses on the technical challenges of each of the above mentioned operations: transfer of the coronary arteries from the native aortic root to the neoaortic root (native pulmonary root); transfer of the pulmonary arteries anterior to the neoascending aorta; reconstruction of the right and left ventricular outflow tracts.
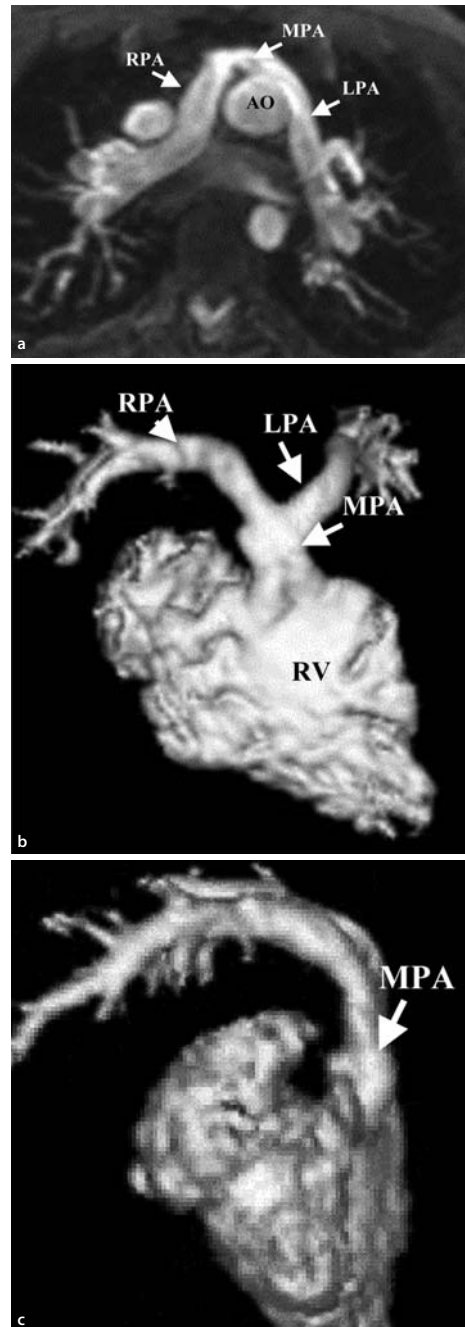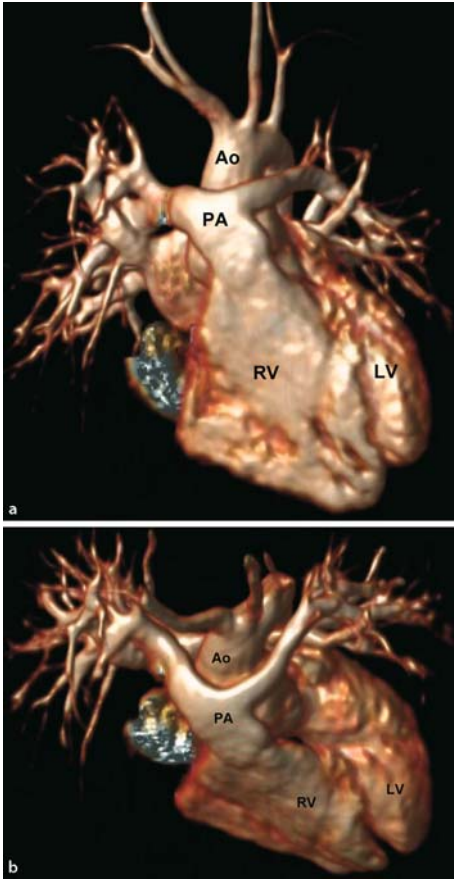

Fig. 3.15.6. Transposition of the great arteries, status post arterial switch. MR angiography maximal intensity projection reconstruction (**a**) and volume rendering reconstruction (**b** and **c**) showing pulmonary stenosis due to the compression between the aorta and the sternum (*AO* aorta, *LPA* left pulmonary artery, *MPA* main pulmonary artery, *RPA* right pulmonary artery, *RV* right ventricle)

Fig. 3.15.7. Transposition of the great arteries, status post arterial switch. **a** MR angiography showing the post-operative images after arterial switch. **b** Different projection with the main pulmonary artery and the origin of the two branches compressed and displaced by the new ascending aorta (*Ao* aorta, *LV* left ventricle, *PA* pulmonary artery, *RV* right ventricle)
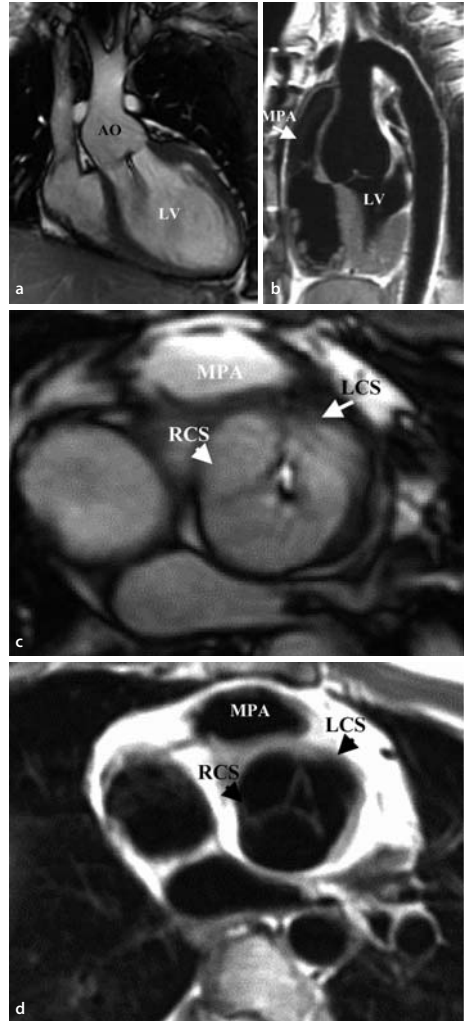
Fig. 3.15.8. Transposition of the great arteries, status post arterial switch. Left ventricular outflow tract steady-state free precession cine MRI (**a**) and fast spin echo parasagittal view (**b**) showing a dilated aortic root leading to a significant aortic valve regurgitation (regurgitation fraction calculated by PVC-MRI = 40%). Note in steady-state free precession (**c**) and FSE (**d**) aortic valve short-axis acquisition with the lack of coaptation of the leaflets (*AO* aorta, *LCS* left coronary sinus, *LV* left ventricle, *MPA* main pulmonary artery, *RCS* right coronary sinus)
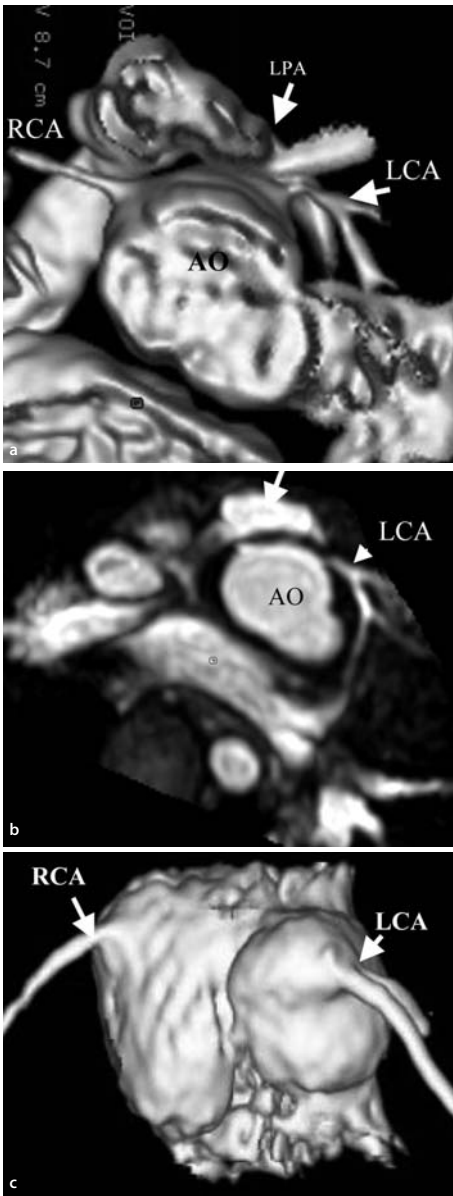
Therefore the goals of the post-operative evaluation in these cases include:

▪ evaluation of global and regional left and right ventricular size and function,
▪ evaluation of the left and right ventricular outflow tracts (Fig. 3.15.5),
▪ qualitative estimation of the right systolic pressure based on the configuration of the interventricular septum,
▪ evaluation of the pulmonary arteries to rule out the presence of stenosis (Figs. 3.15.6 and 3.15.7),
▪ evaluation of the aortic root and coronaries origin (Fig. 3.15.8 and 3.15.9),
▪ other associated anomalies.

The role of myocardial perfusion and viability imaging in this population deserves further studies.

The above objectives can be achieved by the following cardiac MRI protocol:

▪ 3-plane localizing images,
▪ 2-dimensional axial time of flight (see appendix in the "Introduction"),
▪ ECG-gated cine steady-state free precession sequences in 2-chamber, 4-chamber planes, and ventricular short axis for the quantitative assessment of both ventricular dimensions, function and stroke volume as illustrated in the appendix of the "Introduction",
▪ ECG-gated cine steady-state free precession and fast spin echo (if needed) sequence to visualize the left ventricular outflow tract and the aortic arch,

Fig. 3.15.9. Transposition of the great arteries, status post arterial switch. MRI 3-dimensional steady state free precession volume rendering reconstruction (**a**) and maximal intensity projection reconstruction (**b**) showing a suspected mild "kinking" at the origin of the left coronary artery; 3-dimensional steady state free procession volume rendering reconstruction (**c**) in another patient: no coronary artery stenosis is detected (*AO* aorta, *LCA* left coronary artery, *LPA* left pulmonary artery, *RCA* right coronary artery)

- ECG-gated cine steady-state free precession and fast spin echo short axis (if needed) sequences for the aortic root,
- ECG-gated cine steady-state free precession sequence, generally on the sagittal plane, to visualize the right ventricular outflow tract,
- ECG-gated cine steady-state free precession sequence to visualize the intraatrial baffles in case of atrial switch,
- gadolinium-enhanced 3-dimensional MR angiography,
- ECG-gated static 3-dimensional steady-state free precession for the evaluation of origin and proximal course of coronary arteries (Fig. 3.15.9),
- ECG-gated phase velocity contrast MRI sequences perpendicular to the main pulmonary artery, ascending aorta and pulmonary arteries, to assess aortic and pulmonary valve regurgitation and pulmonary blood flow,
- post-gadolinium delayed myocardial enhancement may be used to evaluate the presence of fibrotic tissue.

Imaging of the coronary arteries and pharmacological stress testing (either adenosine or dobutamine) for evaluation respectively of coronary proximal stenosis and myocardial ischemia are increasingly being incorporated into the clinical imaging protocol in the post-operative evaluation of patients with transposition of the great arteries.

▪ References

Babu-Narayan SV, Goktekin O, Moon JC, Broberg CS, Pantely GA, Pennell DJ, Gatzoulis MA, Kilner PJ (2005) Late gadolinium enhancement cardiovascular magnetic resonance of the systemic right ventricle in adults with previous atrial redirection surgery for transposition of the great arteries. Circulation 111: 2091–2098

Bex JP, Lecompte Y, Baillot F, Hazan E (1980) Anatomical correction of transposition of the great arteries. Ann Thorac Surg 29:86–88

Choi BW, Park YH, Choi JY, Choi BI, Kim MJ, Ryu SJ, Lee JK, Sul JH, Lee SK, Cho BK, Choe KO (2001) Using electron beam CT to evaluate conotruncal anomalies in pediatric and adult patients. Am J Roentgenol 177:1045–1049

Cook SC, McCarthy M, Daniels CJ, Cheatham JP, Raman SV (2004) Usefulness of multislice computed tomography angiography to evaluate intravascular stents and transcatheter occlusion devices in patients with d-transposition of the great arteries after Mustard repair. Am J Cardiol 94:967–969

Corno AF, Laks H, George B, Williams RG (1987) Use of in situ pericardium for surgical relief of pulmonary venous obstruction following Mustard's operation. Ann Thorac Surg 43:443–444

Corno AF, Parisi F, Marino B, Ballerini L, Marcelletti C (1987) Palliative Mustard operation: an expanded horizon. Eur J Cardiothorac Surg 1:144–147

Corno AF, George B, Pearl J, Laks (1989) Surgical options for complex transposition of the great arteries. J Am Coll Cardiol 14:742–749

Corno AF, von Segesser LK (2001) Transposition of great arteries and single coronary artery: a new surgical technique for the arterial switch operation. Swiss Med Wkly 131:47–49

Corno AF, Hurni M, Payot M, Sekarski N, Tozzi P, von Segesser LK (2003) Adequate left ventricular preparation allows for arterial switch despite late referral. Cardiol Young 13:49–52

Dorfman AL, Geva T (2006) Magnetic resonance imaging evaluation of congenital heart disease: conotruncal anomalies. J Cardiovasc Magn Reson 8:645–659

Dos L, Pen V, Silversides C, Provost Y, Oechslin E, Horlick E, Paul N (2007) Images in cardiovascular medicine. Cardiac magnetic resonance imaging and multidetector computed tomography scan illustrating Damus-Kaye-Stansel operation. Circulation 115: e440–442

Fogel MA, Hubbard A, Weinberg PM (2001) A simplified approach for assessment of intracardiac baffles and extracardiac conduits in congenital heart surgery with two- and three-dimensional magnetic resonance imaging. Am Heart J 142:1028–1036

Fogel MA, Hubbard A, Weinberg PM (2002) Mid-term follow-up of patients with transposition of the great arteries after atrial inversion operation using two- and three-dimensional magnetic resonance imaging. Pediatr Radiol 32:440–446

Fratz S, Hauser M, Bengel FM, Hager A, Kaemmerer H, Schwaiger M, Hess J, Stern HC (2006) Myocardial scars determined by delayed-enhancement magnetic resonance imaging and positron emission tomography are not common in right ventricles with systemic function in long-term follow up. Heart 92: 1673–1677

Goo HW, Park IS, Ko JK, Kim YH, Seo DM, Yun TJ, Park JJ, Yoon CH (2003) CT of congenital heart disease: normal anatomy and typical pathologic conditions. Radiographics 23:S147–165

Gyarmati G, Simor T, Kadar K, Toth L, Nemeth T, Oprea V, Hartyanszky I (2006) Quantification of right and left ventricular function with magnetic resonance imaging after Senning operation for complete transposition of the great arteries. Orv Hetil 147:171–174

Hornung TS, Anagnostopoulos C, Bhardwaj P, Kilner PJ, Davlouros PA, Bailey J, Francis JM, Pennell DJ, Underwood SR, Gatzoulis MA (2003) Comparison of equilibrium radionuclide ventriculography with cardiovascular magnetic resonance for assessing the systemic right ventricle after Mustard or Senning procedures for complete transposition of the great arteries. Am J Cardiol 92:640–643

Kiaffas MG, Davlouros P, Tsertos F, Andreou J, Danias PG (2005) Cardiovascular magnetic resonance evaluation of patients with transposition of the great arteries following atrial switch surgical correction. Hellenic J Cardiol 46:69–73

Laffon E, Latrabe V, Jimanez M, Ducassou D, Laurent F, Marthan R (2006) Quantitative MRI comparison of pulmonary hemodynamics in Mustard/Senning-repaired patients suffering from transposition of the great arteries and healthy volunteers at rest. Eur Radiol 16:1442–1448

Lecompte Y, Zannini L, Hazan E, Jarreau MM, Bex JP, Tu TV, Neveux JY (1981) Anatomic correction of transposition of the great arteries. J Thorac Cardiovasc Surg 82:629

Lecompte Y, Bex JP (1985) Repair of transposition of the great arteries with ventricular septal defect and left ventricular outflow tract obstruction. J Thorac Cardiovasc Surg 90:151–154

Lissin LW, Li W, Murphy DJ, Hornung T, Swan L, Mullen M, Kilner P, Gatzoulis MA (2004) Comparison of thansthoracic echocardiography versus cardiovascular magnetic resonance imaging for the assessment of ventricular function in adults after atrial switch procedures for complete transposition of the great arteries. Am J Cardiol 93:654–657

Livolsi A, Kastler B, Willard D (1989) Pre- and post-operative study of neonatal transposition of the great vessels by magnetic resonance imaging. Ann Cardiol Angiol 38:261–264

Lorenz CH, Walker ES, Graham TP, Powers TA (1995) Right ventricular performance and mass by use of cine MRI late after atrial repair of transposition of the great arteries. Circulation 92(Suppl-II):233–239

Morell VO, Wearden PD (2007) Aortic translocation for the management of transposition of the great arteries with a ventricular septal defect, pulmonary stenosis, and hypoplasia of the right ventricle. Eur J Cardiothorac Surg 31:552–554

Oosterhof T, Tulevski II, Roest AA, Stendijk P, Vliegen HW, van der Wall EE, de Roos A, Tijssen JG, Mulder BJ (2005) Disparity between dobutamine stress and physical exercise magnetic resonance imaging in patients with an intra-atrial correction for transposition of the great arteries. J Cardiovasc Magn Reson 7:383–389

Ou P, Mousseaux E, Azarine A, Dupont P, Agnoletti G, Vouhé P, Bonnet D (2006) Detection of coronary complications after the arterial switch operation for transposition of the great arteries: first experience with multislice computed tomography in children. J Thorac Cardiovasc Surg 131:639–643

Pettersen E, Helle-Valle T, Edvardsen T, Lindberg H, Smith HJ, Smevik B, Smiseth OA, Andersen K (2007) Contraction pattern of the systemic right ventricle. Shift from longitudinal to circumferential shortening and absent global ventricular torsion. J Am Coll Cardiol 49:2450–2456

Raisky O, Bergoend E, Agnoletti G, Ou P, Bonnet D, Sidi D, Vouhé PR (2007) Late coronary artery lesions after neonatal arterial switch operation: results of surgical coronary revascularization. Eur J Cardiothorac Surg 31:894–898

Raman SV, Cook SC, McCarthy B, Ferketich AK (2005) Usefulness of multidetector row computed tomography to quantify right ventricular size and function in adults with either tetralogy of Fallot or transposition of the great arteries. Am J Cardiol 95:683–686

Salehian O, Schwerzmann M, Merchant N, Webb GD, Siu SC, Therrien J (2004) Assessment of systemic right ventricular function in patients with transposition of the great arteries using the myocardial performance index: comparison with cardiac magnetic resonance imaging. Circulation 110:3229–3233

Sodian R, Weber S, Markert M, Rassoulian D, Kaczmarek I, Lueth TC, Reichart B, Daebritz S (2007) Stereolithographic models for surgical planning in congenital heart surgery. Ann Thorac Surg 83:1854–1857

Sørensen TS, Mosegaard J, Greil GF, Miller S, Seeger A, Hansen OK, Sieverding L (2007) Images in cardiovascular medicine. Virtual cardiotomy for preoperative planning. Circulation 115:e312

Tang T, Chiu IS, Chen HC, Cheng KY, Chen SJ (2001) Comparison of pulmonary arterial flow phenomena in spiral and Lecompte models by computational fluid dynamics. J Thorac Cardiovasc Surg 122:529–534

Taylor AM, Dymarkowski S, Hamaekers P, Razavi R, Gewillig M, Mertens L, Bogaert J (2005) MR coronary angiography and late-enhancement myocardial MR in children who underwent arterial switch surgery for transposition of great arteries. Radiology 234:542–547

Tops LF, Roest AA, Lamb HJ, Vliegen HW, Helbing WA, van der Wall EE, de Roos A (2005) Intraatrial repair of transposition of the great arteries: use of MR imaging after exercise to evaluate regional systemic right ventricular function. Radiology 237:861–867

Tulevski II, van der Wall EE, Groenink M, Dodge-Khatami A, Hirsch A, Stoker J, Mulder BJ (2002) Usefulness of magnetic resonance imaging dobutamine stress in asymptomatic and minimally symptomatic patients with decreased cardiac reserve from congenital heart disease (complete and corrected transposition of the great arteries and subpulmonic obstruction). Am J Cardiol 89:1077–1081

Yeh T, Ramaciotti C, Leonard SR, Roy L, Nikaidoh H (2007) The aortic translocation (Nikaidoh) procedure: midterm results superior to the Rastelli procedure. J Thorac Cardiovasc Surg 133:461–469

Hypoplastic left heart syndrome

▌ Definition

The morphological features of the hypoplastic left heart syndrome are:
- ▌ mitral atresia or severe stenosis
- ▌ aortic atresia or severe stenosis
- ▌ left ventricular hypoplasia or aplasia
- ▌ left atrial hypoplasia
- ▌ interatrial communication
- ▌ patent ductus arteriosus
- ▌ aortic coarctation
- ▌ right atrial dilatation
- ▌ right ventricular dilatation and hypertrophy

The apex is formed by the right ventricle and the epicardial course of the left anterior descending coronary artery defines a very small or non-existent left ventricle. The ascending aorta may be as small as 1 or 2 mm, but enough to supply blood to the coronary arteries in a retrograde fashion from the patent ductus arteriosus. A patent foramen ovale is generally small, with herniation of the valve of the septum primum from left-to-right, or even closed. Premature closure of the patent foramen ovale is usually accompanied by severe hypoplasia of the left heart cavities. Endocardial fibroelastosis can be also present. Connections of the left ventricle to the coronary arteries have been described. The ductus arteriosus is widely patent, serving as a downward-directed conduit from the main pulmonary artery to the descending thoracic aorta. The neonates are generally not born with aortic coarctation, but it frequently develops (80% of cases). Obstructions at the level of the aortic arch are frequently present.

Associated anomalies

Dextrocardia and isomerism are uncommon, as well as juxtaposition of the auricular appendages. Rare is the incidence of an associated partial anomalous pulmonary venous connection. Aortic arch interruption is very rare. Association with the dominant right form of atrioventricular septal defect, double outlet right ventricle or aortic-left ventricular tunnel are possible. Morphological anomalies of the tricuspid valve are unusual, despite a not infrequent presence of tricuspid valve regurgitation. Extremely rare is the association with pulmonary valve stenosis. Extremely rare is the presence of a ventricular septal defect.

▌ Surgical options

Surgical management includes different options:
- ▌ *palliation*: stent of the ductus arteriosus and bilateral pulmonary artery banding,
- ▌ *univentricular type of repair in three stages*: the first stage is the Norwood procedure, followed by a bidirectional Glenn (end-to-side anastomosis of the superior vena cava to the right pulmonary artery) and then by a modified Fontan procedure (total cavo-pulmonary connection by extracardiac or intracardiac connection of the inferior vena cava to the pulmonary artery),
- ▌ *heart transplantation*

■ **Stent of the ductus arteriosus and bilateral pulmonary artery banding:** This palliative approach, consisting of stenting the ductus arteriosus to maintain the patency and surgical (or intravascular) bilateral pulmonary artery banding to maintain adequate systemic perfusion through the ductus arteriosus, has been recently proposed with two potential targets:

■ to improve the clinical condition of the neonate, particularly if the clinical condition is very critical, to increase the chances of tolerating a subsequent Norwood type of procedure,

■ to allow for a stabilization lasting a period long enough to allow for the availability of a donor heart for heart transplantation.

■ **Norwood procedure:** the Norwood procedure consists of an initial palliative procedure (first stage) in view of a univentricular type of repair. Palliation includes using the pulmonary valve and proximal main pulmonary artery as the neoaorta, by transecting the distal main pulmonary artery and connecting the proximal main pulmonary artery to the aortic arch and ascending aorta. Then the pulmonary blood flow is provided by a systemic-to-pulmonary artery shunt from the right subclavian artery or the innominate artery to the right pulmonary artery. In addition, the atrial septum is removed surgically to create an unrestricted interatrial communication and the patent ductus arteriosus is divided. Even in the absence of evident aortic coarctation, the area of the aortic isthmus can be bypassed by an aortic homograft to avoid the risk of recurrent aortic coarctation.

■ **Norwood procedure with the Sano variation:** the modified Norwood operation, proposed by Sano and nowadays widely adopted, including Norwood himself, replaces the modified Blalock-Taussig shunt with a tubular prosthesis implanted between the anterior aspect of the right ventricle and the pulmonary artery bifurcation. The advantage is to avoid the coronary artery steel of blood during diastole from the systemic-to-pulmonary shunt, difficult to manage after the classical Norwood procedure.

■ **Heart transplantation:** Heart transplantation in a hypoplastic left heart is not different from routine heart transplantation, with two exceptions: a) the need of a special technique for cardiopulmonary bypass, due to the presence of ductal dependency of the systemic perfusion; b) the need for reconstruction of the aortic arch and aortic isthmus.

■ Pre-operative information

Neonatal diagnosis and pre-operative assessment of hypoplastic left heart syndrome is classically performed by echocardiography. CT scan (Fig. 3.16.1) and MRI (Fig. 3.16.2) are very rarely utilized in the preoperative screening.
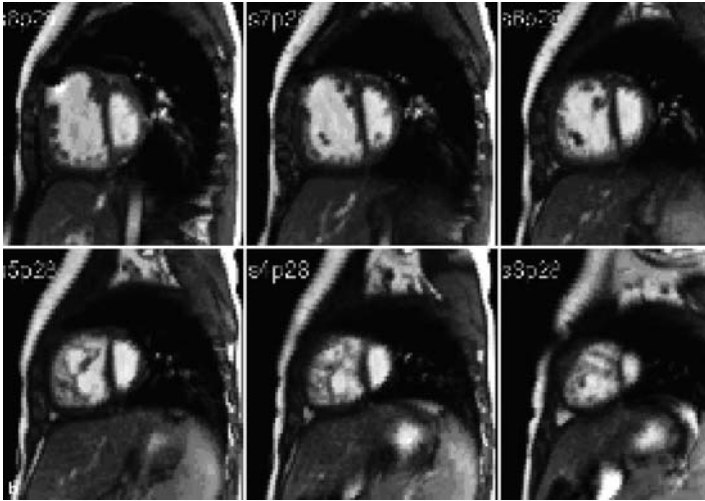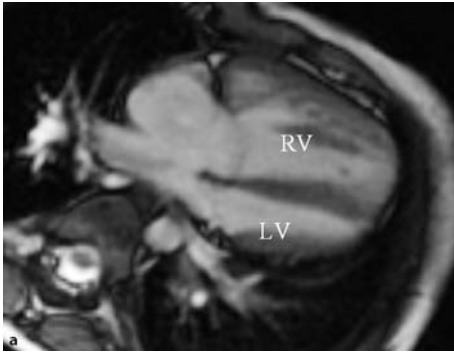
■ Potential complications

■ **Norwood procedure:** the immediate post-operative period is complicated by the very delicate balance between the systemic and
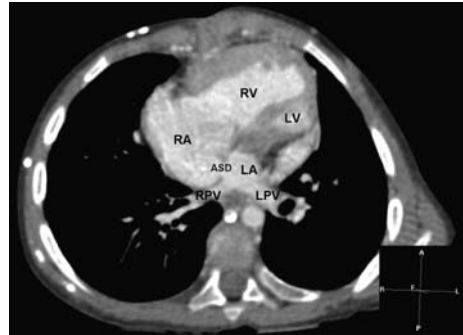
Fig. 3.16.1. Hypoplastic left heart syndrome. CT scan, axial projection, showing the very hypoplastic left ventricle, with small left atrium, dilated right atrium and right ventricle, and atrial septal defect (*ASD* atrial septal defect, *LA* left atrium, *LPV* left pulmonary veins, *LV* left ventricle, *RA* right atrium, *RPV* right pulmonary veins, *RV* right ventricle) (photograph courtesy of Dr. Mohamed Tawil)

pulmonary circulation, in parallel with a single ventricle physiology. Tricuspid regurgitation may develop and become progressive, and this represents a major issue since the right ventricle is functioning as the systemic ventricle. Recurrent aortic coarctation is possible in case of incomplete resection of residual ductal tissue. Rarely the pulmonary veins may develop progressive stenosis, and the ethiology is unclear.


Norwood procedure with the Sano variation: the main problem reported after the modified technique consists in hypoxia, more evident than after the classic Norwood procedure. Concern remains about long-term effects on ventricular function, because of the ventriculotomy performed on the systemic ventricle (Fig. 3.16.3).

▮ **Post-operative follow-up**

After the first stage of the Norwood procedure and before the second stage (bidirectional Glenn), the following targets need to be investigated:

- size of the interatrial septal defect,
- systemic ventricular function and myocardial viability,
- systemic atrioventricular (tricuspid) valve function,
- left ventricular outflow tract and systemic semilunar valve,
- morphology of the aortic arch,

Fig. 3.16.2. Hypoplastic left heart syndrome. Steady state free precession cine MRI 4-chamber (**a**) and short-axis (**b**) view in a 3-year-old patient with an indexed end-diastolic left ventricular volume of 21 ml/m^2 (*LV* left ventricle, *RV* right ventricle)
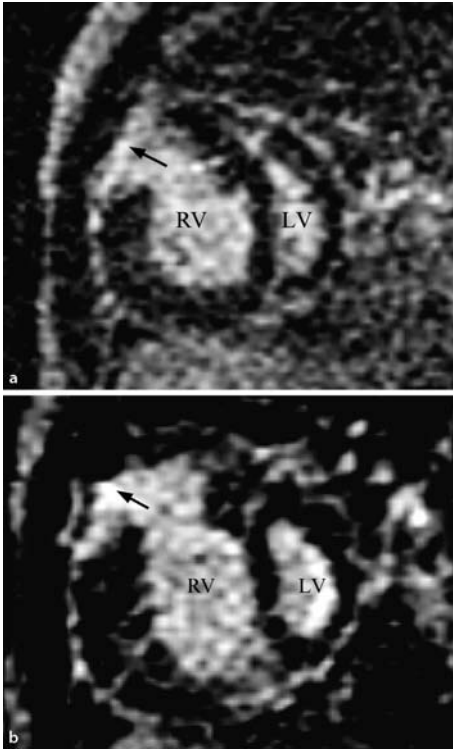
Fig. 3.16.3. Status-post modified Glenn after a Norwood operation with the Sano variation. MRI ventricular short axis "delayed enhancement" showing a large area of fibrosis due to the previous ventriculotomy performed for right ventricle to pulmonary artery conduit insertion (arrow) (*LV* left ventricle, *RV* right ventricle)

■ systemic-to-pulmonary shunt (or right ventricle to pulmonary artery conduit in case of previous Norwood with Sano variation),
■ morphology, flow and resistance of the pulmonary arteries.

The above information was traditionally obtained by echocardiography and cardiac catheterization with angiography. However if pulmonary vascular resistance is not thought to be elevated and CT (Fig. 3.16.4) and/or MRI (Fig. 3.16.5) are able to address all the issues mentioned above, cardiac catheterization can even be avoided. Furthermore, due to MRI's capability to detect myocardial scarring and some other important insights (e.g., biventricular volume), MRI has become a very useful tool in borderline cases where conversion to a biventricular type of repair could still be a suitable option.

The following cardiac MRI protocol is proposed in the evaluation of hypoplastic left heart syndrome after the first stage of the Norwood procedure:

■ 3-plane localizing images,
■ 2-dimensional axial Time-of-flight Angiography (see appendix in the "Introduction"),
■ ECG-gated cine steady-state free precession sequences in 2-chamber, 4-chamber planes, and ventricular short axis for the quantitative assessment of ventricular dimensions, function, mass and stroke volume as illustrated in the appendix of the "Introduction",
■ ECG-gated cine steady-state free precession sequence to visualize the systemic ventricular outflow tract and the neo-aorta (Fig. 3.16.6),
■ ECG-gated cine steady-state free precession and, if needed, fast spin echo sequence to visualize the aortic arch and the native neoaorta anastomosis (Fig. 3.16.7),
■ ECG-gated cine steady-state free precession and, if needed, fast spin echo sequence to visualize the right ventricle to pulmonary artery conduit (in case of Norwood with Sano variation) and the pulmonary artery branches (Fig. 3.16.8),
■ ECG-gated phase velocity contrast MRI sequences perpendicular to the main pulmonary artery, ascending neo- and native aorta, pulmonary arteries, superior vena cava and inferior vena cava to assess the flow pattern,
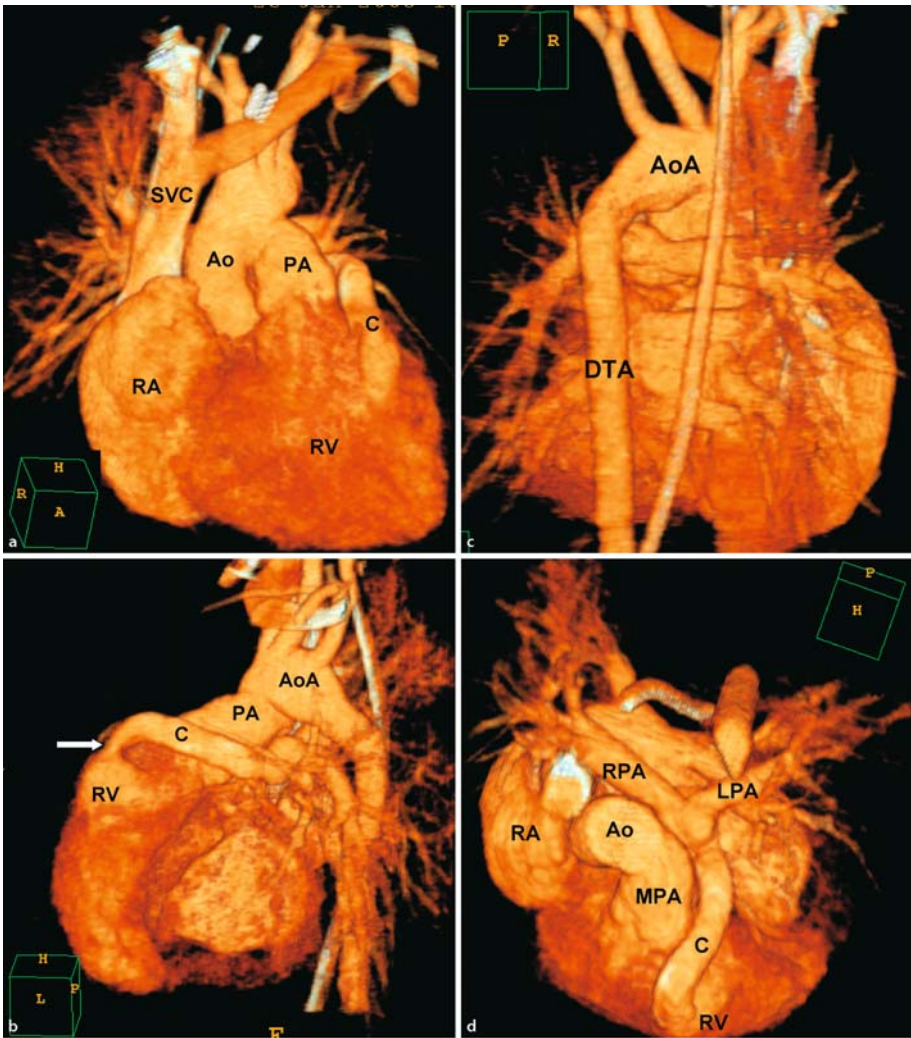
Fig. 3.16.4. Status/post Norwood/Sano modification stage I. **a** CT scan, showing anterior view of the 3-dimensional reconstruction volume rendering image of the end-to-side anastomosis of the transacted pulmonary artery to the ascending aorta and the proximal side of the right ventricle to pulmonary artery conduit. **b** CT scan in the same patient, showing from lateral view the 3-dimensional reconstruction volume rendering image of the end-to-side anastomosis of the divided pulmonary artery to the ascending aorta and right ventricle to pulmonary artery conduit with a narrowing (arrow) at the proximal anastomosis. **c** CT scan, 3-dimensional reconstruction volume rendering image showing from posterior view the adequate reconstruction of the aortic arch. **d** CT scan, 3-dimensional reconstruction volume rendering top-view image showing the end-to-side anastomosis of the divided pulmonary artery to the ascending aorta and the right ventricle to pulmonary artery conduit (*Ao* aorta, *AoA* aortic arch, *C* conduit, *DTA* descending thoracic aorta, *LPA* left pulmonary artery, *PA* pulmonary artery, *MPA* main pulmonary artery, *RA* right atrium, *RPA* right pulmonary artery, *RV* right ventricle, *SVC* superior vena cava) (photographs courtesy of Dr. Mohamed Tawil)
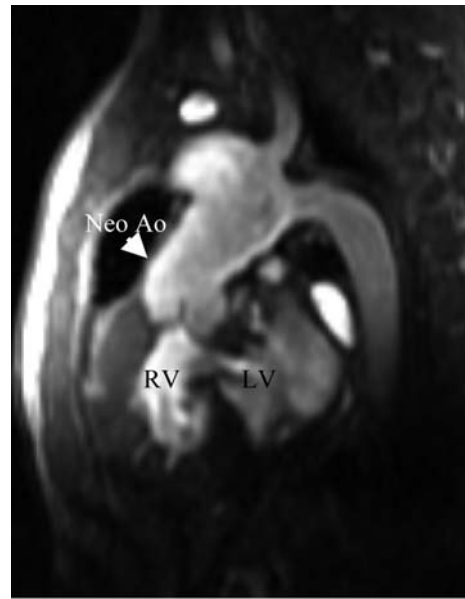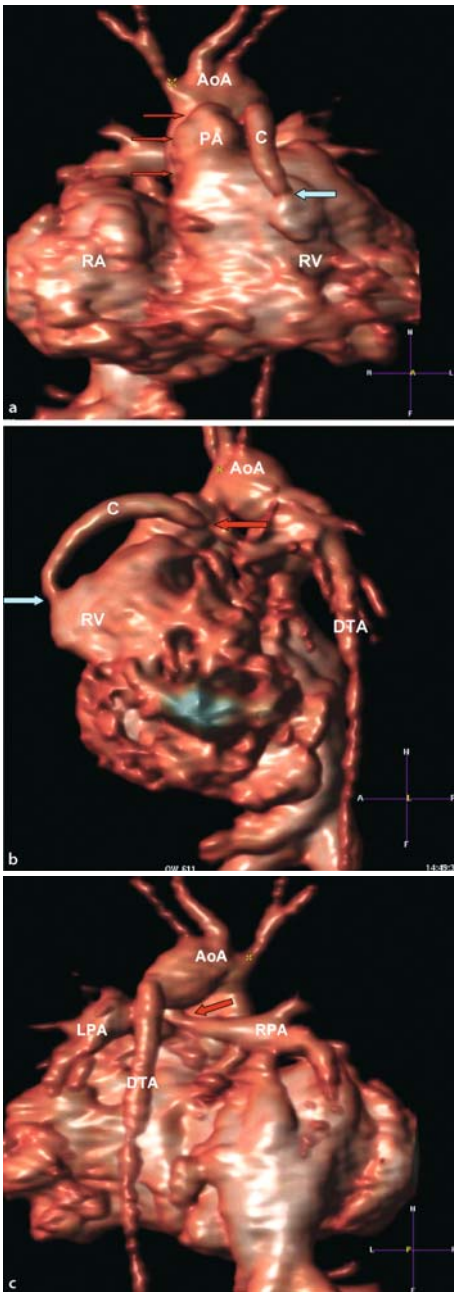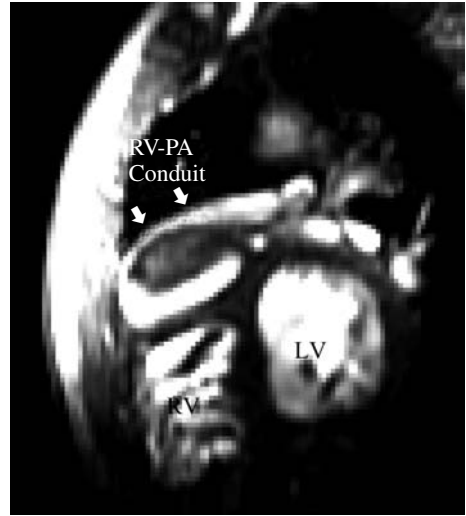
Fig. 3.16.6. Status post Norwood procedure with Sano variation. Cine MRI of the right ventricular outflow tract showing a hypertrophic right systemic ventricle connected to the neoaorta (*LV* left ventricle, *RV* right ventricle)

Fig. 3.16.5 Status post Norwood/Sano for hypoplastic left heart syndrome. **a** Cardiac MR Angiography: 3-dimensional reconstruction, volume rendering anterior view, showing the end-to-side anastomosis of the divided main pulmonary artery to the ascending aorta (red arrows) to create an unobstructed systemic outlet and the proximal anastomosis (blue arrow) of the right ventricle to pulmonary artery conduit (Sano modification). **b** Cardiac MR Angiography: 3-dimensional reconstruction, volume rendering lateral view, showing the stenotic proximal (blue arrow) and distal (red arrow) anastomosis of the right ventricle to pulmonary artery conduit (Sano modification). **c** Cardiac MR Angiography: 3-dimensional reconstruction, volume rendering posterior view, showing the good size of the aortic arch and of the distal pulmonary arteries, but with a long narrowing of the origin of the left pulmonary artery (*AoA* aortic arch, *C* conduit, *DTA* descending thoracic aorta, *LPA* pulmonary artery, *PA* pulmonary artery, *RA* right atrium, *RPA* right pulmonary artery, *RV* right ventricle) (photographs courtesy of Dr. Rob A. Johnson)

Fig. 3.16.8. Status post Norwood/Sano. Cine MRI showing a stenosis of the right ventricle to pulmonary artery conduit after first stage Norwood procedure with Sano variation (*LV* left ventricle, *PA* pulmonary artery, *RV* right ventricle)

Fig. 3.16.7. Status post Norwood procedure. MRI fast spin echo showing the native aorta anastomosed (head arrow) to the neoaorta (*RA* right atrium)
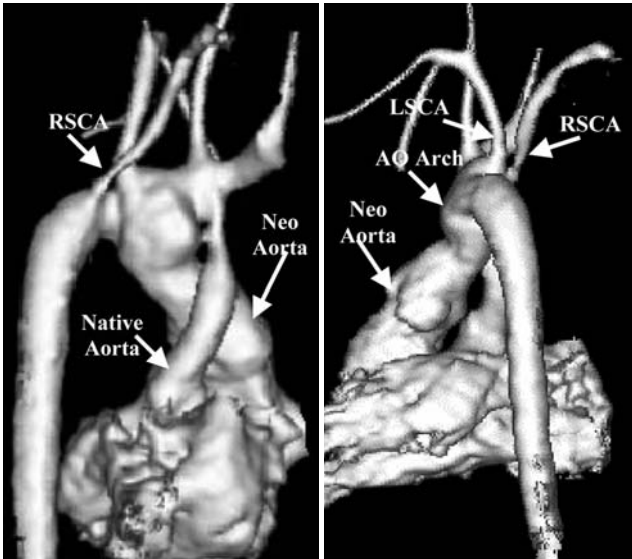
Fig. 3.16.9. Status post first stage of Norwood procedure. MR angiography volume rendering reconstruction showing the reconstructed aortic arch; note the anomalous right sub- clavian artery (*Ao arch* aortic arch, *LSCA* left subclavian artery, *RSCA* right subclavian artery)

- ▌ gadolinium-enhanced 3-dimensional MRI for the evaluation of the pulmonary arteries, the systemic-to-pulmonary artery shunt, the systemic and pulmonary venous returns, and the aortic arch (Fig. 3.16.9).
- ▌ post-gadolinium delayed myocardial enhancement may be used to evaluate the presence of myocardial scar tissue in the 2-chamber and ventricular short-axis planes.

▌ References

Akintuerk H, Michel-Behnke I, Valeske K, Mueller M, Thul J, Bauer J, Hagel KJ, Kreuder J, Vogt P, Schranz D (2002) Stenting of the arterial duct and banding of the pulmonary arteries: basis for combined Norwood stage I and II repair in hypoplastic left heart. Circulation 105:1099–1103

Corno AF (2000) Surgery for congenital heart disease. Curr Opinion Cardiol 15:238–243

Dent CL, Spaeth JP, Jones BV, Schwartz SM, Glauser TA, Hallinan B, Pearl JM, Khoury PR, Kurth CD (2005) Brain magnetic resonance imaging abnormalities after the Norwood procedure using regional cerebral perfusion. J Thorac Cardiovasc Surg 130:1523–1530

Dos L, Pen V, Silversides C, Provost Y, Oechslin E, Horlick E, Paul N (2007) Images in cardiovascular medicine. Cardiac magnetic resonance imaging and multidetector computed tomography scan illustrating Damus-Kaye-Stansel operation. Circulation 115:e440–442

Funabashi N, Rubin GD (2001) Direct identification of patency achieved by a bi-directional Glenn shunt procedure: images by volume rendering using electron-beam computed tomography. Jpn Circ J 65:457–461

Giannico S, Corno AF, Marino B, Cicini MP, Gagliardi MG, Amodeo A, Picardo S, Marcelletti C (1992) Total extracardiac right heart bypass. Circulation 86(Suppl 2):110–117

Greenberg SB, Drummond-Webb J (2005) Gadolinium-enhanced magnetic resonance angiography of right ventricle to pulmonary artery shunts following Norwood I palliation in infants. Pediatr Radiol 35:186–190

Harris MA, Johnson TR, Weinberg PM, Fogel MA (2007) Delayed-enhancement cardiovascular magnetic resonance identifies fibrous tissue in children after surgery for congenital heart disease. J Thorac Cardiovasc Surg 133:676–681

Lilje C, Habermann CR, Weil J (2005) Magnetic resonance imaging follow-up ot total cavopulmonary connection. Heart 91:395

Marcelletti C, Corno AF, Giannico S, Marino B (1990) Inferior vena cava to pulmonary artery extracardiac conduit: a new form of right heart bypass. J Thorac Cardiovasc Surg 100:228–232

Mitani Y, Takabayashi S, Sawada H, Ohashi H, Hayakawa H, Ikeyama Y, Imanaka-Yoshida K, Maruyama K, Shimpo H, Komada Y (2007) Fate of the "opened" arterial duct: lessons learned from bilateral pulmonary artery banding for hypoplastic left heart syndrome under the continuous infusion of Prostaglandin E1. J Thorac Cardiovasc Surg 133:1653–1654

Muthurangu V, Taylor AM, Hedge SR, Johnson R, Tulloh R, Simpson JM, Qureshi S, Rosenthal E, Baker E, Anderson D, Razavi R (2005) Cardiac magnetic resonance imaging after stage I Norwood operation for hypoplastic left heart syndrome. Circulation 112:3256–3263

Norwood WI, Lang P, Castaneda AR, Campbell DN (1981) Experience with operations for hypoplastic left heart syndrome. J Thorac Cardiovasc Surg 82:511–519

Robinson A (2003) Air embolism following CAT scan in a patient with hypoplastic left heart syndrome. Pediatr Cardiol 24:186

Sano S (2007) New era in management of hypoplastic left heart syndrome. Asian Cardiovasc Thorac Ann 15:83–85

Shiraishi I, Kajiyama Y, Yamagishi M, Hamaoka K (2006) Stereolithographic biomodeling of congenital heart disease by multislice computed tomography imaging. Circulation 113:e733–734

Sundareswaran KS, Kanter KR, Krishnankutty R, Sabatier JF, Parks WJ, Sharma S, Yoganathan AP, Fogel M (2006) Impaired power output and cardiac index with hypoplastic left heart syndrome: a magnetic resonance imaging study. Ann Thorac Surg 82:1267–1275

Yamagishi M, Fujiwara K, Yamada Y, Yoshida M, Shuntoh K, Shiraishi I, Hayano T, Itoi T, Hamaoka K, Kitamura N (2001) Norwood operation for left isomeric heart with aortic atresia: evaluation with three-dimensional computed tomography. J Thorac Cardiovasc Surg 121:1205–1207

Chapter 3.17 Cor triatriatum

▊ Definition

When used in isolation, the term *cor tria-triatum* almost always refers to division of the left atrium. The divided right atrium is called *cor triatriatum dexter*.

Several patterns exist in which the left atrial chamber is divided, often in association with anomalous venous connections or other lesions. In the great majority of cases, nonetheless, there is a pattern which can be considered as the "classic" lesion. In this variant, the left atrium is divided by a diaphragm (membrane) into two components: 1) the proximal (superior) left atrial chamber, typically thick-walled, somewhat larger than the distal chamber, above the subdividing diaphragm, receiving the four pulmonary veins; 2) the distal (inferior) left atrial chamber, generally thin-walled, with the opening of the fossa ovalis, the left auricular appendage and the mitral valve. The diaphragm between the two components, which may have one or more variably sized openings in it, is usually rather thick and fibromuscular. Typically, the foramen ovale (which may be deficient, probe-patent or intact) is in actual or potential communication with the distal chamber, and the left auricular appendage is located in the distal chamber; these two features provide a means to distinguish between cor triatriatum and supravalvular mitral ring (see the chapter "Mitral valve disease"). The severity of the lesion depends upon the size of the orifice between the divided components of the left atrium.

Associated anomalies

Cor triatriatum is seen most frequently as an isolated lesion but it can coexist with any other defect. Notable associations include persistent left superior vena cava and un-roofed coronary sinus. Other associated lesions can be supravalvular mitral ring, atrial septal defect, partial or total anomalous pulmonary venous connection, stenosis of the pulmonary veins, atrioventricular septal defect, mitral valve regurgitation, ventricular septal defect, tetralogy of Fallot, double outlet right ventricle, double discordance, hypoplastic left heart syndrome, aortic valve stenosis, pulmonary stenosis, anomalous origin of the right pulmonary artery from the aorta, aortic coarctation; rarely asplenia or polysplenia.

▊ Surgical options

Complete resection of the diaphragm, taking care not to injure the mitral valve or the interatrial septum, is approached from the left atrium or from the right atrium (through an already present or a surgically created interatrial communication), depending on the size of the proximal left atrial chamber and on the presence of associated anomalies.

In the classical form of cor triatriatum, the surgical approach through a right atriotomy is recommended, with enlargement of the patent foramen ovale (or interatrial septal defect) to obtain better exposure of the left atrial diaphragm. After identification and complete resection of the diaphragm, the remaining interatrial communication is

closed with an autologous (or heterologous) pericardial patch.

In the left atrial approach, the common pulmonary venous proximal chamber is opened through a vertical incision anterior to the pulmonary veins, and the diaphragm is exposed by appropriate retraction; one or two radial incisions from the opening of the diaphragm outward to the atrial wall or interatrial septum substantially enhance the exposure; the diaphragm is excised only after precise identification of the pulmonary veins.

▪ Pre-operative information

In addition to the information already obtained with echocardiography, CT scan and MRI can provide details useful to precisely localize the fibromuscular diaphragm (membrane), its relationship with the interatrial septum, the position and the size of its opening connecting the proximal (superior) with the distal (inferior) left atrial chamber, the pulmonary venous connections as well as the presence of associated intracardiac defects (Fig. 3.17.1).

MRI in particular axial and coronal fast spin echo sequences can delineated very well the morphology of the left atrial chamber with the fibromuscular diaphragm (membrane) and its relationship to the near cardiovascular structures. Furthermore, the visualization of a normal left auricular appendage, with a signal void indicating unobstructed flow, excludes other related intracardiac malformations, such as congenital mitral stenosis or supravalvular mitral ring.
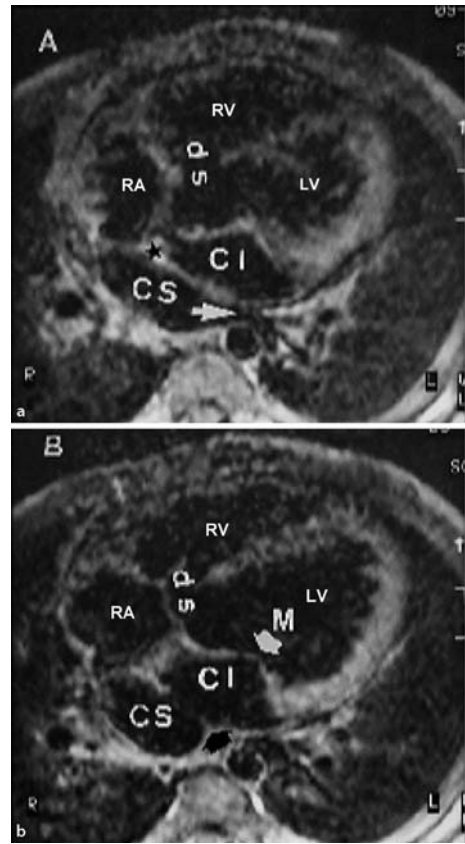
Fig. 3.17.1. Cor triatriatum. **a** MRI axial projection showing the pulmonary veins (arrow) connected to the proximal (superior) left atrial chamber, the distal (inferior) left atrial chamber emptying through the mitral valve into the left ventricle, and the attachment to the interatrial septum (asterisk) of the fibromuscular diaphragm (membrane) dividing the left atrium. Note the presence of a ventricular septal defect. **b** MRI axial projection in the same patient showing the absence of atrial septal defect, the central opening of the fibromuscular diaphragm (membrane) and its lateral insertion (black arrow) (*CI* inferior chamber, *CS* superior chamber, *DS* ventricular septal defect, *LV* left ventricle, *M* mitral valve, *RA* right atrium, *RV* right ventricle) (modified with permission from Cabrera A, Angulo P, Martinez P, Romero C, Pastor E, Galdeano JM (1997) Cor triatriatum with interventricular communication: Doppler color ultrasonography and magnetic resonance diagnosis. Repair in the first months. Rev Esp Cardiol 50:290–292, © Elsevier)
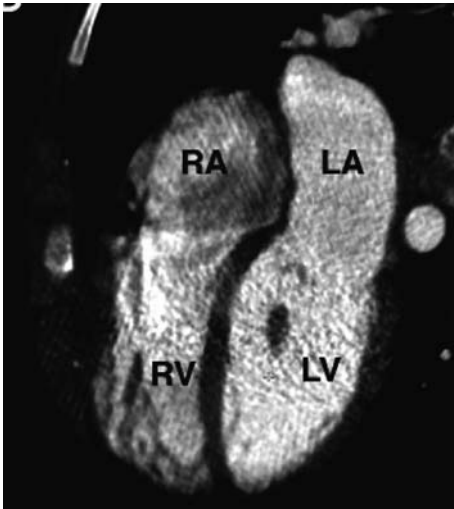
■ Potential complications

Inadequate membrane resection, residual atrial septal defect, mitral valve damage, air embolism, supraventricular arrhythmias; in neonates and infants post-operative crises of pulmonary hypertension requiring treatment are frequent. Pulmonary vein stenosis or restenosis in association with the orifice between the proximal and distal left atrial chambers, generally due to incomplete resection, are quite rare.

■ Post-operative follow-up

Both CT scan and MRI in the post-operative period can investigate the pulmonary veins and confirm the adequacy of the surgical repair (Fig. 3.17.2) or can show the presence of a residual segment of unresected fibromuscular diaphragm (membrane) or even other residual intracardiac defects.

Fig. 3.17.2. Status post repair of cor triatriatum. CT scan angiogram, 4-chamber view showing unobstructed left atrium after resection of the fibromuscular diaphragm (membrane) previously dividing the left atrial chamber and well balanced ventricles (*LA* left atrium, *LV* left ventricle, *RA* right atrium, *RV* right ventricle)

■ References

Bartel T, Müller S, Geibel A (1994) Preoperative assessment of cor triatriatum in an adult by dynamic three dimensional echocardiography was more informative than transoesophageal echocardiography or magnetic resonance imaging. Br Heart J 72:498–499

Bisset GS, Kirks DR, Strife JL, Schwartz DC (1987) Cor triatriatum: diagnosis by MR imaging. Am J Radiol 149:567–568

Cabrera A, Angulo P, Martinez P, Romero C, Pastor E, Galdeano JM (1997) Cor triatriatum with interventricular communication: Doppler color ultrasonography and magnetic resonance diagnosis. Repair in the first months. Rev Esp Cardiol 50:290–292

Chen K, Thng CH (2001) Multislice computed tomography and two-dimensional echocardiographic images of cor triatriatum in a 46-year-old man. Circulation 104, p 2117

Di Cesare E, Marsili L, Di Rienzi P, Paparoni S, De Curtis G, Pecce P (1991) Magnetic resonance in the diagnosis of cor triatriatum. A case report. Radiol Med 82:863–866

Godoy I, Tantibhedhyangkul W, Karp R, Lang R (1998) Images in cardiovascular medicine: cor triatriatum. Circulation 98, p 2781

Goldfarb A, Weinreb J, Daniel WG, Kronzon I (1989) A patient with right and left atrial membranes: the role of transesophageal echocardiography and magnetic resonance imaging in diagnosis. J Am Soc Echocardiogr 2:350–353

Horike K, Matsumura C, Egawa Y, Kirino A, Ohshio T, Kawahito T, Miyauchi T, Ishibashi H, Ohta A, Akita H (1993) A case report of cor triatriatum benefit of MRI for preoperative diagnosis and surgical method. Kyobu Geka 46:1063–1065

Ibrahim T, Schreiber K, Dennig K, Schömig A, Schwaiger M (2003) Images in cardiovascular medicine. Assessment of cor triatriatum sinistrum by magnetic resonance imaging. Circulation 108, p e107

Kaemmerer H, Kochs M, Gabrielsen F, Deutsch H, Smolorz J, Hombach V, Hilger HH (1987) Diagnosis of cor triatriatum dextrum with imaging procedures. Rontgenblatter 40:338–341

MacMillan RM, Rees MR, Maranhao V, Clark DL (1986) Cine-computed tomography of cor triatriatum. J Comput Assist Tomogr 10:124–125

Ono Y, Fukui K, Munakata M, Narita J, Takahata T, Sudo Y, Hatanaka R, Suzuki S (1996) Usefulness of the preoperative MRI for diagnosis and operative method in a case of cor triatriatum. Kyobu Geka 49:921–923

Rumancik WM, Hernanz-Schulman M, Rutkowski MM, Kiely B, Ambrosino M, Genieser NB, Naidich DP (1988) Magnetic resonance imaging of cor triatriatum. Pediatr Cardiol 9:149–151

Sakamoto I, Matsunaga N, Hayashi K, Ogawa Y, Fuhui J (1994) Cine-magnetic resonance imaging of cor triatriatum. Chest 106:1586–1589

Tanaka F, Itoh M, Esaki H, Isobe J, Inoue R (1991) Asymptomatic cor triatriatum incidentally revealed by computed tomography. Chest 100:272–274

Thakrar A, Shapiro MD, Jassal DS, Neilan TG, King ME, Abbara S (2007) Cor triatriatum: the utility of cardiovascular imaging. Can J Cardiol 23:143–145

Chapter 3.18 Tricuspid atresia

▌ Definition

Tricuspid atresia is characterized by the complete absence of a direct communication between the right atrium and the right ventricle (= absent right atrioventricular connection). Tricuspid atresia may range from an imperforate membrane (rarely) to the total absence of the valve with the area replaced by muscular tissue. The floor of the right atrium is completely muscular, frequently with a tiny dimple (= localized fibrous thickening) in the middle, and is totally separated from the ventricular mass by the atrioventricular sulcus (= absent of any potential right atrioventricular connection). The right atrium is generally dilated, and its wall thickened, particularly in the rare (less than 5% of cases) presence of restrictive interatrial communication (generally the interatrial communication is unrestrictive). The left atrium and the mitral valve are both dilated, since they receive both the pulmonary and the systemic venous returns. The right ventricle is generally poorly developed (sometimes so small that its detection is difficult) and is characterized by total absence of the inlet portion and varying degrees of underdevelopment of the trabecular and infundibular portions. A ventricular septal defect, most frequently of muscular type, is generally present between the hypoplastic right ventricle and the left ventricle, providing access to the rudimentary right ventricle and the pulmonary artery. The atrial situs is almost invariably solitus, and the coronary arteries are generally normal.

▌ Classification

The classification of the various forms of tricuspid atresia is based on the type of ventriculoarterial connection and on the amount of antegrade pulmonary blood flow.

▌ Type of ventriculoarterial connection
▪ *type I:* normally related great arteries (=ventriculoarterial concordance) (2/3 of infants),
▪ *type II:* transposition of the great arteries (=ventriculoarterial discordance) (1/3 of infants).

▌ Amount of antegrade pulmonary blood flow
▪ *type A:* absence or severe reduction of antegrade pulmonary blood flow, because of pulmonary atresia or stenosis with absent ventricular septal defect (18% of infants); the pulmonary circulation can be totally ductus-dependent,
▪ *type B:* balanced antegrade pulmonary blood flow (52% of infants), resulting from a moderate degree of obstruction at the level of the ventricular septal defect, the right ventricular outflow tract and/or the pulmonary valve, bicuspid in 20% of patients,
▪ *type C:* unrestricted antegrade pulmonary blood flow (30% of infants), resulting from absence or minimal degree of obstruction at the level of the ventricular septal defect, the right ventricular outflow tract and/or the pulmonary valve.

Associated anomalies

Systemic and pulmonary venous connections are usually normal, with the exception of a persistent left superior vena cava (15% of cases), and partially unroofed coronary sinus with communication between the coronary sinus and the left atrium (1–5% of cases). An atrial septal defect or stretched patent foramen ovale is generally present (the presence of an interatrial communication is necessary for survival) and ventricular septal defect is very frequently present. Ventriculoarterial discordance is present in 1/3 of the patients.

Other associated cardiac anomalies are pulmonary stenosis, pulmonary atresia, patent ductus arteriosus, juxtaposition of the auricular appendages (10% of cases with ventriculoarterial discordance), dextrocardia, right aortic arch, aortic coarctation (very rare in patients with ventriculoarterial concordance, but present in up to 30% of patients with ventriculoarterial discordance and restrictive ventricular septal defect).

In 5% of patients there is a very large prominent Eustachian valve, partitioning the right atrium, like in cor triatriatum dexter (see chapter "Cor triatriatum"). Anedoctical reports exist of tricuspid atresia with anomalous systemic or pulmonary venous connections, aortic atresia and truncus arteriosus. Situs inversus with ventricular L-loop (mirror imaging pattern) is exceptional. The mitral valve, generally normal, may have a double orifice, isolated anterior cleft or straddling and overriding.

■ Surgical options

■ **Modified Blalock-Taussig shunt:** see chapter "Tetralogy of Fallot".

■ **Pulmonary artery banding:** see chapter "Ventricular septal defect".

■ **Bidirectional Glenn or Hemi-Fontan:** see chapter "Single ventricle".
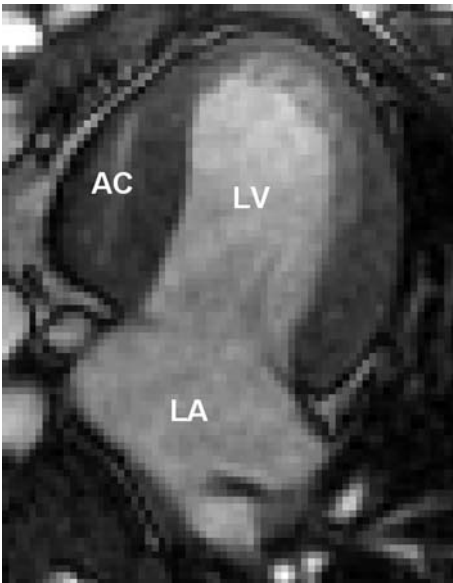
■ **Modified Fontan procedure or total cavo-pulmonary connection:** see chapter "Single ventricle".

■ **One-and-half ventricular repair:** this surgical approach consists of the confection of a bidirectional Glenn: end-to-side anastomosis between the proximal stump of the superior vena cava divided at the level of the cavo-atrial junction and the upper aspect of the right pulmonary artery. The atrial and ventricular septal defects approached through a right atriotomy and a longitudinal incision of the subpulmonary chamber, respectively, are closed with separated patches (pericardium, PTFE, Dacron or Teflon), and then the right atrium is connected with the subpulmonary chamber with interposition of a valved conduit. In the presence of associated pulmonary valve stenosis, a pulmonary valvotomy is required. In the presence of hypoplastic pulmonary valve annulus, the incision of the subpulmonary chamber is prolonged becoming a transannular opening, and the distal end of the conduit is anastomosed to both the subpulmonary chamber and the wall of the pulmonary artery.
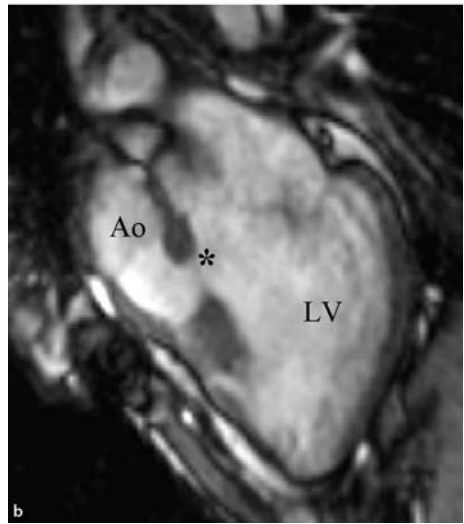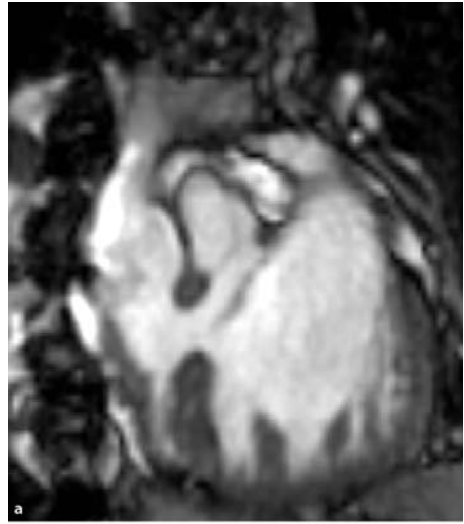
■ **Subaortic resection:** the technique consists of a longitudinal incision of the subaortic right ventricular outlet chamber in the direction of the ascending aorta, of course avoiding major coronary artery branches. After careful identification of the ventricular septal defect (= bulboventricular foramen), a full-thickness of interventricular septum is resected from the anterosuperior aspect of the defect, on the opposite side of the conduction tissue, carefully avoiding lesions to the adjacent aortic valve. Subaortic resection is completed with excision of obstructing muscle bundles, and the outlet chamber is further enlarged by patch (autologous or heterologous pericardium, PTFE) closure of the incision.
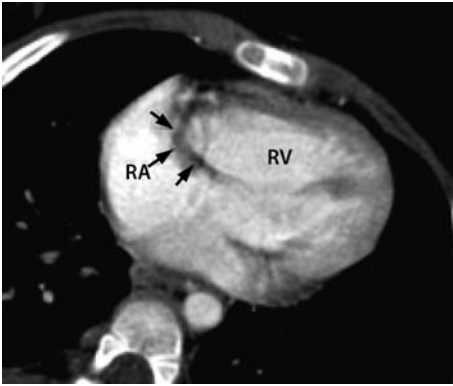
Fig. 3.18.1. Tricuspid atresia. CT scan axial projection showing absence of a direct connection (arrowheads) between the right atrium and the right ventricle (*RA* right atrium, *RV* right ventricle)

Fig. 3.18.3. Tricuspid atresia, restrictive ventricular septal defect and ventriculoarterial discordance. Cine MRI left ventricular outflow tract (**a** and **b**) showing the aorta arising from the hypoplastic right ventricle with restrictive ventricular septal defect (*) (*Ao* aorta, *LV* left ventricle)

Fig. 3.18.2. Tricuspid atresia. Typical MRI aspect of tricuspid atresia with nearly virtual accessory chamber (*AC* accessory chamber, *LA* left atrium, *LV* left ventricle)

■ Pre-operative information

The pre-operative information is the same as acquired from CT scan (Fig. 3.18.1) and MRI (Fig. 3.18.2) for the evaluation of single ventricle (see chapter "Single ventricle"), paying particular attention to the ventricular septal defect and the left ventricular outflow tract in patients with tricuspid atresia and transposition of the great arteries (= ventriculoarterial discordance) (Fig. 3.18.3), and to the interatrial septum.
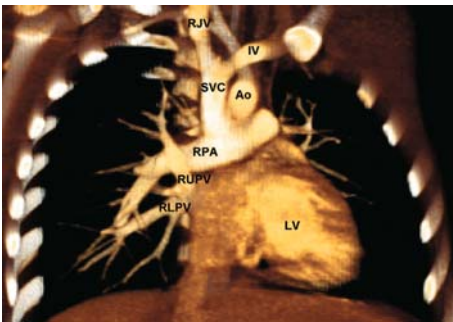
■ Potential complications

■ **Modified Blalock-Taussig shunt:** see chapter "Tetralogy of Fallot".

■ **Pulmonary artery banding:** see chapter "Ventricular septal defect".

■ **Bidirectional Glenn or hemi-Fontan:** see chapter "Single ventricle".

■ **Modified Fontan procedure or total cavopulmonary connection:** see chapter "Single ventricle".

Fig. 3.18.4. Status post bidirectional Glenn anastomosis. CT scan, 3-dimensional angiographic reconstruction, with visualization of the end-to-side superior vena cava to the right pulmonary artery anastomosis and the phase of the pulmonary venous return to the left heart (*Ao* aorta, *IV* innominate vein, *LV* left ventricle, *RJV* right jugular vein, *RLPV* right lower pulmonary vein, *RPA* right pulmonary artery, *RUPV* right upper pulmonary vein, *SVC* superior vena cava) (photograph courtesy of Dr. Mohamed Tawil and Cinzia Crawley)
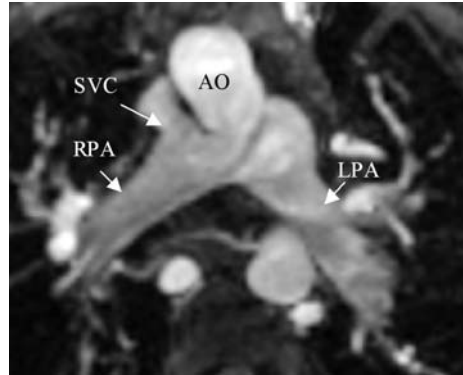
Fig. 3.18.5. Tricuspid atresia, restrictive ventricular septal defect and ventriculoarterial discordance, status post bidirectional Glenn. Same patient of Fig. 3.18.3 MR angiography (maximal intensity projection reconstruction) showing the cavopulmonary anastomosis and normal sized pulmonary arteries (*Ao* aorta, *LPA* left pulmonary artery, *RPA* right pulmonary artery, *SVC* superior vena cava)

■ **Subaortic resection:** complete atrioventricular block occurs very rarely, while the risk for either residual or recurrent subaortic obstruction is higher.

■ Post-operative follow-up

Patients with tricuspid atresia are treated as the patients with a single ventricle (see chapter "Single ventricle").

Postoperative CT and MRI investigations can provide information on the bidirectional Glenn and on the size and morphology of the right and left pulmonary artery, particularly with regard to the presence and extension of any narrowing (Figs. 3.18.4 and 3.18.5).

■ References

Babu-Narayan SV, Gatzoulis MA, Kilner PJ (2007) Non-invasive imaging in adult congenital heart disease using cardiovascular magnetic resonance. J Cardiovasc Med 8:23–29

Brown DW, Gauvreau K, Powell AJ, Lang P, Colan SD, del Nido PJ, Odegard KC, Geva T (2007) Cardiac

magnetic resonance versus routine cardiac catheterization before bidirectional Glenn anastomosis in infants with functional single ventricle. Circulation 116:2718–2725

Choi BW, Park YH, Lee JK, Kim DJ, Kim MJ, Choe KO (2003) Patency of cavopulmonary connection studied by single phase electron beam computed tomography. Int J Cardiovasc Imaging 19:447–455

Corno AF, Horisberger J, Jegger D, von Segesser LK (2004) Right atrial surgery with unsnared inferior vena cava. Eur J Cardiothorac Surg 26:219–220

Festa P, Ait-Ali L, Bernabei M, De Marchi D (2005) The role of magnetic resonance imaging in the evaluation of the functionally single ventricle before and after conversion to the Fontan circulation. Cardiol Young 15:Suppl.3:51–56

Fogel MA, Weinberg PM, Chin AJ, Fellows KE, Hoffman EA (1996) Late ventricular geometry and performance changes of functional single ventricle throughout staged Fontan reconstruction assessed by magnetic resonance imaging. J Am Coll Cardiol 28:212–221

Fogel MA, Weinberg PM, Rychik J, Hubbard A, Jacobs M, Spray TL, Haselgrove J (1999) Caval contribution to flow in the branch pulmonary arteries of Fontan patients with a novel application of magnetic resonance presaturation pulse. Circulation 99:1215–1221

Fogel MA (2006) Cardiac magnetic resonance of single ventricles. J Cardiovasc Magn Reson 8:661–670

Fratz S, Hess J, Schwaiger M, Martinoff S, Stern HC (2002) More accurate quantification of pulmonary blood flow by magnetic resonance imaging than by lung perfusion scintigraphy in patients with Fontan circulation. Circulation 106:1510–1513

Giannico S, Corno AF, Marino B, Cicini MP, Gagliardi MG, Amodeo A, Picardo S, Marcelletti C (1992) Total extracardiac right heart bypass. Circulation 86(Suppl II):110–117

Giannico S, Hammad F, Amodeo A, Michielon G, Drago F, Turchetta A, di Donato R, Sanders SP (2006) Clinical outcome of 193 extracardiac Fontan patients. J Am Coll Cardiol 47:2065–2073

Goo HW, Yang DH, Park IS, Ko JK, Kim YH, Seo DM, Yun TJ, Park JJ (2007) Time-resolved three-dimensional contrast-enhanced magnetic resonance angiography in patients who have undergone a Fontan operation or bidirectional cavopulmonary connection: initial experience. J Magn Reson Imaging 25:727–736

Hayabuchi Y, Mori K, Kitagawa T, Sakata M, Kagami S (2007) Polytetrafluoroethylene graft calcification in patients with surgically repaired congenital heart disease: evaluation using multidetector-row computed tomography. Am Heart J 153:806.e1–808

Hjortdal VE, Emmertsen K, Stenbog E, Frund T, Schmidt MR, Kromann O, Sorensen K, Pedersen EM (2003) Effects of exercise and respiration on blood flow in total cavopulmonary connection: a real-time magnetic resonance flow study. Circulation 108:1227–1231

Kaemmerer H, Stern H, Fratz S, Prokop M, Schwaiger M, Hess J (2000) Imaging in adults with congenital cardiac disease (ACCD). Thorac Cardiovasc Surg 48:328–335

Klimes K, Abdul-Khaliq H, Ovroutski S, Hui W, Alexi-Meskishvili V, Spors B, Hetzer R, Felix R, Lange PE, Berger F, Gutberlet M (2007) Pulmonary and caval blood flow patterns in patients with intracardiac and extracardiac Fontan: a magnetic resonance study. Clin Res Cardiol 96:160–167

Marcelletti C, Corno AF, Giannico S, Marino B (1990) Inferior vena cava to pulmonary artery extracardiac conduit: a new form of right heart bypass. J Thorac Cardiovasc Surg 100:228–232

Mazzera E, Corno AF, Picardo S, Di Donato RM, Marino B, Costa D, Marcelletti C (1989) Bidirectional cavopulmonary shunts: clinical applications as staged or definitive palliation. Ann Thorac Surg 47:415–420

Mochizuki T, Ohtani T, Higashino H, Sugawara Y, Tsuda T, Sekiya M, Miyagawa M, Ohmoto K, Ikezoe J (2000) Tricuspid atresia with atrial septal defect, ventricular septal defect, and right ventricular hypoplasia demonstrated by multidetector computed tomography. Circulation 102:E164–165

Morgan VL, Graham TP, Roselli RJ, Lorenz CH (1998) Alterations in pulmonary artery flow patterns and shear stress determined with three-dimensional phase-contrast magnetic resonance imaging in Fontan patients. J Thorac Cardiovasc Surg 116:294–304

Nakano T, Kado H, Tachibana T, Hinokiyama K, Shiose A, Kajimoto M, Ando Y (2007) Excellent midterm outcome of extracardiac conduit total cavopulmonary connection: results of 126 cases. Ann Thorac Surg 84:1619–1626

Pedersen EM, Strenbog EV, Frund T, Houlind K, Kromann O, Sorensen KE, Emmertsen K, Hjortdal VE (2002) Flow during exercise in the total cavopulmonary connection measured by magnetic resonance velocity mapping. Heart 87:554–558

Rebergen SA, Ottenkamp J, Doornbos J, van der Wall EE, Chin JG, de Roos A (1993) Postoperative pulmonary flow dynamics after Fontan surgery: assessment with nuclear magnetic resonance velocity mapping. J Am Coll Cardiol 21:123–131

Robbers-Visser D, ten Harkel D, Strengers JLM (2007) Cardiac MRI combined with low-dose dobutamine stress reveals an abnormal stress response in children and young adults after Fontan operation at young age. J Cardiovasc Magn Reson 9:107

Socci L, Gervaso F, Migliavacca F, Pennati G, Dubini G, Ait-Ali L, Festa P, Amoretti F, Scebba L, Luisi VS (2005) Computational fluid dynamics in a model of the total cavopulmonary connection reconstructed using magnetic resonance images. Cardiol Young 15(Suppl 3):61–67

Venkatachari AK, Halliburton SS, Setser RM, White RD, Chatzimavroudis GP (2007) Noninvasive quantification of fluid mechanical energy losses in the total cavopulmonary connection with magnetic resonance phase velocity mapping. Magn Reson Imaging 25:101–109

Chapter 3.19 Single ventricle

▌ Definition

Single ventricle (or univentricular heart) is considered a congenital cardiac malformation in which both atria connect to only one ventricular chamber by either two separate atrioventricular valves (double inlet) or a common atrioventricular valve (common inlet). The ventricle to which both atrioventricular valves or a common atrioventricular valve connects is generally well formed, whereas the ventricle not receiving the largest amount of the venous return to the heart is often a rudimentary chamber.

By definition, the term double inlet single ventricle is used only if more than 50% of the overriding valve lies over the main ventricular chamber. When both atrioventricular valves are present, they often cannot be designated as either mitral or tricuspid and are commonly straddling or stenotic. When there is a common atrioventricular valve, it presents frequently with regurgitation.

Most of the hearts described as "single ventricle" or "univentricular heart" in reality possess two ventricular chambers, with one main (dominant) chamber and a second (incomplete) rudimentary chamber which lacks of one or more of its components (generally the inlet, but occasionally also the outlet).

There are three basic patterns of ventricular morphology:

▌ main ventricular chamber of left ventricular morphology, with rudimentary right ventricle (= single ventricle of left ventricular type),

▌ main ventricular chamber of right ventricular morphology, with or without rudimentary left ventricle (= single ventricle of right ventricular type),

▌ single ventricular chamber of indeterminate morphology.

The combination of the type of inlet (double inlet or common inlet) with the type of ventricular morphology (left, right or indeterminate) provide a variety of univentricular atrioventricular connections. This variety is further complicated when other morphological variables are taken in consideration, like the cardiac position (levocardia, mesocardia or dextrocardia), the atrial situs (solitus, inversus, right or left isomerism), the ventriculoarterial connections, the spatial relationship between the main chamber and rudimentary chamber, and the associated cardiac anomalies. The most frequent arrangement is the main chamber of left ventricular morphology with a rudimentary chamber of right ventricular morphology (= single ventricle of left ventricular type). The rudimentary chamber is separated from the main chamber by a septum, which does not extend to the crux of the heart, and is connected to the main chamber via a ventricular septal defect, variously described with interchangeable terms, such as outlet foramen, interventricular foramen, or bulboventricular foramen. Since these hearts do not have a membranous septum, the ventricular septal defect is generally of completely muscular type, with the potential reduction in size typical of the muscular ventricular septal defect in biventricular hearts.

In order to evaluate if the size of the ventricular septal defect is restrictive or unrestrictive, generally its dimensions are related to the size of the corresponding aortic root. The second chamber is always anterior, and is located either to the left or the right. The size of the outlet chamber is related to the degree of development and straddling of the tricuspid valve, in addition to the size of the ventricular septal defect. The ventriculoarterial connections are most commonly discordant and more rarely concordant. Unusual forms of ventriculoarterial connections in double inlet ventricle include double outlet or single outlet (= pulmonary atresia).

Outflow obstruction to the pulmonary artery is common and is the most important determinant of the clinical course. The obstruction may be subvalvular and/or valvular (hypoplastic annulus and/or thickened leaflets), or may be complete (= pulmonary atresia). In the presence of ventriculoarterial concordance the obstruction, mostly dynamic, due to infundibular narrowing, is generally localized at the subvalvular level. In hearts with ventriculoarterial concordance, the obstruction to the pulmonary blood flow is generally due to the presence of a restrictive ventricular septal defect.

Obstruction to the systemic outflow can occur at the subvalvular level and/or the level of the aortic arch and/or isthmus, or at multiple levels. Usually it occurs at the level of the ventricular septal defect in hearts with discordant ventriculoarterial connections; in fact, in these patients, the presence of aortic coarctation and/or aortic arch hypoplasia is a strong marker for the presence of a restrictive ventricular septal defect.

The conduction tissues, with respect to the ventricular septal defect, have a directly comparable arrangement to that seen in tricuspid atresia. This arrangement is seen irrespective of whether the rudimentary right ventricle is right or left sided. The position of the rudimentary ventricle affects only the relationship of the atrioventricular bundle to the outflow tract from the dominant left ventricle. From the surgical point of view, the atrioventricular node can be anywhere around the perimeter of the right-sided (= draining the right-sided atrium) atrioventricular valve.

Associated anomalies

Associated cardiac anomalies occur in about one-third of cases with double inlet ventricle. Anomalous pulmonary and/or systemic venous connections are relatively frequent, particularly in patients with atrial isomerism (see chapter "Isomerism"); the most frequent are persistent left superior vena cava, interruption of the inferior vena cava, partial or total anomalous pulmonary venous connection.

Malformations of the atrioventricular valves are also quite common, including straddling, leaflet dysplasia, leaflet cleft and tags, and annular hypoplasia. Aortic arch anomalies such as coarctation, interrupted aortic arch and hypoplastic aortic arch are strongly associated with a restrictive ventricular septal defect in cases in which the aorta arises from the rudimentary chamber (= ventriculoarterial discordance).

■ Surgical options

■ Pulmonary artery banding: In these patients, the achievement of an adequate pulmonary artery banding is particularly difficult, considering several interrelated variables that continue to evolve, particularly the need to obtain and maintain a low pulmonary artery pressure, an adequate balance between systemic and pulmonary circulation, at the same time avoiding excessive ventricular pressure overload. A solution to these requirements is pulmonary artery banding with a telemetrically adjustable device (FloWatch-PAB®).

■ Shunt: A modified Blalock-Taussig shunt (see chapter "Tetralogy of Fallot") is always the choice for a systemic-to-pulmonary artery shunt.

▪ **Bidirectional Glenn:** The bidirectional Glenn procedure consists of end-to-side anastomosis of the divided superior vena cava to the upper aspect of the right pulmonary artery.

In patients with persistent left superior vena cava, a bilateral bidirectional Glenn procedure (= end-to-side anastomosis of the right superior vena cava to the right pulmonary artery and of the persistent left superior vena cava to the left pulmonary artery, respectively) is performed with the same surgical technique for both anastomoses.

▪ **Hemi-Fontan:** The medial aspect of the superior vena cava and the superior portion of the right atrium are incised as well as the confluence of the right and left pulmonary arteries. In the absence of pulmonary atresia, the proximal stump of the pulmonary artery is divided and oversewn. The superior vena cava is side-to-side anastomosed to the right pulmonary artery, and the same is done in the presence of a persistent left superior vena cava, which is side-to-side anastomosed to the ipsilateral pulmonary artery. A patch of biological (homograft, heterologous pericardium) or prosthetic (PTFE) material is used to augment the pulmonary arteries anteriorly to create a roof over the anastomosis of the vena cava and the pulmonary artery and a dam occluding the inflow of the superior vena cava into the right atrium, leaving a potential connection for the entire systemic venous return larger than the size of the inferior vena cava. An unrestrictive interatrial communication is also created, whenever necessary.

▪ **Modified Fontan:** The completion of the Fontan circulation, rerouting the systemic venous return from the inferior vena cava to the pulmonary arteries, can be accomplished with several different surgical techniques, but nowadays the most used remain the following:

Intracardiac lateral tunnel consisting of baffling the inferior vena cava, the superior vena cava and the upper portion of the right atrium with the inferior aspect of the right pulmonary artery with a patch (pericardium, PTFE). The divided stump of the superior vena cava requires augmentation (by a roof of autologous or heterologous pericardium or PTFE) to accommodate the higher systemic venous return coming from the inferior vena cava. The coronary sinus is left in the lower pressure pulmonary venous atrium. An unrestrictive interatrial communication is also created, whenever necessary.

Extracardiac connection consisting of an extracardiac connection of the divided inferior vena cava (the cardiac stump is oversewn) to the inferior aspect of the right pulmonary artery by interposition of a nonvalved conduit (PTFE, pericardium, in situ pedicled pericardial tunnel), or in exceptional circumstances by direct anastomosis of the transected inferior vena cava to the divided main pulmonary artery.

▪ **Fenestration (= incomplete atrial partitioning):** Different types of *fenestration* exist to allow for an incomplete separation between the caval and pulmonary venous pathways in order to decompress the systemic venous return. In the lateral tunnel technique, an interatrial communication (generally 4–5 mm diameter) is created in the central part of the prosthetic (PTFE) patch (= fixed fenestration), or is left on the lateral aspect of the suture of the patch. In the extracardiac connection, the extracardiac conduit and the morphologically right atrium (now functioning as the pulmonary venous atrium = collecting chamber for the pulmonary veins and the coronary sinus) are off-bypass connected (= fenestration) either by a tubular prosthesis (PTFE, 6–8 mm diameter) or by side-to-side direct anastomosis. All these types of fenestration will either spontaneously close in the late postoperative period, or they can be electively closed by a percutaneous intervention.

▪ **Ventricular septation:** This procedure can be performed as a single stage with a large patch dividing the two atrioventricular valves and the ventricular cavity, taking

great care to avoid obstruction to the systemic and pulmonary outflow tracts.

Staged ventricular septation consists of placing an apical patch and a second patch at the superior portion between the atrioventricular valves, using widely spaced interrupted sutures, with the addition of pulmonary artery banding. Ventricular septation (with debanding) is completed 6–18 months later with a third patch.

▮ Pre-operative information

Classically single ventricle is fully diagnosed and evaluated by echocardiography and cardiac catheterization. The following pre-operative information is required at all stages:

- situs and position of the heart,
- systemic and pulmonary venous connections,
- interatrial communication,
- ventricular septal defect,
- atrioventricular valves (morphology and function),
- ventricular anatomy, function, mass and myocardial viability,
- ventricular outflow tract (level of potential obstruction),
- ventriculoarterial connections,
- aortic arch (morphology and potential obstruction),
- sources of pulmonary blood flow,
- pulmonary arteries morphology, pressures and resistance.

Due to the high potential diagnostic value already discussed in the "Introduction", cardiac CT (Fig. 3.19.1) and MRI (Fig. 3.19.2) are gaining widespread interest in such patients as they could provide, in conjunction with echocardiography, all the required information with exception of the pulmonary pressure and resistance. There is general agreement that, in selected patients without suspected high pulmonary artery pressure, cardiac MRI could be used to avoid cardiac catheterization in many instances as patients progress through staged Fontan circulation. Furthermore, MRI's unique ability to accu-
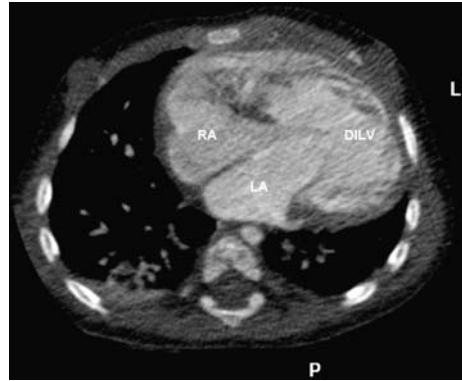
Fig. 3.19.1. Double inlet left ventricle. CT scan, axial projection, showing the double inlet of the left and right atrium into a single ventricle of left ventricular type (*DILV* double inlet left ventricle, *LA* left atrium, *RA* right atrium) (photograph courtesy of Dr. Mohamed Tawil)

rately detect volume and mass of such bizarre shaped ventricles makes it capable of providing us anatomical and functional information not available by any other diagnostic tool.

The following MRI protocol is used in the evaluation of functionally single ventricle:

- 3-plane localizing images,
- 2-dimensional axial Time-of-flight Angiography (see appendix in the "Introduction"); the two previous types of imaging, mainly the latter, can greatly help in defining the bronchial anatomy, hence allowing potential sidedness anomalies to be confirmed (Fig. 3.19.2 a–c),
- ECG-gated cine steady-state free precession sequences in straight axial, sagittal, coronal and additional oblique planes in order to show the whole heart on three orthogonal planes; even if it is of long duration, it better visualizes the intracardiac anatomy, its connections and spatial disposition inside the thorax (Fig. 3.19.2 f–h),
- ECG-gated cine steady-state free precession sequences on the ventricular long and short axis plane, for the quantitative assessment of ventricular dimensions, function, mass and stroke volume,
- ECG-gated cine steady-state free precession and fast spin echo sequences to vi-
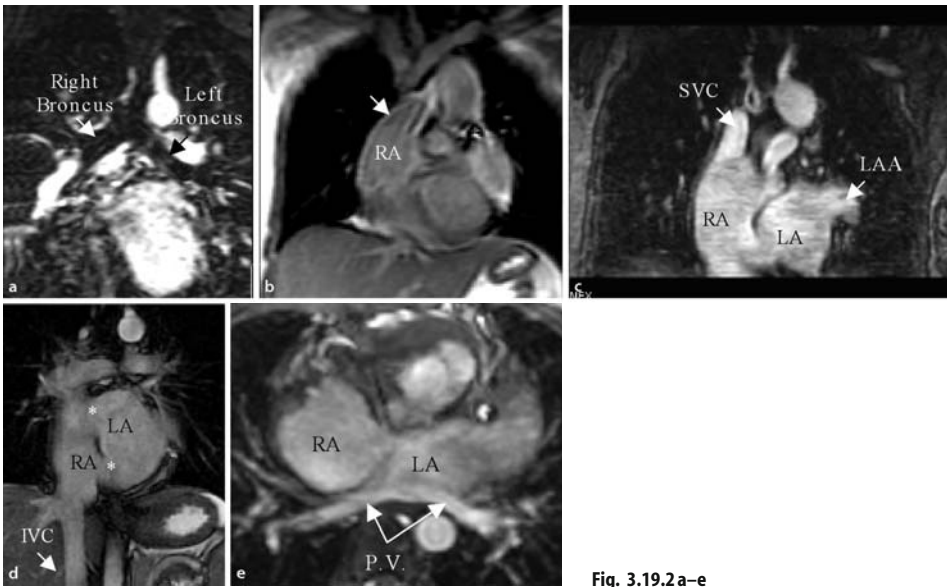
Fig. 3.19.2 a–e

Fig. 3.19.2. Single ventricle. Cardiac MRI in a patient with functionally single ventricle. Angiography (**a, c**) and coronal localizer (**b**) showing bronchial and atrial situs solitus. Time of flight maximal intensity projection reconstruction (**d, e**) illustrating normal systemic and pulmonary venous connections and double interatrial communication (asterisk). Stack of axial (**f**), sagittal (**g**) and coronal (**h**) cine steady-state free precession acquisitions showing atrioventricular discordance with left atrioventricular valve atresia (^), hypoplastic left ventricle, large ventricular septal defect, double outlet right ventricle, malposition of the great arteries and subvalvular and valvular pulmonary stenosis. Para-coronal cine steady-state free precession in diastole (**i**) and systole (**j**) confirms the tricuspid mor-

phology of the right atrioventricular valve. Sagittal ventricular outflow tract cine steady-state free precession (**l**) and fast spin echo (**k**) clearly shows the anterior positioned aorta arising from the right ventricle with severe subvalular and valvular pulmonary stenosis. MR angiography maximal intensity projection reconstruction illustrates mild pulmonary arteries hypoplasia (**m**) and small aortopulmonary collaterals (**n**) (*AO* aorta, *IVC* inferior vena cava, *LA* left atrium, *LAA* left auricular appendage, *LPA* left pulmonary artery, *PA* pulmonary artery, *PV* pulmonary veins, *RA* right atrium, *RV* right ventricle, *RPA* right pulmonary artery, *SVC* superior vena cava, *TV* tricuspid valve, *VSD* ventricular septal defect)

sualize the ventricular outflow tract, the ventricular septal defect and their relationship (Fig. 3.19.2 k and l)),
- ECG-gated phase velocity contrast MRI sequences perpendicular to the main pulmonary artery, ascending aorta, and pulmonary arteries, to assess the flow pattern in the great arteries,
- gadolinium-enhanced MR angiography for the evaluation of the pulmonary arteries and veins, systemic venous connections, aortic arch and any aortopulmonary collaterals (Fig. 3.19.2 m and n).

■ Potential complications

■ **Pulmonary artery banding:** potential for pulmonary artery distortion, development of pulmonary valvular regurgitation or damage to the pulmonary valve, progressive ventricular hypertrophy, decreased ventricular compliance, and development of subvalvular aortic stenosis. Subaortic stenosis often follows palliative pulmonary artery banding, in which the resultant hypertrophy of muscle around the ventricular septal defect may play a contributing role (Fig. 3.19.3).
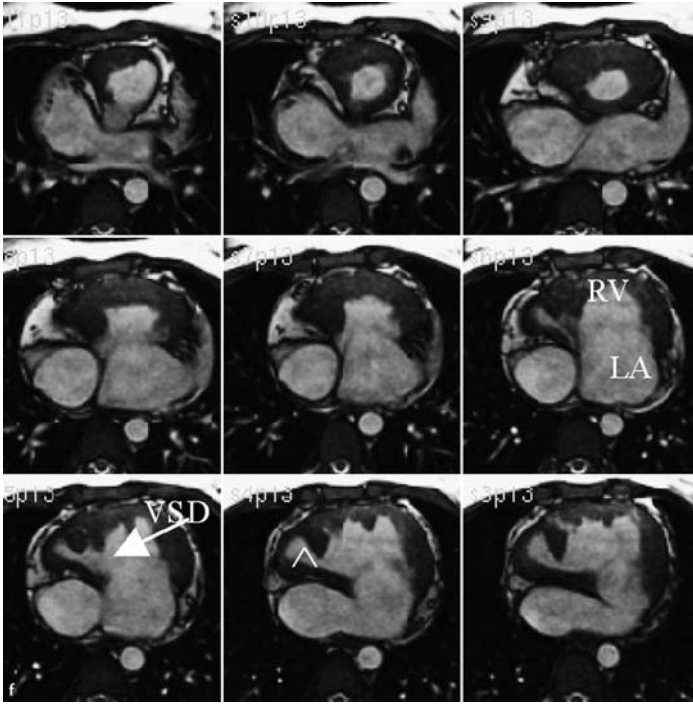
Fig. 3.19.2 f

∎ **Bidirectional Glenn:** prolonged pleural and/or pericardial effusions, chylothorax, phrenic nerve lesion. A persistently high pulmonary vascular resistance results in insufficient pulmonary blood flow and severe cyanosis, manifested by high superior vena cava pressure (over 18–20 mmHg). An elevated superior vena cava pressure may significantly decrease cerebral perfusion by decreasing the pressure gradient across the cerebral bed. This may be clinically manifested as fullness and pulsatility of the fontanelle, persistently irritability, systemic hypertension and relative bradycardia. Following the bidirectional Glenn procedure, potential late development of pulmonary arteriovenous malformations or venovenous collaterals may cause severe cyanosis. The latter results in right-to-left shunt, and, if severe, precludes successful conversion to Fontan operation.

∎ **Hemi-Fontan operation:** distortion or degeneration of the biological or prosthetic materials used for the central pulmonary arteries augmentation and early or late supraventricular arrhythmias are potential complications in addition to those listed for the bidirectional Glenn procedure.

∎ **Modified Fontan procedure:** in the presence of a failing Fontan procedure, the potential obstruction at any level of the cavopulmonary connections, as well as the persistence of intracardiac shunts (other than the surgically created fenestration), must always be ruled out. The most frequent early complications are prolonged pleural effusion and chylothorax; chronic venous stasis, recurrent pericardial effusion, ascites, fluid retention, renal failure, hepatic failure and gastrointestinal dysfunction are more frequent
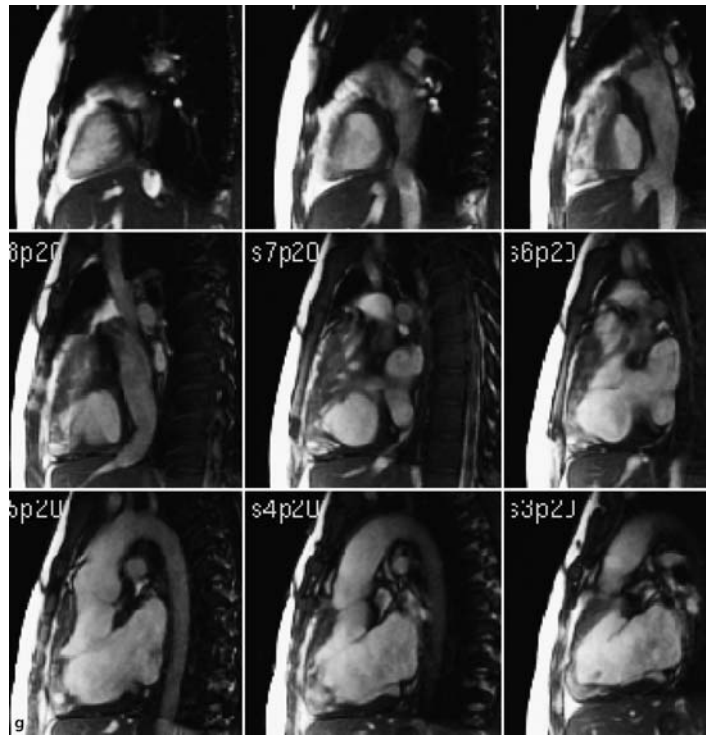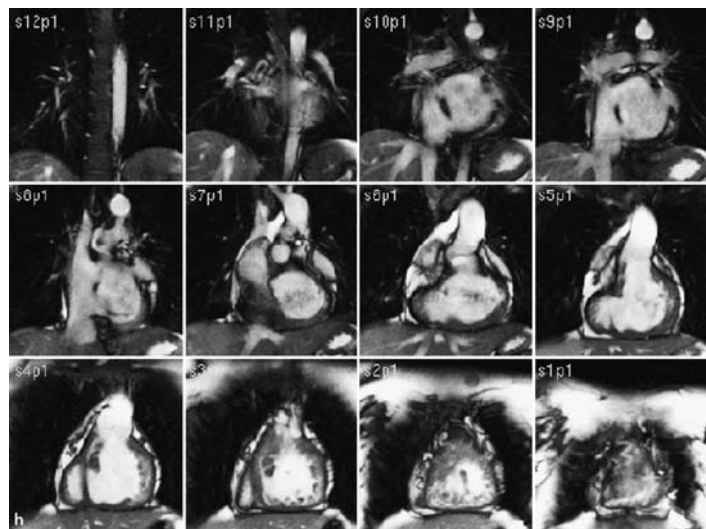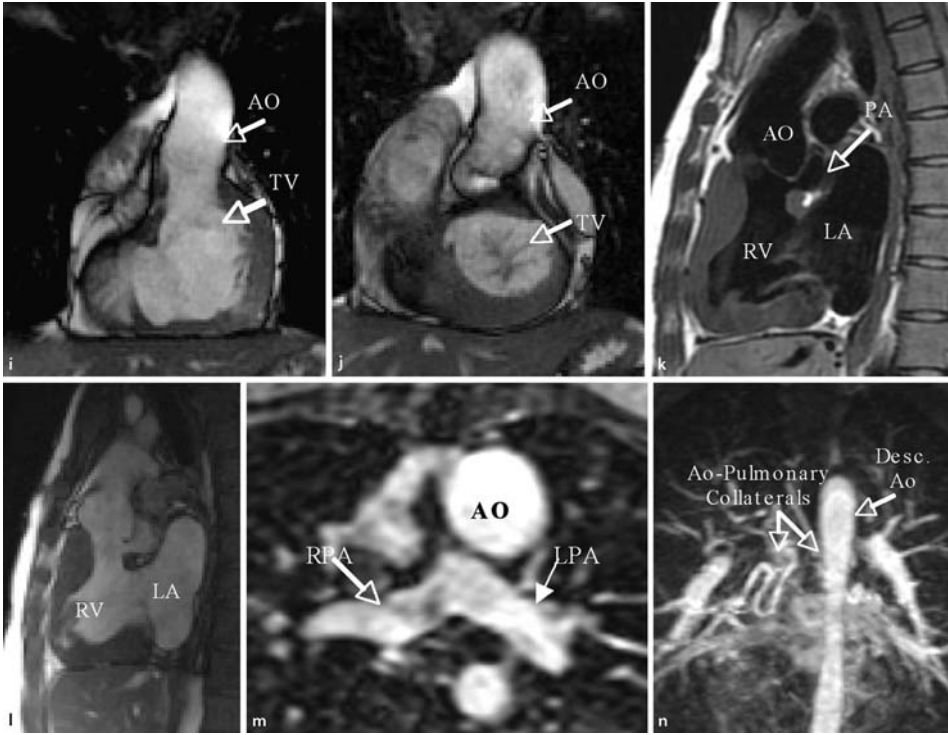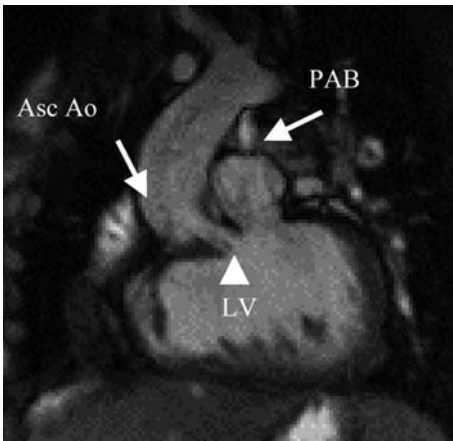
Fig. 3.19.2 g

Fig. 3.19.2 h

Fig. 3.19.2 i–n

in higher risk patients. While sinus node dysfunction, atrial fibrillation or flutter is more frequent, ventricular arrhythmias are less frequent, and complete atrioventricular block is very rare. Thromboembolism can occur in about 10% of patients, particularly in the presence of a low-output state with low velocity flow through the venous pathway.

Protein-losing enteropathy (reduced serum albumin concentration accompanied by diarrhea, poor appetite, failure to grow), pulmonary arteriovenous malformations and venovenous collateral formation (between brachiocephalic angles and pericardial veins, azygos and hemiazygos system, Thebesian veins and epidiaphragmatic veins) with systemic arterial desaturation are the most fre-

quent late complications. Exercise intolerance (or reduced exercise capacity) is observed in a certain percentage of patients as well as progression of atrioventricular valve regurgitation. Persistent and/or progressive hypoxemia can occur after the Fontan procedure, further increased with exercise, even in the absence of evident intracardiac right-to-left shunt. The reason is probably the presence of a mild intrapulmonary shunt and the drainage of the coronary sinus into the pulmonary venous atrium. Plastic bronchitis is very rare but mostly accompanied by dramatic consequences.

Either a fenestration (when absent or inadequate) or the early or late take-down of the total cavopulmonary connection is sometimes necessary, with or without associated

Fig. 3.19.3. Double inlet ventricle, status-post pulmonary artery banding. MRI para-coronal cine steady-state free precession double inlet ventricle and transposition of the great arteries after pulmonary banding with subaortic turbulent flow (head arrow) (*Asc Ao* ascending aorta, *LV* left ventricle, *PAB* pulmonary banding)

treatment for the supraventricular arrhythmias. Heart transplant is sometimes the only available solution, when pulmonary vascular resistance is still within the normal range.

■ **Ventricular septation:** the incidence of complications with ventricular septation, except for a very well selected cases, remains elevated. Potential complications are obstruction to the systemic and/or pulmonary inflow and/or outflow tracts, distortion of the atrioventricular valve(s) with resulting regurgitation, lesion of the coronary arteries, residual interventricular shunt, complete atrioventricular block.
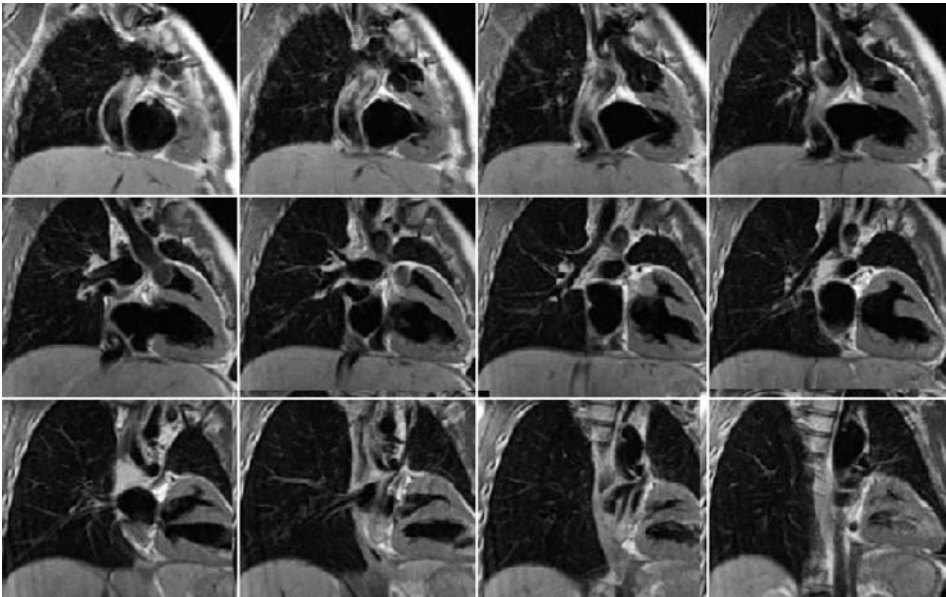
Fig. 3.19.4. Single ventricle with restrictive ventricular septal defect, status post Fontan procedure. MRI fast spin echo para-coronal scan showing a restrictive ventricular septal defect in a patient after Fontan procedure. Note the malalignment of the trabecular septum with a restrictive inlet type of ventricular septal defect extended to the outlet septum, leading to subaortic stenosis
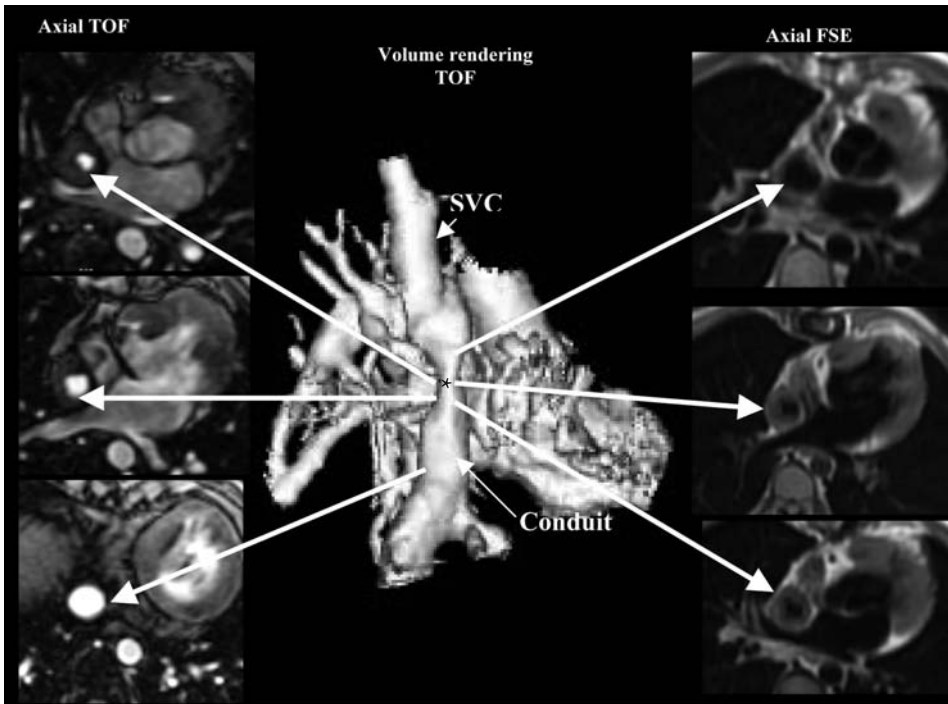
Fig. 3.19.5. Single ventricle, status post extracardiac Fontan with conduit stenosis. MRI volume rendering reconstruction from time of flight acquisition. Axial images at the level indicated by the arrows (fast spin echo images on the right and reformatted time of flight on the left) are shown on the sides. The conduit stenosis (*) was an unexpected finding, not suspected by echocardiography (*FSE* fast spin echo, *SVC* superior vena cava, *TOF* time of flight)
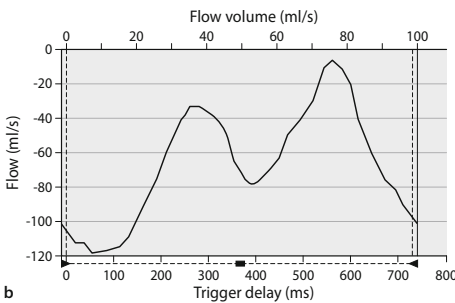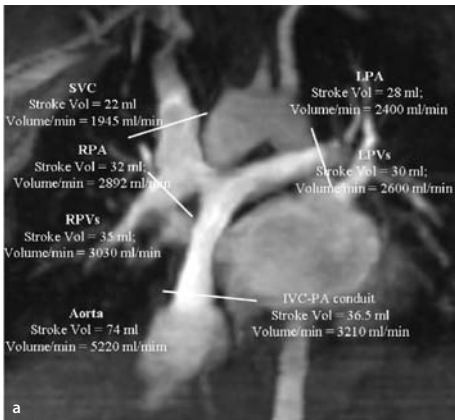
∎ Post-operative follow-up

The following targets have to guide the post-operative evaluation:
- ∎ anatomy, size and flow pattern of the bi-directional cavopulmonary anastomosis or of the total cavopulmonary anastomosis,
- ∎ ventricular volume, mass and function,
- ∎ atrioventricular valve (or valves) evaluation,
- ∎ anatomy of the ventricular septal defect, particularly in case of aorta arising from the accessory chamber (Fig. 3.19.4),
- ∎ detection of thrombi, particularly at atrial level, in case of "old fashion" Fontan procedure, consisting in direct atriopulmonary anastomosis leading to huge right atrial enlargement.

Echo-Doppler, as the first line diagnostic tool, is very useful. However, previous surgical scars, growing body mass, baffles and conduits deeply located inside the thorax and bizarre ventricular geometry make this type of echocardiographic investigation technically challenging and sometimes is not exhaustive enough to accurately cover all the previously mentioned targets, like ventricular function and flow pattern assessment.

On the other hand, cardiac MRI is gaining an increasingly important role in the evaluation of such patients by overcoming some of the echocardiography drawbacks (Fig. 3.19.5). By means of steady-state free precession and phase velocity contrast acquisition, today MRI is the best way to assess ventri-

Fig. 3.19.7. Single ventricle, status post atriopulmonary connection. MRI axial fast spin echo imaging after direct atriopulmonary connection with a huge right atrium prone to thrombi formation due to slow flow (arrowhead) (*LV* left ventricle, *RA* right atrium)

Fig. 3.19.6. Single ventricle, status post extracardiac Fontan. Flow pattern assessment after extracardiac Fontan procedure by means of phase velocity contrast MRI (**a**). Volumetric flow graph at the conduit level showing a typical venous profile (**b**) (*IVC* inferior vena cava, *LPA* left pulmonary artery, *LPVs* left pulmonary veins, *RPA* right pulmonary artery, *RPVs* right pulmonary veins, *SVC* superior vena cava)

cular volume, mass and function, and flow pattern, respectively, in patients with single ventricle after bidirectional Glenn or Fontan procedures. Moreover, by means of the "delay enhancement" technique, myocardial fibrosis can also be detected. Myocardial "tagging" is performed in some MRI laboratories to further evaluate ventricular function and mechanics. In selected patients with normal pulmonary artery pressure and resistance, a comprehensive cardiac MRI, in addition to clinical and echocardiography evaluation, can avoid the need of cardiac catheterization before Fontan completion.

The post-operative protocols used are the same as in the pre-operative evaluation, with the addition of the evaluation of the bidirectional Glenn or Fontan pathways:

■ ECG-gated cine steady-state free precession and fast spin echo sequence targeted at the cavopulmonary anastomosis and the fenestration,

■ ECG-gated phase velocity contrast MRI sequences perpendicular to the ascending aorta, pulmonary arteries, superior and inferior vena cava, Fontan conduit, and pulmonary veins to assess the Fontan pathway flow (Fig. 3.19.6),

■ ECG-gated axial double inversion fast spin echo at the atrial level to check for clots or masses, mainly in case of direct atriopulmonary anastomosis (Fig. 3.19.7),

■ gadolinium-enhanced 3-dimensional MR angiography for the evaluation of the Fontan pathway including systemic venous return, conduit, pulmonary arteries and pulmonary veins, and the aortic arch (Fig. 3.19.8). Because of the particular Glenn or Fontan "physiology", the technique of the contrast medium injection
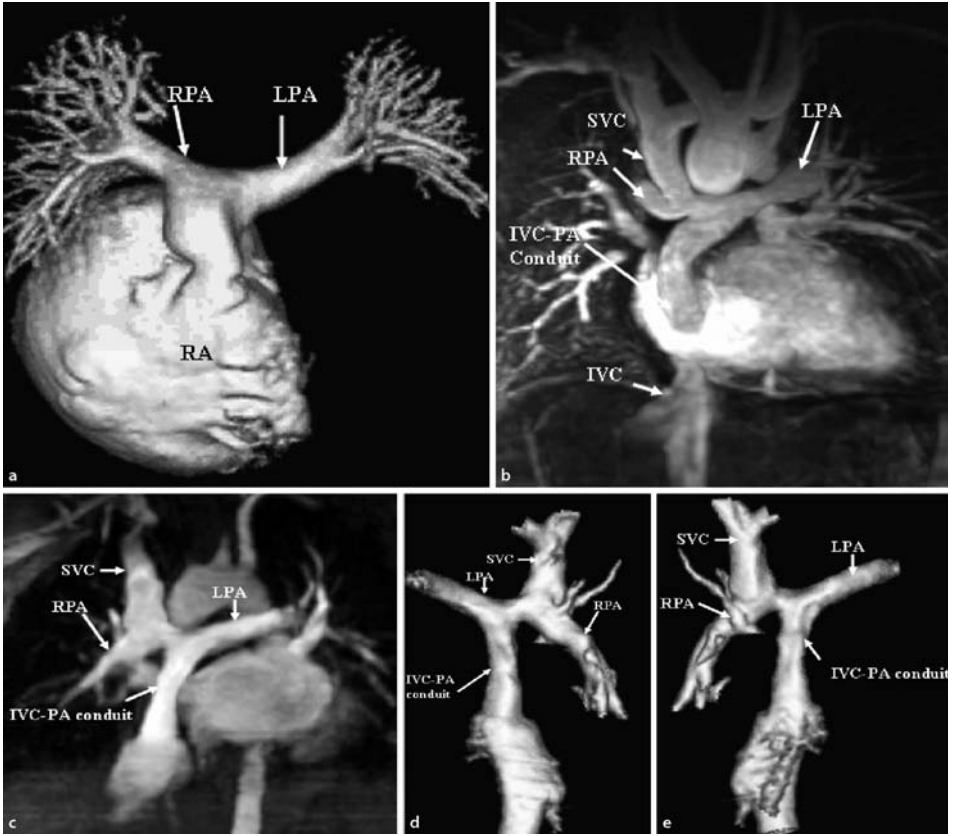
Fig. 3.19.8. MR angiography after different types of Fontan procedures. Volume rendering reconstruction of classic atrio-pulmonary connection in a patient with a huge right atrium (**a**). Maximal intensity projection reconstruction of intra-extra-cardiac Fontan procedure (**b**). Different post-processing of the same patient after extracardiac Fontan procedure: maximal intensity projection reconstruction (**c**); volume rendering selected to the Fontan pathways (**d**) and (**e**) (*IVC* inferior vena cava, *LPA* left pulmonary artery, *PA* pulmonary artery, *RA* right atrium, *RPA* right pulmonary artery, *RPVs* right pulmonary veins, *SVC* superior vena cava)

(site of injection, bolus velocity and amount contrast) is challenging; sometimes it is useful to inject the contrast medium through an inferior limb vein instead of using a superior limb vein as normally done to better visualize the inferior vena cava-pulmonary artery conduit,

■ post-gadolinium delayed myocardial enhancement to evaluate the presence of scar tissue in 2-chamber and ventricular short-axis plane (Fig. 3.19.9).

Adequate information from the CT scan can be obtained using the early phase acquisition protocol with injection of contrast material into the right cubital vein and using the step volume scan mode of electron-beam CT. With 3-dimensional image reconstruc-
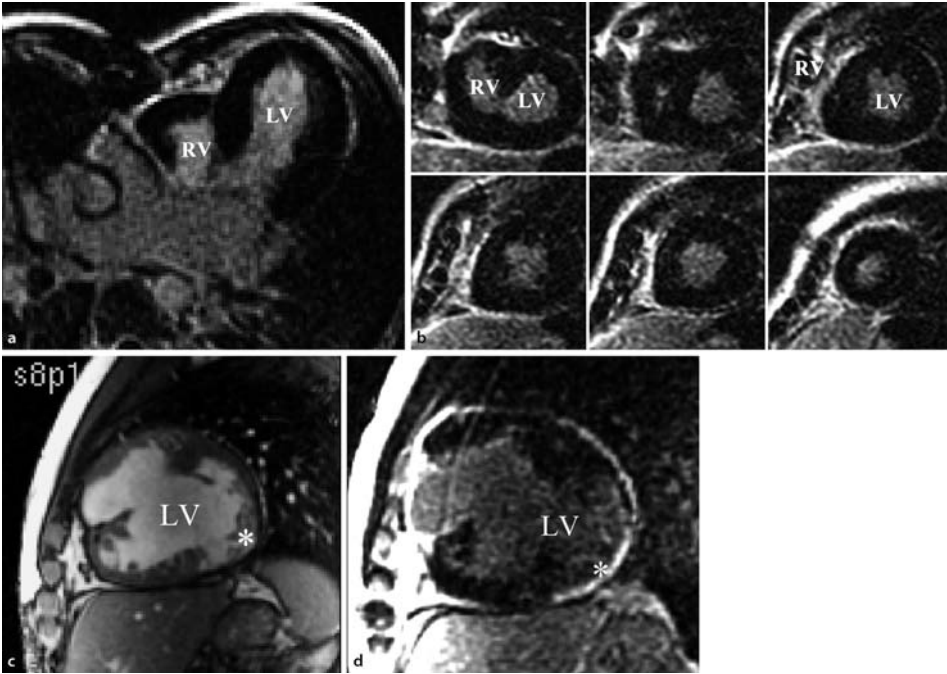
Fig. 3.19.9. Myocardial viability after Fontan procedure. Negative delay enhancement ventricular long-axis (**a**) and short-axis (**b**) view. Positive delay enhancement in double inlet ventricle with impaired ventricular function with two different areas of extended scar (*) at the anterior and posterior ventricular wall (**d**) corresponding in short-axis cine steady-state free precession (**c**) to thin and discynetic areas (*) (*LV* left ventricle, *RV* right ventricle)

tion, the blood flow through the bidirectional Glenn anastomosis and the complex morphology and relationship between adjacent structures can be directly demonstrated (Fig. 3.19.10). Information is provided on the size and morphology of the right and left pulmonary arteries, particularly with regard to the presence and extent of any narrowing.
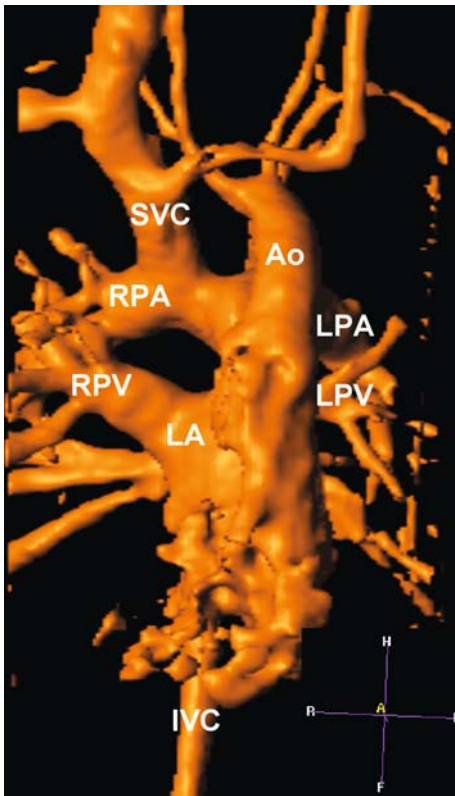
Fig. 3.19.10. Status post bidirectional Glenn anastomosis. CT scan, anterior view 3-dimensional angiographic reconstruction, with visualization of the end-to-side superior vena cava to right pulmonary artery anastomosis and the pulmonary venous return to the left heart (*Ao* aorta, *IVC* interior vena cava, *LA* left atrium, *LPA* left pulmonary artery, *LPV* left pulmonary veins, *RPV* right pulmonary veins, *RPA* right pulmonary artery, *SVC* superior vena cava) (photograph courtesy of Dr. Mohamed Tawil)

■ References

Almond CSD, Mayer JE, Thiagarajan RR, Blume ED, del Nido PJ, McElhinney DB (2007) Outcome after Fontan failure and takedown to an intermediate palliative circulation. Ann Thorac Surg 84:880–887

Babu-Narayan SV, Gatzoulis MA, Kilner PJ (2007) Noninvasive imaging in adult congenital heart disease using cardiovascular magnetic resonance. J Cardiovasc Med 8:23–29

Be'eri E, Maier SE, Landzberg MJ, Chung T, Geva T (1998) In vivo evaluation of Fontan pathway flow dynamics by multidimensional phase-velocity magnetic resonance imaging. Circulation 98:2873–2882

Brown DW, Gauvreau K, Powell AJ, Lang P, Colan SD, del Nido PJ, Odegard KC, Geva T (2007) Cardiac magnetic resonance versus routine cardiac catheterization before bidirectional Glenn anastomosis in infants with functional single ventricle. Circulation 116:2718–2725

Casolo G, Rega L, Gensini GF (2004) Detection of right atrial and pulmonary artery thrombosis after the Fontan procedure by magnetic resonance imaging. Heart 90:825

Choi BW, Park YH, Lee JK, Kim DJ, Kim MJ, Choe KO (2003) Patency of cavopulmonary connection studied by single phase electron beam computed tomography. Int J Cardiovasc Imaging 19:447–455

Corno AF, Becker AE, Bulterijs AHK, Lam J, Nijveld A, Schuller C, Marcelletti C (1982) Univentricular heart: can we alter the natural history? Ann Thorac Surg 34:716–726

Corno AF (1996) Considerations on the cavopulmonary connection. Am Coll Cardiol Curr J Rev 5:38

Corno AF, Bonnet D, Sekarski N, Sidi D, Vouhé PR, von Segesser LK (2003) Remote control of pulmonary blood flow: initial clinical experience. J Thorac Cardiovasc Surg 126:1775–1780

Corno AF, Horisberger J, Jegger D, von Segesser LK (2004) Right atrial surgery with unsnared inferior vena cava. Eur J Cardiothorac Surg 26:219–220

DiSessa TG, Child JS, Perloff JK, Wu L, Williams RG, Laks H, Friedman WF (1984) Systemic venous and pulmonary arterial flow patterns after Fontan's procedure for tricuspid atresia or single ventricle. Circulation 70:898

Dos L, Pen V, Silversides C, Provost Y, Oechslin E, Horlick E, Paul N (2007) Images in cardiovascular medicine. Cardiac magnetic resonance imaging and multidetector computed tomography scan illustrating Damus-Kaye-Stansel operation. Circulation 115:e440–e442

Eichen A, Fratz S, Gutfried C, Balling G, Schwaiger M, Lange R, Busch R, Hess J, Stern H (2003) Hearts late after Fontan operation have normal mass, normal volume, and reduced systolic function: a magnetic resonance imaging study. J Am Coll Cardiol 42:1061–1065

Festa P, Ait-Ali L, Bernabei M, De Marchi D (2005) The role of magnetic resonance imaging in the evaluation of the functionally single ventricle before and after conversion to the Fontan circulation. Cardiol Young 15(Suppl 3):51–56

Fogel MA, Weinberg PM, Fellows KE, Hoffman EA (1993) Magnetic resonance imaging of constant total heart volume and center of mass in patients with functional single ventricle before and after staged Fontan procedure. Am J Cardiol 72:1435–1443

Fogel MA, Gupta KB, Weinberg PM, Hoffman EA (1995) Regional wall motion and strain analysis across stages of Fontan reconstruction by magnetic resonance imaging. Am J Physiol 269:H1132–1152

Fogel MA, Weinberg PM, Chin AJ, Fellows KE, Hoffman EA (1996) Late ventricular geometry and performance changes of functional single ventricle throughout staged Fontan reconstruction assessed by magnetic resonance imaging. J Am Coll Cardiol 28:212–221

Fogel MA, Weinberg PM, Rychik J, Hubbard A, Jacobs M, Spray TL, Haselgrove J (1999) Caval. Caval contribution to flow in the branch pulmonary arteries of Fontan patients with a novel application of magnetic resonance presaturation pulse. Circulation 99:1215–1221

Fogel MA, Durning S, Wernovsky G, Pollock AN, Gaynor JW, Nicolson S (2004) Brain versus lung: hierarchy of feedback loops in single-ventricle patients with superior cavopulmonary connection. Circulation 110(Suppl II):47–52

Fogel MA (2005) Is routine cardiac catheterization necessary in the management of patients with single ventricles across staged Fontan reconstruction? No! Pediatr Cardiol 26:154–158

Fogel MA (2006) Cardiac magnetic resonance of single ventricles. J Cardiovasc Magn Reson 8:661–670

Frakes DH, Smith MJ, Parks J, Sharma S, Fogel SM, Yoganathan AP (2005) New techniques for the reconstruction of complex vascular anatomies from MRI images. J Cardiovasc Magn Reson 7:425–432

Fratz S, Hess J, Schwaiger M, Martinoff S, Stern HC (2002) More accurate quantification of pulmonary blood flow by magnetic resonance imaging than by lung perfusion scintigraphy in patients with Fontan circulation. Circulation 106:1510–1513

Garg R, Powell AJ, Sena L, Marshall AC, Geva T (2005) Effects of metallic implants on magnetic resonance imaging evaluation of Fontan palliation. Am J Cardiol 95:688–691

Giannico S, Hammad F, Amodeo A, Michielon G, Drago F, Turchetta A, di Donato R, Sanders SP (2006) Clinical outcome of 193 extracardiac Fontan patients. J Am Coll Cardiol 47:2065–2073

Goo HW, Yang DH, Park IS, Ko JK, Kim YH, Seo DM, Yun TJ, Park JJ (2007) Time-resolved three-dimensional contrast-enhanced magnetic resonance angiography in patients who have undergone a Fontan operation or bidirectional cavopulmonary connection: initial experience. J Magn Reson Imaging 25:727–736

Greenberg SB, Morrow WR, Imamura M, Drummond-Webb J (2004) Magnetic resonance flow analysis of classic and extracardiac Fontan procedures: the seesaw sign. Int J Cardiovasc Imaging 20:397–405

Hayabuchi Y, Mori K, Kitagawa T, Sakata M, Kagami S (2007) Polytetrafluoroethylene graft calcification in patients with surgically repaired congenital heart disease: evaluation using multidetector-row computed tomography. Am Heart J 153:806.e1–808

Hjortdal VE, Emmertsen K, Stenbog E, Frund T, Schmidt MR, Kromann O, Sorensen K, Pedersen EM (2003) Effects of exercise and respiration on blood flow in total cavopulmonary connection: a real-time magnetic resonance flow study. Circulation 108:1227–1231

Kiesewetter CH, Sheron N, Vettukattil JJ, Hacking N, Stedman B, Millward-Sadler H, Haw M, Cope R, Salmon AP, Sivaprakasam MC, Kendall T, Keeton BR, Iredale JP, Veldtman GR (2007) Hepatic changes in the failing Fontan circulation. Heart 93:579–584

Klimes K, Abdul-Khaliq H, Ovroutski S, Hui W, Alexi-Meskishvili V, Spors B, Hetzer R, Felix R, Lange PE, Berger F, Gutberlet M (2007) Pulmonary and caval blood flow patterns in patients with intracardiac and extracardiac Fontan: a magnetic resonance study. Clin Res Cardiol 96:160–167

Lilje C, Habermann CR, Weil J (2005) Magnetic resonance imaging follow-up ot total cavopulmonary connection. Heart 91:395

Marcelletti C, Corno AF, Giannico S, Marino B (1990) Inferior vena cava to pulmonary artery extracardiac conduit: a new form of right heart bypass. J Thorac Cardiovasc Surg 100:228–232

Mazzera E, Corno AF, Picardo S, Di Donato RM, Marino B, Costa D, Marcelletti C (1989) Bidirectional cavopulmonary shunts: clinical applications as staged or definitive palliation. Ann Thorac Surg 47:415–420

Morgan VL, Graham TP, Roselli RJ, Lorenz CH (1998) Alterations in pulmonary artery flow patterns and shear stress determined with three-dimensional phase-contrast magnetic resonance imaging in Fontan patients. J Thorac Cardiovasc Surg 116:294–304

Pedersen EM, Stenbog EV, Frund T, Houlind K, Kromann O, Sorensen KE, Emmertsen K, Hjortdal VE (2002) Flow during exercise in the total cavopulmonary connection measured by magnetic resonance velocity mapping. Heart 87:554–558

Rebergen SA, Ottenkamp J, Doornbos J, van der Wall EE, Chin JG, de Roos A (1993) Postoperative pulmonary flow dynamics after Fontan surgery: assessment with nuclear magnetic resonance velocity mapping. J Am Coll Cardiol 21:123–131

Robbers-Visser D, ten Harkel D, Strengers JLM (2007) Cardiac MRI combined with low-dose dobutamine stress reveals an abnormal stress response in children and young adults after Fontan operation at young age. J Cardiovasc Magn Reson 9:107

Socci L, Gervaso F, Migliavacca F, Pennati G, Dubini G, Ait-Ali L, Festa P, Amoretti F, Scebba L, Luisi VS (2005) Computational fluid dynamics in a model of the total cavopulmonary connection reconstructed using magnetic resonance images. Cardiol Young 15 (Suppl 3):61–67

Sundareswaran KS, Kanter KR, Kitajima HD, Krishnankutty R, Sabatier JF, Parks WJ, Sharma S, Yoganathan AP, Fogel M (2006) Impaired power output and cardiac index with hypoplastic left heart syndrome: a magnetic resonance imaging study. Ann Thorac Surg 82:1267–1275

Weiss F, Habermann CR, Lilje C, Sasse K, Kuhne T, Weil J, Adam G (2002) MRI in postoperative assessment of univentricular heart disease: correlation with echocardiography and angiography. Rofo 174:1537–1543

Pulmonary atresia
with ventricular septal defect

∎ Definition

Hearts with pulmonary atresia with ventricular septal defect have a biventricular arrangement, concordant atrioventricular connections, unrestrictive ventricular septal defect, single aortic outlet and absent luminal continuity between the right ventricle and the pulmonary arterial circulation.

The ventricular septal defect, usually unrestrictive, is generally of the malalignment type, resulting from extreme anterior deviation of the infundibular septum. The aorta can be entirely connected to the left ventricle or may override the interventricular septum (26–50% of cases). Pulmonary atresia resulting from anterior deviation of the infundibular septum (like in tetralogy of Fallot) with underdevelopment of the right infundibular outflow tract and atretic infundibulum is the most common type (70% of the cases). More rarely, pulmonary atresia can involve the pulmonary valve alone or the pulmonary valve and the proximal portion of the main pulmonary artery, or it may involve a longer segment of the main pulmonary artery. In any case, there is absence of luminal continuity between the right ventricle and the main pulmonary artery or both the right and left pulmonary arteries. The main pulmonary artery can be present and be of reasonable size but in most of cases is severely hypoplastic; more rarely, it consists of only a fibrous cord without lumen and in 5% of the patients is completely absent.

The morphology of the central pulmonary arteries is highly variable. The central right and left pulmonary arteries may be present and communicate freely (confluent pulmonary arteries) or may not communicate (nonconfluent pulmonary arteries, 20–30% of patients) or may be absent. Stenosis at the origin of the right pulmonary artery is present in 10% of the cases, while there is stenosis of the left pulmonary artery in 20% of cases, probably because of the process of closure of the ductus arteriosus. The size of the prebranching pulmonary arteries is extremely variable, and it can be quantitated with two different indexes: the *McGoon ratio* (see reference: Piehler JM), consisting of the ratio between the sum of the diameters of the right plus the left pulmonary artery divided by the diameter of the descending thoracic aorta at the level of the diaphragm, and the *Nakata index* (see reference: Nakata S), consisting of the ratio between the sum of the crosssectional areas of the right plus left pulmonary artery divided by the body surface area of the patient.

The pulmonary circulation is highly variable and it may be supplied by a patent ductus arteriosus, major aortopulmonary collateral arteries (in 60–70% of cases), or plexuses of bronchial and pleural arteries (5%). Only about half (53%) of patients with confluent pulmonary arteries present with pulmonary arteries reaching all 20 pulmonary segments, while less than 20% of patients with nonconfluent and/or hypoplastic pulmonary arteries have complete distribution of pulmonary arteries to all pulmonary segments. The major aortopulmonary collateral arteries may anastomose at any site in the pulmonary vascular tree: extrapulmonary, hilar, lobar and segmental levels. Rare

complex cases have been reported with simultaneous presence of patent ductus arteriosus and major aortopulmonary collateral arteries, and exceptionally with the presence of bilateral (right and left) ductus arteriosus. Major collateral arteries typically arise from the descending thoracic aorta, less commonly from the subclavian arteries, and rarely from the internal mammary (thoracic) arteries, intercostal arteries, carotid arteries or abdominal aorta; extremely rare cases have been reported with collateral arteries arising from coronary arteries. After a complex course in the posterior mediastinum, collaterals provide pulmonary blood flow either terminally or communicating with native proximal or distal pulmonary arterial branches. They may feed one side of the lungs, both sides or cross to the opposite side. Because of processes of intimal proliferation, major collaterals can develop stenosis in up to 60% of the patients. They may evolve quite variably and unpredictably, and may have a protective effect on pulmonary microvasculature. However, they may also complicate the surgical treatment of the disease.

Associated anomalies

Like tetralogy of Fallot with pulmonary stenosis, 25–30% of these patients have a dilated right aortic arch. Other anomalies include dextrocardia, heterotaxia, anomalous pulmonary or systemic venous connections, atrial septal defect or patent foramen ovale (50%), atrioventricular septal defect, tricuspid atresia, double inlet single left ventricle, aortic valve stenosis, complete transposition of the great arteries, double discordance (= congenitally corrected transposition of the great arteries), anomalous coronary arteries or coronary artery-to-pulmonary artery fistulas.

■ Surgical options

■ Unifocalization with central shunt or right ventricular outflow tract reconstruction without closure of the ventricular septal defect.
Through a median sternotomy all the major aortopulmonary collateral arteries are separated from their systemic origin and joined together to construct a pulmonary artery confluence, either with direct anastomoses or with the interposition of an autologous or heterologous pericardial roll; the pulmonary blood flow is obtained either with a central shunt (PTFE tubular prosthesis) or a valveless conduit (PTFE or pericardial) or a biological valved conduit interposed between a right ventriculotomy and the pulmonary artery reconstructed confluence. The ventricular septal defect is left open, or it may be closed with a fenestrated PTFE patch to allow right ventricular decompression, with later closure by interventional cardiology.

■ Single-stage unifocalization and complete repair.
The unifocalization of the major aortopulmonary collateral arteries is performed as for the two-stage repair (see above); the ventricular septal defect is closed from a longitudinal right ventriculotomy with a prosthetic patch, leaving the aortic valve in communication with the left ventricle; the right ventricle to pulmonary artery continuity is obtained with a biological valved conduit (rarely a monocusp valve patch or a valveless conduit is used) interposed between the same right ventriculotomy used for closure of the ventricular septal defect and the pulmonary artery reconstructed confluence.

In the presence of favorable anatomy with adequate right ventricular outflow tract and confluent pulmonary arteries, the first step consists of right ventricular outflow tract reconstruction with pericardial patch and closure of the ventricular septal defect.

■ **Alternative surgical approach.** The segment of descending thoracic aorta containing the origin of all the collaterals is transected and replaced with a PTFE conduit. The distal end of the above segment is closed by running suture, while the proximal end is end-to-side anastomosed to the native pulmonary artery confluence. At this point, the conventional intracardiac repair is performed, with patch closure of the ventricular septal defect and interposition of a biological valved conduit between the right ventricle and the confluence between the native pulmonary arteries and the transected aortic segment.

■ Pre-operative information

Pulmonary atresia with ventricular septal defect requires a pre-operative approach similar to tetralogy of Fallot (see chapter), with the only difference being that antegrade pulmonary blood flow, by definition, is lacking. Therefore, the pre-operative identification of any pulmonary blood flow source (patent ductus arteriosus and/or major aortopul-
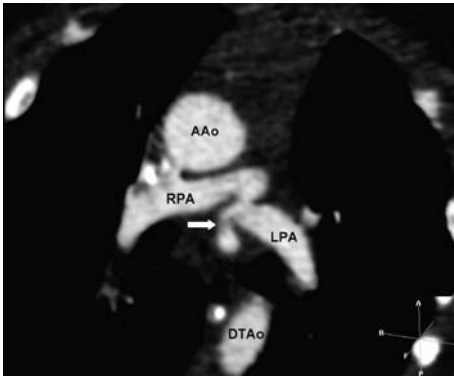
Fig. 3.20.1. Pulmonary atresia with ventricular septal defect. CT contrast angiography, maximal intensity projection reconstruction, showing a long and tortuous patent ductus arteriosus (arrow) providing pulmonary blood flow to confluent pulmonary arteries (*AAo* ascending aorta, *DTAo* descending thoracic aorta, *LPA* left pulmonary artery, *RPA* right pulmonary artery) (photograph courtesy of Dr. Mohamed Tawil)

monary collateral arteries) and the morphology of the pulmonary arteries is mandatory for the decision-making process (either unifocalization of the sources of pulmonary blood flow or shunt or even interventional embolization). This is particularly true in neonates with pulmonary atresia, ventricular septal defect and nonconfluent pulmonary arteries and/or high suspicion of the presence of major aortopulmonary collateral arteries. In these cases, CT scan and/or MRI, each one with its own advantages and disadvantages already discussed in the "Introduction", are very useful (Figs. 3.20.1–3.20.4).

■ Potential complications

Inadequate and/or dishomogeneous distribution of pulmonary blood flow; congestive heart failure, due to the persistence of uncontrolled major aortopulmonary collateral arteries; residual or recurrent ventricular septal defect; complete atrioventricular block, ventricular or supraventricular arrhythmias; persistent airway hyperresponsiveness with or without bronchomalacia; bronchospasm due to tracheobronchial epithelial necrosis or ischemia due to airway ischemia resulting from interruption of the tracheobronchial blood supply during dissection and mobilization of major aortopulmonary collaterals; pulmonary artery aneurysm; development of pulmonary vascular obstructive disease; development or progressive increase of aortic valve regurgitation; need for biological conduit replacement because of conduit calcification and/or valve degeneration (= pulmonary valve regurgitation) or because patient outgrew the conduit size (= right ventricular outflow tract obstruction).

■ Post-operative follow-up

Targets of the postoperative evaluation are the same as for patients with tetralogy of Fallot, with the addition of the unifocaliza-
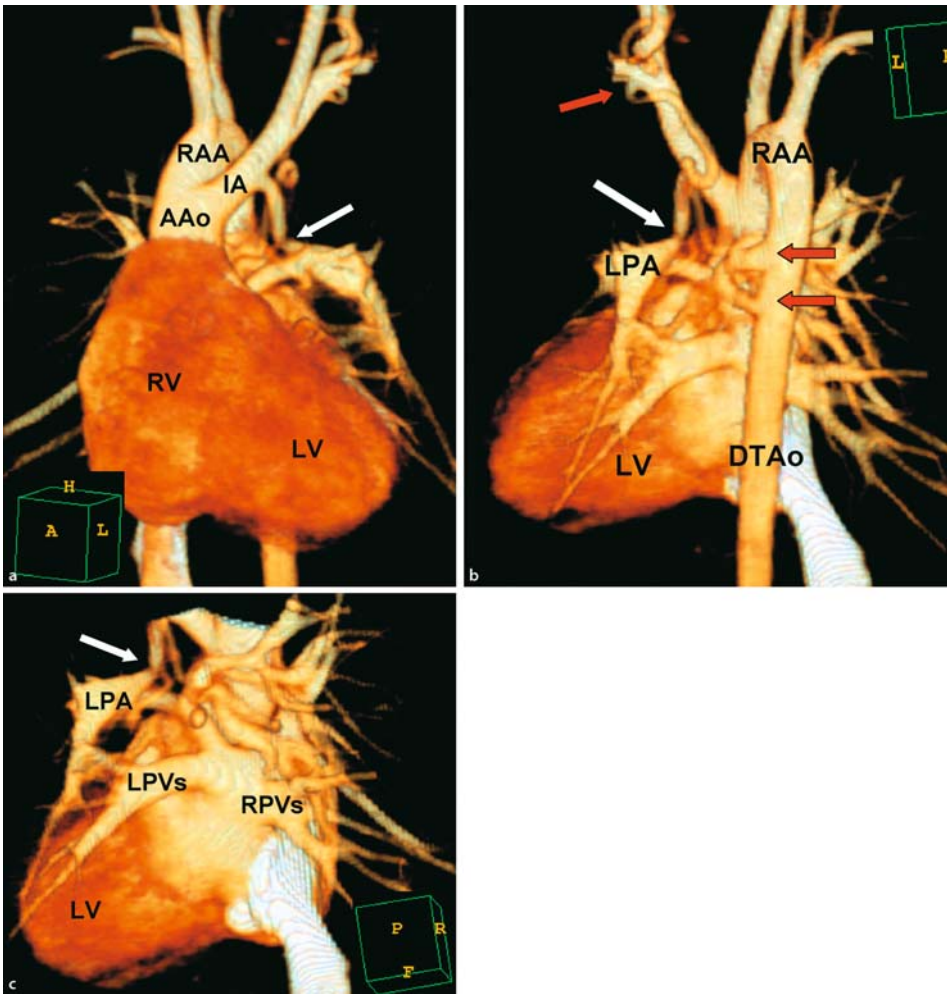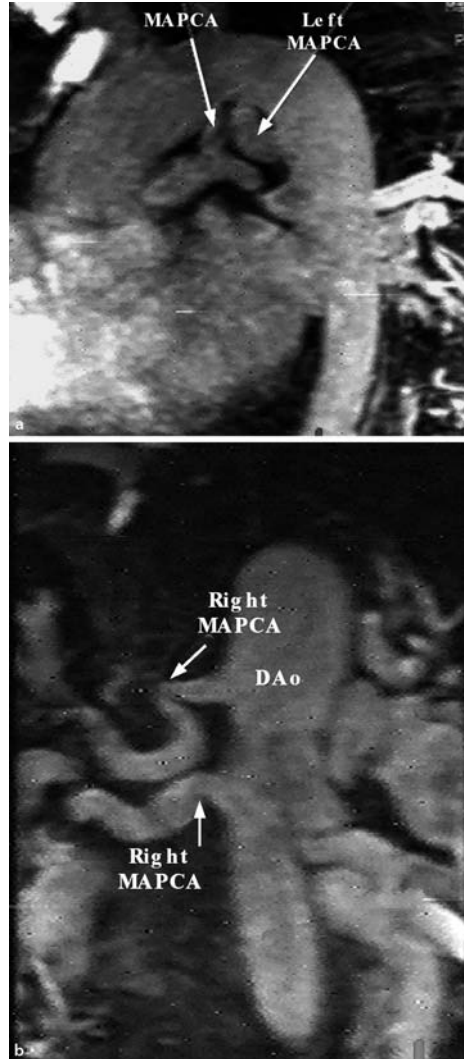
Fig. 3.20.2. Pulmonary atresia with ventricular septal defect. **a** CT contrast angiography, anterior projection, showing a single great artery (aorta) coming from the heart, right aortic arch, and a long patent ductus arteriosus originating from the left innominate artery with a stenotic connection to the left pulmonary artery (arrow) (*AAo* ascending aorta, *IA* innominate artery, *LV* left ventricle, *RAA* right aortic arch, *RV* right ventricle). **b** CT contrast angiography, posterior projection in the same neonate, showing the right aortic arch, the patent ductus arteriosus originating from the left innominate artery with a stenotic connection to the left pulmonary artery (white arrow), and several major aorto-pulmonary artery collaterals (red arrows) originating from the left subclavian artery (X1) and from the descending thoracic aorta (X2) (*DTAo* descending thoracic aorta, *LPA* left pulmonary artery, *LV* left ventricle, *RAA* right aortic arch). **c** CT contrast angiography, in the same neonate, showing the patent ductus arteriosus with a stenotic connection to the left pulmonary artery (white arrow), and several major aorto-pulmonary artery collaterals mostly perfusing the right lung (*LPA* left pulmonary artery, *LPVs* left pulmonary veins, *LV* left ventricle, *RPVs* right pulmonary veins) (photographs courtesy of Dr. Mohamed Tawil)
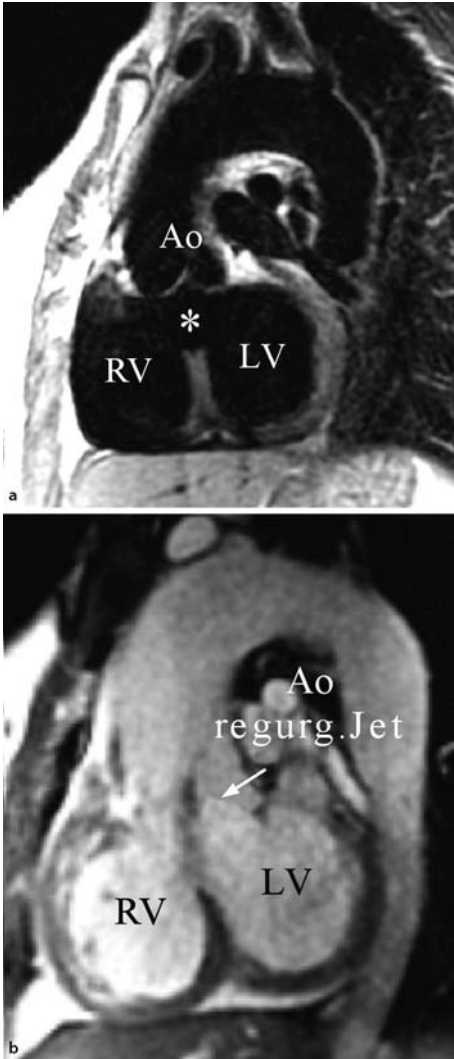
Fig. 3.20.3. Pulmonary atresia with ventricular septal defect. MRI sagittal fast spin echo (**a**) and cine steady-state free precession (**b**) showing a malalignment ventricular septal defect (asterisk) and a overriding and dilated aorta with trivial regurgitation (*Ao* aorta, *LV* left ventricle, *RV* right ventricle

Fig. 3.20.4. Pulmonary atresia with ventricular septal defect, major aortopulmonary collateral arteries and absent main pulmonary artery. MR angiography (maximal intensity projection reconstruction) showing several major aortopulmonary collateral arteries at different aortic levels (**a** and **b**) (*DAo* descending aorta, *MAPCA* major aortopulmonary collateral artery)
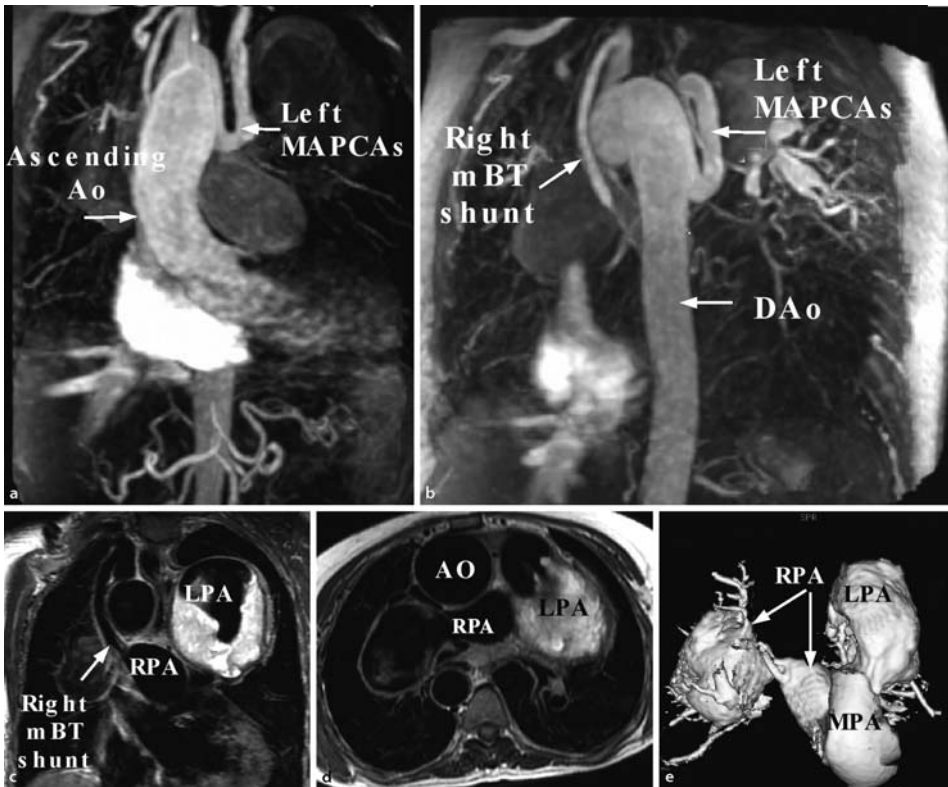
Fig. 3.20.5. Pulmonary atresia with ventricular septal defect, status post right modified Blalock-Taussig shunt and huge left and right pulmonary aneurysm. Maximal intensity projection reconstruction from MR angiography: anterior (**a**) and posterior (**b**) view showing a left major aortopumonary collateral arteries. Fast spin echo in the oblique frontal plane (**c**) illustrating a patent right modified Blalock-Taussig shunt and left pulmonary aneurysm with thrombi stratification. **d** Axial projection. **e** MR angiography volume rendering reconstruction: note the unusual anatomy of the pulmonary arteries and the right and left pulmonary aneurysm (*Ao* aorta, *DAo* descending aorta, *LPA* left pulmonary artery, *MAPCAs* major aortopulmonary collaterals, *MPA* main pulmonary artery, *mBT* modified Blalock-Taussig shunt, *RPA* right pulmonary artery)

tion of the major aortopulmonary collateral arteries. After palliative procedures, CT and MR angiography are valuable tools to show the surgically created systemic-to-pulmonary artery shunts, the relationship between the surgical shunts and the pulmonary arteries, the presence of pulmonary artery aneurysm (Fig. 3.20.5) and particularly the results of surgical procedures of unifocalization of the major aortopulmonary collateral arteries.

After repair, MRI is particularly useful to evaluate biventricular function, pulmonary vascularization, potential residual lesions like residual ventricular septal defect, pulmonary valve regurgitation, right ventricular outflow tract obstruction, and finally ascending aortic dilatation and aortic valve regurgitation (Figs. 3.20.6 and 3.20.7). Therefore, the MRI protocol of postoperative pulmonary atresia with ventricular septal defect
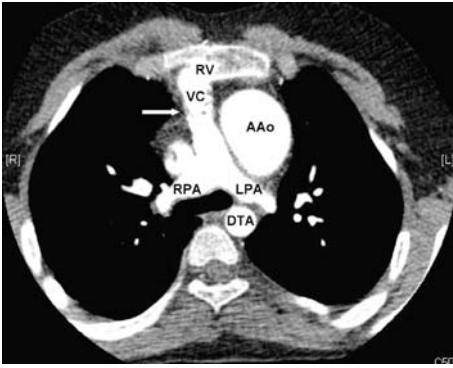
Fig. 3.20.6. Pulmonary atresia with ventricular septal defect. Post-operative CT scan, axial projection, after repair with closure of the ventricular septal defect and implantation of a homograft between the right ventricle and the pulmonary artery showing an obstructed conduit at the proximal anastomosis with the right ventricle and in association with the conduit valve (arrow) (*AAo* ascending aorta, *DTA* descending thoracic aorta, *LPA* left pulmonary artery, *RPA* right pulmonary artery, *RV* right ventricle, *VC* valved conduit)
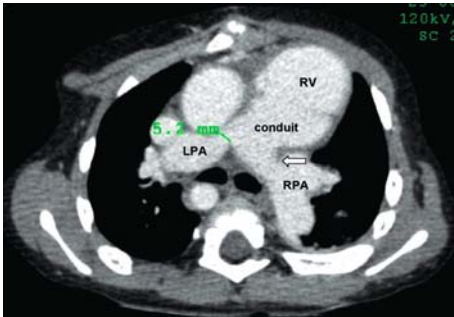
Fig. 3.20.7. Pulmonary atresia with ventricular septal defect. Post-operative CT scan, axial projection, after repair with closure of the ventricular septal defect and implantation of a biological conduit between the right ventricle and the pulmonary artery showing a stenosis at the origin of both the pulmonary arteries (measured diameter 5.2 mm at the left pulmonary artery and arrow at the left pulmonary artery) and a dilatation of the proximal part of the conduit (*LPA* left pulmonary artery, *RPA* right pulmonary artery, *RV* right ventricle) (photograph courtesy of Dr. Mohamed Tawil)

is similar to the postoperative Fallot (see chapter "Tetralogy of Fallot"). In case of multiple previous interventional procedures of embolization, MRI can be nondiagnostic due to major artifacts coming from coils positioned during the embolization procedures.

■ References

Boechat MI, Ratib O, Williams PL, Gomes AS, Child JS, Allada V (2005) Cardiac MR imaging and MR angiography for assessment of complex tetralogy of Fallot and pulmonary atresia. Radiographics 25: 1535–1546

Carotti A, Albanese SB, Minniti G, Guccione P, di Donato RM (2003) Increasing experience with integrated approach to pulmonary atresia with ventricular septal defect and major aortopulmonary collateral arteries. Eur J Cardiothorac Surg 23:719–727

Choi BW, Park YH, Lee JK, Kim MJ, Kim DJ, Ryu SJ, Cho BK, Choe KO (2003) Evaluation of the post-shunt status with electron beam computed tomography in cyanotic congenital heart disease. Yonsei Med J 44:249–258

Corno AF, Giamberti A, Giannico S, Marino B, Rossi E, Marcelletti C, Kirklin JK (1990) Airway obstruction associated with congenital heart disease in infancy. J Thorac Cardiovasc Surg 99:1091–1098

Corno AF, Hurni M, Tozzi P, von Segesser LK (2003) Accordion-like prosthesis for modified Blalock-Taussig shunt. Asian Cardiovasc Thorac Ann 11:229–232

Corno AF, Qanadli SD, Sekarski N, Artemisia S, Hurni M, Tozzi P, von Segesser LK (2004) Bovine valved xenograft in pulmonary position: medium-term follow-up with excellent hemodynamics and freedom from calcifications. Ann Thorac Surg 78:1382–1388

Dorfman AL, Geva T (2006) Magnetic resonance imaging evaluation of congenital heart disease: conotruncal anomalies. J Cardiovasc Magn Reson 8:645–659

Eichhorn J, Schoenberg S, Ulmer HE (2003) Cardiac-gated multislice computerised tomographic angiography in the preoperative evaluation of an infant with tetralogy of Fallot and pulmonary atresia. Cardiol Young 13:466–468

Geva T, Greil GF, Marshall AC, Landzberg M, Powell AJ (2002) Gadolinium-enhanced three-dimensional magnetic resonance angiography of pulmonary blood supply in patients with complex pulmonary stenosis or atresia: comparison with X-ray angiography. Circulation 106:473–478

Goo HW, Park IS, Ko JK, Kim YH, Seo DM, Yun TJ, Park JJ, Yoon CH (2003) CT of congenital heart disease: normal anatomy and typical pathologic conditions. Radiographics 23:S147–165

Holmqvist C, Hochbergs P, Bjorkhem G, Brockstedt S, Laurin S (2001) Preoperative evaluation with MR in tetralogy of Fallot and pulmonary atresia with ventricular septal defect. Acta Radiol 42:63–69

Horisberger J, Jegger D, Boone Y, Seigneul I, Pierrel N, Hurni M, Corno AF, von Segesser LK (1999) Impact of a remote pump head on neonatal priming volumes. Perfusion 14:351–356

Lee HS, Park YH, Cho BK (2001) External compression of bronchus by aneurysm from divided major aortopulmonary collateral artery after unifocalization. Eur J Cardiothorac Surg 19:221–222

Livolsi A, Kastler B (1990) Pre- and postoperative MRI study of 3 newborn infants with pulmonary atresia and interventricular communication. Ann Cardiol Angiol 39:301–304

Marino B, Corno AF, Pasquini L, Guccione P, Carta MG, Ballerini L, De Simone G, Marcelletti C (1987) Indication for systemic-pulmonary artery shunts guided by two-dimensional and Doppler echocardiography: criteria for patient selection. Ann Thorac Surg 44:495–498

Marino B, Digilio MC, Toscano A, Anaclerio S, Giannotti A, Feltri C, de Ioris MA, Angioni A, Dallapiccola B (2001) Anatomic patterns of conotruncal defects associated with deletion 22q11. Genet Med 3:45–48

Murai S, Hamada S, Yamamoto S, Khankan AA, Sumikawa H, Inoue A, Tsubamoto M, Honda O, Tomiyama N, Johkoh T, Nakamura H (2004) Evaluation of major aortopulmonary collateral arteries (MAPCAs) using three-dimensional CT angiography: two case report. Radiat Med 22:186–189

Nakata S, Imai Y, Takanashi Y, Kurosawa H, Tezuka M, Nakazawa M, Ando M, Takao A (1984) A new method for the quantitative standardization of cross sectional areas of the pulmonary arteries in congenital heart diseases with decreased pulmonary blood flow. J Thorac Cardiovasc Surg 88:610–619

Ngan EM, Rebeyka IM, Ross DB, Hirji M, Wolfaardt JF, Seelaus R, Grosvenor A, Noga M (2006) The rapid prototyping of anatomic models in pulmonary atresia. J Thorac Cardiovasc Surg 132:264–269

Oosterhof T, Mulder BJ (2005) Visualization of aortopulmonary connections in tetralogy of Fallot. Int J Cardiovasc Imaging 21:373–374

Paul JF, Lambert V, Losay J, Petit J, Macé L, Belli E, Serraf A, Planché C, Angel C (2002) Three-dimensional multislice CT scanner: value in patients with pulmonary atresia with septal defect. Arch Mal Coeur Vaiss 95:427–432

Piehler JM, Danielson GK, McGoon DC, Wallace RB, Fulton RE, Mair DD (1980) Management of pulmonary atresia with ventricular septal defect and hypoplastic pulmonary arteries by right ventricular outflow construction. J Thorac Cardiovasc Surg 80:552–567

Powell AJ, Chung T, Landzberg MJ, Geva T (2000) Accuracy of MRI evaluation of pulmonary blood supply in patients with complex pulmonary stenosis or atresia. Int J Card Imaging 16:169–174

Prasad SK, Soukias N, Hornung T, Khan M, Pennell DJ, Gatzoulis MA, Mohiaddin RH (2004) Role of magnetic resonance angiography in the diagnosis of major aortopulmonary collateral arteries and partial anomalous pulmonary venous drainage. Circulation 109:207–214

Reddy VM, McElhinney DB, Amin Z, Moore P, Parry AJ, Teitel DF, Hanley FL (2000) Early and intermediate outcomes after repair of pulmonary atresia with ventricular septal defect and major aortopulmonary collateral arteries: experience with 85 patients. Circulation 101:1826–1832

Schoen P, Poerner M, Hausleiter J, Wacker A, Martinoff S, Kaemmerer H, Redington A, Hess J (2004) Images in cardiovascular medicine. Multislice computed tomography in complex pulmonary atresia after stent implantation. Circulation 110:e299–300

Shiraishi I, Kajiyama Y, Yamagishi M, Hamaoka K (2006) Stereolithographic biomodeling of congenital heart disease by multislice computed tomography imaging. Circulation 113:e733–734

Vick GW, 3rd, Wendt RE, 3rd, Rokey R (1994) Comparison of gradient echo with spin echo magnetic resonance imaging and echocardiography in the evaluation of major aortopulmonary collateral arteries. Am Heart J 127:1341–1347

CHAPTER **3.21** **T**runcus arteriosus

▮ Definition

There is only one great artery (truncus arteriosus) originating from the base of the heart providing both pulmonary and systemic circulation. The truncal valve is obviously larger than a normal semilunar valve, with a variable number of leaflets from only one up to five and even six leaflets (extremely rare); most frequently the truncal valve has three (42–61% of cases) or four leaflets (24–31% of cases); a truncal valve with two leaflets is rare (5% of cases). The valve is generally located above the ventricular septal defect, almost always present, and the leaflets can be dysplastic and/or thickened with resulting stenosis, regurgitation (in at least 20% of cases), or both. The ventricular septal defect results from the absence of the infundibular septum, and is generally high, anterior and unrestrictive. Absence of the ventricular septal defect is anecdotal.

The pulmonary arteries can originate as a single main pulmonary artery from the lateral aspect of the truncus arteriosus (type I of the Collett and Edwards classification, the most frequent), or with two very close but separate origins from the posterolateral aspect of the truncus arteriosus (type II, the second frequent), or with the two pulmonary arteries independently originating from a lateral aspect of the truncus arteriosus (type III). The truncus arteriosus with neither pulmonary arterial branch arising from the truncus arteriosus (so called type IV) is considered as a variant of pulmonary atresia and ventricular septal defect with absent pulmonary arteries (see chapter "Pulmonary atresia with ventricular septal defect"). Stenosis at the origin of one or both branches of the pulmonary arteries is reported in 2 to 10% of patients. The origin of the coronary arteries presents with variable pattern, independent of the number of truncal valve leaflets.

Associated anomalies

Ventricular septal defect is almost always present, right aortic arch is frequent (18–36%), as well as truncal valve regurgitation (23%) or stenosis and coronary arteries abnormalities (18%), including single coronary artery and intramural course; aortic arch interruption, usually of type B (11–14%), and aortic coarctation are accompanied by patent ductus arteriosus; more rare (5%) is the association with nonconfluent pulmonary arteries, the so-called "absent" pulmonary artery, where one of the pulmonary arteries originates either from a patent ductus arteriosus or from a major aortopulmonary collateral; persistent left superior vena cava, total anomalous pulmonary venous connection, tricuspid atresia, complete atrioventricular septal defect, single ventricle, double aortic arch, anomalous origin of circumflex coronary artery from right pulmonary artery, situs inversus, dextrocardia have been exceptionally reported.

▮ Surgical options

Palliative approaches with bilateral pulmonary artery banding or plication of the origin of the pulmonary artery component have been practically abandoned in favor of surgical repair.

The surgical technique consists of three major components:

▮ separation of the pulmonary artery component from the truncus; at this point the truncus becomes the new aorta; the remaining opening in the lateral aspect of the truncus can be closed either directly or with a patch (pericardium or PTFE), based on the size and particularly on the presence of a coronary artery originating in the proximity of the opening itself; either technique to close the residual opening (direct or patch) needs to avoid traction or tension of the coronary arteries, and in this regard patch closure is the preferable technique,

▮ closure of the ventricular septal defect with a patch from a longitudinal right ventriculotomy, leaving the remaining systemic artery (becoming the aorta) in connection only with the left ventricle, and avoiding damage to the truncal valve (becoming the aortic valve),

▮ connection of the pulmonary artery component with the right ventricle by interposition of a biological valved conduit; valveless conduits are more rarely used; alternatively it is possible to perform direct anastomosis of the posterior wall of the pulmonary component to the posterior edge of the right ventriculotomy, completing the connection with a pericardial or PTFE roof, with or without a monocusp pulmonary valve (technique rarely utilized).

Associated lesions, particularly the presence of aortic coarctation or aortic arch interruption, need to be treated during the same procedure.

In the presence of moderate to severe truncal valve regurgitation, particularly with a quadrileaflet valve, a plasty by reduction to three leaflets with leaflet excision and annular remodeling can substantially reduce the degree of valvular regurgitation. More difficult to perform is the surgical opening of a stenotic truncal valve with adequate results. Truncal valve replacement (with a homograft or mechanical valve) needs to be taken into consideration in case reconstructive valvular surgery fails.

▮ Pre-operative information

Truncus arteriosus can be sufficiently evaluated, mainly in neonates, by transthoracic echocardiography. Nevertheless in older patients or if more anatomical details about the pulmonary arteries and venous connections as well as aortic arch are needed, CT scan and MRI can give more valuable insight. The role of CT scan and cardiac MRI is to delineate the precise morphology of the arterial trunk, with identification of the origin of the pulmonary arteries accordingly with the type of truncus arteriosus (type I, II or III), the distance between the origin of the pulmonary component and the origin of the left main coronary artery, and potential anomalies of the coronary arteries (Fig. 3.21.1).

CT scan and MRI are particularly useful in case of associated anomalies, in particular of disconnected pulmonary arteries or a so-called absent pulmonary artery, where the left or the right pulmonary artery originates
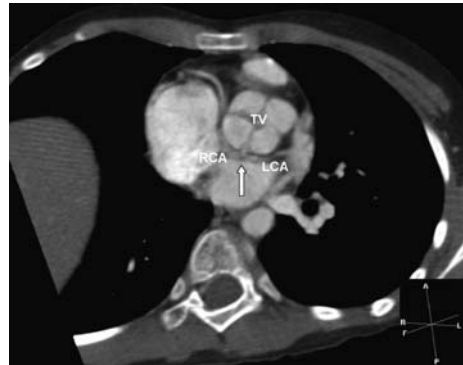
Fig. 3.21.1. Truncus arteriosus. CT scan, axial projection, showing a quadricuspid truncal valve with single origin of the coronary arteries with association with the posterior commissura (arrow) (*LCA* left coronary artery, *RCA* right coronary artery, *TV* truncal valve) (photograph courtesy of Dr. Mohamed Tawil)
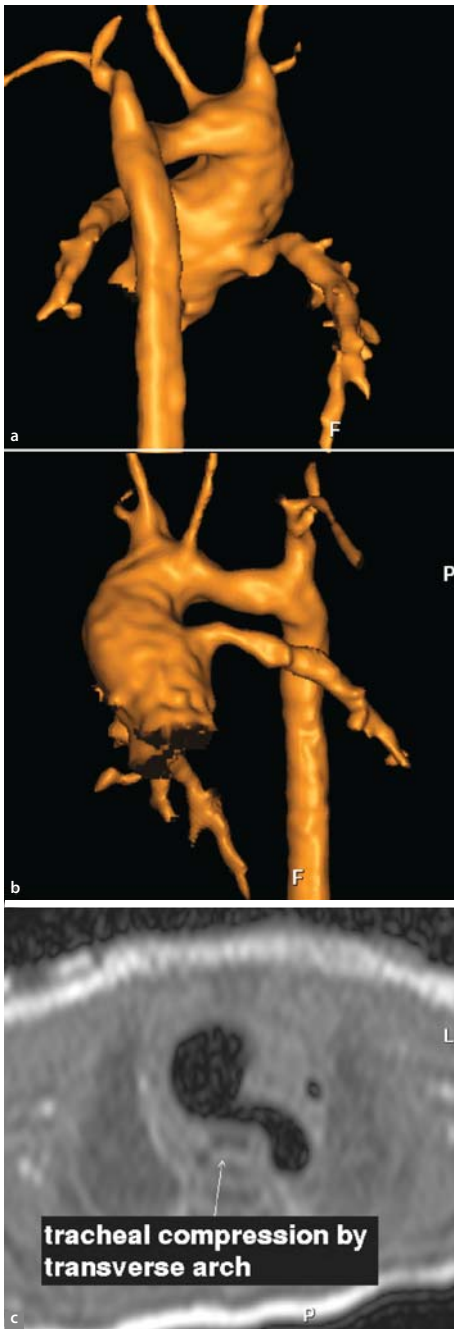
from a ductus arteriosus or from a major aortopulmonary collateral artery. In these cases, even angiography can fail to reveal the presence and location of the absent pulmonary artery, well visualized by CT scan or MRI.

CT scan and MRI play the same important role in the presence of aortic coarctation or aortic arch interruption, where the precise identification of the aortic arch morphology can allow better surgical planning (Fig. 3.21.2).

Finally, in the presence of airway compression, particularly frequent with right aortic arch, where tracheal and left bronchial compression are often associated, the simultaneous visualization of the great arteries and the airways provides vital information for the decision-making process when planning surgical repair of the truncus arteriosus associated with surgical relief of airway compression.

Due to radiation exposure considerations already highlighted in the introduction, MRI is considered the second choice diagnostic tool after echocardiography for the evaluation of truncus arteriosus with complex anatomy.

The pre-operative MRI protocol includes:
▪ 3-plane localizing images,
▪ 2-dimensional axial Time-of-flight Angiography (see appendix in the "Introduction"),
▪ ECG-gated cine steady-state free precession sequences in 2-chamber, 4-chamber planes, and ventricular short axis for the quantitative assessment of both ventricular dimensions, function and stroke volume (as illustrated in appendix in the introduction chapter),

Fig. 3.21.2. Truncus arteriosus. MR Angiography volume rendering reconstruction, posterior (**a**) and lateral (**b**) view, showing the truncus arteriosus type III with separate origin from its lateral and posterior aspect of relatively small pulmonary arteries and severe kinking of the transverse aortic arch. (**c**) MRI fast spin echo imaging showing the tracheal compression due to the transverse aortic arch (photographs courtesy of Dr. Philipp Beerbaum and Dr. Robert A. Johnson)

- ECG-gated steady-state free precession left ventricular outflow tract,
- ECG-gated steady-state free precession short axis of the truncal valve,
- ECG-gated fast speed echo to visualize potential airway obstruction,
- ECG-gated phase velocity contrast MRI sequences perpendicular to the main trunk for the quantification of truncal valve regurgitation,
- gadolinium-enhanced 3-dimensional MRI for the evaluation of the aortic arch, pulmonary arteries and ductus arteriosus if patent.

▪ Potential complications

Residual ventricular septal defect, complete atrioventricular block, arrhythmias, residual or progressive truncal valve stenosis or regurgitation, residual right ventricular outflow tract obstruction, pulmonary hypertension, airways compression (particularly in the presence of right aortic arch and aortic coarctation or aortic arch interruption). Late complications are progressive truncal valve dysfunction and obstruction of the right ventricle to pulmonary artery conduit.

▪ Post-operative follow-up

The role of CT scan and MRI in patients after repair of truncus arteriosus increases with their age. The anatomic and functional issues in these patients are similar to those encountered in patients after repair of tetralogy of Fallot with pulmonary atresia and pulmonary atresia with ventricular septal defect (Fig. 3.21.3). In addition, neoaortic valve dysfunction, aortic arch obstruction and potential airway compression are additional issues that may require further investigation.

Fig. 3.21.3. Truncus arteriosus, status post-repair. **a** CT scan, sagittal projection, showing the valved conduit with calcifications (arrows) on the free wall. **b** CT scan in the same patient, axial projection, showing the truncal valve (*Ao* aorta, *LA* left atrium, *LPA* left pulmonary artery, *LV* left ventricle, *MP* main pulmonary artery, *RPA* right pulmonary artery, *RV* right ventricle, *TV* truncal valve, *VC* valved conduit) (photographs courtesy of Dr. Mohamed Tawil)
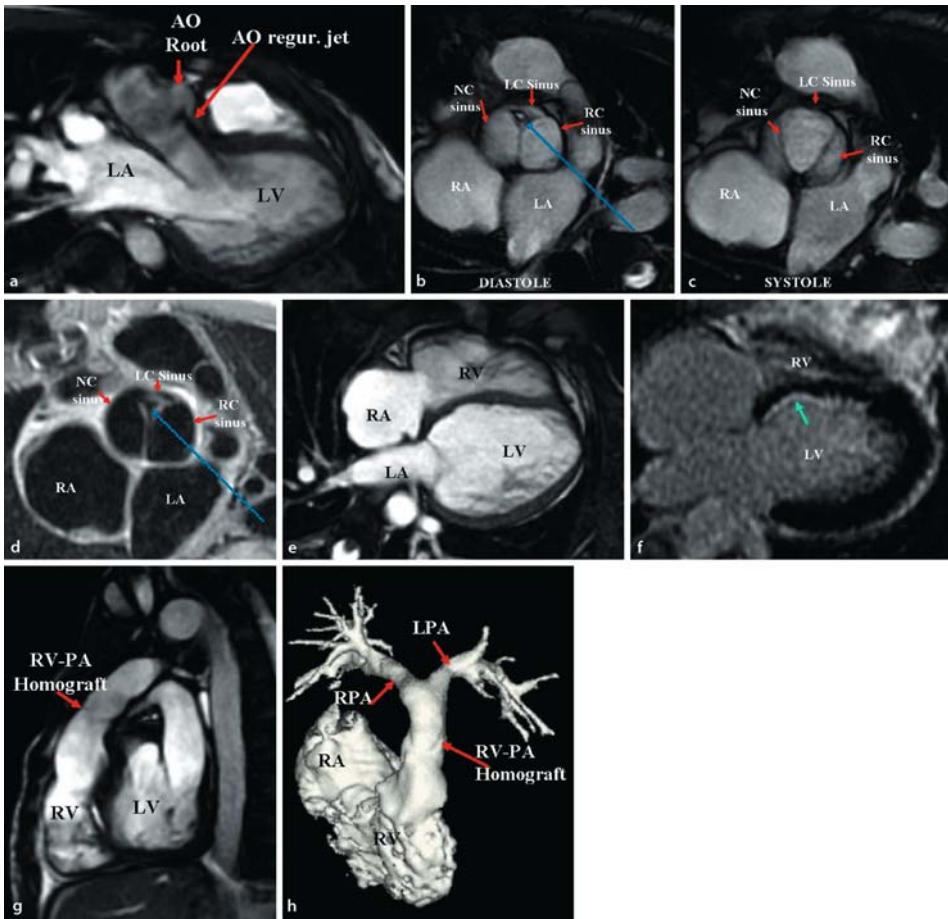
Fig. 3.21.4. Truncus arteriosus Type I, status post repair with a homograft. Cardiac MRI late after repair of truncus arteriosus, with severe aortic regurgitation. Steady-state free precession cine imaging of the left ventricular outflow tract (**a**) showing the aortic regurgitation jet (40% regurgitant fraction calculated by phase velocity contrast-MRI). Short-axis cine imaging steady-state free precession of the aortic valve in diastole (**b**) and systole (**c**) and fast spin echo in diastole (**d**): note the defect of coaptation (blue arrow) secondary to hypoplastic left coronary leaflet. The left ventricle, shown in the steady-state free precession 4-chamber view (**e**), is dilated (Z-score = +4 in diastole). The acquisition late after I.V. injection of gadolinium (delayed enhancement) (**f**) demonstrate a 3 cm long subendocardial fibrosis (arrow) in association with the left side of the lower portion of the interventricular septum. Cine imaging (steady-state free precession) of the right ventricular outflow tract (**g**) and 3-dimensional MR angiography (volume rendering reconstruction) (**h**) showing mild stenosis of the pulmonary homograft and pulmonary arteries (*AO* aorta, *LA* left atrium, *LC* left coronary artery, *LPA* left pulmonary artery, *LV* left ventricle, *NC* noncoronary, *PA* pulmonary artery, *RA* right atrium, *RC* right coronary, *RPA* right pulmonary artery, *RV* right ventricle)
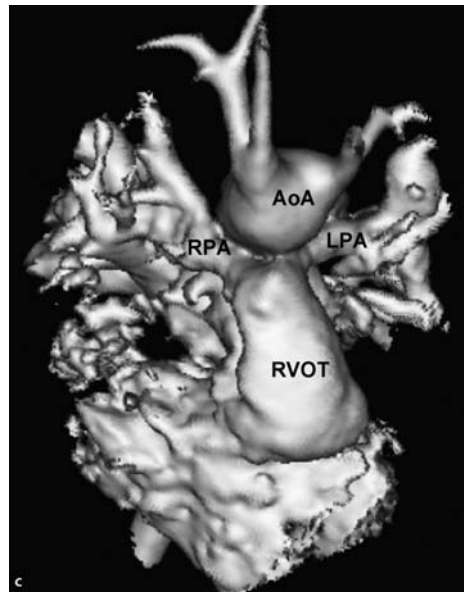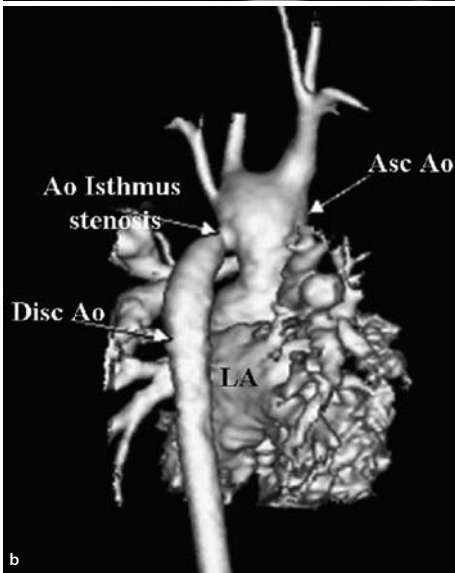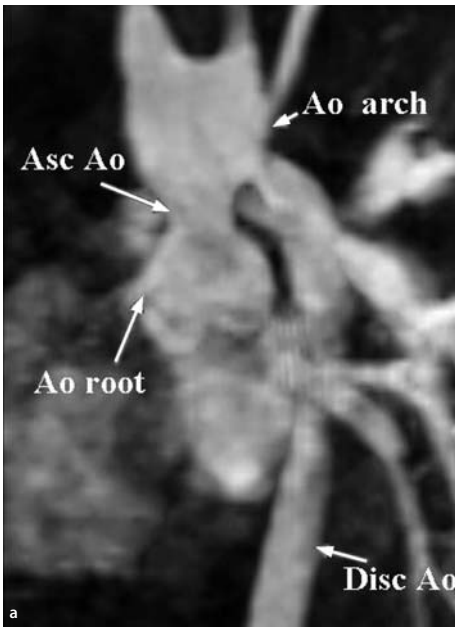
Fig. 3.21.5. Truncus arteriosus Type IV, status post repair with a pericardial patch for right ventricular outflow tract reconstruction and end-to-end anastomosis for the interrupted aortic arch. Cardiac MRI maximal intensity projection (**a**) and volume rendering reconstruction (**b**) showing the stamped ascending aorta and aortic isthmus stenosis. Volume rendering reconstruction (**c**) showing the pulmonary bifurcation shifted anterior to the ascending aorta during the Lecompte maneuver (*Ao Arch* aortic arch, *Ao root* aortic root, *Asc Ao* ascending aorta, *Disc Ao* descending aorta, *LA* left atrium, *LPA* left pulmonary artery, *Pulm* pulmonary, *RPA* right pulmonary artery, *RVOT* right ventricular outflow tract)

The goals of the post-operative MRI examination include: 1) quantitative assessment of left and right ventricular volumes, function, and mass; 2) measurements of pulmonary and neoaortic valve regurgitation; 3) imaging of the right ventricular outflow tract, the valved conduit, and the branch pulmonary arteries; 4) assessment of residual shunts; and 5) imaging of the aortic arch and isthmus (Figs. 3.21.4 and 3.21.5).

Modifications of the MRI protocol described for tetralogy of Fallot are individualized for the patient's anatomic and hemodynamic characteristics:

▮ 3-plane localizing images,
▮ 2-dimensional axial Time-of-flight Angiography (see appendix in the "Introduction"),
▮ ECG-gated cine steady-state free precession sequences in 2-chamber, 4-chamber planes, and ventricular short axis for the quantitative assessment of both ventricular dimensions, function and stroke volume (as illustrated in the appendix in the "Introduction"),
▮ ECG-gated cine steady-state free precession para-sagittal sequence to visualize the left ventricular outflow tract and the aortic arch,
▮ ECG-gated cine steady-state free precession sequence short axis of aortic (previous truncal) valve,
▮ ECG-gated cine steady-state free precession sequence, generally on the sagittal plane, to visualize the right ventricular outflow tract,
▮ ECG-gated fast spin echo of the aortic arch when required,
▮ gadolinium-enhanced 3-dimensional MRI for the evaluation of great arteries and aortic arch,
▮ ECG-gated phase velocity contrast MRI sequences perpendicular to main pulmonary artery, ascending aorta and pulmonary arteries, to assess aortic and pulmonary valve regurgitation, pulmonary blood flow,
▮ post-gadolinium delayed myocardial enhancement may be used to evaluate the presence of fibrotic tissue.

▮ References

Corno AF (2000) Surgery for congenital heart disease. Curr Opinion Cardiol 15:238–243

Corno AF, Qanadli SD, Sekarski N, Artemisia S, Hurni M, Tozzi P, von Segesser LK (2004) Bovine valved xenograft in pulmonary position: medium-term follow-up with excellent hemodynamics and freedom from calcifications. Ann Thorac Surg 78:1382–1388

Davtyan HG, Corno AF, Drinkwater DC, George B, Laks H (1986) Valve replacement for congenital heart disease. Circulation 74:II–250

Dorfman AL, Geva T (2006) Magnetic resonance imaging evaluation of congenital heart disease: conotruncal anomalies. J Cardiovasc Magn Reson 8:645–659

Ebert PA, Turley K, Stanger P, Hoffman JIE, Heymann MA, Rudolph AM (1984) Surgical treatment of truncus arteriosus in the first 6 months of life. Ann Surg 200:451–456

Gomes MMR, McGoon DC (1971) Truncus arteriosus with interrupted aortic arch: report of a case successfully repaired. Mayo Clin Proc 46:40

Goo HW, Park IS, Ko JK, Kim YH, Seo DM, Yun TJ, Park JJ, Yoon CH (2003) CT of congenital heart disease: normal anatomy and typical pathologic conditions. Radiographics 23:S147–165

Harris MA, Johnson TR, Weinberg PM, Fogel MA (2007) Delayed-enhancement cardiovascular magnetic resonance identifies fibrous tissue in children after surgery for congenital heart disease. J Thorac Cardiovasc Surg 133:676–681

Kalavrouziotis G, Purohit M, Ciotti G, Corno AF, Pozzi M (2006) Truncus arteriosus communis: early and midterm results of early primary repair. Ann Thorac Surg 82:2200–2206

McGoon DC, Rastelli GC, Ongley PA (1968) An operation for the correction of truncus arteriosus. JAMA 205:69–73

Muhler MR, Rake A, Schwabe M, Chaoui R, Heling KS, Planke C, Lembcke A, Fischer T, Kivelitz D (2004) Truncus arteriosus communis in a midtrimester fetus: comparison of prenatal ultrasound and MRI with postmortem MRI and autopsy. Eur Radiol 14:2120–2124

Murashita T, Hatta E, Imamura M, Yasuda K (2002) Giant pseudoaneurysm of the right ventricular outflow tract after repair of truncus arteriosus: evaluation by MR imaging and surgical approach. Eur J Cardiothorac Surg 22:849–851

Paul JF, Serraf A (2002) Images in cardiovascular medicine. Truncus arteriosus and double aortic arch. Circulation 105:170

Rastelli GC, Tituts JL, McGoon DC (1967) Homograft of ascending aorta and aortic valve as a right ventricular outflow: an experimental approach to the repair of truncus arteriosus. Arch Surg 95:698–707

Rodefeld MD, Hanley FL (2002) Neonatal truncus arteriosus repair: surgical techniqus and clinical management. Semin Thorac Cardiovasc Surg Pediatr Card Surg Ann 5:212–217

Sano S, Brawn WJ, Mee RBB (1990) Repair of truncus arteriosus and interrupted aortic arch. J Card Surg 5:157

▌ Definition

Aortopulmonary window is a communication, usually nonrestrictive, between the ascending aorta and the main pulmonary artery, in the presence of two semilunar valves. In most patients, there is little or no length to the communication, as the term window implies, while a ductus-like type of communication is rare. The aortopulmonary window is generally located in the left lateral wall of the ascending aorta, usually close to the orifice of the left coronary artery (Fig. 3.22.3); therefore it is not infrequent to find an anomalous origin of the coronary artery from the pulmonary artery, close to the edge of the defect.

Associated anomalies

Associated defects are present in 30–50% of patients, the most frequent being aortic arch interruption type A, tetralogy of Fallot with or without pulmonary atresia, ventricular septal defect, anomalous origin of a coronary artery and anomalous origin of a pulmonary artery; occasional an association with atrial septal defect, cor triatriatum, complete atrioventricular septal defect, transposition of the great arteries, subaortic obstruction (extremely rare), bicuspid aortic valve, aortic atresia, critical pulmonary valve stenosis, aortic arch hypoplasia, aortic coarctation, double aortic arch, and patent ductus arteriosus.

▌ Surgical options

▌ **Ligature:** nowadays, this surgical approach is limited to exceptional cases with aortopulmonary window with "ductus-like" morphology, with relatively small diameter and long shape.

▌ **Closure on cardiopulmonary bypass:** the surgical approach can be transaortic, transpulmonary, transdefect or combined transaortic and transpulmonary, according to the morphology of the defect and the personal experience of the surgeon. In any case, after initial opening of the aortic side or of the anterior wall of the defect, the origin of the coronary arteries and the origin of the right pulmonary artery must be very carefully identified. Thus, the transpulmonary approach is not ideal, because it does not allow adequate visualization of the origin of the coronary arteries.

Patch closure with a prosthetic or pericardial patch is always preferred to direct closure to avoid distortion of the surrounding structures, particularly the origin of the coronary arteries. In the presence of anomalous origin of a coronary artery, tunnel or coronary artery reimplantation is required in order to leave the origin of the anomalous coronary artery connected with the aortic side of the circulation.
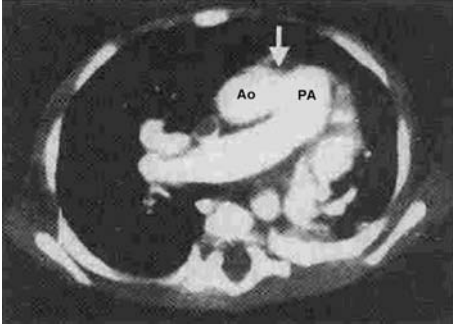
Fig. 3.22.1. Aortopulmonary window. CT scan, axial projection, showing a distal type of aortopulmonary window (arrow), with a diameter of 1.1 cm (*Ao* aorta, *PA* pulmonary artery) (modified with permission from Zhang X, Wu ZK, Yao JP, Sun PW (2004) Aortopulmonary window: a case diagnosed and surgery confirmed by ultra-fast computed tomography. Chin Med J 117:1750–1752)
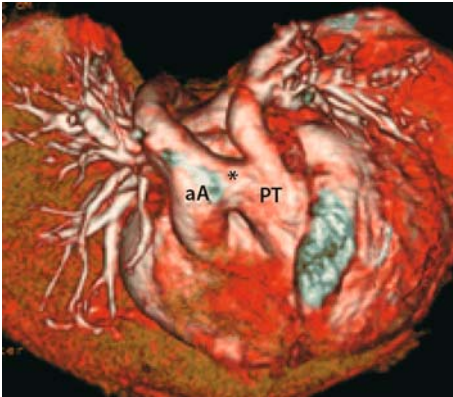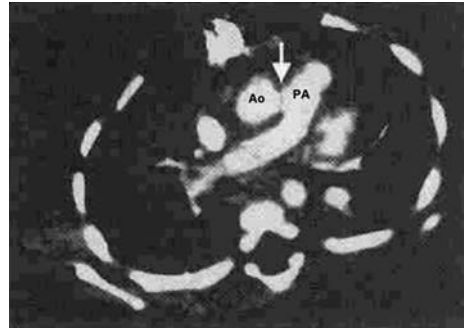

Fig. 3.22.2. Aortopulmonary window. CT scan, volume rendering imaging showing a distal aortopulmonary window (asterisk) (*aA* ascending aorta, *PT* pulmonary trunk) (reproduced with permission from Goo HW, Park IS, Ko JK, Kim YH, Seo DM, Yun TJ, Park JJ, Yoon CH (2003) CT of congenital heart disease: normal anatomy and typical pathologic conditions. Radiographics 23:S147–165)
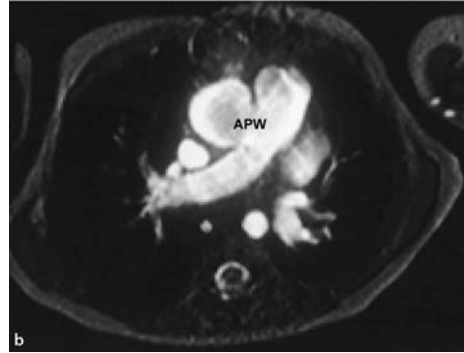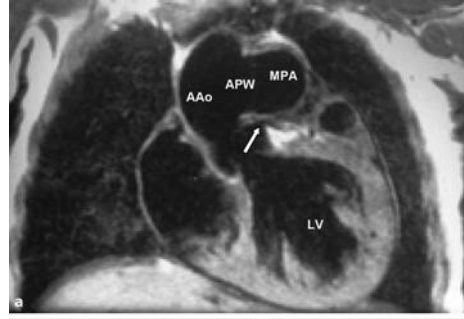
Fig. 3.22.3. Aortopulmonary window. **a** MRI, fast spin echo, showing a large communication between the ascending aorta and the main pulmonary artery, immediately above the origin of the left main coronary artery (arrow). **b** MR angiography maximal intensity projection reconstruction in the same patient, showing the large aortopulmonary window (*AAo* ascending aorta, *APW* aortopulmonary window, *LV* left ventricle, *MPA* main pulmonary artery)

■ Pre-operative information

The clinical data and the echocardiographic investigation generally provide enough information for the diagnosis of aortopulmonary window. Other noninvasive investigations, such as CT scan (Figs. 3.22.1 and 3.22.2) and/or MRI (Figs. 3.22.3 and 3.22.4), allow clear visualization of the location of the aortopulmonary window and can precisely show its relationship with the origin of the coronary arteries. CT scan and MRI become extremely important in order to better plan the surgical approach in the presence of asso-

Fig. 3.22.5. Aortopulmonary window, status post repair. Post-operative CT scan in the same patient of Fig. 3.22.1, axial projection, showing absence of any residual shunt or stenosis in the ascending aorta and main pulmonary artery (*Ao* aorta, *PA* pulmonary artery) (modified with permission from Zhang X, Wu ZK, Yao JP, Sun PW (2004) Aortopulmonary window: a case diagnosed and surgery confirmed by ultra-fast computed tomography. Chin Med J 117:1750–1752)

ciated anomalies, e.g., aortic arch interruption, aortic arch hypoplasia with or without aortic coarctation, anomalous origin of a pulmonary artery, and anomalous origin of a coronary artery from the pulmonary artery.

The cardiac MRI protocol used in the presence of aortopulmonary window is the following:

- 3-plane localizing images,
- 2-dimensional axial Time-of-flight Angiography (see the appendix in the "Introduction"),

Fig. 3.22.4. Aortopulmonary window. **a** MR angiography axial maximal intensity projection reconstruction in a neonate showing the aortopulmonary window (arrow). **b** MR angiography maximal intensity projection reconstruction in the same neonate showing the aortopulmonary window (arrow). **c** MR angiography maximal intensity projection reconstruction in the same neonate, showing the aortopulmonary window (arrow) (*AAo* ascending aorta, *AoA* aortic aortic arch, *MPA* main pulmonary artery)

- ECG-gated cine steady-state free precession sequences in 2-chamber, 4-chamber planes, and ventricular short axis for the quantitative assessment of both ventricular dimensions, function and stroke volume, as illustrated in the appendix of the "Introduction",
- ECG-gated cine steady-state free precession and static fast spin echo sequences on additional planes to better delineate the aortopulmonary window,
- ECG-gated static 3-dimensional steady-state free precession for the evaluation of origin and proximal course of the coronary arteries,
- ECG-gated phase velocity contrast MRI sequences perpendicular to the main pulmonary artery branches and ascending aorta to assess the amount of shunt,
- gadolinium-enhanced 3-dimensional MRI for the evaluation of potential associated anomalies of the aortic arch.

■ Potential complications

Residual or recurrent left-to-right shunt, residual or progressive obstruction of the ascending aorta or the main pulmonary artery, obstruction of a coronary artery origin.

■ Post-operative follow-up

In the follow-up of patients after surgical repair of aortopulmonary window, CT scan and/or MRI are indicated to rule out residual aortopulmonary distortion (Fig. 3.22.5). Meanwhile MRI by means of cine MR and phase velocity contrast acquisitions can respectively visualize and measure residual shunts at the aortopulmonary window, or to rule out residual defects after the repair of associated malformations.

■ References

Atiq M, Rashid N, Kazmi KA, Qureshi SA (2003) Closure of aortopulmonary window with Amplatzer duct occluder device. Pediatr Cardiol 24:298–299

Cetin II, Orun UA, Varan B, Coskun M, Tokel K (2005) A case of aortopulmonary window simulating common arterial trunk presented at the age of 13. Cardiovasc Intervent Radiol 28:533–535

Chen MR, Wu SJ (2006) Unclassified type of aortopulmonary window. Circulation 113:e703–704

Corno AF, Pierli C, Biagioli B, Lisi G, Grossi A (1988) Anomalous origin of the left coronary artery from an aorto-pulmonary window. J Thorac Cardiovasc Surg 96:669–671

Garver KA, Hernandez RJ, Vermilion RP, Martin Goble M (1997) Correlative imaging of aortopulmonary window: demonstration with echocardiography, angiography, and MRI. Circulation 96:1036–1037

Goo HW, Park IS, Ko JK, Kim YH, Seo DM, Yun TJ, Park JJ, Yoon CH (2003) CT of congenital heart disease: normal anatomy and typical pathologic conditions. Radiographics 23:S147–165

Incesu L, Baysal K, Kalayci AG, Erk K (1998) Magnetic resonance imaging of proximal aortopulmonary window. Clin Imaging 22:23–25

Kervancioglu S, Soydine S, Davutoglu V, Kervancioglu R, Sirikci A, Bayram M (2004) Aortopulmonary window: a rare adult case demonstration by echocardiography, MRI, CE-MRA and angiography. Cardiovasc Intervent Radiol 27:175–178

Yoo SJ, Choi HY, Park IS, Hong MG, Kim SH (1991) Distal aortopulmonary window with aortic origin of the right pulmonary artery and interruption of the aortic arch (Berry syndrome): diagnosis by MR imaging. Am J Roentgenol 157:835–836

Wong MN, Chang LG, Sim KH (2007) Interrupted aortic arch and aortopulmonary window demonstrated on 64-slice multidetector computed tomography angiography. Heart 93:95

Zhang X, Wu ZK, Yao JP, Sun PW (2004) Aortopulmonary window: a case diagnosed and surgery confirmed by ultra-fast computed tomography. Chin Med J 117:1750–1752

▊ Definition

The anomalous origin of the pulmonary artery (also called "hemitruncus") is a rare congenital malformation in which only one pulmonary artery branch, usually the right (opposite to the laterality of the aortic arch), originates from the posterior aspect of the ascending aorta just above the aortic sinotubular junction, without any defect between the ascending aorta and the main pulmonary artery, whereas the main pulmonary artery and the other pulmonary artery branch arise in their normal position and, therefore, are connected with the morphological right ventricle. The other main difference with persistent truncus arteriosus is the presence of two well-separated semilunar valves, aortic and pulmonary valves, and the usual absence of ventricular septal defect. Therefore, hemitruncus defines only the anomalous origin of one pulmonary artery. The anomalous pulmonary artery, most frequently the right, has unrestricted origin, and normal structure, course and distribution. The anomalous origin of the left pulmonary artery (isolated lesion in 40% of patients) usually occurs in the presence of a right aortic arch. Very rarely, the anomalous pulmonary artery can originate from the descending thoracic aorta or from either the right or the left coronary artery. Extremely rare cases have been reported of anomalous origin of one pulmonary artery from the innominate artery, the right pulmonary artery with normal left aortic arch, and the left pulmonary artery in the presence of right aortic arch.

Associated anomalies

Left (rarely right) patent ductus arteriosus is present in 50–75% of patients. Other associated anomalies are atrial or ventricular septal defect (8–10% of patients), tetralogy of Fallot with or without absent pulmonary valve, pulmonary stenosis or atresia with ventricular septal defect, aortopulmonary window, right aortic arch (50–75% of cases with anomalous left pulmonary artery), aortic coarctation, aortic arch interruption.

▊ Surgical options

The surgical repair can be performed either with or without cardiopulmonary bypass. The use of cardiopulmonary bypass, particularly in infants, allows adequate mobilization of the anomalous pulmonary artery, safe separation from the ascending aorta and reimplantation on the main pulmonary artery. Various surgical techniques have been reported for reimplantation of the anomalous pulmonary artery to the main pulmonary artery, posterior to the ascending aorta, including the direct anastomosis (definitely the preferred technique), an extension with either an aortic flap or an autologous pericardial patch, or the interposition of a synthetic tubular prosthesis, now practically abandoned.

▮ Pre-operative information

The CT scan (Fig. 3.23.1) and MRI can provide full visualization of the pulmonary arteries and their origins, particularly of the proximal segment of the left pulmonary artery, a frequent blind spot for transthoracic and transesophageal echocardiography. The side of the aortic arch and the presence of other associated anomalies can also be visualized.

▮ Potential complications

In the immediate post-operative period, episodes of pulmonary hypertension have been reported, while in the later follow-up residual or recurrent stenosis at the site of the anastomosis with the main pulmonary artery, and inhomogeneous lung perfusion have been observe with the nuclear scan.

▮ Post-operative follow-up

CT scan and/or MRI can be helpful in the post-operative evaluation of surgery for hemitruncus especially if a pulmonary artery branch stenosis is suspected. In addition to information on the morphology of the pulmonary arteries, cardiac MRI can provide information on the lung perfusion.

For post-operative evaluation of hemitruncus, the following cardiac MRI protocol is used:

▮ 3-plane localizing images,
▮ 2-dimensional axial Time-of-flight Angiography (see the appendix of the "Introduction"),
▮ ECG-gated cine steady-state free precession and fast spin echo sequence along the long axis of both pulmonary arteries (Fig. 3.23.2 b),
▮ ECG-gated cine steady-state free precession and fast spin echo sequence on the axial plane to evaluate the pulmonary arteries (Fig. 3.23.2 a),
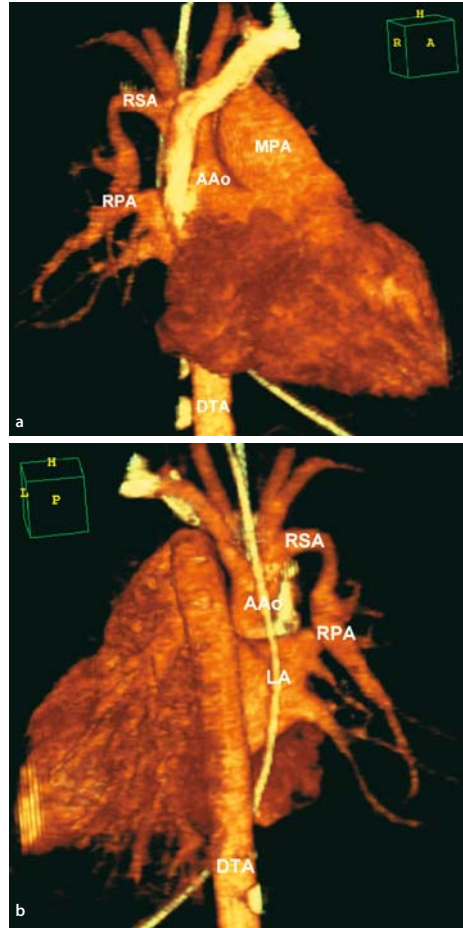
Fig. 3.23.1. Anomalous pulmonary artery. **a** CT Angiography volume rendering reconstruction, anterior view, coronal projection, showing the anomalous right pulmonary artery originating from the right subclavian artery, in a neonate with associated type A aortic arch interruption. **b** CT in the same neonate with postero-lateral view, showing the anomalous right pulmonary artery originating from the right subclavian artery and the type A aortic arch interruption (*AAo* ascending aorta, *DTA* descending thoracic aorta, *LA* left atrium, *MPA* pulmonary artery, *RPA* right pulmonary artery, *RSA* right subclavian artery) (photographs courtesy of Dr. Mohamed Tawil)
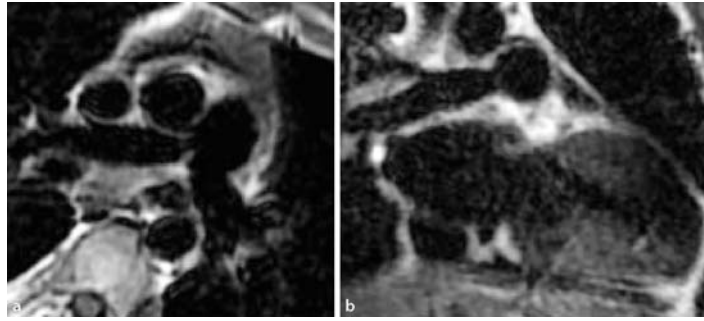
Fig. 3.23.2. Post-operative evaluation of anomalous origin of the right pulmonary artery from the ascending aorta. MRI fast spin echo axial (**a**) and coronal (**b**) view showing a mild stenosis at the origin of the right pulmonary artery. The PVC technique demonstrates a mild reduction of the right lung perfusion compared to the left (36 versus 64% of the total pulmonary flow)

■ ECG-gated phase velocity contrast sequences perpendicular to the main pulmonary artery and the branch pulmonary arteries in order to assess and quantify the flow pattern,

■ gadolinium-enhanced 3-dimensional MR Angiography for pulmonary arteries morphology.

■ References

Abu-Sulaiman RM, Hashmi A, McCrindle BW, Williams WG, Freedom RM (1998) Anomalous origin of one pulmonary artery from the ascending aorta: 36 years' experience from one centre. Cardiol Young 8:449–454

Choi BW, Park YH, Choi JY, Choi BI, Kim MJ, Ryu SJ, Lee JK, Sul JH, Lee SK, Cho BK, Choe KO (2001) Using electron beam CT to evaluate conotruncal anomalies in pediatric and adult patients. Am J Roentgenol 177:1045–1049

Dodo H, Alejos JC, Perloff JK, Laks H, Drinkwater DC, Williams RG (1995) Anomalous origin of the left main pulmonary artery from the ascending aorta associated with DiGeorge syndrome. Am J Cardiol 75:1294–1295

Fucci C, di Carlo D, di Donato R, Marino B, Calcaterra F, Marcelletti C (1989) Anomalous origin of the right pulmonary artery from the ascending aorta: repair without cardiopulmonary bypass. Int J Cardiol 23:309–313

Goo HW, Park IS, Ko JK, Kim YH, Seo DM, Yun TJ, Park JJ, Yoon CH (2003) CT of congenital heart disease: normal anatomy and typical pathologic conditions. Radiographics 23:S147–165

Gupta K, Livesay JJ, Lufschanowski R (2001) Absent right pulmonary artery with coronary collaterals supplying the affected lung. Circulation 104:E12–13

Livolsi A, Donato L, Kastler B, Willard D, Geisert J (1991) Magnetic resonance imaging in the diagnosis of retrotracheal pulmonary artery. Ann Cardiol Angiol 40:29–32

Mee RBB (1987) Surgical repair of hemitruncus: principles and techniques. J Cardiovasc Surg 2:247–256

Nathan M, Rimmer D, Piercey G, del Nido PJ, Mayer JE (2007) Early repair of hemitruncus: excellent early and late outcomes. J Thorac Cardiovasc Surg 133:1329–1335

Razavi R, Miquel M, Baker E (2004) Diagnosis of hemi-truncus arteriosus by three-dimensional magnetic resonance angiography. Circulation 109:e15–16

Rosa U, Wade KC (1987) CT findings in hemitruncus. J Comput Assist Tomogr 11:698–700

Sechtem U, Jungehulsing M, de Vivie R, Mennicken U, Hopp HW (1991) Left hemitruncus in adulthood: diagnostic role of magnetic resonance imaging. Eur Heart J 12:1040–1044

Sun AM, Alhabshan F, Branson H, Freedom RM, Yoo SJ (2005) MRI diagnosis of isolated origin of the left subclavian artery from the left pulmonary artery. Pediatr Radiol 35:1259–1262

Tsai SK, Chang CI, Wang MJ, Chen SJ, Chiu IS, Chen YS, Lue HC (2001) The assessment of the proximal left pulmonary artery by transoesophageal echocardiography and computed tomography in neonates and infants: a case series. Anesth Analg 93:594–597

Chapter 3.24 Anomalous coronary arteries

▌ Definition

Regardless of the position of the heart within the chest and the position and origin of the great arteries, aortic and pulmonary valves normally have a single point of contact, with commissural apposition; coronary arteries almost always originate normally from the facing sinuses of Valsalva on either side of this point of commissural contact; coronary arteries do not normally originate from the nonfacing or most distant sinus. Various types of coronary artery anomalies exist, sometime isolated or with more than one abnormal component.

▌ Isolated anomalous origin of a coronary artery.

From the pulmonary artery (historically called Bland-White-Garland syndrome): the anomalous coronary artery is most often the left coronary artery. Two clinical forms, infantile and adult, are recognized, representing two ends of a morphologic and pathophysiologic spectrum, which may reflect the degree of retrograde flow from the right coronary system to the anomalous left coronary artery via collateral channels; a myocardial steel-like syndrome may develop with ischemia and infarction if collateral development is not adequate. These patients may develop cardiomegaly and mitral valve regurgitation due to papillary muscle infarction.

From the wrong sinus of Valsalva (with or without intramural course): the presence of origin of the left main coronary artery or the left anterior descending coronary artery from the right sinus of Valsalva and intramural course (inside the aortic wall) is known to be malignant (= at risk of sudden death) due to compression of the vessel during or immediately after exercise. An "interarterial" course between the aortic root and the main pulmonary artery is also malignant, mainly if associated with intramural course of the coronary artery. On the other hand, a retroaortic course of the left coronary artery is most frequently (but not always) extramural and clinically benign.

From another coronary artery: there might be a single origin for the coronary arteries from the aortic root or even a double orifice for the coronary artery, but with an anomalous left anterior descending coronary artery originating from the right coronary artery and the left facing sinus giving only origin to the circumflex coronary artery.

From an additional coronary ostium: sometimes there are three coronary artery ostia, because either the conal branch of the right coronary artery originates separately from the right sinus of Valsalva, or because the left anterior descending and circumflex coronary arteries arise separately from the left sinus instead of from the main common coronary trunk.

▌ Anomalous course of a coronary artery.

Intramural course: defined as the coronary artery running in the wall of the aorta, sharing an adventitial origin.

Intramyocardial course (myocardial bridging): defined as an epicardial segment of a coronary artery that courses through the myocardium. The fact that such bridges are reported in >1% of the general population suggests that they may be a normal benign

variant. Therefore, only "severe" myocardial bridges (whose criteria are not well defined) leading to angina pectoris, myocardial ischemia or infarction are counted as pathological entities.

■ **Atresia of a coronary artery orifice:** several variations are possible, although very rare:
- atresia of the origin of the main trunk of the left coronary artery,
- atresia or the origin of the left anterior descending coronary artery,
- atresia of the origin of the circumflex artery,
- atresia of the origin of the right coronary artery.

■ **Coronary artery fistula:** a coronary artery fistula consists of single or multiple communication(s) between a normally distributed coronary artery or its branches, and either a cardiac cavity (= coronary-cameral fistula) or any segment of the systemic or pulmonary circulation (= coronary arteriovenous fistula); coronary artery fistula from either the right (60% of the cases) or left coronary artery (35%) or both coronary arteries (5%) is in 90–92% of patients connected to the right side of the heart, but it may be connected to one of the following: pulmonary artery, right ventricle, right atrium, coronary sinus, superior vena cava, pulmonary vein, left atrium, left ventricle, multiple sites. Congenital coronary artery fistulas may be associated (20 to 45% of cases) with a congenital heart defect.

■ **Anomalous coronary artery associated with a congenital heart defect:** coronary anomalies may be associated with several other congenital heart defects, most notably transposition of the great arteries, tetralogy of Fallot and pulmonary atresia.

■ **Associated anomalies**

Ventricular septal defect, tetralogy of Fallot, pulmonary atresia, truncus arteriosus, aorto-pulmonary window, transposition of the great arteries, congenitally corrected transposition of the great arteries (= double discordance), double-chambered right ventricle, aortic valve disease, supravalvular aortic stenosis (with Williams syndrome), hypoplastic left heart syndrome, aortic coarctation.

Particularly important is the potential association of an anomalous origin of the left coronary artery from the pulmonary artery with patent ductus arteriosus or aortopulmonary window: even if this combination is extremely rare, there are reports of death after closure of the ductus arteriosus or aortopulmonary window. Atresia of a coronary artery orifice is more frequently associated with supravalvular aortic stenosis and anomalies of the aortic or truncal valve, where excess tissue can obstruct the coronary orifice, or where the angle of origin of the coronary artery produces a valve-like obstruction. Quadricuspid aortic valves can be associated with single coronary ostium, and displacement of the left or right coronary orifice.

■ **Surgical options**

■ **Anomalous origin of the left coronary artery from the pulmonary artery:**
- ligation,
- end-to-side anastomosis of the left subclavian artery or the internal mammary artery (= thoracic artery) to the anomalous coronary artery,
- Takeuchi procedure (= intrapulmonary baffling technique),
- reimplantation,
- heart transplant.

■ **Anomalous origin of a coronary artery from the wrong aortic sinus:** the coronary artery with anomalous origin from a wrong sinus, frequently with an intramural segment, is moved to the appropriate sinus without unroofing. An alternative technique consists of a coronary artery bypass graft, preferably

with implantation of the internal mammary artery (= thoracic artery) to the anomalous coronary artery. In the presence of compression of the anomalous coronary artery between the aorta and pulmonary artery, a feasible surgical technique consists of transection of the main pulmonary artery at the level of its bifurcation, patch closure of the distal opening and reimplantation of the main pulmonary artery to the left pulmonary artery branch. This technique allows for separation of the main pulmonary artery from the aorta with elimination (or at least reduction) of coronary artery compression.

∎ **Coronary artery fistula:** through a median sternotomy, the feeding artery of the coronary artery fistula, its course and site of insertion are identified. In rare cases where the fistula is a terminal coronary artery, surgical occlusion by means of a direct ligature can be performed without cardiopulmonary bypass. In the vast majority of patients, the surgical procedure requires cardiopulmonary bypass and includes opening of the chamber where the anomalous fistula is draining, identification of the fistula, and suture of the anomalous coronary connection; large aneurysms may require surgical resection.

∎ **Atresia of a coronary artery orifice:** angioplasty of the origin of a coronary artery is the surgical technique used to treat the atresia of a coronary artery orifice, or to enlarge the coronary artery main stem in the presence of left main coronary artery atresia. Enlargement can be obtained on cardiopulmonary bypass with an autologous saphenous vein or pericardium patch, or with a PTFE patch.

∎ **Pre-operative information**

Since in children with anomalous coronary arteries, the incidence of wrong diagnosis with conventional coronary angiography is reported to be as high as 50%, noninvasive techniques (echocardiography, CT and MR angiography) are considered more reliable; the favored modalities are transthoracic echocardiography in children and multidetector CT in teenagers and adults. The recent improvements of multidetector row CT for cardiac imaging, particularly with regard to spatial and temporal resolution and sophisticated ECG gating, allow motion-free, fast, accurate, detailed, contrast-enhanced cardiac imaging, offering a noninvasive alternative diagnostic tool, useful also to delineate abnormal origin and branching of the coronary arteries. However, the elevated heart rate in small children still represents a major technical limit.

The presence of a "malignant" right coronary artery can be simulated by motion artifacts in front of the aortic root imitating an anomalous right coronary artery originating from the left posterior sinus of Valsalva. These artifacts can be avoided by using retrospective ECG gating (Fig. 3.24.1). However, the use of ionizing radiation and potentially nephrotoxic agents may limit its use particularly in small children.
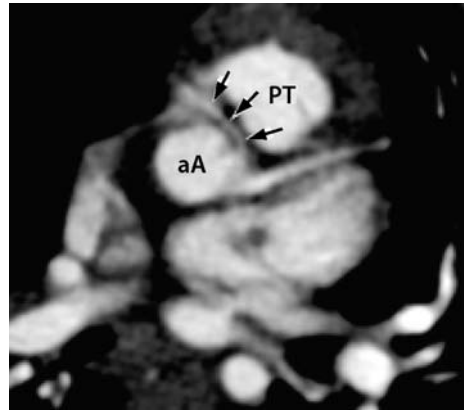
Fig. 3.24.1. Anomalous right coronary artery. CT scan oblique axial view showing the anomalous origin of the right coronary artery from the left aortic sinus, with course between the great arteries (arrow) (*aA* ascending aorta, *PT* pulmonary trunk) (reproduced with permission from Goo HW, Park IS, Ko JK, Kim YH, Seo DM, Yun TJ, Park JJ, Yoon CH (2003) CT of congenital heart disease: normal anatomy and typical pathologic conditions. Radiographics 23:S147–165)

Coronary MR angiography places particularly high demands on planning, spatial resolution, high signal-to-noise ratio, and precise cardiac and respiratory motion correction. However, recent advances in hardware, MRI sequences, and motion detection techniques allow coronary MR angiography that includes volumetric acquisition of the entire heart as well as imaging of the arterial walls within a clinically acceptable scan time to be performed. As a tomographic imaging technique, MR angiography allows 3-dimensional reconstruction and omni-directional visualization of an anomalous coronary artery origin and course, thereby eliminating some problems of selective traditional coronarography. In particular, MR angiography facilitates the differential diagnosis of "interarterial" and "intraseptal" coronary artery courses, which are very important for prognostic evaluation.

The spatial resolution of MR angiography is satisfactory in defining the course of the coronary arteries but remains limited in defining the detailed anatomy of the critically important proximal ectopic arteries, particularly in small children, where the intramural course and degree of compression inside the aortic wall can only be guessed at. Nonetheless, because of its 3-dimensional visualization abilities, MRI can clarify the acuity of the proximal coronary artery origin (tangential take-off), its location at the level of the sinotubular junction or above it, and the sinus of origin. By itself, the presence of a coronary artery with tangential origin does not necessarily mean a stenotic effect. However, it is usually associated with an intramural course, which is clearly correlated with obstruction.

Furthermore, in addition to anatomical data, cardiac MRI allows the functional consequences of coronary artery anomalies to be evaluated: the amount of shunt and flow in the case of a coronary artery fistula, and the global and regional function of the left ventricle. Myocardial ischemia can be detected by means pharmacological stress testing either with adenosine or dobutamine. Finally by means of gadolinium delayed enhancement, fibrotic areas can be detected as well.

The MRI protocol proposed for detection of coronary artery anomalies is the following:

- 3-plane localizing images,
- 2-dimensional axial Time-of-flight Angiography (see appendix in the "Introduction"),
- axial fast spin echo and oblique sequences at the level of aortic root followed by a series of oblique images perpendicular to the axial plane, with slice thickness 3–4 mm (Fig. 3.24.2),
- ECG-gated cine steady-state free precession sequences in 2-chamber, 4-chamber planes, and ventricular short axis for the quantitative assessment of both ventricular dimensions, function and stroke volume as illustrated in the appendix of the "Introduction",
- fat suppressed 3-dimensional steady-state free precession pulse sequence, (breath hold for small slab, or free breathing with Navigator to allow a larger slab) parallel to the plain of each main coronary artery (Fig. 3.24.3),
- gadolinium-enhanced 3-dimensional MR angiography,
- ECG-gated phase velocity contrast MRI sequences perpendicular to the main pulmonary artery, ascending aorta and coronary fistula (when required),


Fig. 3.24.2. Intramural left coronary artery. MRI axial fast spin echo showing intramural course of the left coronary artery (arrowhead) (*AO* aorta)
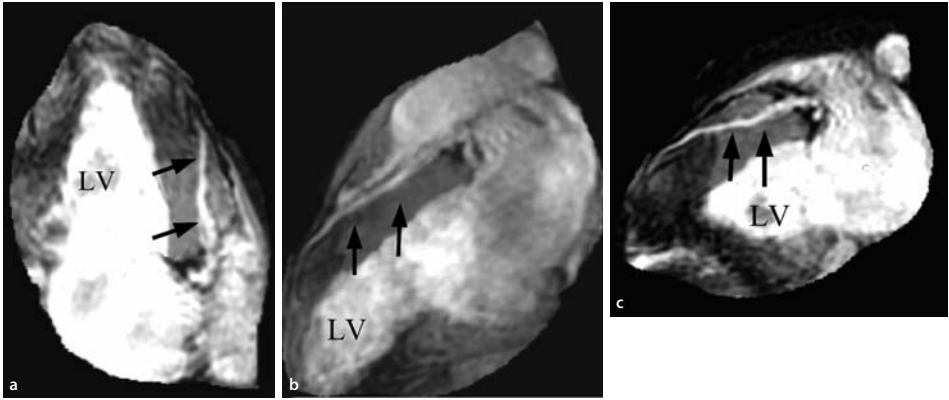
Fig. 3.24.3. Myocardial bridging. MRI 3-dimensional steady-state free precession (**a, b** and **c**) showing myocardial bridging of the left anterior descending coronary artery (arrow) in a patient with symptomatic hypertrophic cardiomyopathy (*LV* left ventricle)
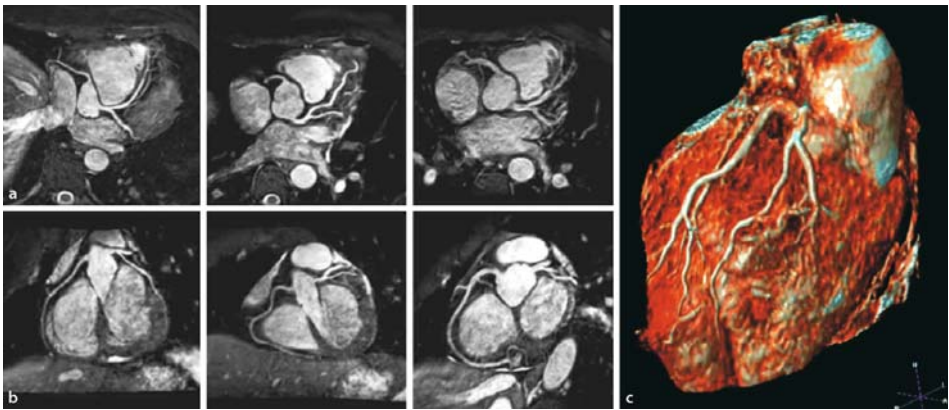
Fig. 3.24.4. MRI with sensitivity encoding (SENSE) technique. Whole heart coronary magnetic resonance angiography (CMRA) in healthy volunteers. **a** The angiograms of the left coronary artery system (LM/LAD/LCX, upper row) and **b** the right coronary artery (RCA, lower row) were reformatted retrospectively from a volumetric whole heart data set. A volume rendered view is shown in **c**. A steady-state free precession (SSFP) sequence with an additional T_2 preparation pulse was employed for optimal contrast. To maintain a clinically acceptable scan time, sensitivity encoding (SENSE) in concert with partial Fourier encoding was employed, resulting in a total scan time of 4 min during free breathing. A nearly isotropic resolution ($1.3 \times 1.3 \times 1.5$ mm^3) was obtained (reproduced with permission from Stehning C, Boernert P, Nehrke K (2007) Advances in coronary MR angiography from vessel wall to whole heart imaging. Magn Reson Med Sci 6:157–170)

▪ post-gadolinium delayed myocardial enhancement may be used to evaluate potential presence of fibrotic tissue,

▪ more recently, the use of 32-channel coil sensitivity encoding (SENSE) permits whole heart MR angiography to be performed (Fig. 3.24.4).

Pharmacological stress testing either with adenosine or dobutamine is increasingly being incorporated into the MRI protocol in patients with suspected myocardial ischemia.

▪ Potential complications

▪ Anomalous origin of the left coronary artery from the pulmonary artery.

Takeuchi procedure: potential complications include residual or recurrent stenosis of the new coronary artery channel, with subsequent myocardial ischemia, as well as baffle leaks, residual or recurrent supravalvular pulmonary stenosis, due to the obstruction created by the space occupied by the new coronary artery channel constructed inside the main pulmonary artery. Another potential complication is injury to the aortic valve when creating the aortopulmonary window.

Reimplantation: low cardiac output with hemodynamic instability can complicate the post-operative period, particularly in patients with severely compromised myocardial function and/or operated on after late referral. Another potential complication is the obstruction of the reimplanted coronary artery, due to excessive tension, kinking or twisting of the coronary artery, with potential subsequent myocardial ischemia or infarction. Ventricular arrhythmias can accompany poor ventricular function and severe ventricular dilatation.

Angioplasty of the origin of a coronary artery: despite patch enlargement of the orifice of a coronary artery generally providing adequate coronary artery perfusion, residual or recurrent coronary artery stenosis can require re-operation, in most cases with a cor-

onary artery bypass graft accomplished with the internal thoracic (=mammary) artery.

▪ Anomalous origin of a coronary artery from the wrong aortic sinus: inadequate coronary artery perfusion can persist after surgery, as well as malfunctioning of the aortic valve, damaged by the coronary artery reimplantation.

▪ Coronary artery fistulas: myocardial ischemia or infarction, recurrence of the coronary artery fistula.

▪ Atresia of a coronary artery orifice: myocardial ischemia or infarction.

▪ Post-operative follow-up

The aim and information requested for the post-operative evaluation of anomalous coronary artery are similar that seen in the pre-operative setting, paying attention to individualize each investigation to the previously performed operative procedure and to the current clinical condition of the patient.

▪ References

Alphonso N, Anagnostopoulos PV, Nölke L, Moon-Grady A, Azakie A, Raff GW, Karl TR (2007) Anomalous coronary artery from the wrong sinus of Valsalva: a physiologic repair strategy. Ann Thorac Surg 83:1472–1476

Angelini P (2007) Coronary artery anomalies: an entity in search of an identity. Circulation 115:1296–1305

Aris A, Carreras F, Leta R, Fuentes M (2005) Diagnosis of anomalous origin of the circumflex artery by multidetector CT. Eur J Cardiothorac Surg 27:918

Barriales-Villa R, Moris C (2001) Usefulness of helical computed tomography in the identification of the initial course of coronary anomalies. Am J Cardiol 88:719

Bruder O, Sabin GV, Barkhausen J (2005) Magnetic resonance imaging of anomalous origin of the left coronary artery from the pulmonary artery (Bland-White-Garland syndrome). Heart 91:656

Bunce NH, Lorenz CH, Keegan J, Lesser J, Reyes EM, Firmin DN, Pennell DJ (2003) Coronary artery anomalies: assessment with free-breathing three-

dimensional coronary MR angiography. Radiology 227:201–208

Cademartiri F, Mollet N, Nieman K, Szili-Torok T, de Feyter PJ (2004) Images in cardiovascular medicine. Right coronary artery arising from the left circumflex demonstrated with multislice computed tomography. Circulation 109:e185–186

Cademartiri F, Runza G, Luccichenti G, Galia M, Mollet NR, Alaimo V, Brambilla V, Gualerzi M, Coruzzi P, Midiri M, Lagalla R (2006) Coronary artery anomalies: incidence, pathophysiology, clinical relevance and role of diagnostic imaging. Radiol Med 111:376–391

Casolo G, Del Meglio J, Rega L, Manta R, Margheri M, Villari N, Gensini G (2005) Detection and assessment of coronary artery anomalies by three-dimensional magnetic resonance coronary angiography. Int J Cardiol 103:317–322

Chen SJ, Lee WJ, Lin MT, Liu KL, Wang JK, Lue HC (2007) Coronary artery diameters in infants and children with congenital heart disease as determined by computed tomography. Am J Cardiol 100:1696–1701

Chiurlia E, Ligabue G, Ratti C, Modena MG (2003) Type IV dual left anterior descending coronary artery evaluated using multislice computed tomography: anatomy of a rare coronary anomaly. Ital Heart J 4:900–901

Coles DR, Wilde P, Baumbach A (2004) An anomalous right coronary artery shown by multislice CT coronary angiography. Heart 90:1188

Corno AF, Pierli C, Biagioli B, Lisi G, Grossi A (1988) Anomalous origin of the left coronary artery from an aorto-pulmonary window. J Thorac Cardiovasc Surg 96:669–671

Corno AF (2000) Surgery for congenital heart disease. Curr Opinion Cardiol 15:238–243

Culham JAG (1997) Abnormalities of the coronary arteries. In: Freedom RM, Mawson JB, Yoo SJ, Benson LN (eds) Congenital Heart Disease: Textbook of Angiocardiography. Futura Publishing, Armonk NY, pp 849–867

Deibler AR, Kuzo RS, Vohringer M, Page EE, Safford RE, Patron JN, Lane GE, Morin RL, Gerber TC (2004) Imaging of congenital coronary anomalies with multislice computed tomography. Mayo Clin Proc 79:1017–1023

Dewey M, Teige F, Stangl K (2007) Split coronary artery seen with computed tomography and magnetic resonance imaging. Heart 93:538

Eicken A, Vogt M, Marinovic B, Stern H (2007) Aberrant origin of the left coronary artery from the right-facing sinus of Valsalva with intramural course: preoperative and postoperative imaging. Heart 93:362

Gerber TC, Kuzo RS, Safford RE (2002) Computed tomographic imaging of anomalous coronary arteries. Circulation 106:67

Ghersin E, Litmanovich D, Ofer A, Lessick J, Dragu R, Rispler S, Beyar R, Engel A (2004) Anomalous origin of right coronary artery: diagnosis and dynamic evaluation with multidetector computed tomography. J Comput Assist Tomogr 28:293–294

Girish R (2006) Images in cardiology. Multislice cardiac computed tomographic images of anomalous origin of the left coronary artery from the pulmonary artery (ALCAPA). Heart 92:2

Goitein O, Lacomis JM (2005) Myocardial bridging: non-invasive diagnosis with multidetector CT. J Comput Assist Tomogr 29:238–240

Goo HW, Park IS, Ko JK, Kim YH, Seo DM, Yun TJ, Park JJ (2005) Visibility of the origin and proximal course of coronary arteries on non-ECG-gated heart CT in patients with congenital heart disease. Pediatr Radiol 35:792–798

Hague C, Andrews G, Forster B (2004) MDCT of a malignant anomalous right coronary artery. Am J Roentgenol 182:617–618

Hong C, Woodard PK, Bae KT (2004) Congenital coronary artery anomaly demonstrated by three dimensional 16 slice spiral CT angiography. Heart 90:478

Horisaki T, Yamashita T, Yokoyama H, Urasawa K, Kitabatake A (2003) Three-dimensional reconstruction of computed tomographic images of anomalous origin of the left main coronary artery from the pulmonary trunk in an adult. Am J Cardiol 92:898–899

Ichikawa M, Komatsu S, Asanuma H, Iwata A, Ishito T, Hirayama A, Lim YJ, Kodama K, Mishima M (2005) Acute myocardial infarction caused by "malignant" anomalous right coronary artery detected by multidetector row computed tomography. Circ J 69:1564–1567

Karadag B, Spieker LE, Wildermuth S, Boehm T, Corti R (2005) Cardiac arrest in a soccer player: a unique case of anomalous coronary origin detected by 16-row multislice computed tomography coronary angiography. Heart Vessels 20:116–119

Katoh M, Wildberger JE, Gunther RW, Buecker A (2005) Malignant right coronary artery anomaly simulated by motion artefacts on MDCT. Am J Roentgenol 185:1007–1010

Khanna A, Torigian DA, Ferrari VA, Bross RJ, Rosen MA (2005) Anomalous origin of the left coronary artery from the pulmonary artery in adulthood on CT and MRI. Am J Roentgenol 185:326–329

Khouzam R, Marshall T, Lowell D, Siler JR (2003) Left coronary artery originating from right sinus of Valsalva with diagnosis confirmed by CT: a case report. Angiology 54:499–502

Kim CK, Park CB, Jin U, Lee BY, Song KS (2005) Evaluation of unroofing procedure of anomalous origin of right coronary artery from the left sinus of Valsalva between aorta and pulmonary trunk by multidetector computed tomography. J Comput Assist Tomogr 29:752–755

Komocsi A, Simor T, Toth L, Szabados S, Magel F, Printer T, Aradi D, Konyi A, Horvath IG, Papp L (2007) Magnetic resonance studies in management of adult cases with Bland-Whire-Garland syndrome. Int J Cardiol 122:e8–11

Lee J, Choe YH, Kim HJ, Park JE (2003) Magnetic resonance imaging demonstration of anomalous origin

of the right coronary artery from the left coronary sinus associated with acute myocardial infarction. J Comput Assist Tomogr 27:289–291

Lessick J, Kumar G, Beyar R, Lorber A, Engel A (2004) Anomalous origin of a posterior descending artery from the right pulmonary artery: report of a rare case diagnosed by multidetector computed tomography angiography. J Comput Assist Tomogr 28:857–859

Lembcke A, Dübel HP, Elgeti T, Rutsch W (2007) Multislice spiral computed tomography of a malignant single coronary artery. Eur J Cadiothorac Surg 32: 801

Li W, Ferret C, Henein M (2003) Images in cardiovascular medicine. Anomalous coronary arteries by electron beam angiography. Circulation 107:2630

Lumia D, Carrafiello G, Laganá D, Caní A, Ghiringhelli S, Salerno-Uriatre JA, Fugazzola C (2007) MDCT coronary angiography for diagnosis of anomalous origin right coronary artery: a case report. Emerg Radiol 14:237–240

Manghat NE, Morgan-Hughes GJ, Marshall AJ, Roobottom CA (2005) Multidetector row computed tomography: imaging congenital coronary artery anomalies in adults. Heart 91:1515–1522

Mavrogeni S, Spargias K, Karagiannis S, Kariofilis P, Cokkinos DD, Douskou M, Cokkinos DV (2006) Anomalous origin of right coronary artery: magnetic resonance angiography and viability study. Int J Cardiol 109:195–200

Mesurolle B, Qanadly SD, Mignon F, Lacombe P (2005) Anomalous origin of the left coronary artery arising from the pulmonary trunk. Am J Roentgenol 185: 326–329

Mohrs OK, Nowak B, Fach WA, Kober G, Voigtlaender T (2004) Assessment of nonviable myocardium due to Bland-White-Garland syndrome using contrast-enhanced MRI. J Cardiovasc Magn Reson 6:941–944

Montaudon M, Latrabe V, Iriart X, Caix P, Laurent F (2007) Congenital coronary arteries anomalies: review of the literature and multidetector computed tomography (MDCT)-appearance. Surg Radiol Anat 29:343–345

Ou P, Iserin F, Vouhé P, Bonnet D (2006) Anomalous origin of the left coronary artery from the right aortic sinus: surgery based on diagnosis by 64-slice CT. Eur J Cardiothorac Surg 29:610

Parga JR, Ikari NM, Bustamante LN, Rochitte CE, de Avila LF, Oliveira SA (2004) Case report: MRI evaluation of congenital coronary artery fistulae. Br J Radiol 77:508–511

Post JC, van Rossum AC, Bronzwaer JG, de Cock CC, Hofman MB, Valk J, Visser CA (1995) Magnetic resonance angiography of anomalous coronary arteries: a new gold standard for delineating the proximal course? Circulation 92:3163–3171

Rathi VK, Mikolich B, Patel M, Doyle M, Yamrozik J, Biederman RW (2005) Coronary artery fistula; non-invasive diagnosis by cardiovascular magnetic resonance imaging. J Cardiovasc Magn Reson 7:723–725

Ropers D, Gehling G, Pohle K, Maeffert R, Regenfus M, Moshage W, Schuster P, Daniel WG, Achenbach S (2002) Images in cardiovascular medicine. Anomalous course of the main or left anterior descending coronary artery originating from the right sinus of Valsalva: identification of four common variations by electron beam tomography. Circulation 106:67

Said SA, Hofman MB, Beek AM, van der Werf T, van Rossum AC (2007) Feasibility of cardiovascular magnetic resonance of angiographically diagnosed congenital solitary coronary artery fistulas in adults. J Cardiovasc Magn Reson 9:575–583

Sahn DJ, Vick GW (2001) Review of new techniques in echocardiography and magnetic resonance imaging as applied to patients with congenital heart disease. Heart 86(Suppl II):41–53

Salm LP, Bax JJ, Lamb HJ, Hazekamp MG, de Roos A, van der Wall EE, Vliegen HW (2003) Evaluation of rerouting surgery of a coronary artery anomaly by magnetic resonance angiography. Ann Thorac Surg 76:1748

Sato Y, Inoue F, Matsumoto N, Tani S, Takayama T, Yoda S, Kunimasa T, Ishii N, Uchiyama T, Saito S, Tanaka H, Furuhashi S, Takahashi M, Koyama Y (2005) Detection of anomalous origin of the coronary artery by means of multislice computed tomography. Circ J 69:320–324

Schmitt R, Froehner S, Brunn J, Wagner M, Brunner H, Cherevatyy O, Gietzen F, Christopoulos G, Kerber S, Fellner F (2005) Congenital anomalies of the coronary arteries: imaging with contrast-enhanced, multidetector computed tomography. Eur Radiol 1110–1121

Seguchi O, Terashima M, Awano K (2003) Multiple coronary artery fistulas visualised by three dimensional computed tomography. Heart 89:1381

Sevrukov A, Aker N, Sullivan C, Jelnin V, Candipan RC (2002) Identifying the course of an anomalous left coronary artery using contrast-enhanced electron beam tomography and three-dimensional reconstruction. Catheter Cardiovasc Interv 57:532–536

Stehning C, Boernert P, Nehrke K (2007) Advances in coronary MRA from vessel wall to whole heart imaging. Magn Reson Med Sci 6:157–170

Su JT, Krishnamurthy R, Chung T, Vick GW, Kovalchin JP (2007) Anomalous right coronary artery from the pulmonary artery: nonivasive diagnosis and serial evaluation. J Cardiovasc Magn Reson 9:57–61

▌ Definition

Double outlet right ventricle defines a heterogeneous group of cardiac malformations unified by an abnormal ventriculoarterial connection. General agreement about the definition of double outlet right ventricle is when both great arteries, or one great artery and more than half of the other originates from the right ventricle. However, as clearly demonstrated with noninvasive investigations, this definition could be misleading due to the fact that the ventriculoarterial connections, lying on different planes, could be visualized in different ways, leading to different results, depending upon the orientation plan of the examination, independent of whether echocardiography, CT scan or MRI is used (Fig. 3.25.2). According to Yves Lecompte, the classification and terminology of this complex group of patients with anomalous ventriculoarterial connection is less important than the precise pre-operative definition of the anatomic criteria useful to determine the best surgical approach. The most general definition of "malposition of the great arteries with ventricular septal defect" should be used. Nevertheless the categorization of patients with double outlet right ventricle is necessary to compare the results of different surgical treatments.

A morphological feature characteristic of the double outlet right ventricle is absence of the normal fibrous continuity between the mitral and semilunar valves (either aortic valve in the presence of ventriculoarterial concordance, or pulmonary valve in the presence of ventriculoarterial discordance), referred to the presence of a subaortic or subpulmonary conus, respectively.

The relationship between the great arteries may vary and many relative positions have been reported; more frequently they are side by side and parallel, with the aortic valve positioned to the right of the pulmonary valve.

Patients with double outlet right ventricle have been categorized accordingly to:

The type of the ventriculoarterial connection:
▌ concordant (85%): the pulmonary artery originates entirely from the right ventricle,
▌ discordant (15%): the aorta originates entirely from the right ventricle.

The position of the associated ventricular septal defect:
▌ subaortic ventricular septal defect (50%),
▌ subpulmonary ventricular septal defect (30%),
▌ doubly-committed ventricular septal defect (immediately underneath the semilunar valves) (10%),
▌ noncommitted (remote) ventricular septal defect (far from both the semilunar valves) (10%).

The type of pulmonary blood flow:
▌ restricted (= with pulmonary stenosis),
▌ unrestricted (= without pulmonary stenosis).

The most frequent combination is *double outlet right ventricle with concordant ventriculoarterial connection, subaortic ventricular septal defect and obstruction to the pulmo-*

nary outflow tract (so-called tetralogy of Fallot-type). Typical cardiac anomalies associated with this type of double outlet right ventricle are mitral stenosis and subaortic obstruction, as well as anomalous attachments (straddling) of the anterior and septal leaflets of the tricuspid valve.

The second most frequent type is *double outlet right ventricle with discordant ventriculoarterial connection and subpulmonary ventricular septal defect, without obstruction to the pulmonary outflow tract (so-called Taussig-Bing malformation)*. Typical cardiac anomalies associated to this type of double outlet right ventricle are straddling mitral valve, subaortic obstruction and aortic coarctation.

Another combination is *double outlet right ventricle with concordant ventriculoarterial connection and subaortic ventricular septal defect, without obstruction to the pulmonary outflow tract*. Typical cardiac anomalies associated with this type of double outlet right ventricle are straddling mitral valve and aortic coarctation.

More rare are the combinations of *double outlet right ventricle with doubly committed or with noncommitted (remote) ventricular septal defect*. In patients with noncommitted (remote) ventricular septal defect, the defect is frequently of muscular or inlet (atrioventricular) type, therefore distant from both the semilunar valves. There is ventriculoarterial concordance, and pulmonary stenosis is very rare.

Associated anomalies

Dextrocardia, juxtaposition of left auricular appendages, total anomalous pulmonary venous connection, anomalous systemic venous connections, cor triatriatum, mitral stenosis, cleft of the mitral valve, common atrioventricular valve, straddling mitral and/or tricuspid valve, superoinferior ventricles with or without criss-crossing atrioventricular connections, multiple ventricular septal defects, hypoplastic left ventricle, left ventricular outflow tract obstruction, discrete subaortic stenosis, aortic coarctation, aortic

arch interruption, absent pulmonary valve, absent left pulmonary artery, and ectopia cordis have all been reported in association with double outlet right ventricle.

The origin and course of the coronary arteries are associated with the relationship between the aorta and pulmonary artery. Several variations are described, including anomalous origin of the right coronary artery from the left main coronary artery, duplication of the left anterior descending coronary artery, anomalous origin of the left anterior descending coronary artery from the right coronary artery, anomalous origin of the left circumflex artery from the right coronary artery, and single right or single left coronary artery as the most frequent anomalies.

▪ Surgical options

▪ Palliation:

Modified Blalock-Taussig shunt can be considered in neonates with *double outlet right ventricle with concordant ventriculoarterial connection, subaortic ventricular septal defect and obstruction to the pulmonary outflow tract (so-called tetralogy of Fallot-type)*.

Pulmonary artery banding can be considered for *double outlet right ventricle with concordant ventriculoarterial connection and subaortic ventricular septal defect, without obstruction to the pulmonary outflow tract*.

▪ Repair: according to each different type of morphology, several surgical techniques have been reported, referring to one of the following principles:
- *intraventricular repair* connecting the left ventricle to the aorta and the right ventricle to the pulmonary artery,
- *arterial switch* operation with closure of the ventricular septal defect by a prosthetic patch connecting the left ventricle to the neoaorta,
- *univentricular type of repair*, with end-to-side superior vena cava to pulmonary ar-

tery anastomosis (= bidirectional Glenn) followed by total cavopulmonary connection (= modified Fontan procedure).

Because the large variability of intracardiac morphologies, with various associated cardiac lesions, and the different surgical experiences, several alternative surgical options are available for each single patient, depending on the match of the individual patient with the individual surgeon.

■ **Intraventricular repair:** there are different types of intraventricular repair. In all of them the left ventricle is connected to the aorta and the right ventricle to the pulmonary artery, either directly or with the interposition of a conduit.

Intraventricular tunnel repair, suitable for the more simple type of *double outlet right ventricle with concordant ventriculoarterial connection and subaortic ventricular septal defect*, can be performed either through right atriotomy (rarely) or right ventriculotomy. Right ventriculotomy allows easier evaluation of the adequate shape and positioning of the prosthetic patch needed to connect the left ventricle with the aorta. The ventricular size and position, combined with the relationship between the diameter of the aortic valve and the distance between the tricuspid and pulmonary valve, dictate the need for enlargement of the tunnel between the left ventricle and the aorta. When needed, the ventricular septal defect is enlarged by an anterior incision, with muscular resection. The prosthetic material used to create the intraventricular tunnel is generally a prosthetic tubular prosthesis (PTFE, Dacron) about 20% larger than the aortic diameter, cut at a length equal to the distance between the anterior edge of the ventricular septal defect and the aortic annulus. Two-thirds of the entire circumference of the tubular prosthesis are used, in a manner leaving an unobstructed left ventricle to aorta tunnel, but at the same time avoiding the potential bulging of the patch to obstruct the right ventricular outflow tract.

In the presence of severe *obstruction to the pulmonary outflow tract,* a transannular patch or a biological valved conduit implanted between the right ventriculotomy and the pulmonary artery are used to relieve the obstruction. An alternative option is the Lecompte procedure (see below for details).

In *double outlet right ventricle with discordant ventriculoarterial connection and subpulmonary ventricular septal defect, without obstruction to the pulmonary outflow tract (so-called Taussig-Bing malformation)*, the intraventricular tunnel is more complicated to design and accomplished. In the *Kawashima technique,* the intraventricular tunnel is positioned posterior to the orifice of the pulmonary valve, if there is enough distance between the tricuspid and pulmonary valves. If the distance between the tricuspid and pulmonary valves is inadequate, the intraventricular tunnel has to remain anterior to the orifice of the pulmonary valve. In both cases, the ventricular septal defect needs to be enlarged by anterior resection of the infundibular septum.

In patients with *double outlet right ventricle with discordant ventriculoarterial connection and obstruction to the pulmonary outflow tract,* the best surgical option is the *Lecompte procedure (or REV = Réparation à l'Etage Ventriculaire)*. After right ventriculotomy and infundibular resection, the left ventricle is connected to the aorta by closure of ventricular septal defect with a straight patch; after transection and shortening of the ascending aorta and transfer of the pulmonary artery bifurcation anterior to the aorta (*Lecompte maneuver*), the right ventricle-to-pulmonary artery continuity is obtained with reimplantation of the transected pulmonary artery directly on the right ventricle to its posterior wall, while the anterior aspect is connected to the rest of the right ventriculotomy with a monocusp pericardial patch.

■ **Arterial switch operation:** the crucial point is the surgical approach for closure of the ventricular septal defect. The possibilities

are through right atriotomy (ideal for perimembranous and inlet defects), through the aortic valve (neopulmonary valve) after resection of the aortic buttons with the orifices of the coronary arteries (ideal for outlet types of subaortic defects), or through the pulmonary valve (neoaortic valve) (ideal for the subpulmonary type of defects). The rest of the procedure is like that for the conventional arterial switch.

An alternative surgical technique is the *Bex-Nikaidoh aortic translocation*, where the aortic root, including aortic valve and coronary arteries, is isolated from the right ventricle. The pulmonary artery is transected and the area between the ventricular septal defect and the proximal stump of the transected pulmonary artery is widely incised; the left ventricle is connected to the aorta with a patch roofing the opened ventricular septal defect, while the right ventricle is connected to the transected pulmonary artery like in the Lecompte procedure.

In the Taussig-Bing type of double outlet right ventricle with aortic arch obstruction, a surgical technique recently proposed (Dr. Sano) consists of the transection of the great arteries, ductus arteriosus, descending thoracic aorta, and aortic arch with aortotomy incision from the aortic arch to the distal ascending aorta, followed by creation of an aortopulmonary window, anastomosis of the descending thoracic aorta to the posterior wall of the aortic arch, anastomosis of the neoaorta to the aortic arch with rerouting of the coronary arteries (without need for coronary arteries reimplantation), and reconstruction of the neo-right ventricular outflow tract after the Lecompte maneuver.

■ **Univentricular type of repair:** in the presence of complicated intracardiac anatomy (e.g., the presence of inlet type of noncommitted ventricular septal defect with straddling tricuspid valve, or common atrioventricular valve, or hypoplasia of the right ventricular chamber), the biventricular type of repair is either not feasible or the associated risk is too high. In these patients, the uni-

ventricular type of repair is the preferred surgical option.

In these cases the first step is a bidirectional Glenn, followed by the modified Fontan procedure, preceded or not by a pulmonary artery banding, depending upon the presence or absence of obstruction to the pulmonary blood flow.

■ Pre-operative information

As already described above, the so-called double outlet right ventricle includes a spectrum of different types of morphology, where, in the presence of normal ventricular size, the pathophysiology and the subsequent surgical treatment depend upon the spatial relationship between the ventricular septal defect and the great arteries, the morphology and length of the ventricular outlets, and the orientation of the infundibular septum. All combinations are possible, making
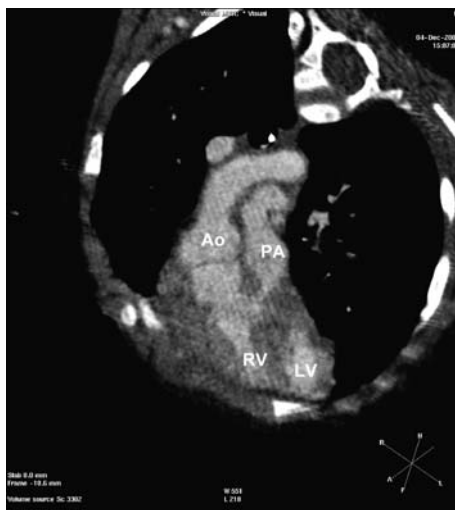
Fig. 3.25.1. Double outlet right ventricle. CT scan showing the double outlet right ventricle, ventriculoarterial discordance, ventricular septal defect (far from the aortic valve) and pulmonary stenosis (*Ao* aorta, *LV* left ventricle, *PA* pulmonary artery, *RV* right ventricle) (photograph courtesy of Dr. Mohamed Tawil)

any classification useless and even misleading with regard to the decision-making process among the available surgical options.

Echocardiography is certainly the first and the best tool to define the anatomy in children with double outlet right ventricle, and it is fundamental in planning the surgical repair; CT scan (Fig. 3.25.1) and/or MRI (Fig. 3.25.2) are rarely required. Exceptions include patients with complex anomalies of the aortic arch and/or pulmonary arteries, aortopulmonary collaterals, anomalous systemic or pulmonary venous connections not completely defined by echocardiography.

However, as echocardiography is limited in the assessment of all the cardiac structures from a single approach, sometimes it might be difficult to determine the 3-dimensional reconstruction of the complex ventricular septal defect/outlets/great arteries. Cardiac MRI is particularly attractive for the development of stereolithographic models able to create accurate and realistic 3-dimensional models for the pre-operative assessment of such complex congenital heart defects. A virtual incision-making tool allowing arbitrary incisions to be made on 3-dimensional MRI reconstructions has already been experimentally developed, but is not yet commercially available.

When MRI is indicated to better delineate the spatial relationship between the ventricular septal defect and the ventricular outlets and, in some instances the aortic arch and pulmonary arteries, the MRI protocol proposed has already been described in the chapters on "Tetralogy of Fallot" and "Transposition of the great arteries", respectively. In particular cases with complex ventriculoarterial connection, it can be useful to represent the heart and great arteries on the 3 main orthogonal planes to better delineate the intraventricular morphology (Fig. 3.25.3).
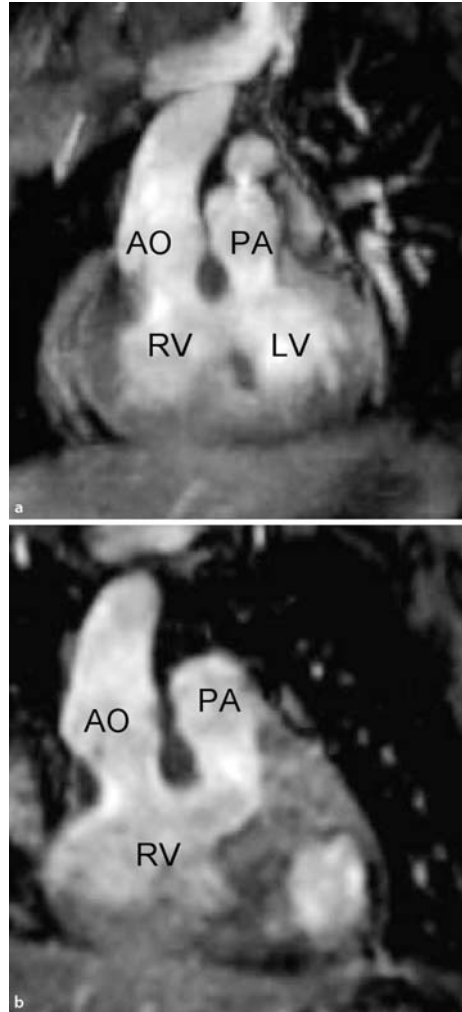
Fig. 3.25.2. Double outlet right ventricle. MR Angiography maximal intensity projection in the same patient delineating apparently different ventriculoarterial connections: **a)** the aorta seems to originate from the anterior right ventricle and the pulmonary artery from the posterior left ventricle, **b)** the plane is slightly rotated and both great arteries seem to be connected to the anterior right ventricle (*AO* aorta, *LV* left ventricle, *PA* pulmonary artery, *RV* right ventricle)
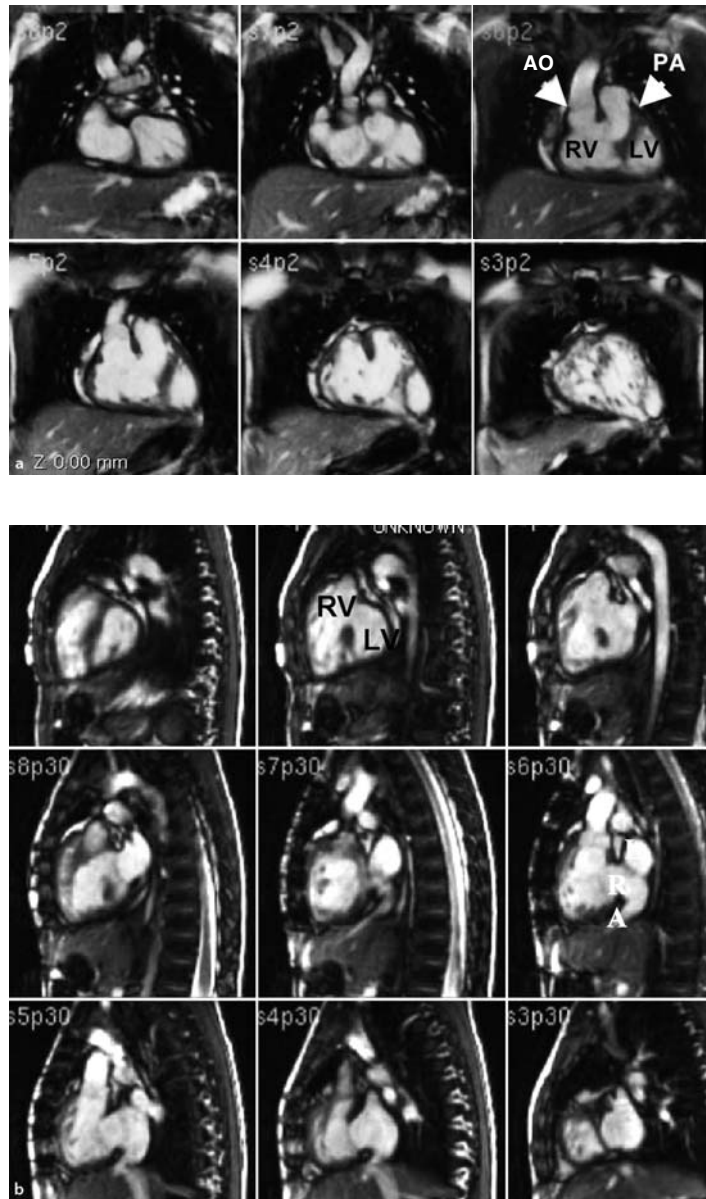
Fig. 3.25.3. Double outlet right ventricle. Cine MRI of heart and great arteries on the 3 orthogonal main planes: **a** coronal plane from posterior (upper left) to anterior (lower right), **b** sagittal plane from left (upper left) to right (lower right), and **c** axial plane from inferior (upper left) to superior (lower right). The great arteries are side-by-side; the left ventricle is hypoplastic, with left and posterior position; the left atrium is superior and left sided (*AO* aorta, *LV* left ventricle, *PA* pulmonary artery, *RV* right ventricle)
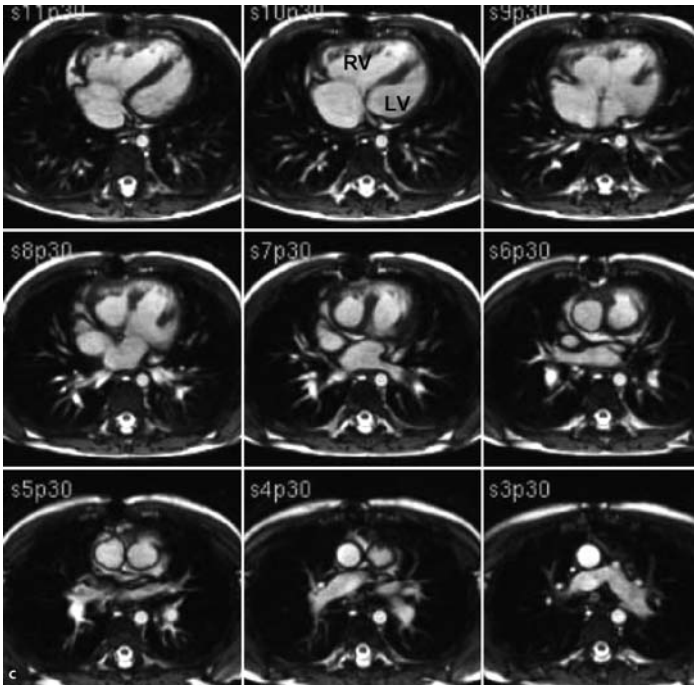
Fig. 3.25.3 c

■ Potential complications

■ **Intraventricular repair:** potential complications after intraventricular repair include residual or recurrent ventricular septal defect, residual or recurrent right and/or left ventricular outflow tract obstruction, arrhythmias, complete atrioventricular block, atrioventricular valve regurgitation.

■ **Arterial switch operation:** the most frequent complications are residual or recurrent right ventricular outflow tract obstruction, and residual or recurrent neoaortic valve regurgitation.

■ **Univentricular type of repair:** see chapter "Single ventricle".

■ Post-operative follow-up

The role of cardiac CT scan and MRI after surgery for double outlet right ventricle increases in adult patients when their acoustic window for echocardiography becomes more limited. The examination strategy is tailored to the underlying morphology and the type of surgery performed. Patients with a "tetralogy of Fallot type" of double outlet right ventricle repair have similar long-term course as those after repair for tetralogy of Fallot, and the CT scan and MRI protocols have already been highlighted in the related chapter. Similarly, in those with "Transposition of the great arteries or Taussig-Bing type" (see the relative chapter) of double outlet right ventricle, the post-operative is-

Fig. 3.25.5. Status post repair of double outlet right ventricle. CT scan 3-dimensional reconstruction of contrast angiography, lateral view, showing the valved conduit implanted between the right ventricle and the pulmonary artery (*AoA* aortic arch, *DTA* descending thoracic aorta, *RV* right ventricle, *VC* valved conduit) (photograph courtesy of Dr. Mohamed Tawil)

Fig. 3.25.4. Status post repair of double outlet right ventricle. **a** CT scan contrast angiography, axial projection, showing the valved conduit implanted between the right ventricle and the pulmonary artery, with a narrowing near the distal anastomosis (arrow). **b** CT scan in the same patient contrast angiography, sagittal projection, showing the valved conduit implanted end-to-side to pulmonary artery leaving open the native right ventricular outflow tract, with the measurement of the narrowing near the distal anastomosis (diameter = 5.9 mm) (*AAo* ascending aorta, *DTA* descending thoracic aorta, *LPA* left pulmonary artery, *nRVOT* native right ventricular outflow tract, *RPA* right pulmonary artery, *RV* right ventricle, *SVC* superior vena cava, *VC* valved conduit) (photographs courtesy of Dr. Mohamed Tawil)

sues are similar to those encountered after the Rastelli procedure (Figs. 3.25.4–3.25.6) or REV procedure (Figs. 3.25.7 and 3.25.8), respectively. Of course in these cases, it is very important to adapt and modify, if necessary, the investigation protocol to address morphologic and functional abnormalities specific to the individual patient; this requires on-line evaluation of the imaging data since previously unsuspected abnormalities may only be detected during the scan.
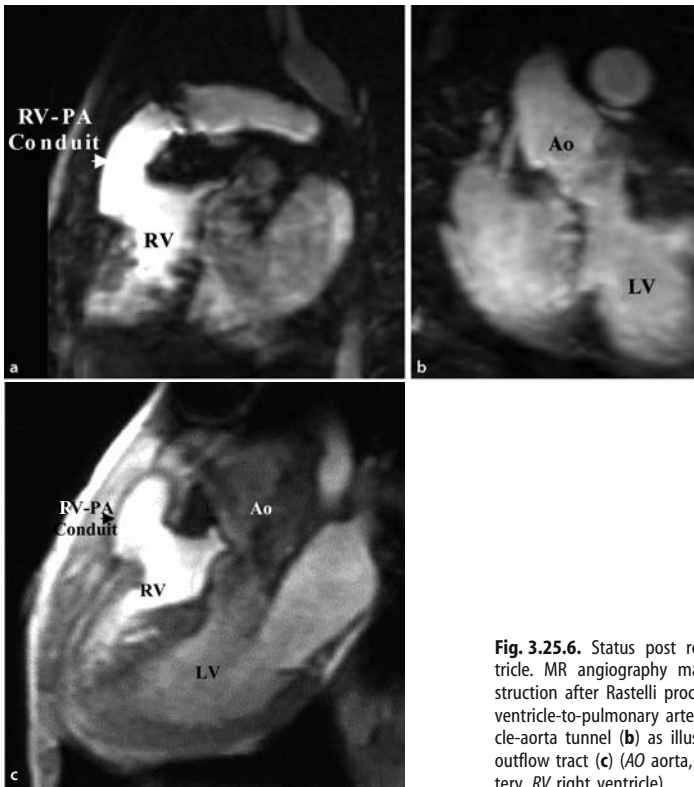
Fig. 3.25.6. Status post repair of double outlet right ventricle. MR angiography maximal intensity projection reconstruction after Rastelli procedure showing a good sized right ventricle-to-pulmonary artery conduit (**a**), and the left ventricle-aorta tunnel (**b**) as illustrated in cine MRI left ventricular outflow tract (**c**) (*AO* aorta, *LV* left ventricle, *PA* pulmonary artery, *RV* right ventricle)
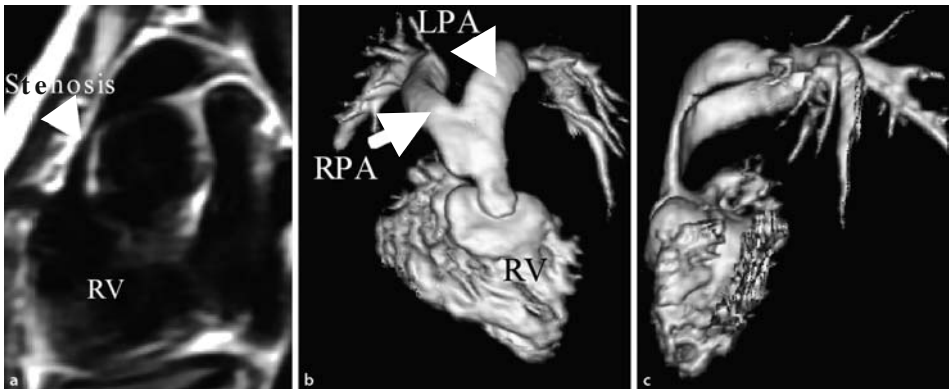
Fig. 3.25.7. Status post repair of double outlet right ventricle. Para-sagittal fast spin echo (**a**) and MR angiography volume rendering reconstruction (**b** and **c**) after REV procedure showing a severe stenosis of the right ventricular outflow tract with anterior compression by the sternum and posterior by the aorta (*LPA* left pulmonary artery, *RPA* right pulmonary artery, *RV* right ventricle)
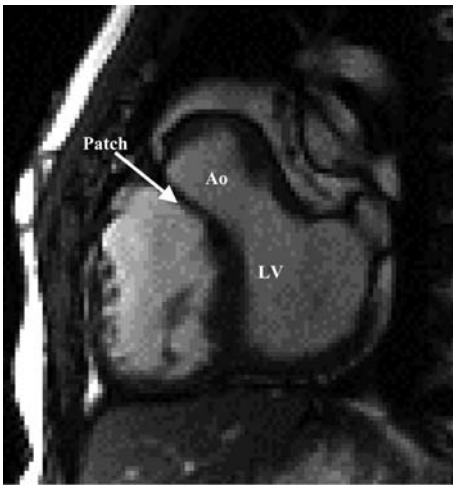
Fig. 3.25.8. Status post repair of double outlet right ventricle. Cine MRI of the left ventricular outflow tract after REV procedure showing the unobstructed left ventricle-aorta tunnel (*Ao* aorta, *LV* left ventricle)

▌ References

Bex JP, Lecompte Y, Baillot F, Hazan E (1980) Anatomical correction of transposition of the great arteries. Ann Thorac Surg 29:86

Borromée L, Lecompte Y, Batisse A, Lemoine G, Vouhé P, Sakata R, Leca F, Zannini L, Neveux JY (1988) Anatomic repair of anomalies of ventriculoarterial connection associated with ventricular septal defect. II. Clinical results in 50 patients with pulmonary outflow tract obstruction. J Thorac Cardiovasc Surg 95:96

Choi BW, Park YH, Choi JY, Choi BI, Kim MJ, Ryu SJ, Lee JK, Sul JH, Lee SK, Cho BK, Choe KO (2001) Using electron beam CT to evaluate conotruncal anomalies in pediatric and adult patients. Am J Roentgenol 177:1045–1049

Corno AF, Hurni M, Griffin H, Galal OM, Payot M, Sekarski N, Tozzi P, von Segesser LK (2002) Bovine jugular vein as right ventricle-to-pulmonary artery valved conduit. J Heart Valve Dis 11:242–247

Corno AF, Bonnet D, Sekarski N, Sidi D, Vouhé PR, von Segesser LK (2003) Remote control of pulmonary blood flow: initial clinical experience. J Thorac Cardiovasc Surg 126:1775–1780

Corno AF, Qanadli SD, Sekarski N, Artemisia S, Hurni M, Tozzi P, von Segesser LK (2004) Bovine valved xenograft in pulmonary position: medium-term follow-up with excellent hemodynamics and freedom from calcifications. Ann Thorac Surg 78:1382–1388

Dorfman AL, Geva T (2006) Magnetic resonance imaging evaluation of congenital heart disease: conotruncal anomalies. J Cardiovasc Magn Reson 8:645–659

Dos L, Pen V, Silversides C, Provost Y, Oechslin E, Horlick E, Paul N (2007) Images in cardiovascular medicine. Cardiac magnetic resonance imaging and multidetector computed tomography scan illustrating Damus-Kaye-Stansel operation. Circulation 115: e440–442

Goo HW, Park IS, Ko JK, Kim YH, Seo DM, Yun TJ, Park JJ, Yoon CH (2003) CT of congenital heart disease: normal anatomy and typical pathologic conditions. Radiographics 23:S147–165

Lecompte Y, Neveux JY, Leca F, Zannini L, Tu TV, Duboys Y, Jarreau MM, Starr A (1982) Reconstruction of the pulmonary outflow tract without prosthetic conduit. J Thorac Cardiovasc Surg 84:727–733

Lecompte Y, Batisse A, di Carlo D (1993) Double-outlet right ventricle: a surgical synthesis. Adv Card Surg 4:109–136

Sodian R, Weber S, Markert M, Rassoulian D, Kaczmarek I, Lueth TC, Reichart B, Daebritz S (2007) Stereolithographic models for surgical planning in congenital heart surgery. Ann Thorac Surg 83:1854–1857

Sørensen TS, Mosegaard J, Greil GF, Miller S, Seeger A, Hansen OK, Sieverding L (2007) Images in cardiovascular medicine. Virtual cardiotomy for preoperative planning. Circulation 115:e312

Uehara M, Funabashi N, Ogawa Y, Minamino T, Komuro I (2007) Double outlet right ventricle demonstrated by multislice computed tomography. Int J Cardiol 121:218–220

Chapter 3.26 Double discordance

▋ Definition

In this fascinating cardiac malformation, the morphologically left atrium (=pulmonary venous atrium) is connected via a tricuspid valve with the morphologically right ventricle, from which originates the aorta, while the morphologically right atrium (=systemic venous atrium) is connected via a mitral valve with the morphologically left ventricle, from which originates the pulmonary artery. Therefore two discordant connections, atrioventricular and ventriculoarterial (=double discordance), occur in sequence in each side of the heart. The classical definition of "congenitally corrected transposition of the great arteries" derived from the observation that the effects of transposition of the great arteries are "corrected" by the congenital inversion of the two ventricles, with the two circulatory pathways "physiologically" in series, despite the anatomic derangements.

In these hearts an atrial situs solitus or inversus can be present, as well as superoinferior disposition of the ventricular chambers can occur, with a more or less horizontal interventricular septum. Dextrocardia is present in 25% of the cases. The ascending aorta is typically located anterior and to the left of the pulmonary artery (Figs. 3.26.1 and 3.26.2). The coronary arteries originate from the facing sinuses of the aortic valve, generally with a mirror-image distribution, following the appropriate ventricle.

Associated anomalies

In double discordance, probably less than 1% of individuals have no associated malformations. The most frequent and important associated lesions are ventricular septal defect (up to 80% of cases), tricuspid valve anomalies (=Ebstein-like malformation), corresponding to abnormalities of the systemic atrioventricular valve (in up to 60% of cases), pulmonary stenosis or atresia (30–50%), dextrocardia
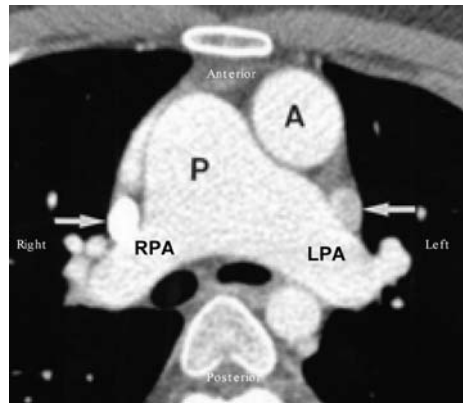
Fig. 3.26.1. Double discordance. CT scan contrast angiography, axial projection, showing the aorta with anterior-left position in relationship with the pulmonary artery, and the presence of bilateral superior vena cava (arrows). The left superior vena cava is more faintly opacified because contrast material was injected in a vein of the right arm (*A* aorta, *LPA* left pulmonary artery, *P* pulmonary artery, *RPA* right pulmonary artery) (reproduced with permission from Choi BW, Park YH, Choi JY, Choi BI, Kim MJ, Ryu SJ, Lee JK, Sul JH, Lee SK, Cho BK, Choe KO (2001) Using electron beam CT to evaluate conotruncal anomalies in pediatric and adult patients. Am J Roentgenol 177:1045–1049)
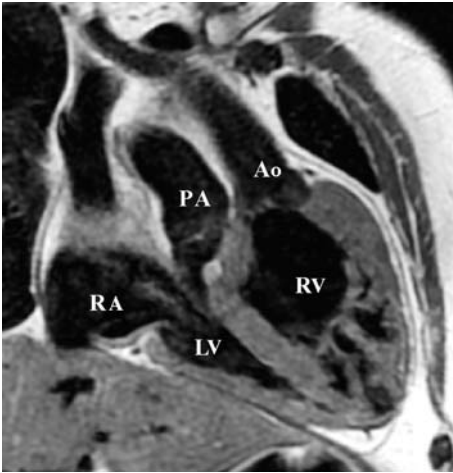
Fig. 3.26.2. Double discordance. Fast spin echo ventricular outflow tract showing the ventriculoarterial discordance (*Ao* aorta, *LV* ventricle, *PA* pulmonary artery, *RA* right atrium, *RV* right ventricle)

(25%) and complete atrioventricular block (12–33% of cases). Mitral valve anomalies are also quite frequent (up to 55% of cases). Straddling of an atrioventricular valve can be associated with hypoplasia of the ipsilateral ventricle.

Coronary artery anomalies potentially complicating anatomical repair have been reported in 45% of patients, including single coronary artery orifice (the most frequent coronary artery anomaly), left anterior coronary artery originating from the right coronary artery, and eccentric coronary orifices. Hypoplasia of one of the two ventricles generally occurs in the presence of a straddling atrioventricular valve (ipsilateral to the hypoplastic ventricle).

Less frequently have been reported situs inversus (with mirror-image relation), supravalvular left atrial ring, atrial septal defect, complete atrioventricular septal defect, straddling mitral valve, double outlet right ventricle, discrete subvalvular or valvular aortic stenosis (Fig. 3.26.3), patent ductus arteriosus, aortic coarctation, aortic arch inter-

ruption, aortic atresia, pulmonary atresia with intact ventricular septum, coarctation of the left pulmonary artery. The isolated atrioventricular discordance, without ventriculoarterial discordance (also called isolated ventricular inversion), has rarely been observed, generally with associated ventricular septal defect.

■ Surgical options

The surgical management of even the simple associated defects, such as ventricular septal defect or pulmonary stenosis, has been reported to be associated with much higher mortality and morbidity rates in these patients than in patients with an otherwise normal heart. From the technical point of view, the surgical approach to address the ventricular septal defect or pulmonary stenosis is difficult, and the risk of inducing a complete atrioventricular block is high. Furthermore, despite technical success, the above procedures may not result in functional improvement.

■ **Palliations:** the initial surgical approach in infancy can be a palliative procedure, including pulmonary artery banding in the presence of a large ventricular septal defect with pulmonary hypertension, or a modified Blalock-Taussig shunt in the presence of severe cyanosis due to pulmonary stenosis.

■ **Conventional repair:** depending on the age at presentation and on the specific combination of the associated lesions, conventional surgical repair of double discordance may involve tricuspid valve repair or replacement, closure of the ventricular septal defect, implantation of a biological valved conduit between the left ventricle and the pulmonary artery and pacemaker implantation.

With the conventional repair the morphologically right ventricle remains the systemic ventricle, while the morphologically right atrioventricular valve (tricuspid valve) remains the systemic valve.

▌ **Double (= atrial and arterial) switch procedure:** because of the disappointing medium and long-term results of the conventional approach, surgical treatment in the last few years has been directed toward repair where the morphologically left ventricle and the morphologically left atrioventricular valve (mitral valve) are restored to the systemic circulation.

The following conditions are required for a double switch procedure:
▌ absence of major atrioventricular valve straddling,
▌ balanced ventricular chambers,
▌ adequate left ventricular function and pressure (at least 75% of the systemic right ventricle), either because of the presence of an unrestrictive ventricular septal defect or because of a previous pulmonary artery banding,
▌ coronary arteries not precluding transfer and reimplantation.

With the double switch procedure, the patients without pulmonary stenosis or atresia undergo atrial switch (Mustard or Senning procedure) and arterial switch (Jatene procedure), with closure of ventricular septal defect when present.

Patients with left ventricular outflow tract obstruction (= pulmonary stenosis or atresia) undergo atrial switch (Mustard or Senning procedure), closure of ventricular septal defect and implantation of an extracardiac biological valved conduit between the right ventricle and the pulmonary artery (Rastelli operation) or the direct implantation of the transected pulmonary artery on the right ventriculotomy (Lecompte procedure).

In the presence of severe heart failure, particularly biventricular failure, heart transplant has to be taken into consideration.

▌ **One-and-half ventricular repair:** in the presence of a relatively hypoplastic ventricle, the one-and-half ventricular repair (end-to-side anastomosis of the superior vena cava to the right pulmonary artery in addition to intracardiac repair, in order to reduce the volume overload of the small/malfunctioning right ventricle) is the procedure of choice.

▌ Pre-operative information

Sequential chamber localization is the fundamental first step in the diagnosis of double discordance. Accurate morphological characterization of the cardiac chambers and the great arteries is essential for the diagnosis of double discordance. The criteria to distinguish the morphologic right ventricle (functionally systemic ventricle) include course trabeculation, typical papillary muscles pattern with a septal origin as well as a vascular conus, presence of a moderator band, and more apical insertion of the atrioventricular valve (in this case the tricuspid valve) in the body of the right ventricle.

On the other hand, the morphologic left ventricle is recognized by its fine trabeculation and less apical insertion of the atrioventricular valve (in this case the mitral valve) to the septum than to the contralateral side. The aortic arch with its branches and the take-off of the coronary arteries allow recognition of the aorta, with the atypical coronary artery pattern. Identification of the short trunk and the immediate bifurcation is key for identifying the main pulmonary artery.

Echocardiographic investigation generally provides all the information required for correct diagnosis and decision making for surgery, particularly in infants and children.

However, cardiac MRI assumes an increasing role in several important pre-operative issues, mainly in older children, such as ventricular volumes and functions, morphology of the outflow tracts, relationship between ventricular septal defect and intracardiac structures, morphology of the pulmonary arteries, origin and course of the coronary arteries, and morphology and location of the auricular appendages as well, to rule out juxtaposition of the auricular appendages as well, in case anatomical correction is taken into consideration.

To achieve these goals the following cardiac MRI protocol is suggested:

■ 3-plane localizing images,

■ 2-dimensional axial Time-of-flight Angiography (see the appendix in the "Introduction"),

■ ECG-gated cine steady-state free precession sequences in the 2-chamber, 4-chamber planes, and ventricular short axis for the quantitative assessment of both ventricular dimensions, function and stroke volume (Fig. 3.5.3) as illustrated in the appendix of the "Introduction"; 4-chamber acquisition is very informative to confirm the diagnosis of double discordance, highlighting the attachment of the atrioventricular valve septal leaflets to the septum and the different trabeculation pattern of both ventricles (Fig. 3.26.4),

■ ECG-gated cine steady-state free precession sequence to visualize the left ventricular outflow tract and pulmonary valve to rule out any obstruction on the pulmonary pathway,

■ ECG-gated cine steady-state free precession sequence, generally on the sagittal plane, to visualize the right ventricular outflow tract and the aorta located anterior and to the left,

■ ECG-gated static 3-dimensional steady-state free precession for the evaluation of the origin and proximal course of the coronary arteries,

■ ECG-gated cine steady-state free precession sequence on different oblique planes to evaluate the presence of a ventricular septal defect and its relationship to both outflow tracts (Fig. 3.26.5),

■ gadolinium-enhanced 3-dimensional MR angiography for the evaluation of the great arteries, the aortic arch, and the pulmonary and systemic veins,

■ ECG-gated phase velocity contrast MRI sequences perpendicular to the main pulmonary artery, ascending aorta, and pulmonary arteries, to assess flow pattern in the great vessels, mainly to quantify shunts if present. Tricuspid valve regurgitation in these patients is very common due to the
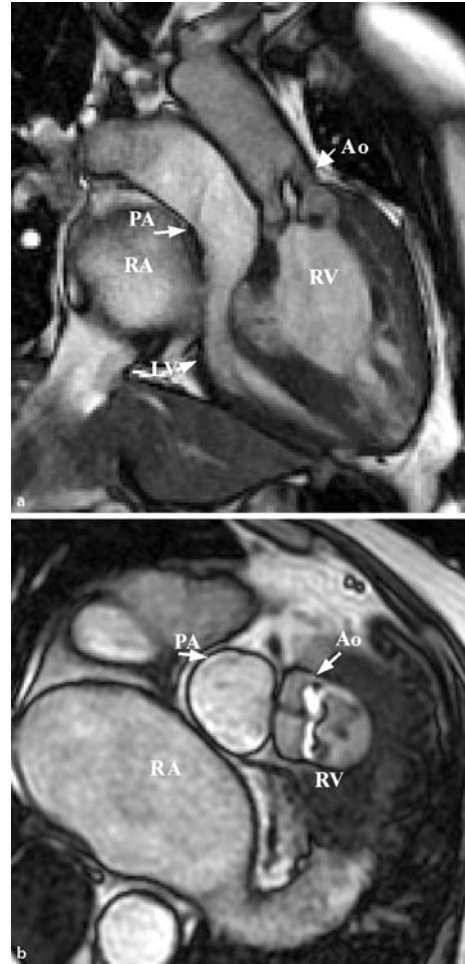
Fig. 3.26.3. Double discordance and aortic stenosis. Cardiac MRI steady-state free precession right ventricular outflow tract (**a**) and aortic valve short axis (**b**) of an unusual case of double discordance and aortic stenosis (*AO* aorta, *LV* ventricle, *PA* pulmonary artery, *RA* right atrium, *RV* right ventricle)

presence of systemic pressure in the right ventricle and may be due to the ventricular septal shift as well, leading to a tricuspid valve regurgitation due to malfunction of the tricuspid chordae attached to the septum. This is confirmed by the observation that in patients with double discordance
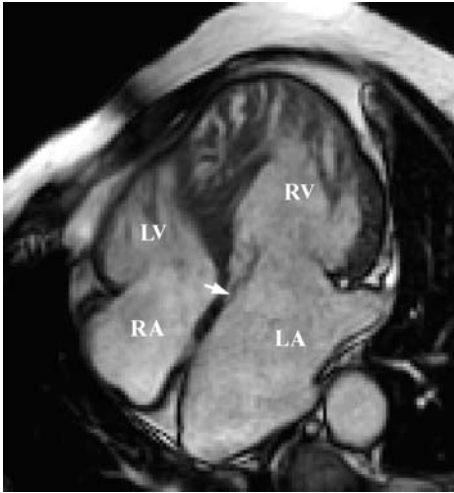
Fig. 3.26.4. Double discordance. Cardiac MRI steady-state free precession 4-chamber view showing the coarse right ventricular muscular trabeculations and the apical displacement of the septal leaflet of the left atrioventricular valve (arrowhead), confirming atrioventricular discordance (*LA* left atrium, *LV* ventricle, *RA* right atrium, *RV* right ventricle)
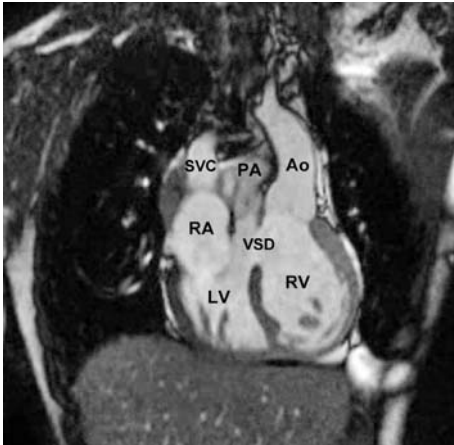
Fig. 3.26.5. Double discordance. Cine cardiac MRI showing the ventriculoarterial discordance, the ventricular septal defect and the outflow tracts relationship (*Ao* aorta, *LV* morphologically left ventricle, functionally right (pulmonary) ventricle, *PA* pulmonary artery, *RA* right atrium, *RV* morphologically right ventricle, functionally left (systemic) ventricle, *SVC* superior vena cava, *VSD* ventricular septal defect)

with large ventricular septal defect, where the ventricular septum is straight and not shifted to the left, tricuspid valve regurgitation is generally less progressive than in the case of low subpulmonary ventricle pressure. This hypothesis is confirmed in patients with double discordance and large ventricular septal defect after pulmonary artery banding (see section "Post-operative follow-up", Fig. 3.26.6). Tricuspid regurgitation can be quantified by subtracting the right ventricular stroke volume from the aorta stroke volume, if the accuracy of both measurements is good.

■ post-gadolinium delayed myocardial enhancement may be used to evaluate the presence of scar tissue. In case of double discordance, one major concern is the capacity of the morphologic right ventricle to sustain (lifelong) the systemic circulation due to both the characteristics of the myocardial fibers disposition and the possibility of progressive tricuspid valve regurgitation. To address this issue, in addition to assessment of right ventricular volumes and ejection fraction, it is possible to assess the contractile reserve of the systemic right ventricle during and after beta-adrenergic stimulation, taking advantage of the high accuracy of MRI compared to echocardiography because of the bizarre shape of the right ventricle. The clinical significance of such studies, even in the preoperative setting, requires more extended investigations.

In patients with double discordance, when the descending thoracic aorta is located on the contralateral side of the ascending aorta, the ascending aorta is positioned more laterally and the aortic arch is located more posterior, and as a consequence tracheal compression can be caused by the elongated aortic arch. In these cases, CT or MRI show a transversely oriented aortic arch and severe tracheal compression in the anteroposterior direction by the aortic arch. Aortic size (larger than normal), posterior position, elongation, and end-on appearance of the aortic arch are useful predictors of tracheal compression.
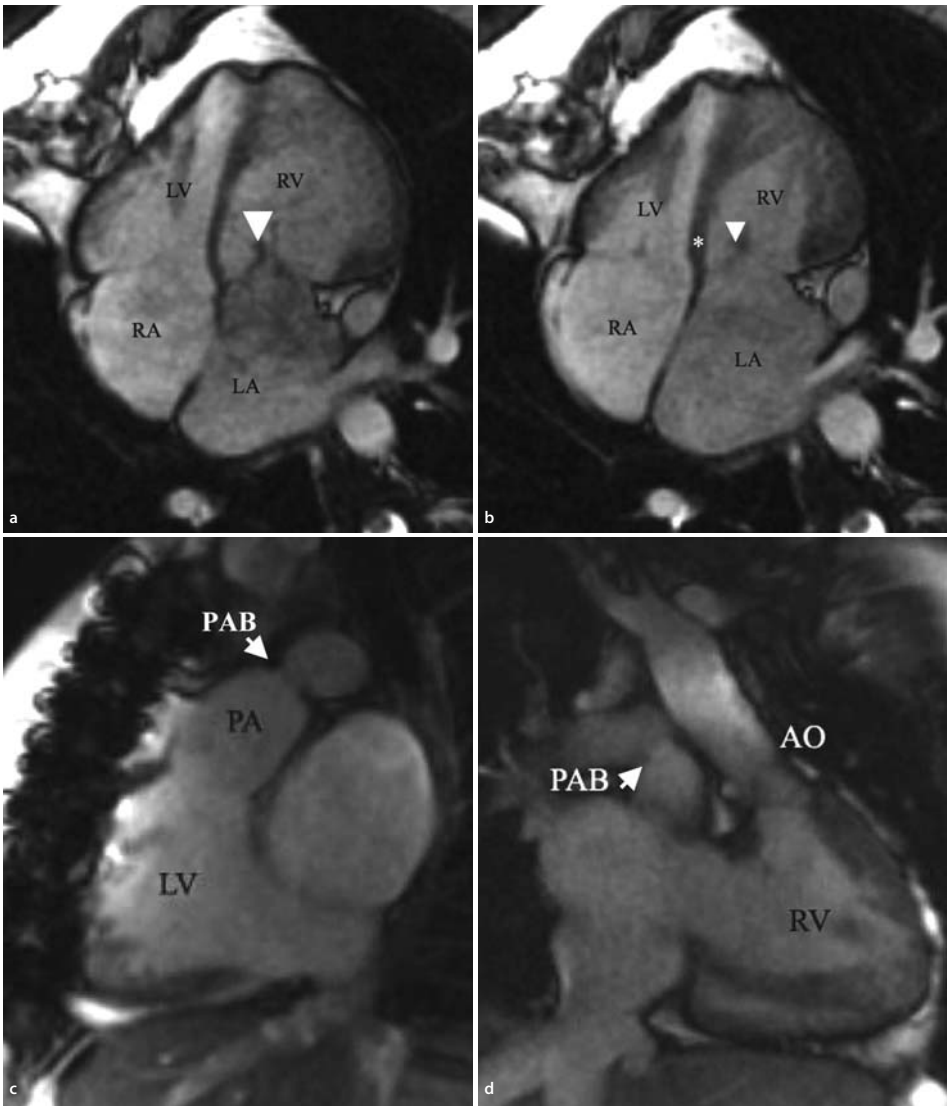
Fig. 3.26.6. Double discordance, status post pulmonary banding. Cardiac MRI steady-state free precession 4-chamber view in proto-systole (**a**) and in tele-systole (**b**), left ventricular outflow tract (**c**) and right ventricular outflow tract (**d**). Note in **a** the tricuspid lack of coaptation (headarrow) disappearing at the end of the systole (**b**), probably because the septum (asterisk) where the tricuspid valve chordae are attached, is shifted toward the right ventricle due to the high pressure in the left subpulmonary ventricle (*AO* aorta, *LA* left atrium, *LV* ventricle, *PA* pulmonary artery, *PAB* pulmonary artery banding, *RA* right atrium, *RV* right ventricle)
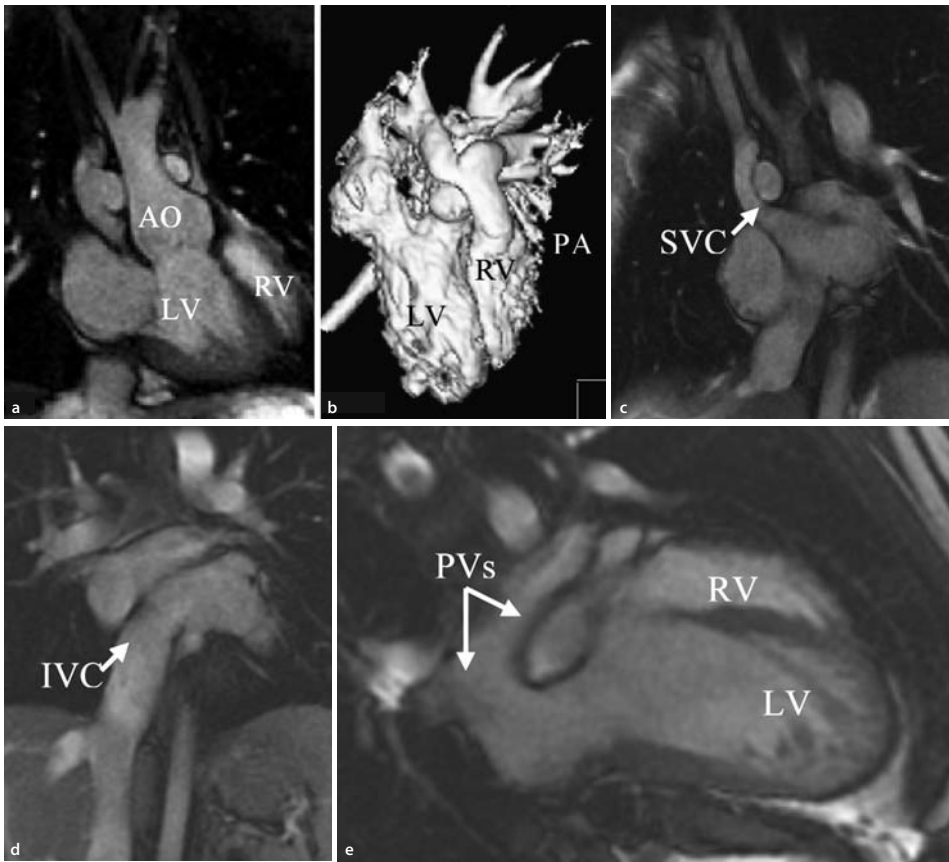
Fig. 3.26.7. Double discordance with ventricular septal defect, status post atrial (Senning) and arterial switch. Cine steady-state free precession (**a**, **c**, **d**, **e**) and volume rendering MR angiography reconstruction (**b**). No evidence of pulmonary (**e**) and systemic veins (**c**, **d**) baffle stenosis (*AO* aorta, *IVC* inferior vena cava, *LV* left ventricle, *PA* pulmonary artery, *PVs* pulmonary veins, *RV* right ventricle, *SVC* superior vena cava)

■ Potential complications

■ Conventional repair: early potential complications are arrhythmias, complete atrioventricular block, residual ventricular septal defect, residual tricuspid valve regurgitation and residual right ventricular outflow tract obstruction.

In the follow-up, a substantial percentage (up to 67%) of patients treated with conventional repair develops congestive heart failure and dysfunction with morphological right ventricular failure. These complications are strongly associated with regurgitation of the morphologically right atrioventricular valve (tricuspid valve), and particularly with tricuspid valve repair or replacement.

■ Double (= atrial and arterial) switch procedure: myocardial failure with low cardiac output can occur after such a long and complicated procedure, particularly in the presence of previous surgical treatment(s). Other potential complications are the occurrence of complete atrioventricular block, residual or recurrent systemic and/or pulmonary venous obstructions (because of the atrial rerouting), residual or recurrent atrial septal defect, residual or recurrent tricuspid valve regurgitation, residual or recurrent ventricular septal defect, residual or recurrent left or right ventricular outflow tract obstruction.

■ Post-operative follow-up

Cardiac MRI is particularly useful in the follow-up of these patients particularly because of the complex intracardiac anatomy and the surgical baffle, which are difficult to visualize by any other diagnostic technique.

Post-operatively, cardiac MRI provides quantitative evaluation of the left and right ventricular mass, size and function, and also the presence of residual intracardiac shunts and the presence and degree of potential tricuspid valve regurgitation. Thus, after palliation with pulmonary artery banding in the presence of double discordance, cardiac MRI can beautifully show the tricuspid (systemic) leaflet coaptation throughout the systole demonstrating its variation depending upon the ventricular septal shifting (Fig. 3.26.6).

Cardiac MRI is also able to rule out any baffle obstruction or leak after atrial rerouting (Mustard or Senning procedures) as well as to visualize the outflow tracts (Fig. 3.26.7).

After arterial switch (Jatene procedure), because of the potential complication of neoaortic valve regurgitation, cine MRI is useful to visualize the aortic root and leaflets and to detect the mechanisms of aortic valve regurgitation, as well as to monitor its progression by means of serial assessment of the aortic flow and regurgitation fraction.

In patients with pre-operative tracheal compression, the postoperative investigation with CT scan should demonstrate decreased size of the aorta and ascending aorta restored to its anterior position, with reduction or disappearance of the tracheal compression.

■ References

Ando M, Duncan BW, Mee RBB (2003) Anatomic correction for corrected transposition after pulmonary unifocalization. Ann Thorac Surg 75:1012–1014

Bautista-Hernandez V, Marx GR, Gauvreau K, Mayer JE, Cecchin F, del Nido PJ (2006) Determinants of left ventricular dysfunction after anatomic repair of congenitally corrected transposition of the great arteries. Ann Thorac Surg 82:2059–2066

Chang DS, Barack BM, Lee HY (2007) Congenitally corrected transposition of the great arteries: imaging with 16-MDCT. Am J Roentgenol 188:W428–430

Choi BW, Park YH, Choi JY, Choi BI, Kim MJ, Ryu SJ, Lee JK, Sul JH, Lee SK, Cho BK, Choe KO (2001) Using electron beam CT to evaluate conotruncal anomalies in pediatric and adult patients. Am J Roentgenol 177:1045–1049

Corno AF (2000) Surgery for congenital heart disease. Curr Opinion Cardiol 15:238–243

Corno AF (2002) Surgical treatment of complex cardiac anomalies: the "one and half ventricle repair. Eur J Cardiothorac Surg 22:436–437 (editorial comment)

Corno AF, Bonnet D, Sekarski N, Sidi D, Vouhé PR, von Segesser LK (2003) Remote control of pulmonary blood flow: initial clinical experience. J Thorac Cardiovasc Surg 126:1775–1780

Corno AF, Qanadli SD, Sekarski N, Artemisia S, Hurni M, Tozzi P, von Segesser LK (2004) Bovine valved xenograft in pulmonary position: medium-term follow-up with excellent hemodynamics and freedom from calcifications. Ann Thorac Surg 78:1382–1388

Delius RE, Rademecker MA, de Leval MR, Elliott MJ, Stark J (1996) Is a high-risk biventricular repair always preferable to conversion to a single ventricle repair? J Thorac cardiovasc Surg 112:1561–1567

Dodge-Khatami A, Tulevski II, Bennink GB, Hitchcock JF, de Mol BA, van der Wall EE, Mulder BJ (2002) Comparable systemic ventricular function in healthy adults and patients with unoperated congenitally corrected transposition using MRI dobutamine stress testing. Ann Thorac Surg 73:1759–1764

Fratz S, Hauser M, Bengel FM, Hager A, Kaemmerer H, Schwaiger M, Hess J, Stern HC (2006) Myocardial scars determined by delayed-enhancement magnetic resonance imaging and positron emission tomography are not common in right ventricles with systemic function in long-term follow up. Heart 92:1673–1677

Giannico S, Corno AF, Marino B, Cicini MP, Gagliardi MG, Amodeo A, Picardo S, Marcelletti C (1992) Total extracardiac right heart bypass. Circulation 86(Suppl 2):110–117

Giardini A, Lovato L, Donti A, Formigari R, Oppido G, Gargiulo G, Picchio FM, Fattori R (2006) Relation between right ventricular structural alterations and markers of adverse clinical outcome in adults with systemic right ventricle and either congenital complete (after Senning operation) or congenital corrected transposition of the great arteries. Am J Cardiol 98:1277–1282

Goo HW, Park IS, Ko JK, Kim YH, Seo DM, Yun TJ, Park JJ, Yoon CH (2003) CT of congenital heart disease: normal anatomy and typical pathologic conditions. Radiographics 23:S147–165

Graham TP, Bernard YD, Mellen BG, Celermajer D, Baumgartner H, Cetta F, Connolly HM, Davidson WR, Dellborg M, Foster E, Gersony WM, Gessner IH, Hurwitz RA, Kaemmerer H, Kugler JD, Murphy DJ, Noonan JA, Morris C, Perloff JK, Sanders SP, Sutherland JL (2000) Long-term outcome in congenitally corrected transposition of the great arteries: a multi-institutional study. J Am Coll Cardiol 36:255–261

Hoeffel JC (2001) Congenitally corrected transposition of the great arteries (L-TGA) with situs inversus totalis in adulthood: findings with magnetic resonance imaging. Magn Reson Imaging 19:762

Imai Y, Seo K, Aoki M, Shin'oka T, Hiramatsu K, Ohta A (2001) Double-switch operation for congenitally corrected transposition. Pediatr Card Surg Ann Semin Thorac Cardiovasc Surg 4:16–33

Karl TR, Weintraub RG, Brizard CP, Cochrane AD, Mee RBB (1997) Senning plus arterial switch operation for discordant (congenitally corrected) transposition. Ann Thorac Surg 64:495–502

Lembcke A, Koch C, Dohmen PM, Rutsch W, Abbara S, Krug LD, Muehler MR, Rogalla P (2005) Electrocardiographic-gated multislice computed tomography for visualization of cardiac morphology in congenitally corrected transposition of the great arteries. J Comput Assist Tomogr 29:234–237

Losekoot TG, Anderson RH, Becker AE, Danielson GK, Soto B (1983) Congenitally corrected transposition. Churchill Livingstone, Edinburgh

Lundstrom U, Bull C, Wyse RK, Somerville J (1990) The natural and "unnatural" history of congenitally corrected transposition. Am J Cardiol 65:1222–1229

Marcelletti C, Maloney JD, Ritter DG, McGoon DC, Wallace RB (1980) Corrected transposition and ventricular septal defect: surgical experience. Ann Surg 191:751–759

Marino B, Corno AF (2003) Spiral pattern: universe, normal heart, and complex congenital defects. J Thorac Cardiovasc Surg 126:1225–1226

Mazzera E, Corno AF, Picardo S, Di Donato RM, Marino B, Costa D, Marcelletti C (1989) Bidirectional cavopulmonary shunts: clinical applications as staged or definitive palliation. Ann Thorac Surg 47:415–420

Piran S, Veldtman G, Siu S, Webb GD, Liu PP (2002) Heart failure and ventricular dysfunction in patients with single or systemic right ventricles. Circulation 105:1189–1194

Scardi S, Pagnan L, Perkan A (2005) Magnetic resonance assessment of an adult patient with congenitally corrected transposition of the great arteries. Ital Heart J 6:939–940

Schwab JO, Ehlgen A, Sommer T (2003) Congenitally corrected transposition of the great arteries in a 70-year-old woman diagnosed using single-detector helical CT. Am J Roentgenol 181:598

Steinhoff JP, Hyslop B, Menon V, Willis PW (2004) Images in cardiology. Congenitally corrected transposition of the great arteries with subpulmonic stenosis. Clin Cardiol 27:551

Tulevski II, van der Wall EE, Groenink M, Dodge-Khatami A, Hirsch A, Stoker J, Mulder BJ (2002) Usefulness of magnetic resonance imaging dobutamine stress in asymptomatic and minimally symptomatic patients with decreased cardiac reserve from congenital heart disease (complete and corrected transposition of the great arteries and subpulmonic obstruction). Am J Cardiol 89:1077–1081

Chapter 3.27 Isomerism

▋ Definition

In patients with incomplete lateralization of thoracic and visceral organs, the atrial appendages are also not lateralized. Thus, in the vast majority of these patients both atrial appendages present with similar internal and external morphology, characteristic of either the right or the left atrial appendage. Atrial isomerism is the designation for hearts with bilaterally right atrial appendages (Fig. 3.27.1) or bilaterally left atrial appendages.

Anomalous systemic venous connections are generally associated with atrial isomerism.

These so-called heterotaxic syndromes are characterized by failure of many "right-left" differentiations, leading to situs inversus or ambiguity in the visceroatrial situs, along with anomalies of systemic and/or pulmonary venous connections (Fig. 3.27.2).

In patients with *left atrial isomerism* the infrahepatic portion of the inferior vena cava is frequently (75% of the cases) absent (= inferior vena cava interruption), and the venous return from the lower part of the body reaches the superior vena cava via the azygos vein (= azygos continuation) (Fig. 3.27.3) or via the hemiazygos vein (= hemiazygos continuation) emptying into either a right-sided superior vena cava or into a persistent left superior vena cava. Inferior vena cava interruption has never been observed in *right atrial isomerism*.
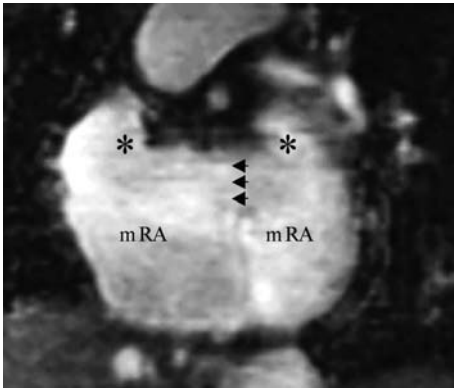
Fig. 3.27.1. Right atrial isomerism. Cardiac MRI time of flight, maximal intensity projection reconstruction showing two morphologic right atria with two symmetrical right auricular appendages (asterisk) and wide interatrial communication (arrows) (*mRA* morphologic right atrium)
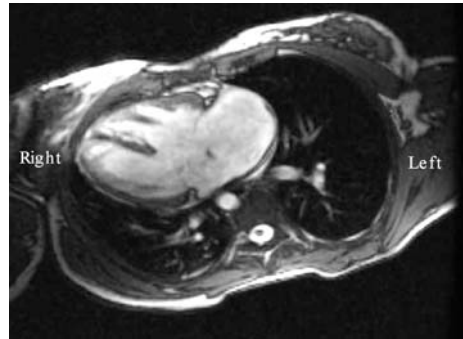
Fig. 3.27.2. Situs inversus. Cine MRI showing situs inversus with dextrocardia, right atrial isomerism, atrioventricular septal defect, total anomalous pulmonary venous connection. Note the common atrium and the common atrioventricular valve
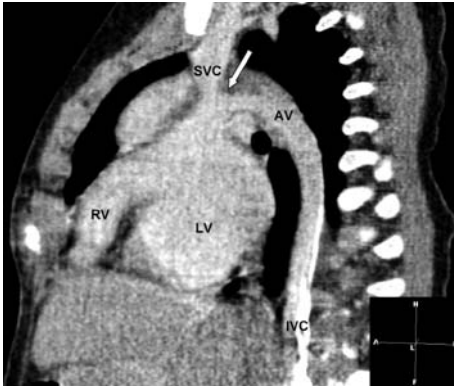
Fig. 3.27.3. Inferior vena cava interruption with azygos continuation. CT scan, sagittal projection, showing the azygos continuation of the inferior vena cava and the connection of the azygos vein to the superior vena cava (arrow) (*AV* azygos vein, *IVC* inferior vena cava, *LV* left ventricle, *RV* right ventricle, *SVC* superior vena cava) (photograph courtesy of Dr. Mohamed Tawil)
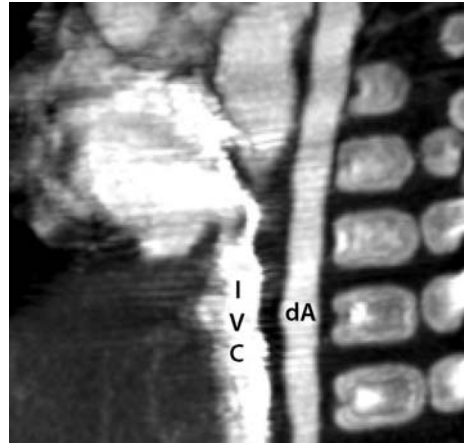
Fig. 3.27.4. Right isomerism. CT scan sagittal reformatted image showing the inferior vena cava and the abdominal aorta running along the same side of the spine (=juxtaposition of the inferior vena cava and abdominal aorta) with the vena cava in anterolateral position (*dA* descending thoracic aorta, *IVC* inferior vena cava) (reproduced with permission from Goo HW, Park IS, Ko JK, Kim YH, Seo DM, Yun TJ, Park JJ, Yoon CH (2003) CT of congenital heart disease: normal anatomy and typical pathologic conditions. Radiographics 23: S147–165)

In patients with *right atrial isomerism* the inferior vena cava and the abdominal aorta may run along the same side of the spine (Fig. 3.27.4); the right and the left hepatic veins may enter the ipsilateral sides of the common atrium, remaining separate from the connection of the inferior vena cava.

Persistent left superior vena cava is present in 50% of patients with *right atrial isomerism* and in 70% of patients with *left atrial isomerism*, and in both situations, particularly in *right atrial isomerism*, it can be connected to the upper left side of the left atrium instead of the coronary sinus.

The coronary sinus orifice can often be absent, more frequently in *right atrial isomerism* than in *left atrial isomerism*.

Abnormalities of the pulmonary veins are also common in both left and right atrial isomerism; total anomalous pulmonary venous connection to the superior or inferior vena cava is more frequent in *right atrial isomerism* (in 40% of these patients with obstruction to the pulmonary venous return), whereas anomalous pulmonary venous connection into the same side of the atrium as

the systemic venous drainage is more frequent in *left atrial isomerism* (generally unobstructed).

The atrial septum and ventricular septum are very rarely normal in patients with atrial isomerism; a common atrium is present in about 50% of the cases, atrioventricular septal defect in about 80% of cases, with most patients having a common atrioventricular orifice, and various types of ventricular septal defect can be present, in the vast majority of cases of atrioventricular type.

Frequently, there is outflow obstruction to pulmonary arterial blood flow at the valvular and/or subvalvular level. Pulmonary atresia is slightly more common in *right atrial isomerism*, whereas pulmonary stenosis is more common in *left atrial isomerism*.

Ventriculoarterial discordance is very frequent (75–90% of cases).
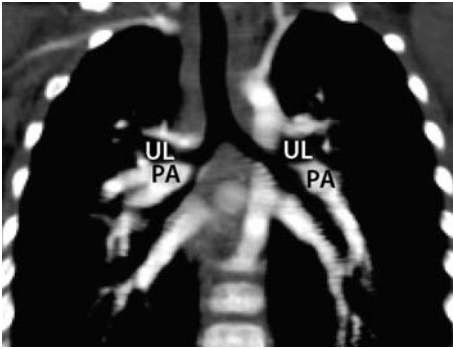
Fig. 3.27.5. Right isomerism. CT scan, oblique coronal projection, showing right bronchial isomerism: both upper lobe bronchi, symmetrically short, are located above the descending lower pulmonary arteries (*PA* pulmonary artery, *UL* upper bronchus) (reproduced with permission from Goo HW, Park IS, Ko JK, Kim YH, Seo DM, Yun TJ, Park JJ, Yoon CH (2003) CT of congenital heart disease: normal anatomy and typical pathologic conditions. Radiographics 23:S147–165)
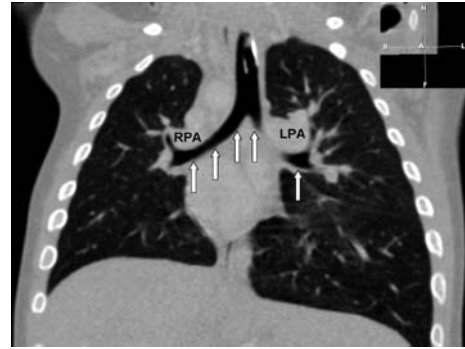
Fig. 3.27.6. Left isomerism. CT scan, coronal projection, showing the right and left bronchus (arrows) below the ipsilateral pulmonary artery at the hilum (hypoarterial bronchus), as is the case for a morphologically left pulmonary artery (=two left pulmonary arteries) (*LPA* left pulmonary artery, *RPA* right pulmonary artery) (photograph courtesy of Dr. Mohamed Tawil)

Pulmonary artery anomalies are not rare, particularly when there is pulmonary atresia with the ductus arteriosus as the only source of pulmonary blood flow. After closure of the ductus arteriosus, a "coarctation" commonly develops at the origin of the left pulmonary artery, at the insertion of the ductus arteriosus.

The branching pattern of the pulmonary arteries generally assumes one of two forms, depending on whether left or right atrial isomerism is present. In *right atrial isomerism,* both right and left pulmonary arteries tend to look like a normal right pulmonary artery (=two right pulmonary arteries), with the bronchus for the upper lobe being above the first segmental artery for the right upper lobe (epiarterial bronchus) (Fig. 3.27.5). In contrast, in *left atrial isomerism,* the bronchus is below the pulmonary artery at the hilum (hypoarterial bronchus), as is the case for a normal left pulmonary artery (=two left pulmonary arteries) (Fig. 3.27.6).

Atrial isomerism generally corresponds to thoracic isomerism; therefore, in *right atrial isomerism* both lungs tend to be trilobed (=two right lungs), whereas in *left atrial iso-*merism both lungs tend to be bilobed (=two left lungs).

Finally, *asplenia* is more commonly present in *right atrial isomerism*, whereas *polysplenia* is more frequently associated with *left atrial isomerism.*

These features have contributed to the general rule (with several exceptions) that patients with *right atrial isomerism* tend to have bilateral "right-sidedness" (asplenia), whereas those with *left atrial isomerism* tend to have bilateral "left-sidedness" (polysplenia).

Because of the extreme morphological variability within the cases with atrial isomerism, the term "heterotaxy" has been suggested to define the presence of any of the numerous possible anomalies of lateralization.

Associated anomalies

■ **Left isomerism:** polysplenia, anomalous systemic and/or pulmonary venous connection are very frequent, with interruption of the inferior vena cava and azygos continuation as the most frequent (56–92% of cases), followed by anomalous pulmonary venous connection (56%) that in a certain percentage of

patients is potentially obstructive, common atrioventricular valve (46–49%), common atrium (38%), cor triatriatum (30%), pulmonary atresia or stenosis (28%), aortic coarctation (16%), congenital atrioventricular block (7%).

∎ **Right isomerism:** asplenia, valvular and subvalvular pulmonary stenosis or pulmonary atresia are predominant (89% of cases), followed by discordant ventriculoarterial connection (72–75%) either with transposition of the great arteries or double outlet right ventricle, atrioventricular septal defect (72%) with or without a common atrium, single ventricle (55%), extracardiac total anomalous pulmonary venous connection (50%), persistent left superior vena cava, bilateral right auricular appendages (20%).

∎ Surgical options

∎ **Palliation:** pulmonary artery banding or modified Blalock-Taussig shunt in the presence of increased or reduced pulmonary blood flow, respectively.

∎ **Biventricular repair:** in the presence of anomalous systemic and/or pulmonary venous connection(s) a complex interatrial baffle (pericardium, Teflon, PTFE) is very frequently required to obtain adequate re-routing of the systemic and pulmonary venous returns. In the presence of persistent left superior vena cava, particularly when it is connected to the left atrium, the extracardiac connection of the left superior vena cava either to the right superior vena cava or to the right auricular appendage can simplify the partitioning of the atrial chambers. The techniques to repair a atrioventricular or ventricular septal defect have been described in the relative chapters.

∎ Univentricular repair
∎ Bidirectional Glenn or hemi-Fontan.
∎ Modified Fontan or total cavopulmonary connection.

∎ In the presence of interruption of the inferior vena cava and azygos continuation, the preferred surgical option is the *Kawashima operation*, consisting of the end-to-side anastomosis between the transected superior vena cava and the right pulmonary artery, like in the bidirectional Glenn, but without dividing the azygos vein. In this way, the entire systemic venous return, excluding the splanchnic veins and the coronary sinus, is deviated directly into the pulmonary circulation. The Kawashima operation, therefore, represents an almost complete univentricular type of repair, like the total cavopulmonary connection.

∎ Pre-operative information

CT and MRI investigations can show the presence of multiple abnormally positioned spleens (polysplenia), right-sided stomach, left-sided liver, short pancreas and dextrocardia.

CT and MRI studies are particularly helpful in defining the presence and location of anomalous hepatic, pulmonary and/or systemic venous connections. Important for surgical decision making and the management of cardiopulmonary bypass is the identification of the connections between the hepatic and pulmonary veins and the atria, and the association of other anomalous systemic venous connections such as the interrupted left-sided inferior vena cava with azygos continuation.

To achieve these goals in such patients, a MRI 2-dimensional axial time of flight sequence from below the diaphragm up to the neck (see the appendix in the "Introduction") is particular useful in order to define with high spatial resolution both the pulmonary and systemic venous connections and the cardiac and great arteries complex arrangement, without using contrast medium, ready to be post-processed (Fig. 3.27.1).

Airway morphology is better demonstrated by CT scan (Figs. 3.27.5 and 3.27.6); however a
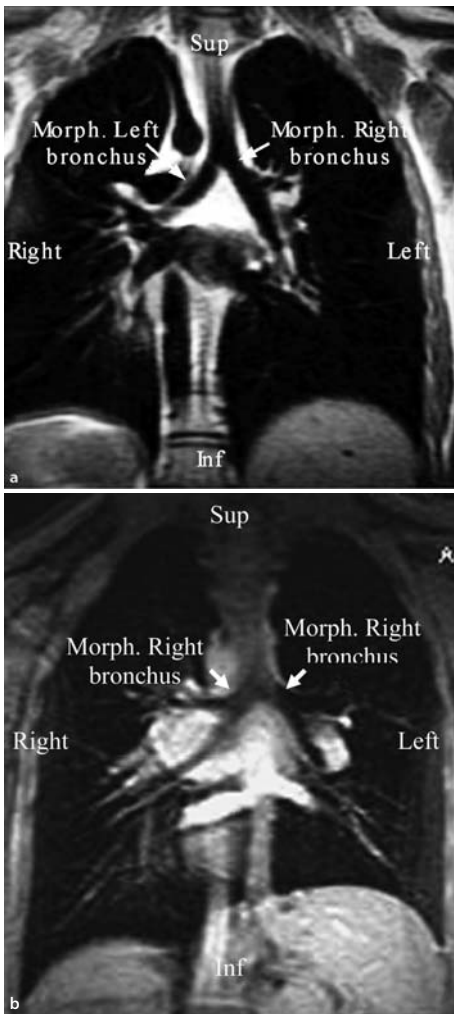
Fig. 3.27.7. Bronchial sidedness. **a** Cardiac MRI coronal fast spin echo showing situs inversus bronchial disposition. **b** Cardiac MRI coronal localizer showing two morphologically right bronchi in right isomerism

targeted frontal fast spin echo slice, or even localizer, can fully delineate the bronchial sidedness (Fig 3.27.7).

A complete protocol to evaluate the frequently associated anomalies is listed in detail in other chapters (see particularly the chapters "Single ventricle" and "Anomalous systemic venous connections").

■ Potential complications

The main differences with regard to the complications compared to the patients with functionally univentricular hearts without isomerism are the following:

■ after bidirectional Glenn (see chapter "Single ventricle"), there is a higher incidence of prolonged pleural effusions and chylothorax,

■ after modified Fontan or total cavopulmonary connection (see chapter "Single ventricle"), there is a higher incidence of prolonged pleural effusions, supraventricular arrhythmias, pulmonary arteriovenous malformations and venovenous collaterals (particularly after *Kawashima operation*).

■ Post-operative follow-up

For the post-operative follow-up after univentricular type of surgery see the relative chapter ("Single ventricle"), paying particular attention to the associated anomalies.

■ References

Da Cruz E, Milella L, Corno AF (1998) Left isomerism with tetralogy of Fallot and anomalous systemic and pulmonary venous connections. Cardiol Young 8: 131–133

Deanfield JE, Leanage R, Stroobant J, Chrispin AR, Taylor JFN, Macartney FJ (1980) Use of high kilovoltage filtered beam radiographs for detection of bronchial situs in infants and young children. Br Heart J 44:577–583

Geva T, Vick GW, Wendt RE, Rokey R (1994) Role of spin echo and cine magnetic resonance imaging in presurgical planning of heterotaxy syndrome. Comparison with echocardiography and catheterization. Circulation 90:348–356

Giannico S, Corno AF, Marino B, Cicini MP, Gagliardi MG, Amodeo A, Picardo S, Marcelletti C (1992) Total extracardiac right heart bypass. Circulation 86(Suppl 2):110–117

Giannico S, Hammad F, Amodeo A, Michielon G, Drago F, Turchetta A, di Donato R, Sanders SP (2006) Clinical outcome of 193 extracardiac Fontan patients. J Am Coll Cardiol 47:2065–2073

Goo HW, Park IS, Ko JK, Kim YH, Seo DM, Yun TJ, Park JJ, Yoon CH (2003) CT of congenital heart disease: normal anatomy and typical pathologic conditions. Radiographics 23:S147–165

Marcelletti C, di Donato R, Nijveld A, Squitieri C, Bulterijs AH, Naeff M, Schuller J, Becker AE (1983) Right and left isomerism: the cardiac surgeon's view. Ann Thorac Surg 35:400–405

Mazzera E, Corno AF, Picardo S, Di Donato RM, Marino B, Costa D, Marcelletti C (1989) Bidirectional cavopulmonary shunts: clinical applications as staged or definitive palliation. Ann Thorac Surg 47:415–420

Nigg C, Kolyvanos Naumann U, Kaser L, Vetter W (2007) Situs inversus, situs inversus totalis. Schweiz Rundsch Med Prax 96:713–718

Partridge JB, Scott O, Deverall PB, Macartney FJ (1975) Visualization and measurement of the main bronchi by tomography as an objective indicator of thoracic situs in congenital heart disease. Circulation 51:188–196

Ratib O, Perloff JK, Child JS (2004) Images in cardiovascular medicine. Unique discordance: thoracic situs solitus with left isomerism. Circulation 109:2252–2253

Rossi G, Corno AF, Montemurro G (1992) Prenatal diagnosis of isomerism of the right atrial appendages. Cardiol Young 2:298–301

Sugiyama H, Kadono T, Hoshiai M, Tan T, Koizumi K, Sakamoto H, Nakazawa S (2004) Gadolinium-based balloon angioplasty for pulmonary artery stenosis in an infant with a right isomerism. Catheter Cardiovasc Interv 63:346–350

Vanhoenacker FM, De Ruysscher D, De Backer AI, De Schepper AM (2001) Heterotaxy syndrome in an adult, with polysplenia, visceral and cardiovascular malposition. JBR-BTR 84:1–4

Yamagishi M, Fujiwara K, Yamada Y, Yoshida M, Shuntoh K, Shiraishi I, Hayano T, Itoi T, Hamaoka K, Kitamura N (2001) Norwood operation for left isomeric heart with aortic atresia: evaluation with three-dimensional computed tomography. J Thorac Cardiovasc Surg 121:1205–1207

CHAPTER 3.28 Slings and rings

This chapter considers the two most frequent anatomical situations with slings and/or rings: pulmonary artery sling and vascular ring.

Pulmonary artery sling

Definition

In pulmonary artery sling (= anomalous left pulmonary artery), the left pulmonary artery originates extrapericardial from the posterior aspect of the right pulmonary artery, encircles the right main bronchus and courses right-to-left, posterior to the distal tracheal bifurcation and anterior to the esophagus, before entering the hilum of the left lung.

The ligamentum arteriosum is posterior to the aorta from the origin of the right pulmonary artery, superior to the left main bronchus, effectively creating a vascular ring (or sling) around the trachea but not around the esophagus.

Approximately 50% of patients with pulmonary artery sling have complete cartilaginous tracheal rings: the posterior membranous component of the trachea is absent, and the tracheal cartilages, rather than being U shaped, are O shaped. As a consequence, the trachea is often narrower than normal. The complete rings may be localized to the region where the sling passes around the trachea, although often they extend the entire length of the trachea, creating a long-segment tracheal stenosis (= sling-ring complex). In the area where the sling passes around the trachea, there is likely to be tracheal compression resulting in important functional stenosis. With prolonged duration of airway compression, tracheomalacia and/or bronchomalacia can be a severe consequence.

Bronchus suis (= "pig bronchus"), consisting of separate high origin of the epiarterial bronchus to the right upper lobe from the trachea, is also relatively frequently associated with pulmonary artery sling.

Congenital heart defects are present in 50% of patients with pulmonary artery sling, most commonly atrial septal defect, ventricular septal defect, patent ductus arteriosus, persistent left superior vena cava, scimitar syndrome (see chapter "Partial anomalous pulmonary venous connection"). Extremely rare is the association with tricuspid atresia, single ventricle, tetralogy of Fallot, transposition of the great arteries, aortic arch anomalies.

Other anomalies in the arterial supply to one or both lungs are also associated with this malformation, e.g. the anomalous left pulmonary artery only supplying the left upper lobe with normal pulmonary artery supply to the left lower lobe, or partial anomalous supply to the right upper lobe from an anomalous left pulmonary artery.

Surgical options

Reimplantation of the anomalous left pulmonary artery is the treatment of choice, with or without tracheal reconstruction according to the degree, extent and duration of the airway involvement.

In the presence of associated malformations of the upper airway, its surgical treatment must be absolutely performed during the same operation for the vascular lesion.

Division of the anomalous left pulmonary artery at the origin and its mobilization and subsequent reimplantation into the main pulmonary artery anterior to the trachea can be accomplished either with or without cardiopulmonary bypass. The mobilization of the pulmonary artery is enhanced by the division of the ligamentum arteriosum. The procedure of reimplantation of the anomalous left pulmonary artery has been reported via left or (very rarely) or right thoracotomy, but the preferred approach is through a median sternotomy to allow better mobilization of the pulmonary artery and the choice between the reimplantation with or without cardiopulmonary bypass, and also for simultaneous tracheal reconstruction (of course with cardiopulmonary bypass) in the presence of complete tracheal rings with or without long-segment tracheal stenosis.

With regard to *tracheal reconstruction*, several techniques have been adopted for circular ring stenosis.

▮ *Resection* is the procedure of choice for short stenosis (< 1/3 of the tracheal length) without involvement of the carina or the main bronchi.
▮ For long segment tracheal stenosis, the technique of *slide tracheoplasty*, feasible even in infants in the presence of very long segment tracheal stenosis, has been demonstrated to provide the most reliable and consistent early and long-term results.
▮ Tracheoplasty with pericardial patch, homograft, prosthetic patch or costal cartilage has been reported in a few cases with very inconsistent results.

▮ Pre-operative information

Artifacts introduced by the lungs and airway negatively affect the ability of ultrasound to accurately assess the relationship between the airways and great vessels and aortic arch, while angiography fails to show the esophagus and airways.

In contrast to echocardiography and angiography, both CT scan and MRI can simultaneously define the anatomical details of both the airway and the vascular structures, facilitating diagnosis and surgical planning.

While CT and MRI seem to be equivalent to conventional cardiac catheterization and angiographic techniques for detecting vascular abnormalities, CT scan is more accurate than MRI in assessing the morphology of the airway (complete tracheal rings and extent of tracheal stenosis) and for the diagnosis of potentially life-threatening complications, such as tracheal, bronchial or esophageal compression.

CT scan can delineate the position of the left pulmonary artery arising from the right pulmonary artery, encircling the trachea, and reaching the hilum of the left lung coursing anteriorly to the esophagus and the aorta (Fig. 3.28.1); furthermore, it shows the presence of complete tracheal rings and the level and extent of tracheal stenosis (Fig. 3.28.2).

In patients with congenital heart defects, the posterior displaced ascending aorta may compress the main bronchus on the side of the aortic arch and right pulmonary artery against the descending thoracic aorta or spine. Even if the bronchial compression is mild with tolerable airway symptoms, these patients must be observed closely.

In these cases, the CT shows on the axial image a significantly larger retrosternal space, smaller interaortic distance, smaller aorto-spinal distance, and bronchial stenosis quantifiable on reformatted images perpendicular to the mainstem bronchi. However, the use of ionizing radiation limits the utilization of CT scan in children.

On the other hand, MRI can provide information on the relationship between the aorta and its branches and trachea and bronchi (Fig. 3.28.3), and phase velocity contrast acquisition of both pulmonary arteries can also provide information on the pulmonary blood flow distribution.
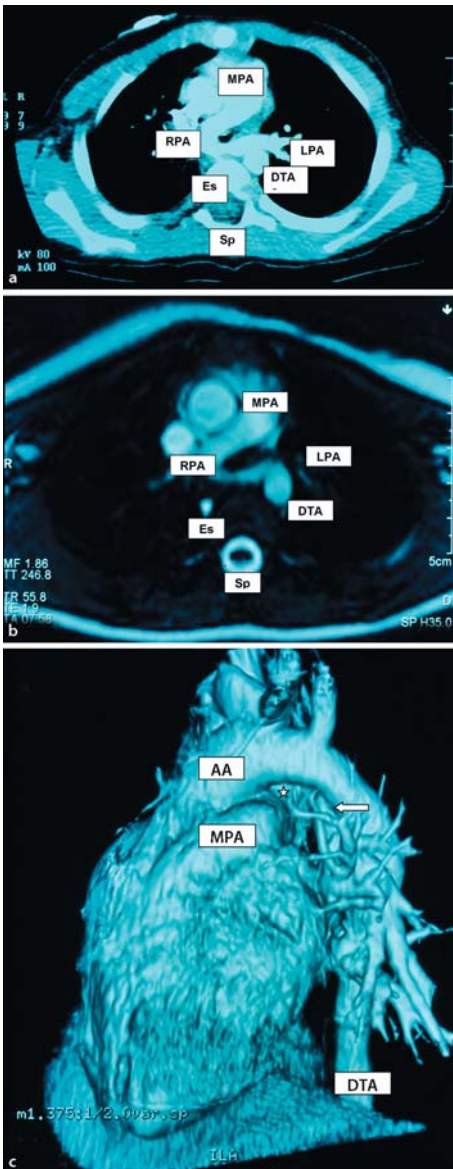
■ Potential complications

Residual or recurrent stenosis (also with reported occlusion) at the origin of the reimplanted left pulmonary artery, residual or recurrent airway obstruction, tracheomalacia, recurrent respiratory infections.

■ Post-operative follow-up

Both CT scan and MRI can evaluate the surgical results and detect the presence of potential complications with the same considerations followed for the pre-operative investigation.

Fig. 3.28.1. Pulmonary artery sling. **a** CT scan, axial projection, showing the left pulmonary artery arising from the right pulmonary artery, encircling the trachea, and reaching the hilum of the left lung coursing anteriorly to the esophagus and the aorta. **b** Contrast MRI, axial projection, in the same child showing the left pulmonary artery arising from the right pulmonary artery, encircling the trachea, and reaching the hilum of the left lung coursing anteriorly to the esophagus and the aorta. **c** Lateral view of the 3-dimensional reconstruction of the CT angiography in the same patient showing the absence of origin of the left pulmonary artery from the main pulmonary artery, and its origin (arrow) from the right pulmonary artery (star) (*AAo* ascending aorta, *DTAo* descending thoracic aorta, *Es* esophagus, *LPA* left pulmonary artery, *MPA* main pulmonary artery, *RPA* right pulmonary artery, *Sp* spine) (reproduced with permission from Corno AF (2004) Congenital Heart Defects. Decision making for surgery. Volume 2, Springer)
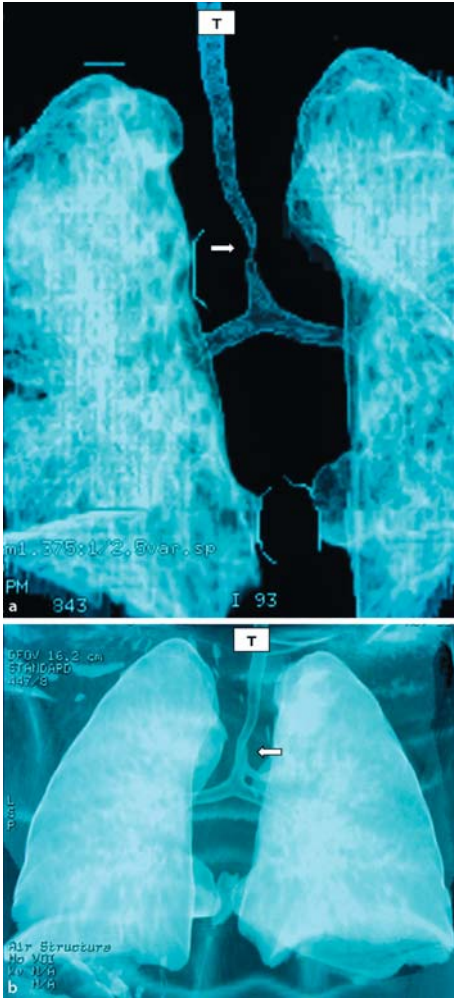
Fig. 3.28.2. Pulmonary artery sling. **a** Coronal projection of the CT scan in the same patient showing the associated long-segment tracheal stenosis with severe distal deviation and obstruction (arrow). **b** Coronal projection of CT scan in the same patient showing the associated long-segment tracheal stenosis with severe distal deviation and obstruction (arrow) (*T* trachea) (reproduced with permission from Corno AF (2004) Congenital Heart Defects. Decision making for surgery. Volume 2, Springer)

Vascular ring

▮ Definition

Various congenital vascular anomalies can result in airway compression at the level of the trachea or of the main bronchi (mostly the left), and esophageal compression, because of the presence of a *complete or incomplete vascular ring* constituted by the aortic arch and its branches. Generally a vascular ring is due to the presence of a double aortic arch or a right aortic arch. However a right aortic arch may occur without forming a vascular ring depending upon branching of brachiocephalic vessels and location of the ductus arteriosus.

▮ Frequent forms:

▮ *Double aortic arch:* one of the two most common forms of complete vascular rings; the trachea and esophagus are completely encircled by connected segments of the aortic arch and its branches. Various forms of double aortic arch exist: both arches may be patent, or an atretic segment may exist at one of several locations in either arch. The right arch, generally dominant (in 50–75% of patients), gives origin to the right common carotid and right subclavian arteries either as an innominate artery or as two separate vessels. The left arch, which gives origin to the left common carotid and left subclavian arteries, is patent in the majority of patients, but it may be hypoplastic or atretic beyond the origin of either the left common carotid (rarely) or the left subclavian artery (more frequently) (Figs. 3.28.4 and 3.28.5). In 15–25% of patients the left arch is dominant, and in these cases the right arch is almost always patent, while in 15–25% of patients the right and left aortic arch present with almost equal size.

▮ *Right aortic arch with anomalous origin of the left subclavian artery and left ductus arteriosus or ligamentum arteriosum:* a
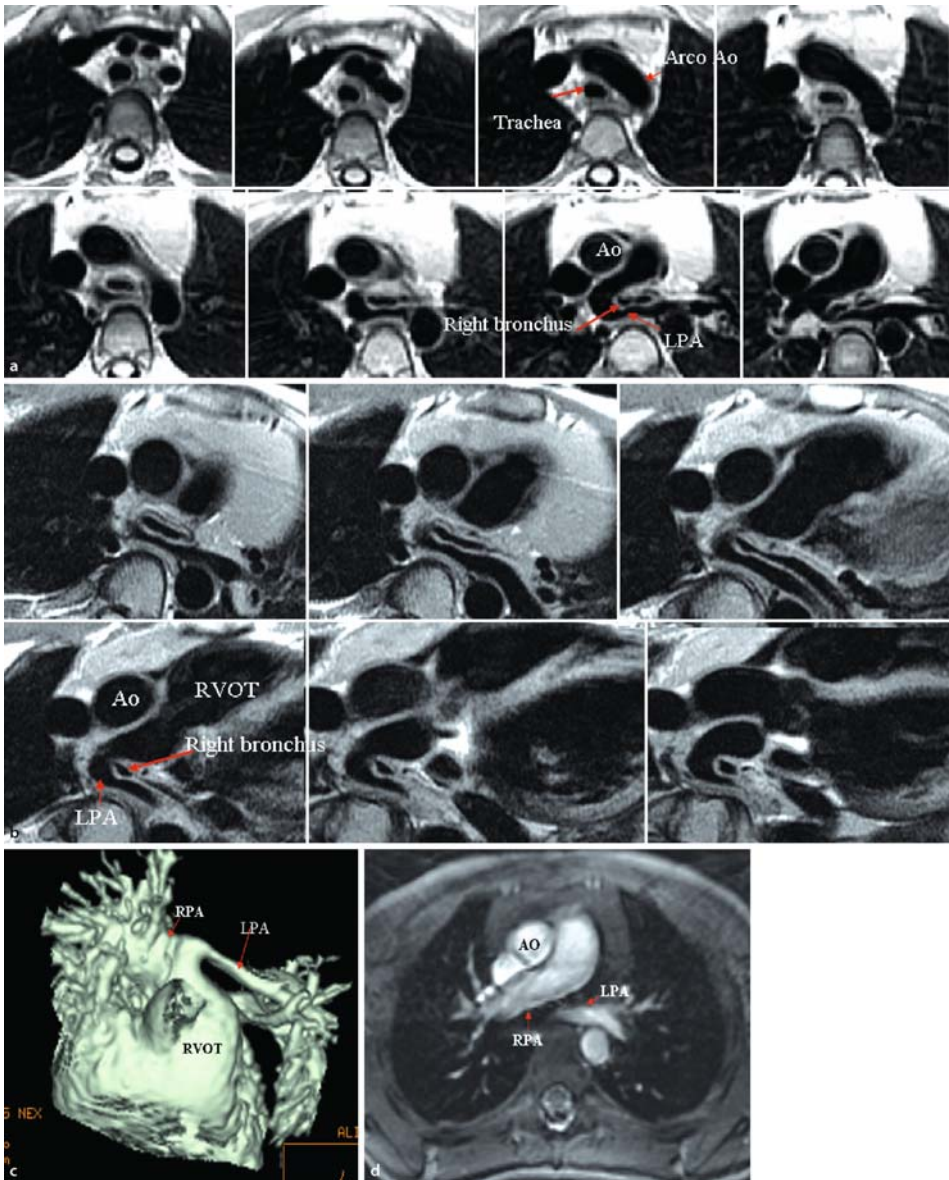
Fig 3.28.3. Pulmonary artery sling. Fast spin echo MRI supero-inferior axial scan (**a**) and para-axial scan, fast spin echo MRI (**b**), and 3-dimensional volume rendering reconstruction (**c**) of anomalous origin of the left pulmonary artery encircling the right bronchus. The left pulmonary artery presents an anterior compression by the distal trachea and proximal bronchi, posterior by the spine. Axial time of flight image of both pulmonary arteries (**d**). Note its different caliber corresponding to different lung perfusion assessed by phase velocity contrast acquisition (68% of pulmonary perfusion to the right and 32% to the left pulmonary artery) (*AO* aorta, *LPA* left pulmonary artery, *RPA* right pulmonary artery, *RVOT* right ventricular outflow tract)
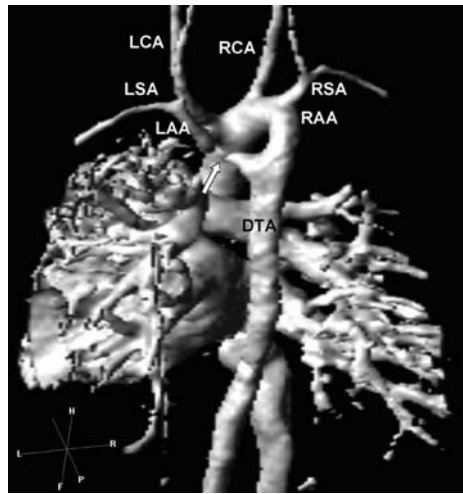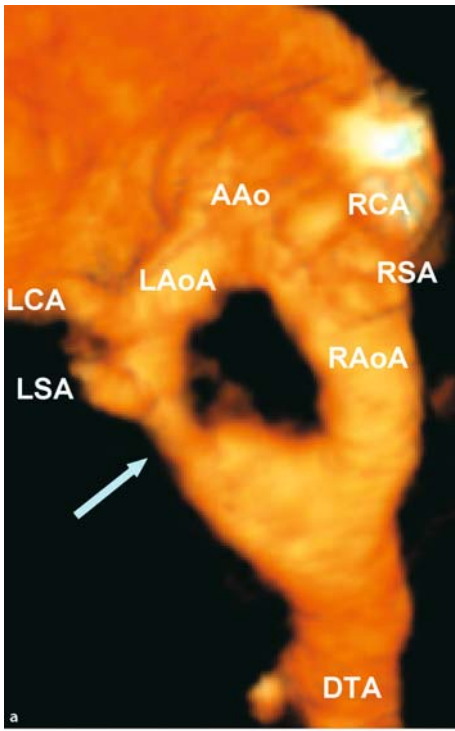
Fig. 3.28.5. Double aortic arch, with atretic left arch. MR angiography volume rendering reconstruction, posterior view, showing the hypoplastic left arch with atretic end segment (arrow) (*DTA* descending thoracic aorta, *LAA* left aortic arch, *LCA* left carotid artery, *LSA* left subclavian artery, *RAA* right aortic arch, *RCA* right carotid artery, *RSA* right subclavian artery) (photograph courtesy of Dr. Mohamed Tawil)
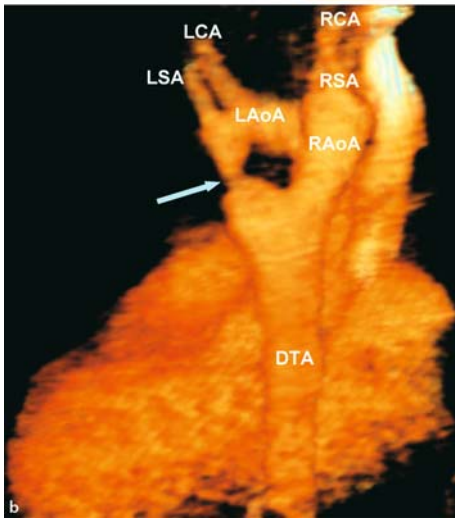
Fig. 3.28.4. Double aortic arch. CT scan, contrast angiography volume rendering reconstruction, viewed from above (**a**) and posterior coronal view (**b**), showing the double aortic arch, with the dominant right arch giving origin to the right carotid and right subclavian arteries and the left arch, from which the left carotid and left subclavian arteries originate and which is hypoplastic (arrow) beyond the origin of the left subclavian artery (*AAo* ascending aorta, *DTA* descending thoracic aorta, *LAoA* left aortic arch, *LCA* left carotid artery, *LSA* left subclavian artery, *RAoA* right aortic arch, *RCA* right carotid artery, *RSA* right subclavian artery) (photographs courtesy of Dr. Mohamed Tawil and Dr. Cinzia Crawley)

right aortic arch gives origin, in sequence, to the left common carotid, the right common carotid, the right subclavian, and the left subclavian arteries. The left subclavian artery, last branch originating from the aortic arch, passes behind the esophagus and then gives origin to the ductus arteriosus or ligamentum arteriosum, which passes anteriorly to connect to the proximal left pulmonary artery, thereby completing the vascular ring.

■ *Right aortic arch with mirror-image branching and left retroesophageal ductus arteriosus or ligamentum arteriosum:* a right aortic arch gives origin, in sequence, to the left innominate artery (left common carotid with left subclavian), the right common carotid, and the right subclavian artery. The final branch, often arising from a prominent ductus diverticulum, is a patent ductus arteriosus or ligamentum arteriosum that passes leftward behind the esophagus and then anteriorly to reach the left pulmonary artery.

■ *Anomalous innominate artery:* the innominate artery originates more posterior than usual from the left aortic arch and crosses posteriorly the trachea, compressing the anterior tracheal wall (*innominate artery compression syndrome*).

■ *Pulmonary artery sling*: see above.

■ **Rare forms:**

■ *Right or left retroesophageal aortic arch.*

■ *Right aortic arch with anomalous left subclavian artery with or without aortic coarctation:* this combination is technically not a complete vascular ring, but it may cause symptoms similar to a ring because of the presence of a right-sided patent ductus arteriosus or ligamentum arteriosum, contributing to the formation of an incomplete vascular ring. The esophageal compression can be more severe in the presence of aneurysmal dilatation of the anomalous left subclavian artery origin (=Kommerel diverticulum) (Figs. 3.28.6 and 3.28.7).

Fig. 3.28.6. Right aortic arch with diverticulum of Kommerell and anomalous origin of the left subclavian artery. **a** CT angiography volume rendering reconstruction viewed from above showing the right aortic arch and the anomalous left subclavian artery originating from the Kommerell diverticulum. **b** CT angiography in the same patient volume rendering reconstruction anterior view showing the right aortic arch and the anomalous left subclavian artery originating from the Kommerell diverticulum (*AAo* ascending aorta, *DTAo* descending thoracic aorta, *KD* Kommerell diverticulum, *LCA* left carotid artery, *LSA* left subclavian artery, *RAA* right aortic arch, *RCA* right carotid artery, *RSA* right subclavian artery) (photographs courtesy of Dr. Mohamed Tawil)
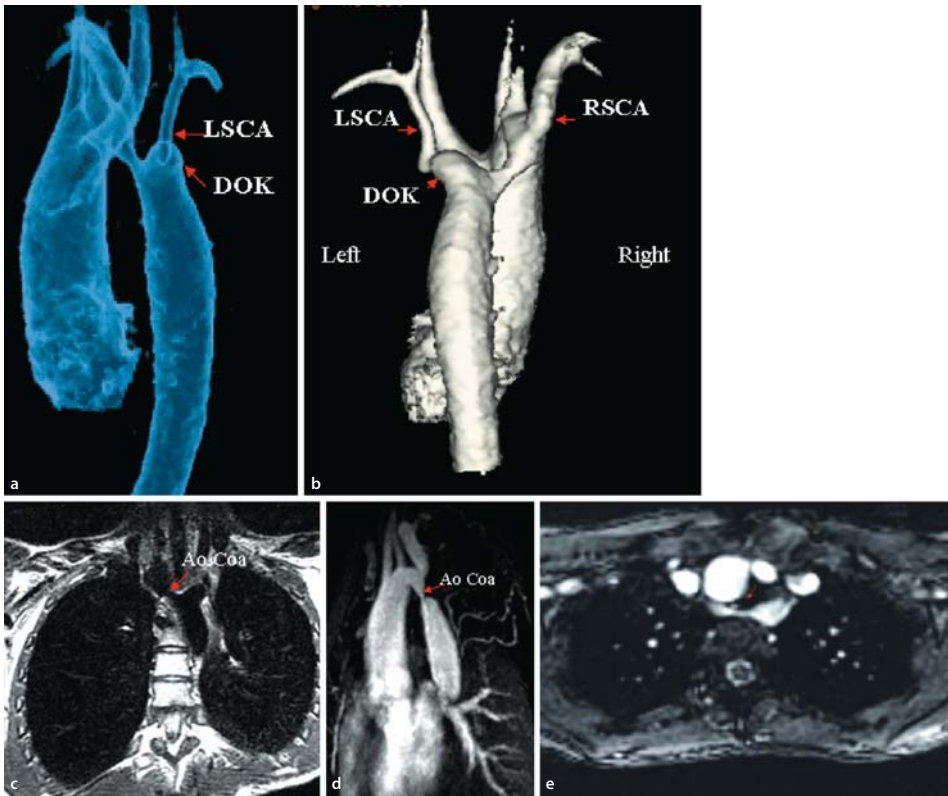
Fig. 3.28.7. Right aortic arch with aortic coarctation and diverticulum of Kommerell. MR angiography volume rendering reconstruction (**a** and **b**), fast spin echo (**c**) maximal intensity projection (**d**) and axial time of flight (**e**) image at the level of the distal stenotic aortic arch: the right aortic arch after the origin of the right subclavian artery shifts to the left posterior to the trachea with a significant narrowing at this level (arrow). The left subclavian artery originates from the diverticulum of Kommerell. The descending aorta is on the left. CT scan transversal projection showing mild tracheal compression (arrow) of a different patient (**f**) and the 3-dimensional reconstruction showing the aneurysmal dilatation near the origin of the left subclavian artery from the Kommerel diverticulum (**g**) (*AO Coa* aortic coarctation, *DOK* diverticulum of Kommerell, *LSCA* left subclavian artery, *RSCA* right subclavian artery)

∎ *Situs inversus with left aortic arch and right ligamentum arteriosum.*
∎ *Dominant left aortic arch, mirror-image branching, right descending aorta, and atretic right aortic arch:* a dominant left aortic arch is extremely rare: the arch vessels arise normally from the normal-sized left aortic arch, while the right arch is atretic.

∎ *Left aortic arch, right descending aorta, and right-sided ligamentum arteriosum to right pulmonary artery:* the reported branching sequence from the left aortic arch is the right common carotid, left common carotid, left subclavian, and, finally, right subclavian as a fourth branch from the proximal descending aorta.

Fig. 3.28.7 (continued)

Fig. 3.28.8. Left aortic arch with diverticulum of Kommerell and anomalous origin of the right subclavian artery. **a** CT scan with axial projection showing the left aortic arch with Kommerell diverticulum and complete compression of the esophagus behind the trachea (arrow). **b** CT scan in the same patient showing the left aortic arch with Kommerell diverticulum and anomalous origin of the right subclavian artery (*AoA* aortic arch, *KD* Kommerell diverticulum, *LB* left bronchus, *RSA* right subclavian artery, *T* trachea) (photographs courtesy of Dr. Mohamed Tawil)

■ *Left aortic arch, anomalous right subclavian artery originating from a Kommerell diverticulum:* this combination can present with esophageal compression due to the anomalous position of the right subclavian artery (Fig. 3.28.8).

A vascular ring is generally an isolated cardiac malformation, with ventricular septal defect and tetralogy of Fallot probably the most common associated anomalies. Very rarely it can be associated with anomalous left subclavian artery, left or right patent ductus arteriosus, aortic coarctation, univentricular heart, pulmonary atresia with ventricular septal defect (unusual), double outlet right ventricle, truncus arteriosus, or transposition of the great arteries.

Since the major clinical impact of the presence of a vascular ring in children is tracheal compression, altered tracheal geometry, e.g., smaller dimensions (area, shorter and longest diameters), has been demonstrated in all symptomatic children with vascular rings compared with asymptomatic children.

Esophageal compression can be associated with airway compression, while esophageal atresia is sometimes found in association with double aortic arch.

▪ Surgical options

The vascular ring is divided through a left thoracotomy. After division, the two stumps generally retract briskly, indicating the tension with which the ring had been surrounding the esophagus and trachea. In all cases the ligamentum arteriosum or the patent ductus arteriosus must also be divided. Frequently, there are additional fibrous strands passing across the esophagus and/or the trachea, and all these have to be divided to completely relieve compression. In the rare case requiring an approach through a right thoracotomy, the same principles are applied. The technique of video-assisted thoracoscopic division has recently been developed as an alternative approach for dividing the vascular ring.

In the case of persistent compression of trachea and/or main bronchus by the aorta or a pulmonary artery branch, "arteriopexy" is performed by suturing the retroesophageal aortic segment to the prevertebral fascia or through the sternum; "extension" of the aorta or the pulmonary artery by a tubular prosthesis may be necessary.

In the presence of *innominate artery compression syndrome,* the approach is through a right anterior thoracotomy with suspension of the innominate artery to the posterior aspect of the sternum; an alternative technique is the transection of the innominate artery at the origin and its reimplantation on the aorta in a more proximal position.

In the presence of right aortic arch with anomalous left subclavian artery originating from a Kommerell diverticulum, the ligamentum arteriosum is divided and the anomalous origin of the left subclavian artery is disconnected from the aneurysmal origin and reimplanted end-to-side of the left carotid artery.

In the presence of associated intracardiac anomalies requiring simultaneous repair with cardiopulmonary bypass through a median sternotomy, the division of the vascular ring is performed during the same procedure from a frontal approach, also advisable in the presence of associated tracheal or esophageal lesions requiring simultaneous surgical treatment.

▪ Pre-operative information

While barium esophagography and echocardiography can accurately determine side of the aortic arch and presence of a vascular ring in the majority of cases, neither modality can reliably delineate the optimal site for division of a ring, particularly in those cases with atretic or hypoplastic segments. Therefore, the surgeon is required to do more extensive dissection to obtain a complete intraoperative diagnosis and to find the best location for division. It is also noteworthy that errors in determining arch sidedness from barium swallow or echocardiography are not that rare. Precise definition of arch anatomy, such as that provided by CT scan and MRI, is superior to the aforementioned techniques as well as to the more invasive angiographic methods.

As for the pulmonary artery sling, CT scan and MRI can simultaneously define the anatomical details of both the airway and the vascular structures, facilitating the diagnosis and the surgical planning. In patients with congenital heart defects, the posterior displaced ascending aorta may compress the main bronchus on the side of the aortic arch and right pulmonary artery against the descending thoracic aorta or spine. In these cases, the CT shows on the axial image a significantly larger retrosternal space, smaller interaortic distance, smaller aortospinal distance, and bronchial stenosis quantifiable on reformatted images perpendicular to the mainstem bronchi.

The aims of the protocol for MRI imaging the aortic arch or pulmonary arteries and

related structures are: 1) rapid identification of the basic arch anatomy or pulmonary arteries; 2) determination of tracheobronchial compression and its relationship to vascular structures; 3) optimal imaging of the aortic arch to determine the ideal site for division in the presence of a vascular ring.

▪ **2-Dimensional imaging:** simple transverse/axial imaging from a level in the neck just below the larynx, down to the level of the diaphragm, allows identification of the trachea and esophagus. Any area of narrowing or distortion of the nearly circular trachea is noted by fast spin echo static images thanks to their better contrast and resolution. Each arch vessel is followed from its respective termination down to the level of the aortic arch. If time permits, simple coronal imaging affords rapid cross-sectional imaging of the aortic arch(es) on either side of the trachea, which is helpful in deciding which arch is larger in case of double aortic arch. This view is also useful in recognizing a diverticulum in vessels running more vertically than horizontally. A series of simple sagittal images is particularly useful for assessing the linear extent and degree of tracheal narrowing.

▪ **3-Dimensional imaging:** after 2-dimensional imaging in one or more standard planes, gadolinium injection is performed to provide a 3-dimensional shaded surface display of the aorta or pulmonary arteries, facilitating the decision-making process for the best approach and position to divide the vascular ring. The other application of 3-dimensional imaging is to allow curved cuts through the great vessels for cases where tortuosity obscures areas of narrowing. By essentially reslicing them along their major axis, areas of stenosis or hypoplasia become more evident.

▪ **Flow assessment:** in cases of double aortic arch with similar size, velocity mapping in the two arches will show which has the lesser blood flow and therefore would be the better one to divide.

▪ Potential complications

Since in infants with severe respiratory symptoms, there is likely to be an element of tracheo/bronchomalacia associated with longstanding compression by the vascular ring during in utero development, it should be anticipated that all respiratory symptoms will not be immediately relieved, even after complete relief of the external airway compression. Nevertheless, residual or recurrent airways obstruction is possible, as well as recurrent respiratory infections, chylothorax (lesion to the thoracic duct), diaphragmatic paresis/paralysis (injury to the phrenic nerve) or vocal cord paresis/paralysis (injury to the recurrent laryngeal nerve).

▪ Post-operative follow-up

As for the pulmonary artery sling, both CT scan and MRI can evaluate the surgical results and detect the presence of potential complications with the same considerations followed for the pre-operative investigation.

▪ References

Azarow KS, Pearl RH, Hoffman MA, Zurcher R, Edwards FH, Cohen AJ (1992) Vascular ring: does magnetic resonance imaging replace angiography? Ann Thorac Surg 53:882–885

Backer CL, Hillman N, Mavroudis C, Holinger LD (2002) Resection of Kommerell's diverticulum and left subclavian artery transfer for recurrent symptoms after vascular ring division. Eur J Cardiothorac Surg 22:64–69

Beekman RP, Beek FJ, Hazekamp MG, Meijboom EJ (1997) The value of MRI in diagnosing vascular abnormalities causing stridor. Eur J Pediatr 156:516–520

Belarbi N, Sebag G, Holvoet L, Delagausie P, Lupoglazoff JM, Hassan M (1998) Left aortic arch with right descending aorta and right ligamentum arteriosum in an infant. J Radiol 79:61–63

Berdon WE, Baker DH, Wung JT, Chrispin A, Kozlowski K, de Silva M, Bales P, Alford B (1984) Complete cartilage-ring tracheal stenosis associated with anomalous left pulmonary artery: the Ring-Sling-Complex. Radiology 152:57–64

Bisset GS, Strife JL, Kirks DR, Bailey WW (1987) Vascular rings: MR imaging. Am J Radiol 149:251–256

Chen HY, Chen LK, Su CT, Chen SJ, Lin CH, Tsai YF, Wu CC, Peng HL, Lu TN (2002) Left cervical aortic arch with aneurism and obstruction: three-dimensional computed tomographic angiography and magnetic resonance appearance. Int J Cardiovasc Imaging 18:463–468

Chen SJ, Lee WJ, Wang JK, Wu MH, Chang CI, Liu KL, Chiu IS, Chen HY, Su CT, Li YW (2003) Usefulness of three-dimensional electron beam computed tomography for evaluating tracheobronchial anomalies in children with congenital heart disease. Am J Cardiol 92:483–486

Chen SJ, Lee WJ, Lin MT, Wang JK, Chang CI, Chiu IS, Wu MH (2007) Left pulmonary artery sling complex: Computed Tomography and hypothesis of embriogenesis. Ann Thorac Surg 84:1645–1650

Corno AF, Monnier Ph, von Segesser LK (2001) Tracheal resection associated with slide tracheoplasty for long-segment congenital tracheal stenosis involving the carina. J Thorac Cardiovasc Surg 122:403–404

Eichhorn J, Fink C, Delorme S, Ulmer H (2004) Rings, slings and other vascular abnormalities. Ultrafast computed tomography and magnetic resonance angiography in pediatric cardiology. Z Cardiol 93:201–208

Fletcher BD, Cohen RC (1989) Tracheal compression and the innominate artery: MR evaluation in infants. Radiology 170:103–107

Fletcher SE, Duncan K, Schroeder B, Danford DA (2004) Coarctation of a right-sided aortic arch and an unusual vascular ring. J Cardiovasc Magn Reson 6:577–581

Gomes AS, Lois JF, George B, Alpan G, Williams RG (1987) Congenital abnormalities of the aortic arch: MR imaging. Radiology 165:691–695

Haramati LB, Glickstein JS, Issenberg HJ, Haramati N, Crooke GA (2002) MR imaging and CT of vascular anomalies and connections in patients with congenital heart disease: significance in surgical planning. Radiographics 22:337–347

Holmes KW, Bluemke DA, Vricella LA, Ravekes WJ, Kling KM, Spevak PJ (2006) Magnetic resonance imaging of a distorted left subclavian artery course: an important clue to an unusual type of double aortic arch. Pediatr Cardiol 27:316–320

Julsrud PR, Ehman RL (1986) Magnetic resonance imaging of vascular rings. Mayo Clin Proc 61:181–185

Hodina M, Wicky S, Payot M, Sekarski N, Gudinchet F (2001) Non-invasive imaging of the ring-sling complex in children. Pediatr Cardiol 22:333–337

Kastler B, Livolsi A, Germain P, Daltroff G, Willard D (1988) Diagnosis of double aortic arch in the neonatal period. Contribution of magnetic resonance imaging. J Radiol 69:625–628

Kim YM, Yoo SJ, Kim TH, Park IS, Kim WH, Lee JY, Han MY (2002) Three-dimensional computed tomography in children with compression of the central airways complicating congenital heart disease. Cardiol Young 12:44–50

Lambert V, Sigal-Cinqualbre A, Belli E, Planchè C, Roussin R, Serraf A, Bruniaux J, Angel C, Paul JF (2005) Preoperative and postoperative evaluation of airways compression in pediatric patients with 3-dimensional multislice computed tomographic scanning: effect on surgical management. J Thorac Cardiovasc Surg 129:1111–1118

Lee KH, Yoon CS, Choe KO, Kim MJ, Lee HM, Yoon HK, Kim B (2001) Use of imaging for assessing anatomical relationship of tracheobronchial anomalies associated with left pulmonary artery sling. Pediatr Radiol 31:269–278

Lee TY, Ng SH, Liang CD, Hsieh MJ, Ko SF (2006) Dissection of Kommerell's aneurysm mimicking aortic arch dissection on echocardiography: multislice computed tomographic diagnosis. J Thorac Cardiovasc Surg 132:1228–1230

Livolsi A, Donato L, Germain P, Kastler B, Binter M, Casanova R, Geisert J, Eisenmann B (1993) Pre- and post-operative MRI study of an aneurysm of the right brachiocephalic artery with tracheal compression. Eur J Pediatr 152:457

McLeary MS, Frye LL, Young LW (1998) Magnetic resonance imaging of a left circumflex aortic arch and aberrant right subclavian artery: the other vascular ring. Pediatr Radiol 28:263–265

Neuhauser EDB (1946) The roentgen diagnosis of double aortic arch and other anomalies of the great vessels. Am J Roentgen Rad Ther Nucl Med 56:1–12

Ou P, Celermajer DS, Agnoletti G, Brunelle F, Vouhé P, Sidi D, Bonnet D (2007) Images in cardiovascular medicine. Definitive diagnosis of pulmonary artery sling in a critically ill infant with high-resolution computed tomography. Circulation 115:e398–399

Rimell FL, Shapiro AM, Meza MP, Goldman S, Hite S, Newman B (1997) Magnetic resonance imaging of the pediatric airway. Arch Otolaryngol Head Neck Surg 123:999–1003

Soler R, Rodriguez E, Requejo I, Fernandez R, Raposo I (1998) Magnetic resonance imaging of congenital abnormalities of the thoracic aorta. Eur Radiol 8:540–546

Weinberg PM (2006) Aortic arch anomalies. J Cardiovasc Magn Reson 8:633–643

Zachary CH, Myers JL, Eggli KD (2001) Vascular ring due to right aortic arch with mirror-image branching and left ligamentum arteriosus: complete preoperative diagnosis by magnetic resonance imaging. Pediatr Cardiol 22:71–73

Subject index